USE OF PARTIAL COHERENCE INTERFEROMETRY IN MEASURING RETINAL SHAPE

Pavan Kumar Verkicharla

Bachelor of Science in Optometry (B. S. Opt)

Submitted in fulfilment of the requirements for the degree of

Doctor of Philosophy

School of Optometry and Vision Science
Institute of Health and Bio-medical Innovation
Faculty of Health
Queensland University of Technology
2015

Keywords

Axial length

Asphericity

Anisomyopia

Conicoids

IOLMaster

Lenstar

Magnetic resonance imaging

Myopia

Partial coherence interferometry

Peripheral refraction

Peripheral eye lengths

Retinal shape

Abstract

Myopia (short-sightedness) is associated with axial elongation of the eye. It is the most common refractive anomaly in children and young adults. Its cause and treatment have been debated for decades; the mechanism of elongation remains unclear. The elongation may be associated with retinal shape.

Retinal shape can be quantified in terms of vertex radius of curvature and asphericity. It can be measured using magnetic resonance imaging (MRI), but this is time consuming and expensive. This study involved development and validation of a simple and inexpensive method for measuring retinal shape, and its use in exploring retinal shape variation with visual field meridian, magnitude of myopia, race, and in anisomyopia.

The method involved partial coherence interferometry (PCI) to measure peripheral (off-axis) eye lengths, combined with other measures and optical modelling. An attachment was developed to take measurements along the horizontal and vertical meridians of the visual field out to ±35° and ±30°, respectively. On the basis of a first preliminary experiment considering two available commercial PCI instruments, the Haag-Streit Lenstar was preferred to Carl Zeiss IOLMaster because the former gave better intra- and inter-sessional repeatability. A second preliminary experiment found that rotating eyes, to look at the peripherally located targets provided by the attachment, did not influence peripheral eye length measurements.

In Experiment 1, retinal shapes estimated using PCI with three different Stages of eye modelling were compared with those obtained from MRI in 58 young adults. Stage 1 used a Le Grand full theoretical model eye without ray deviation at surfaces, Stage 2 involved the same model eye but allowed ray deviation at surfaces, and Stage 3 involved ray deviation at surfaces and individual corneal topography, lens shape and lens equivalent refractive index. Retinal shape was also estimated by Dunne's method, which uses peripheral refraction data and eye modelling. For most participants, all three Stages of PCI and Dunne's method gave slightly flatter retinal estimates than MRI along both meridians with the percentage difference (the average point-by-point height differences between two surfaces over a fixed distance)

between MRI and all Stages of PCI (<4% and <7% along horizontal and vertical field meridians, respectively) and Dunne's method (6% and 9%) being less than the uncertainty of MRI estimates (12–14%). As results for intermediate Stage 2 analysis were similar to those for the more sophisticated Stage 3, Stage 2 was used for further investigations.

In Experiment 2, the validated PCI method was used to compare retinal shapes in young adult Caucasians, East Asians and South Asians. Higher relative peripheral hyperopia, more negative relative peripheral eye lengths and steeper retinas were found a) along the horizontal than along the vertical meridian, b) in myopes than in emmetropes, and c) in East Asian myopes than in Caucasian myopes.

In Experiment 3, the validated PCI method was used to compare retinal shapes of fellow eyes in 11 isomyopes and 9 anisomyopes. The higher myopic eyes of anisomyopic participants had greater relative peripheral hyperopia and steeper retinas than their fellow eyes along the horizontal meridian, but with no obvious differences along the vertical meridian. There was no evidence that the higher myopic eyes of anisomyopes had different retinal shapes than isomyopic eyes with the same refraction.

In conclusion, this study validated a method for estimating retinal shape using partial coherence interferometry in combination with raytracing, and found variation in retinal shape between meridians, with refraction, and between races. The racial differences, combined with the high prevalence of myopia in East Asia, suggest that retinal shape may play a role in myopia development.

Table of Contents

List of Figures

List of Tables

List of Abbreviations

ANOVA – Analysis of variance

AL – Axial length

CCD – Charge coupled device

Cyl – Cylinder

d – Displacement

D – Dioptre

EL – Eye length

FOV – Field of view

FSE – Fast spin echo

H – Height

HASTE – Half-Fourier-acquisition single-shot turbo spin-echo

Hyp – Hyperopia

J_{180} – With/against the rule astigmatism

J_{45} – Oblique astigmatism

L – Length

LED – Light emitting diode

M – Spherical equivalent

MF – Merit function

MRI – Magnetic resonance imaging

Myp – Myopia

NEX – Number of excitations

NHMRC – National Health and Medical Research Council

OPL – Optical path length

PCI – Partial coherence interferometry

PTD – Photo detector

Q – Asphericity

RPEL – Relative peripheral eye length

R_v – Vertex radius of curvature

R_{Eq} – Equivalent radius of curvature

SD – Standard deviation

SNR – Signal to noise ratio

Sph – Sphere

SR – Spectacle refraction

TE – Echo time

TR – Repetition time

TSE – Turbo spin-echo

W – Width

Statement of Original Authorship

The work contained in this thesis has not been previously submitted to meet requirements for an award at this or any other higher education institution. To the best of my knowledge and belief, the thesis contains no material previously published or written by another person except where due reference is made.

Signature:

Date: 9th. January. 2015

Acknowledgements

Firstly, I gratefully thank my principal supervisor Professor David Atchison for his guidance, support and for being a perfect inspiration.

I thank my associate supervisors Assoc/Professor Katrina Schmid, Dr. Ankit Mathur and Dr. Marwan Suheimat for their support. Dr. Mathur wrote routines for estimating retinal co-ordinates with the optical design package Zemax. Dr. Suheimat helped develop instrumentation for preliminary experiments and he wrote routines for comparing the retinal shape estimates with PCI and MRI.

Professor Edward Mallen from the University of Bradford built the attachment to show peripheral targets with partial coherence interferometry instruments, and helped build the phakometer. Dr Mark Dunne from Aston University provided a version of his program to estimate retinal shape. My fellow PhD student Adnan Khan gave advice with phakometry data collection and analysis.

I am grateful to the people involved with magnetic resonance imaging, including Professor James Pope who developed the imaging protocols, radiographers Aiman Al Najjar and Anita Burns for running sessions, and research assistant Farshid Sepehrband for developing imaging analysis routines.

I appreciate recommendations from my Head of School Assoc/Professor Peter Hendicott and Research Coordinator Assoc/Professor Andrew Zele.

I would like to acknowledge the financial support of a scholarship from the Faculty of Health and a Queensland University of Technology postgraduate research award scholarship. Much of my project was funded by a ‘Master myopia eye model’ grant from Johnson and Johnson Vision Care, Inc., Florida.

I thank all my research study participants for their valuable time.

I thank my friends Yash, Anjali, Nishant, Avinash and fellow PhD students Michelle, Prakash and Daniel for their moral support, help and encouragement during my stay in Brisbane.

I extend my gratitude and thank my entire family and friends in India, especially my lovely parents for their unconditional support, encouragement and patience. Amma and Nanna, my success is all yours and I dedicate this thesis to you.

Chapter 1- Introduction

1.1 BACKGROUND

Myopia (short-sightedness) is the most prevalent ocular condition in young children worldwide (see review by Pan et al. (2012)), particularly in East Asian communities where it affects up to 90% of teenagers. It is a leading cause of blindness in later life through associated conditions of retinal detachment, glaucoma, retinal degenerations, posterior staphyloma, chorioretinal atrophy, choroidal neovascularisation, macular holes and macular haemorrhage, and presents healthcare services with a considerable public health burden and individuals with a significant economic burden. The cause and treatment of myopia have been debated for decades, and the mechanism of the development of myopia remains unclear. Both environmental and genetic factors have been associated with the onset and progression of myopia (Wilson and Woo, 1989, Feldkamper and Schaeffel, 2003).

Previously, much attention was given to the central retina and the state of focus along the visual axis, but as the foveal area forms only a small part of the visual field it is reasonable that peripheral retinal areas might be of importance in driving refractive status. Hoogerheide et al. (1971) reported different patterns of peripheral refraction in emmetropes and myopes, with emmetropes usually showing peripheral relative myopia and myopes usually showing peripheral relative hyperopia. From this has developed intense interest in the role that retinal shape and/or peripheral refractive state may have in myopia development (Wallman and Winawer, 2004, Stone and Flitcroft, 2004).

Since Hoogerheide et al.'s work, several other studies have shown different peripheral refraction patterns in emmetropic and myopic groups (Charman, 2011, Berntsen et al., 2010). These studies appear to confirm that relative peripheral hyperopia is likely to result in myopia. The retinal shape may play a causative role in this, with steep retinas likely to be the source (at least in part) of the relative peripheral hyperopia. The occurrence of relative peripheral hyperopia appears to coincide with a more prolate eyeball shape (Atchison et al., 2004). There are measured differences amongst refractive groups in peripheral refraction in vertical

and horizontal visual fields (Atchison et al., 2006, Chen et al., 2010) but it is not known if this is linked to differences in retinal shape in these meridians.

Recent research indicates that the retinal shape may be an important consideration in myopia progression (Charman and Radhakrishnan, 2010, Smith, 2011). Retinal shape has been shown to alter the way in which intraocular pressure and other forces affect the eyeball; particular eyeball shapes may be more vulnerable to subsequent distortion and axial stretch, leading to myopia (Stone and Flitcroft, 2004). Alternately, it may be that peripheral refraction drives axial growth through purely optical factors.

In recent literature, eye and/or retinal shape have been inferred from peripheral refraction, and to a lesser extent, vice versa. Given that both the eye's optics and the retinal shape contribute to the peripheral refraction, and the large variation found in the latter, this inference should be made cautiously. Therefore, it is important to have an appropriate method to determine the relationship between retinal shape and myopia progression. There have been a few studies of retinal shape using the direct method of magnetic resonance imaging (Chen et al., 1992, Atchison et al., 2005a, Gilmartin et al., 2011, Gilmartin et al., 2013). Retinal shape can also be estimated by indirect optical methods that are based on peripheral refraction (Dunne et al., 1987, 1995, Logan et al., 2004) and partial coherence interferometry (Schmid, 2003a, 2003b, 2011, Mallen and Kashyap, 2007, Atchison and Charman, 2011, Ehsaei et al., 2012, Faria-Ribeiro et al., 2013, Ding et al., 2013).

Magnetic resonance imaging is available only in hospitals, is expensive and takes considerable time. Retinal shape can be estimated by measuring central and peripheral eye lengths, followed by some manipulation of peripheral optics of the eye (Verkicharla et al., 2012), but there is no device specifically designed for peripheral measurements. A simple device that is feasible, accurate, non-contact and inexpensive will be of considerable benefit in myopia research.

Partial coherence interferometry (PCI) has been used to determine retinal shape, but there are some assumptions in its use and it has not been assessed for accuracy against magnetic resonance imaging. Two recent commercial instruments, the IOLMaster (Carl-Zeiss Meditec AG Jena, Germany) and the Lenstar (Haag Streit, Bern, Switzerland) contain a Michelson interferometer to create partial coherence and to compare the optical path lengths of two beams, one of which is reflected from

a reference mirror on a moveable stage and the other which travels into the eye and is reflected from one or more surfaces (anterior and posterior corneal surface, anterior and posterior lens surface, retina, and choroid). Only a few studies have used instruments based on partial coherence interferometry for measuring peripheral eye lengths (Schmid, 2003a, 2003b, 2011, Mallen and Kashyap, 2007, Atchison and Charman, 2011, Ehsaei et al., 2012, Faria-Ribeiro et al., 2013, Ding et al., 2013).

This study will compare results obtained by the two commercially-available partial coherence interferometry instruments and determine their repeatability. One of the instruments (Lenstar LS 900) and the magnetic resonance imaging technique will be used to determine retinal shape in eyes with different refractive conditions, the results were compared and recommendations made regarding appropriate corrections to the former method. The retinal shape results will also be compared with those estimated using a method based on peripheral refraction (Dunne, 1995). The validated PCI method will be later used in studies of retinal shape, with the ultimate purpose of assisting in developing preventive strategies for myopia.

Considering that there are differences in biomechanical, structural and optical characteristics of the fellow eyes of anisomyopes (Vincent et al., 2014), retinal shape will be measured in individuals with anisomyopia (where different amounts of myopia occur in the two eyes of a person). In this case the less myopic eye will serve as an experimental control. As both eyes are exposed to the same visual (environmental) influences and the confounding influence of differences in genetic background are avoided, this condition is useful for understanding the relationship between retinal shape and myopia.

Race appears to be associated with myopiogenesis, with East Asians showing high myopia prevalence. Considering structural variations in the eye, it is possible that retinal shapes are different between races. Retinal shape will be measured in participants with different racial backgrounds to determine how the retinal shape and peripheral refraction alter with race. If spectacle lenses for the correction of myopia are going to be designed based on retinal shape, then it is important to know whether retinal contours vary with ethnicities and/or meridians so that anti-myopia specific lenses can be designed accordingly.

1.2 AIMS

This research programme will help the understanding of the role of retinal shape in the development of myopia. The following aims will be addressed:

- To determine the reliability of a simple method of determining retinal shape using off-axis partial coherence interferometry, and to validate this method by comparing the results to that of magnetic resonance imaging.
- To use the validated method to measure retinal shape in East Asian, South Asian and Caucasian emmetropes and myopes to determine how retinal shape and peripheral refraction are related in eyes of people with different racial backgrounds.
- To determine how retinal shape and peripheral refraction vary between the two eyes of individuals with isomyopia and anisomyopia.

By achieving these aims I will contribute an important assessment device with applications for understanding myopia development risk and likely optical treatment effectiveness.

1.3 HYPOTHESES

Research hypotheses are:

1. Retinal shape can be accurately predicted by measuring "off-axis eye lengths" with a commercial partial coherence interferometry instrument.
2. There are differences in retinal shapes among different racial groups.
3. There are meridional (vertical and horizontal) variations in retinal shape.
4. Retinal shapes are different in isomyopic eyes and anisomyopic eyes of the same refraction.

1.4 SCOPE OF THE THESIS

The following chapters will include:

- **Chapter 2** provides a comprehensive literature review of the topics related to the project.
- **Chapter 3** describes methods. It includes two preliminary studies that investigated the repeatability of peripheral eye lengths with partial coherence interferometry instruments and the influence of eye rotation on these measurements.
- **Chapters 4, 5 and 6** are the main experimental chapters.
- **Chapter 4** is a validation experiment, in which comparison was made between the retinal shape results from partial coherence interferometry and magnetic resonance imaging. Details of retinal shape analysis from the various measurements obtained from PCI and MRI are explained here. Aim 1 and hypothesis 1 are addressed by this experiment.
- **Chapter 5** investigates how retinal shape and peripheral refraction alter with race using peripheral eye length and peripheral refraction methods. This experiment will address aim 2 and its associated hypotheses 2 and 3.
- **Chapter 6** investigates the retinal shape in isomyopes and anisomyopes using peripheral refraction and peripheral eye length methods. This experiment will address aim 3 and its accompanying hypothesis 4.
- **Chapter 7** is a concluding chapter summarising the research. It also includes the clinical implications and discusses future directions.

Chapter 2- Literature Review

2.1 DEFINITION OF MYOPIA

Myopia is the refractive condition of the eye in which parallel rays from a distant object come to a focus in front of the retina during relaxed accommodation. This causes blurred distance vision. Common names for myopia are near-sightedness and short-sightedness. Practically myopia is defined according to the distance ophthalmic correction, for example ≤ 0.25 D.

2.2 PREVALENCE

Myopia is the most common refractive anomaly in children and young adults. Its prevalence is affected by country, race, age and environment. It affects a considerable proportion (about 44% in children and 26% in adults) of Western populations (Kempen et al., 2004, Villarreal et al., 2003), but a larger proportion (>60% in children and >30% in adults) of East Asian communities (Lam et al., 2012, You et al., 2013, Kim et al., 2013a). The prevalence of myopia in children is higher in urban Asian regions such as Singapore (Seet et al., 2001) and Taiwan (Lin et al., 2004, Guo et al., 2012) than in developing Asian countries like India (Murthy et al., 2002, Krishnaiah et al., 2009). It has been estimated that 2.5 billion people (30% of the world's population) will be affected by myopia by the year 2020 (reported by VISION 2020). Region and age-wise prevalence of myopia are given in Table 2.1, note that variations in definition and measurement affect these.

Table 2.1: Summary of studies of myopia prevalence

Author	Myopia Definition	Region	Sample size	Age (years)	Prevalence %
You et al. (2013)	≤ −0.50 D	China (Beijing)	15,066 792 1,278	7-18 7 18	64.9 9.7 72.8
Sun et al. (2012)	< −0.50 D	China (Shanghai)	5083	14-42	95.5
Lan et al. (2013)	≤ −0.50 D	China (Guangzhou)	2,478	3-6	1.0
Guo et al. (2012)	not given	Taiwan	20,609 2,978	12-65 12-19	46.7 70.3
Lin et al. (2004)	< −0.25 D	Taiwan	920 937 2,474	12 15 16-18	61 81 84
Kim et al. (2013a)	≤ −0.50 D	Korea	22,562 2,690	20-70 20-29	48.1 78.9
Fan et al. (2004)	≤ −0.50 D	Hong Kong	7,560 1,720 1,035	5-16 11 7	36.7 53.1 28.9
Lam et al. (2012)	≤ −0.50 D	Hong Kong	2,651	6 12	18.3 61.5
Pan et al. (2013a)	< −0.50 D	Singapore	8,772	40-70	31.4
Saw et al. (2002)	≤ −0.50 D	Singapore	1,453	7–9	36.7
Goh et al. (2005)	< −0.50 D	Malaysia	4,634	7–15	20.7
Morgan et al. (2006)	< −0.50 D	Mongolia	1,057	7-17	5.8
Adhikari et al. (2013)	≤ −0.50 D	Nepal	484	3-5	24.2
Ahmed et al. (2008)	≤−0.25	India (North)	4,360	7-18	4.7
Raju et al. (2004)	<−0.50 D	India (South)	2,508	>39	26.9
Krishnaiah et al. (2009)	< −0.50 D	India (South)	3642	40-92	36.5
Murthy et al. (2002)	≤ −0.50 D	India (Urban)	6,447	5-15	7.4
Shah et al. (2008)	< −0.50 D	Pakistan	14 490	30-50	36.5
Hashemi et al. (2012)	≤ −0.50 D	Iran	6,311	40-64	30.2
Montes-Mico et al. (2000)	<−0.25	Spain	7,621	3-93	21.2

Kumah et al. (2013)	≤ −0.50 D	Ghana	2,435	12-15	3.4
Naidoo et al .(2003)	≤ −0.50 D	South Africa	4,890	5–15	4.0
Rudnicka et al .(2010)	≤ −0.50 D	UK South Asian African Caribbean White	1,179 262 142 96 233	10-11	11.9 25.2 12.7 7.9 3.4
O'Donoghue et al. (2010)	≤ −0.50 D	Northern Ireland	1,053	6–7 12-13	2.8 17.7
Villarreal et al. (2003)	≤ −0.50 D	Mexico	1,035	12-13	44.0
Pan et al. (2013b)	≤ −1.00 D	United States Hispanic Black Whites Chinese	4,430 1,046 1,230 1,667 487	45-84	25.1 14.2 21.5 31.0 37.2
Vitale et al. (2008)	< −0.50 D	United States	12,010	20	33.1
Kempen et al. (2004)	≤ −1.00 D	United States Europe Australia	30,058 496,000 471,000	40-80	25.5 26.6 5.8
Wensor et al. (1999)	< −0.50 D	Australia	4,744	40-98	17.0
French et al. (2013)	≤ −0.50 D	Australia	2,760	12 17	14.4 29.6
Ip et al. (2007b)	≤ −0.50 D	Australia	2,353	12	11.9

2.3 CONSEQUENCES OF MYOPIA

The development of myopia is generally irreversible with the majority of cases due to excessive axial elongation of the eye - the elongation leads to stretching of the outer coats of the eye (McBrien and Gentle, 2003, Rada et al., 2006). Its effect on individuals and society is considerable, including direct costs such as spectacles, contact lenses, and refractive surgery, and indirect costs such as vision loss due to the associated ocular complications like glaucoma, macular holes, retinal degenerations, retinal detachment and cataract (Lim et al., 2009, Wong et al., 2003, Saw et al., 2005).

2.3.1 MYOPIA AND GLAUCOMA

Glaucoma is a progressive optic neuropathy and one of the leading causes of irreversible blindness in the adult population (Coleman and Brigatti, 2001). Primary open angle glaucoma is the most common type and is associated with high myopia (Loyo-Berrios and Blustein, 2007, Marcus et al., 2011, Chen et al., 2012). Population-based studies indicate that the risk of glaucoma increases with increasing amounts of myopia.

Because of the changes in the structure and arrangement of the connective tissue, the optic nerve head in myopic eyes may be structurally susceptible to glaucomatous damage. The reduced retinal nerve fiber layer thickness in myopic eyes may be considered a risk factor for the development of glaucomatous changes (Chang, 2011).

2.3.2 MYOPIA AND CATARACT

Cataract is opacification of the lens and is the major cause of avoidable blindness in the world. The association between cataract (both nuclear and posterior sub-capsular) and myopia is well known (Lim et al., 1999, Younan et al., 2002).

Reduced antioxidant properties and increased levels of lipid peroxidation by-products have been found in cataractous lenses of myopes compared with control and non-myopic cataractous lenses. Cataractous lenses had lower levels of glutathione compared to controls, with the lowest levels found in myopic lenses (Micelli-Ferrari et al., 1996). The alteration of the antioxidant defence in myopic lens makes myopia, a risk factor for cataract.

2.3.3 MYOPIA AND RETINAL DEGENERATION

Excessive axial elongation of the eye in myopia can cause mechanical stretching and thinning of the choroid and retinal pigment epithelium layers, resulting in various retinal degenerative changes. In high myopes, there is an increased risk of peripheral retinal degenerations, retinal tears, retinal detachment, posterior staphyloma, chorioretinal atrophy, retinal pigment epithelial atrophy,

lacquer cracks, choroidal neovascularisation and macular haemorrhage (Gozum et al., 1997). Most retinal lesions are associated with severe irreversible vision loss. Lattice degeneration is the most important of the peripheral retinal degenerations and is a risk factor for retinal breaks which can predispose to retinal detachment (Pierro et al., 1992).

2.3.4 MYOPIA AND THE OPTIC DISC

High myopia is a risk factor for optic disc abnormalities. Myopes have significantly tilted, rotated, larger disc areas and longer disc-foveola distances than non-myopes (Hyung et al., 1992, Ramrattan et al., 1999, Vongphanit et al., 2002).

2.3.5 MYOPIA AND POSTERIOR STAPHYLOMA

Excessive axial elongation in high myopic eyes can lead to abnormal protrusions of the posterior segment known as posterior staphyloma. High myopes with posterior staphylomas tend to develop severe macular pathologies such as myopic foveoschisis and macular holes (Takano and Kishi, 1999, Hsiang et al., 2008).

2.3.6 ECONOMIC BURDEN AND PUBLIC HEALTH

The significance of myopia as a public health issue has been underestimated, due to the apparent ease with which myopia can be corrected. Myopia is a leading cause of blindness in later life and presents healthcare services with a considerable public health burden and individuals with considerable economic burden. It has been estimated that Singapore (population ~5 million) spends US$90 million/year on spectacles and US$2.5 million/year on refractive surgery (Seet et al., 2001). While refractive surgery can correct myopia, thus freeing patients from spectacle and contact lenses, the structural changes within the eye due to the elongation are unaffected. It is this stretching of the eye that increases the risk of the ocular pathologies mentioned above (Saw et al., 2005, Timothy, 2007). Prevention of, or the reduction in rate of increase, of myopia is thus an important public health issue.

2.4 AETIOLOGY AND RISK FACTORS

Myopia is a complex ocular refractive condition which may have a multi-factorial etiology. Whether myopia is inherited or environmentally determined has been under debate in recent decades. Several risk factors for myopia have been identified in children, that can be broadly classified as genetic susceptibility (Hammond et al., 2001) and environmental factors including nutrition, socioeconomic background, near work and outdoor activity (Saw et al., 2006, Saw et al., 1996, Saw et al., 2001, Lim et al., 2010, Edwards, 1996, Rose et al., 2008).

2.4.1 GENETICS AND ENVIRONMENT

A range of biochemical pathways are involved in eye growth. Alterations within the retina, choroid and sclera might change the sequence of normal biochemical events. Genes involved in these pathways may contain susceptibility variants for myopia (McBrien and Gentle, 2003, Morgan, 2003, Feldkamper and Schaeffel, 2003). Several genetic loci for myopia (MYP) have been mapped, with most of them (20 loci) linked to high myopia.

It has been observed that children with two myopic parents are at high risk (40%) of developing myopia, which decreases in those with one myopic parent (20-30%), and is lowest (10%) in children with no myopic parents (Mutti et al., 2002, Wu and Edwards, 1999, Ip et al., 2007b). It is possible that shared intense near-work environment as well as shared genes may be associated with myopia running in families. Increased accommodation due to intensive near work is associated with myopia (Ip et al., 2008, Mutti et al., 2002, Mutti and Zadnik, 2009).

Few studies have considered anisomyopia as a means of controlling the confounding effect of genetics and environment on myopia in order to investigate the influence of other factors on myopia development (see review by Vincent et al. (2014)). The fellow eyes of anisomyopes do not seem to be different with respect to anterior ocular biometry (Kim et al., 2013b) and corneal and total higher-order aberrations (Vincent et al., 2011, Hartwig et al., 2013). However, there are differences between the posterior segments of the higher myopic eyes and their fellow eyes: longer vitreous chambers (Kim et al., 2013b), thinner choroids (Vincent

et al., 2013), and more curved retinal surfaces (Logan et al., 2004) determined using peripheral refraction (see section 2.4.2.8). The reason for one eye to be more myopic is not clear, but it is possible that the higher myopic eye of anisomyopic individual might have different properties in the eye compared to the fellow eye which might lead to anisomyopia. *To my knowledge, no studies have investigated whether the biometry or the structural properties of higher myopic eyes of anisomyopes is different from that of eyes of isomyopes with similar refraction*.

2.4.2 RETINALSHAPE

The human retina is a complex light-sensitive tissue forming the inner surface of the eye. The image of the visual world is focused on the retina by the optics of the eye and initiates a cascade mechanism to trigger various visual centres of the brain through the optic nerve fibres. The fovea forms the central 1.5 mm of retina, in the centre of which there is depression called foveola, the most important part of retina as it provides best visual acuity. The peripheral retina stretches to the ora-serrata (about 21 mm from the foveola). The retina occupies approximately 72% of a sphere (Kolb, 1995).

The ability to process visual information is distributed unevenly over the retina. For example, decrease in resolution acuity (Wertheim, 1980 (translated by DUNSKY, IL. Original work published in 1891), Latham and Whitaker, 1996, Land and Tatler, 2009), vernier acuity (Fahle and Schmid, 1988), contrast sensitivity (Anderson et al., 1991, Ehsaei et al., 2013) and orientation discrimination (Paradiso and Carney, 1988) occurs from the fovea into the retinal periphery. This is related to structural variations in the density of photoreceptors and neurons. (Inui et al., 1981, Curcio and Allen, 1990, Wenner et al., 2014, Chui et al., 2005).

Previously, much attention was given to the central retina and the state of focus along the visual axis, but as the foveal area corresponds to only a small part of the visual field it is reasonable that peripheral retinal areas might also be important in driving refractive status. Recent evidence includes work involving animal models showing the presence of ocular growth pathways mediated by peripheral retinal image quality (Smith, 2011). Considering that myopia is mostly due to the axial elongation of the eye (>95%), it is the accelerated stretching of the eye after birth and

not the changes in corneal or lens power that leads to the development of myopia (Zadnik, 1997). The increased axial length must shift the retinal position, altering the structure/anatomy (size and shape) of the posterior part of the eye (McBrien and Adams, 1997, McBrien and Gentle, 2003).

Recent research indicates that the retinal shape may be an important consideration in myopia development/progression (Charman and Radhakrishnan, 2010, Smith, 2011), because it influences the way in which intraocular pressure and other forces affect the eyeball. There is considerable interest in the role that retinal shape (i.e. retinal curvature and asphericity) and/or peripheral refractive state may play in myopia development (Stone and Flitcroft, 2004). Literature related to retinal shape is detailed in subsections below.

2.4.2.1 Conicoids, shapes, axes and sections used to describe eye and retinal shape

The eye is a complex structure containing aspheric surfaces. An aspheric surface varies from the centre towards the periphery, usually becoming either progressively flatter or steeper.

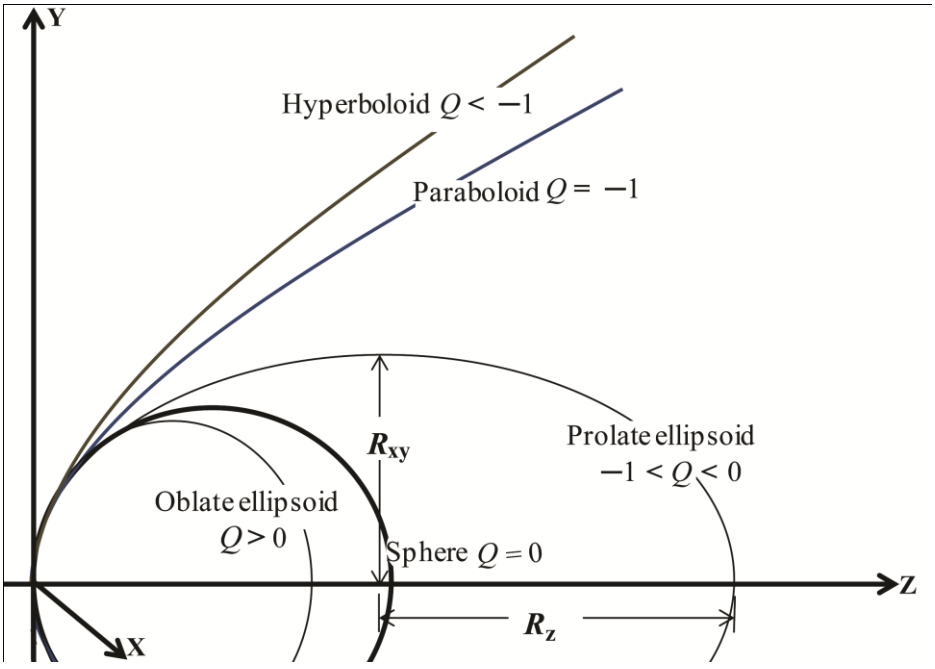

Figure 2:1: Conicoids with the same vertex curvature R_v, based on Atchison and Smith (2000). Semi-axis lengths R_{xy} and R_z are shown for the prolate ellipsoid.

Ocular surfaces are typically described by conic sections. A conic section rotated about one of its principal meridians becomes a rotationally symmetric conicoid. This can be described by the equation

$$X^2 + Y^2 + (1 + Q)\, Z^2 - 2ZR_v = 0 \quad (1)$$

where Z is measured along the optical axis, X and Y are measured along axes perpendicular to the Z-axis and to each other, R_v is the vertex radius of curvature, and Q describes the asphericity (Figure 2:1). $Q > 0$ represents an oblate ellipse (steepening away from the vertex), $Q = 0$ represents a sphere, $-1 < Q < 0$ represents a prolate ellipse (flattening away from the vertex), $Q = -1$ represents a paraboloid and $Q < -1$ represents a hyperboloid. Alternative terms for oblate ellipsoid and prolate ellipsoid are oblate spheroid and prolate spheroid, respectively. Sometimes asphericity is represented by the quantity p where

$$p = 1 + Q \quad (2)$$

and sometimes it is represented by the eccentricity e, where

$$e^2 = -Q \quad (3)$$

An alternate equation to equation (1) that can be applied to ellipsoids is

$$(X^2 + Y^2)/R^2_{xy} + (Z - R_z)^2/R^2_z = 1 \quad (4)$$

where R_{xy}, R_{xy} and R_z are the semi-axis lengths along the X, Y and Z directions, respectively (Figure 2:1). For an oblate ellipsoid $R_{xy} > R_z$ and for a prolate ellipsoid $R_z > R_{xy}$. The vertex radius of curvature R_v and the asphericity Q are related to R_z and R_{xy} by

$$R_v = R^2_{xy}/R_z \quad (5)$$

$$Q = R^2_{xy}/R^2_z - 1 \quad (6)$$

Non-rotationally symmetrical ellipsoids can be described by

$$X^2/R^2_x + Y^2/R^2_y + (Z - R_z)^2/R^2_z = 1 \quad (7)$$

where R_x, R_y, and R_z are the semi-axis lengths along the X, Y and Z axes, respectively. For the X-Z section, the vertex radius of curvature R_{xv} and asphericity Q_x are given by

$$R_{xv} = R^2_x/R_z \quad (8)$$

$$Q_x = R^2_x/R^2_z - 1 \quad (9)$$

Similarly for the Y-Z section,

$$R_{yv} = R^2_y/R_z \quad (10)$$

$$Q_y = R^2_y/R^2_z - 1 \quad (11)$$

Further levels of sophistication would be to rotate and decentre the surfaces, and to have more complex surfaces, which are beyond the scope of this review.

Figure 2:2 shows sections and axes of the eye. Transverse axial sections are parallel to the XZ plane, and taking the visual axis as the Z axis, one is usually selected to match the XZ plane as well as possible. Sagittal sections are parallel to the YZ plane, and similar to the transverse axial sections, one is usually selected to match the YZ plane as well as possible. Coronal sections are parallel to the XY plane, and one is usually selected where the X and Y dimensions are judged to be maximums.

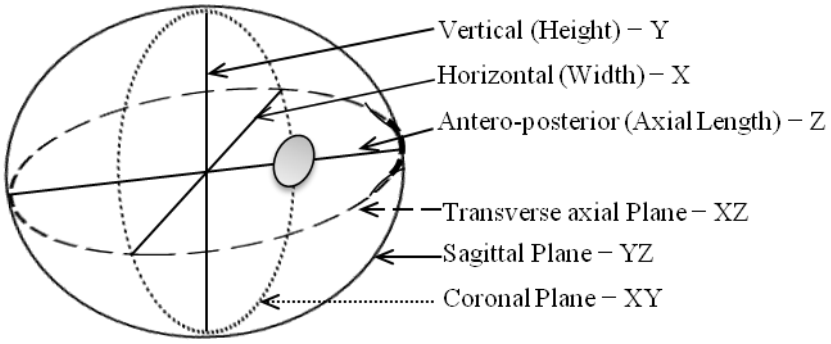

Figure 2:2: Scanning planes and axes of the eye. The sagittal plane (solid line) is a vertical section containing the visual axis, the transverse axial plane (dashed line) is a horizontal section containing the visual axis, and the coronal plane (dotted line) is a vertical section perpendicular to the visual axis.

The antero-posterior length is usually measured from the anterior corneal surface to the posterior pole at the inner retina, generally understood as the axial length, although in some studies it has been measured from the posterior cornea to the posterior pole and in others it has been measured from the anterior cornea to the outer sclera (Table 2.2). This distance can be measured through either transverse axial or sagittal sections.

The vertical length, or height, is the widest distance between the top and bottom of the eye and can be obtained from either sagittal or coronal sections. The horizontal length, or width, is the widest distance between temporal and nasal sides of the eye and can be obtained from either transverse axial or coronal sections. The height and width can be measured from inner retina to inner retina or from outer

sclera to outer sclera. Unless otherwise indicated in this chapter, the distances apply to the inner retina.

Eye shape can be quantified using the axial length, height and width of the eye, with a number of studies using the ratios of axial length to height and/or axial length to width as additional descriptors. Clearly this is an oversimplification as it ignores the rapid change in shape that occurs at the corneo-scleral intersection. Retinal shape can be similarly described by fitting ellipsoids to its posterior part, the functional part of the eye as far as imaging is concerned. Retinal shape may be confused with the more nebulous concept of eye shape. The eye shape and retinal shape components will have similar heights and widths, but the lengths of the ellipsoids used to fit the retina are shorter than the axial length by about 3.1 mm (Atchison et al., 2005a).

2.4.2.2 Models of retinal shape in myopia and their relation to peripheral refraction

Variations in retinal shape in myopic eyes can be related to models of the retinal stretching that accompany the increase in axial length as shown in Figure 2:3. These include a global expansion model (a), a model where the stretching occurs parallel to the optical axis at the equatorial region (b), and a model where the stretching takes place only at the posterior pole (c). A hybrid model, called the axial expansion model is the combination of equatorial and posterior pole expansion models (d). The first three models are shown with spherical surfaces and the hybrid model is shown with a prolate ellipsoid surface.

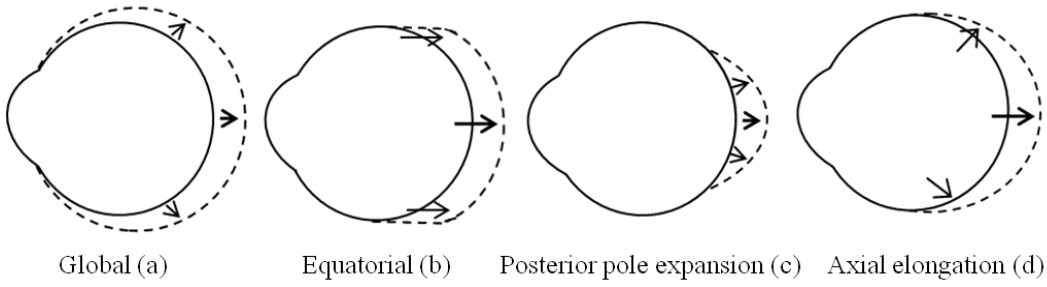

Figure 2:3: Models of retinal stretching in myopia. The solid circles represent the shape of the retina of an emmetropic eye, the dashed shapes represent the myopic retinas, and the arrows indicate the regions of stretching.The first three models were presented by Strang et al. (1998), and Atchison et al. (2004) described the axial elongation model.

A thin beam (pencil) of light from an off-axis object point on a plane surface, passing through a symmetrical optical system, will be focused as lines at two positions, one corresponding to light refracted in the (tangential) plane containing the object point and the optical axis and the other in the (sagittal) plane perpendicular to this plane. For a range of object points across the surface there will be two image shells as shown in the Figure 2:4a. Taking the optical system of an emmetropic eye, and assuming that its normal retinal shape is a sphere with radius of curvature of about 12 mm and that the shell corresponding to the average of the tangential and sagittal shells coincides approximately with this sphere, a retinal shape approximation can be made. Figure 2:4b shows this retinal shape (solid line) along with changes in retinal curvature that make the retina flatter or steeper. Light from a distant off-axis point converges to a point that coincides with the normal retina, is in front of the flatter retina causing peripheral myopia, and is behind the steeper retina causing peripheral hyperopia. The eye with the steeper retina might respond to the peripheral hyperopic defocus by elongating and thus causing myopia.

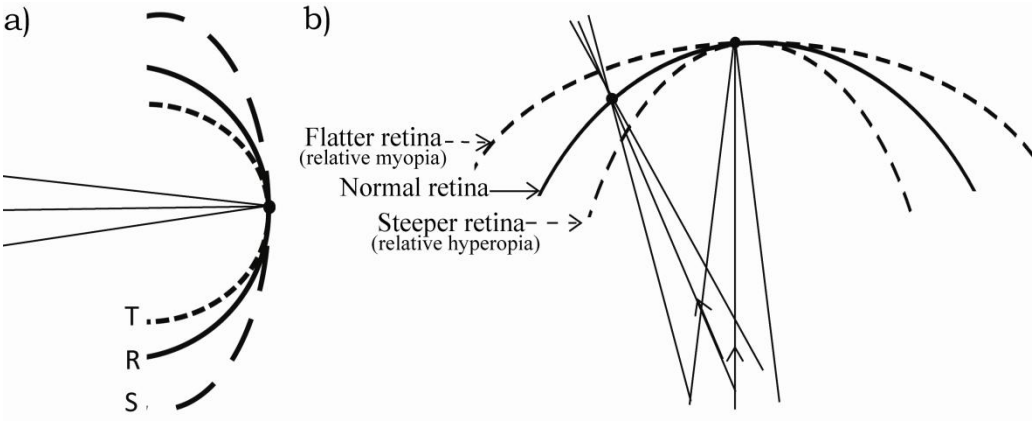

Figure 2:4: Formation of tangential (T-dotted line) and sagittal images (S-dashed line) on either side of retina (R-bold line)(a). Formation of the mean of the image shells, and its location relative to the retina for three different retinal shapes (b).

This description can be extended to a myopic eye. Assuming the optics of the eye are the same as that of the emmetropic eye described above apart from an increase in length, for the flatter retina an off-axis light beam's "mean" focus will be further in front of the retina than for the "normal" retina. The peripheral refraction corresponding to this is referred to as relative peripheral myopic refraction because a

more negative correction is needed that for the normal retina. For the steeper retina, the off-axis light beam's "mean" focus will be closer to the retina than for the normal retina, resulting in a relative peripheral hyperopia. Similar to the emmetropic eye with a steep retina, the eye might respond to the relative hyperopic defocus by becoming yet more myopic.

The situation described above leading to myopia development might be turned around - "excessive" relative peripheral myopia in the young emmetropic or hyperopic eye might result in a "stop" signal to normal emmetropization and lead to an adult hyperopic eye.

The above situation is over-simplified: real eyes do not generally exhibit rotational symmetry and so peripheral refraction varies according to visual field meridian. Most emmetropic eyes have low levels of peripheral myopia, as will be discussed later. Most emmetropic retinas are oblate in shape rather than spherical (Atchison et al., 2005a).

Figure 2:5 shows how models of retinal stretching relate to image position and relative peripheral refraction. For all models, the image surface (the position at which images occur) is closer to the retina in the periphery than in the centre, resulting in relative peripheral hyperopia. This effect is greatest for posterior polar expansion, followed by axial, equatorial and global expansion.

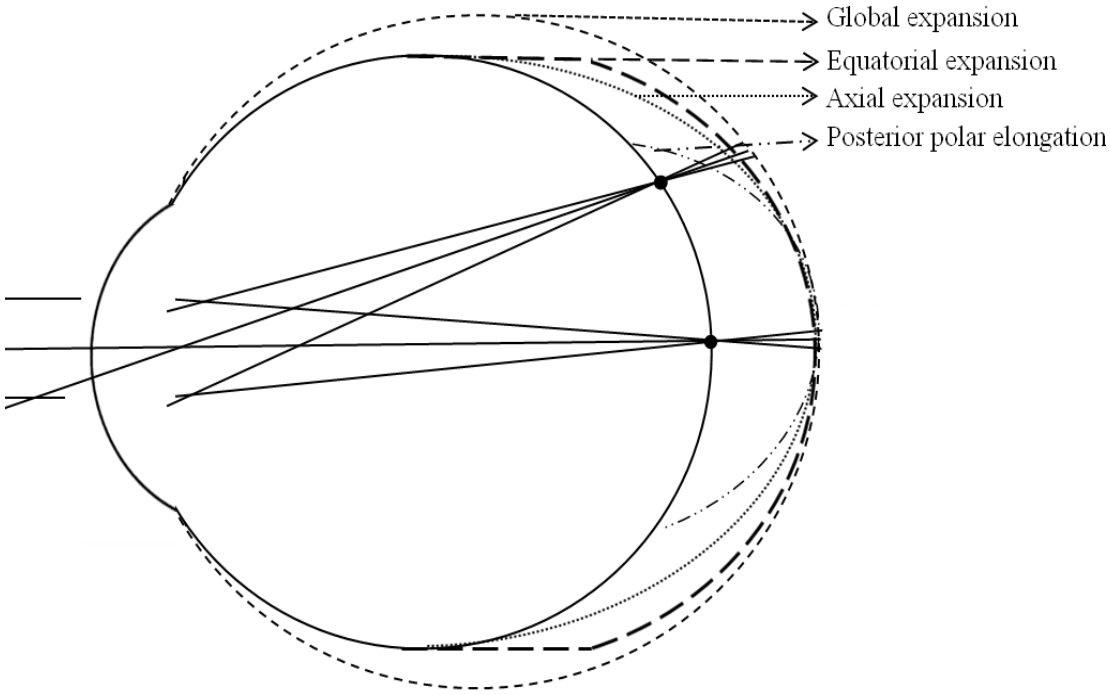

Figure 2:5: Positions of images relative to the myopic retina for the global, equatorial, posterior pole, and axial expansion models. It is assumed that the retinal surfaces remain spherical in the elongated regions for the first three models, while the surface for the axial expansion model is a prolate ellipsoid.

2.4.2.3 Peripheral refraction

Peripheral refraction studies date back to Thomas Young (1801) who determined the tangential and sagittal image shells, for a 25 cm diameter circular object surface, for a schematic eye based on measurements of his own left eye. This was followed by several studies in the late nineteenth and early twentieth centuries as reported by Ames and Proctor (1921). Ferree et al. (1931, 1932, 1933a, 1933b) conducted a well-known study of peripheral refraction along the horizontal meridian up to 60° from fixation in 21 participants using an objective refractometer. They identified three different patterns of peripheral refraction as shown in Figure 2:6. The type A pattern had 'mixed' astigmatism in which the tangential refraction (refraction along the horizontal direction) became more myopic and sagittal refraction (refraction along the vertical direction) became more hyperopic, the type B pattern had relative hyperopic astigmatism in which both tangential and sagittal refraction became more hyperopic into the periphery, and the type C pattern had asymmetrical astigmatism with the peripheral refraction differing between nasal and temporal sides of the horizontal peripheral field.

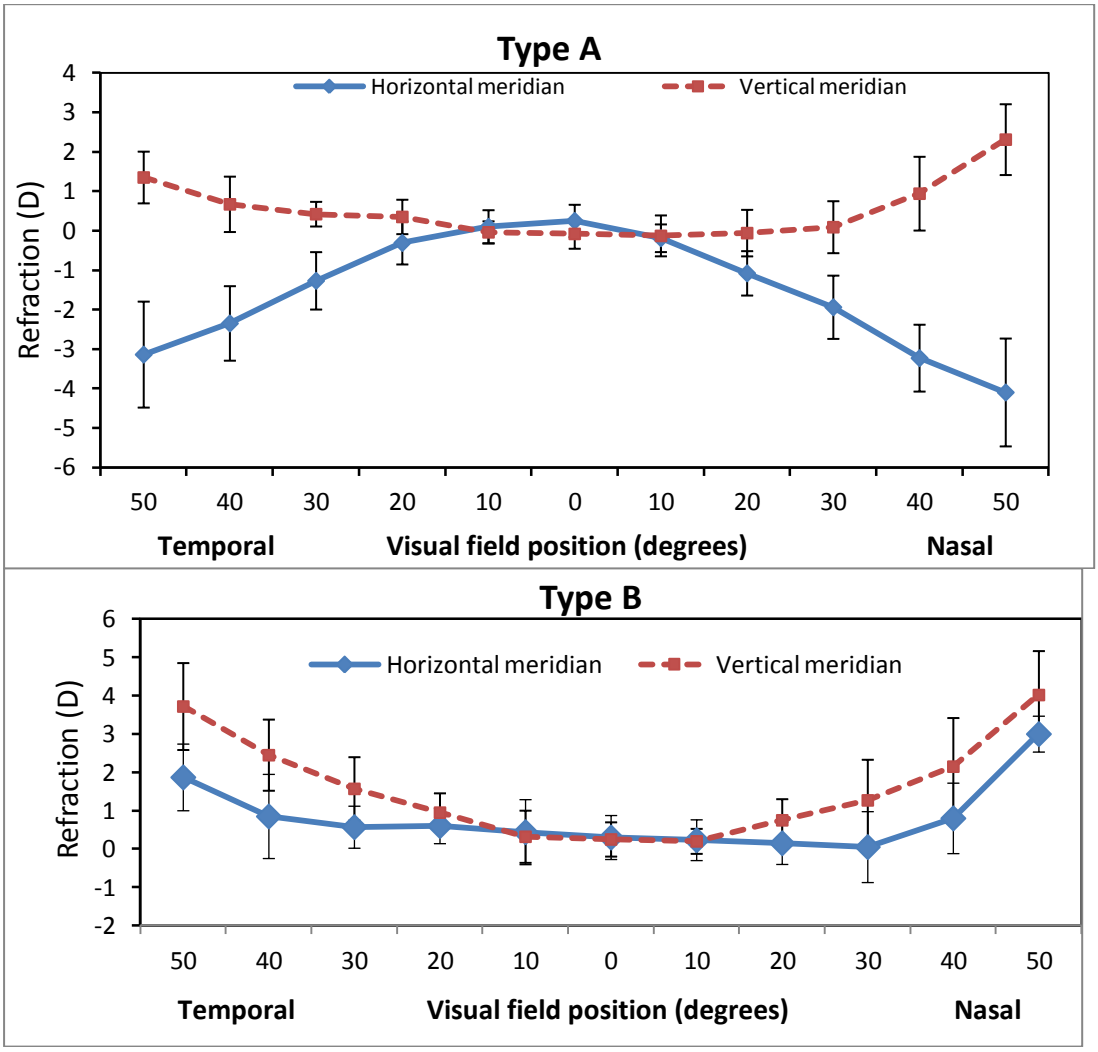

Figure 2:6: Average peripheral refractions along horizontal visual field of 6 eyes for type A and 5 eyes for type B, having only small central refractions, identified by Ferree et al. (1931). Error bars indicate standard deviations.

Ferree and Rand (1933a) related the peripheral refraction patterns to the likely shapes of eyes. They did not use the terms “relative peripheral myopia” or “relative peripheral hyperopia” as are now used, but their assertions were equivalent to suggesting that a prolate ellipsoid shape would increase the relative peripheral hyperopia or decrease the relative peripheral myopia. As should be apparent from Figure 2:1, changing from a spherical shape to oblate elliptical and prolate elliptical shapes, but without changing the vertex curvature, will result in shifts towards relative peripheral hyperopia and relative peripheral myopia, respectively. These are

in the opposite direction to Ferree and Rand's suggestions as they assumed that accompanying the change in asphericities would be a change in vertex curvature. This is made clear at only one point in the paper, when referring to an eye with a pattern of relative peripheral myopia, or "myopic astigmatism" because the nearly emmetropic eye has peripheral myopia in both principal meridians, they refer to "an eyeball flattened at the back, with a shape tending towards that of an oblate spheroid" (Ferree and Rand, 1933a). It is likely that Ferree and Rand did not consider that, accompanying differences in axial length and eye shape, eyes might have different equatorial dimensions as shown in the development of myopia according to the global model of myopia expansion. Figure 2:7 shows the effect of different shaped ellipsoids on peripheral refraction in which the equatorial diameter does not vary, but with variations in both vertex curvature and asphericity between the ellipsoids.

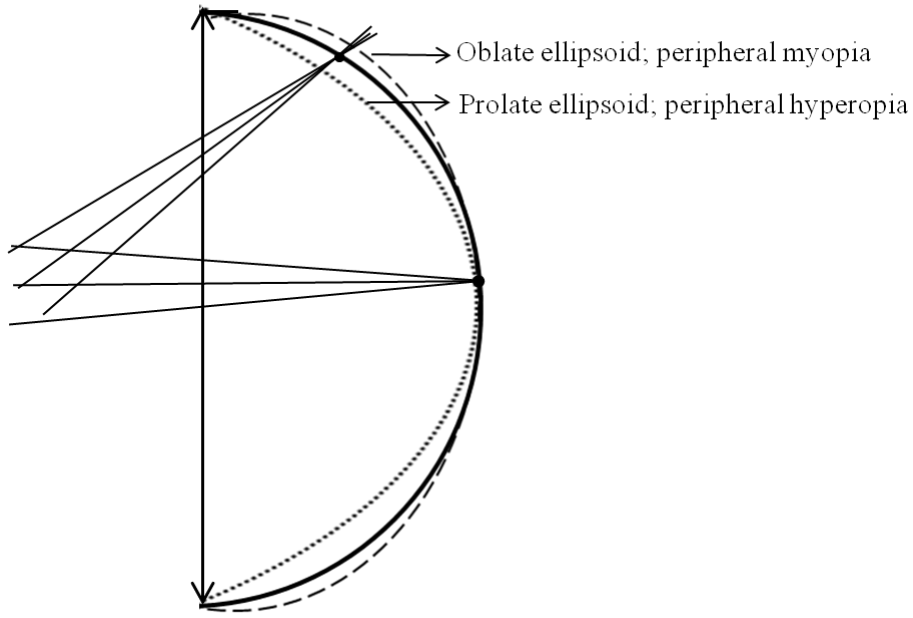

Figure 2:7: Effect of different shaped ellipsoids with constant equatorial diameter on peripheral refraction.

By considering the amount of peripheral astigmatism (the difference in refraction between the two principal meridians), Ferree and Rand inferred the power and length of the eye, considering that eyes with small degrees of peripheral astigmatism were likely to be longer and less powerful, and vice versa for eyes with higher degrees of peripheral astigmatism.

While others involved in peripheral refraction studies since then have been vague about what is eye shape, e.g. is it the retinal shape or an overall shape of the eye, Ferree and Rand (1933a) seemed to have in mind the shape of the retina: "Attention may be called to the following points: the possibility of determining roughly the conformation of the retina and the shape of the posterior half of the eyeball" (pages 937-938).

Rempt et al. (1971) investigated peripheral refraction in 442 young adults out to 60º along the horizontal visual field using retinoscopy. They described five patterns of peripheral refraction (types I to V), shown in stylistic pattern in Figure 2:8. There is a progression in pattern from type I, which is the same as type B identified by Ferree et al., to type II, type IV and type V, in which both horizontal meridian and vertical meridian refractions move in the myopic direction. Type III is an asymmetric pattern similar to Ferree et al.'s type C. The frequency of the patterns was related to the central refraction with 91/141 myopes having the type I pattern, 135/217 emmetropes and 61/84 hyperopes having the type IV pattern, and 17/34 cases of type V occurring for hyperopes.

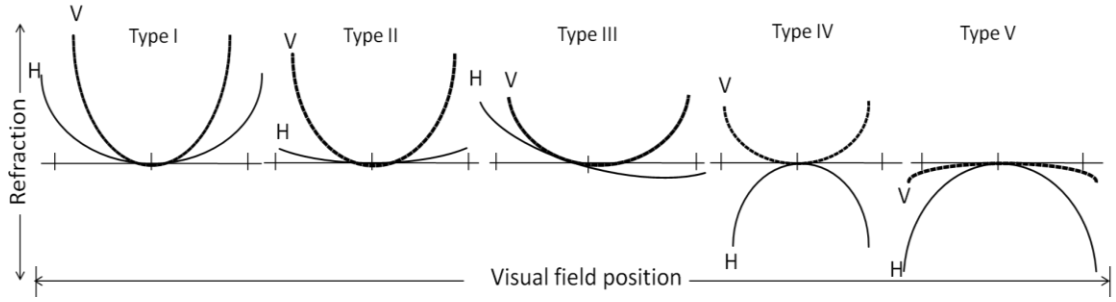

Figure 2:8: Five types (I- V) of skiagrams (peripheral refraction plots), described by Rempt et al. (1971). Type I, III and IV are similar to types B, C, and A, respectively, identified by Ferree et al. The curves are shown as parabolas, but real plots are seldom as regular.

The findings of Rempt et al. (1971) regarding the way in which peripheral refraction patterns change with central refraction have been supported and elaborated by numerous studies. Since this time, results have been shown as the mean refraction combined with a measure, or measures, of astigmatism. A summary of findings along the horizontal visual field is as follows:

1. There is considerable inter participant variation within members of the same group (eg within emmetropes), as occurs for the higher order aberrations.

2. Several studies have found emmetropic groups to have a weak relative peripheral myopia (Mutti et al., 2000, Atchison et al., 2006, Kang et al., 2010, Chen et al., 2010), although some have found a weak tendency in the hypermetropic direction on one or both sides of the visual field (Millodot, 1981). Myopic groups show relative peripheral hyperopia, (Millodot, 1981, Mutti et al., 2000, Atchison et al., 2006, Kang et al., 2010, Chen et al., 2010, Berntsen et al., 2010), which to some extent increases with increase in myopia (Atchison et al., 2006) and hypermetropic groups show relative peripheral myopia (Millodot, 1981, Atchison et al., 2005b). As noted by Charman and Radhakrishnan (2010), there is a tendency for the peripheral refractions of the different refraction groups to converge as field angles get larger and this will occur for the axial elongation model eye of Figure 2:3 (Charman and Jennings, 1982, Dunne et al., 1987).

3. Some participants shift from a relative peripheral myopic pattern to a relative peripheral hyperopic pattern at large angles eg > 45° (Mathur and Atchison, 2013)

4. Peripheral astigmatism decreases with increase in myopia (Atchison et al., 2006); possibly because of small numbers this has not been noted in many studies.

5. The turning point (minimum or maximum) of mean refraction or of regular (J_{180} or 90/°180°) astigmatism is usually a few degrees into the temporal visual field (Druault, 1900, Lotmar and Lotmar, 1974, Dunne et al., 1993) and decreases slowly with increase in myopia (Atchison et al., 2006). This is usually attributed to the angle alpha, the angle between the visual axis and the best fit optical axis at the nodal point; Atchison et al. (2006), but not Dunne et al. (1993), found a significant relationship between the turning point of astigmatism and angle alpha.

6. The oblique component of astigmatism (J_{45} or 45/°135° astigmatism), which was not investigated in most studies before 1981, is much smaller in the periphery than the J_{180} component and is linearly related to peripheral angle (Atchison et al., 2006).

7. Effects of age (Atchison et al., 2005b, Chen et al., 2010) and ethnicity are small (Kang et al., 2010)

8. The effects of accommodation are unclear: Walker and Mutti (2002) found a hyperopic shift in relative peripheral hyperopia upon accommodation. Calver et al. (2007) and Davies and Mallen (2009) found no effect of accommodation on relative peripheral refraction for both emmetropic or myopic groups, and Whatham et al. (2009) found a myopic shift in relative peripheral refraction in a group of myopic children (eg 0.74 D and 0.59 D at 40° temporal and nasal fields, respectively, with nearly 3 D increase in accommodation demand).

9. Manipulating refractive correction in the form of refractive surgery (Ma et al., 2005), orthokeratology (Cho et al., 2005, Charman et al., 2006, Queirós et al., 2010, Kang and Swarbrick, 2011, Santodomingo-Rubido et al., 2011, Kang and Swarbrick, 2013), special contact lenses (Sankaridurg et al., 2011, Ticak and Walline, 2013) and special spectacle lenses (Sankaridurg et al., 2010) has considerable and largely predictable effects on peripheral refraction.

Studies of peripheral refraction have been restricted mainly to the horizontal visual field, with some two dimensional studies measuring across small angles only e.g. 20-25° degrees from fixation (Seidemann et al., 2002, Mathur et al., 2009a). Atchison et al. (2006) measured along the vertical visual field to ±35° from fixation in a subset of 43 of their 116 participants and found different patterns than along the horizontal visual field. For emmetropes the relative peripheral myopia was greater along the vertical than in the horizontal visual field. With increase in myopia, there was little change in relative peripheral refraction. These findings have since been replicated (Berntsen et al., 2010, Chen et al., 2010). Atchison et al. found that the regular astigmatism was similar in vertical and horizontal fields, apart from a change in sign. In the vertical visual field the turning point of regular astigmatism was

≈(–)3° in the inferior field, without any dependence on central refraction. The oblique astigmatism changed at three times the rate with increasing angle along the vertical field than along the horizontal field, and this was attributed to angle alpha along the horizontal visual field.

Without any changes in the optics of the eye apart from the shape and position of the retinal surface, all models of retinal stretching predict, to various degrees, the trend of increasing relative peripheral hyperopia along the horizontal visual field with increase in myopia (Figure 2:5), but only the global stretching model comes close to predicting the relative lack of change of relative peripheral refraction along the vertical visual field.

Atchison (2006) modelled peripheral optics according to biometric measurements in 121 emmetropic and myopic young adults. The models showed increase in corneal curvature, increase in vitreous length, and change in retinal shape with increase in myopia. The retinal vertex radii of curvature and the retinal asphericities in XZ and YZ sections were given by

$$R_{xv}\ (\text{mm}) = -12.91 - 0.094SR$$

$$Q_x = +0.27 + 0.0026SR$$

$$R_{yv}\ (\text{mm}) = -12.72 + 0.004SR$$

$$Q_y = +0.25 + 0.0017SR$$

where *SR* is the spectacle refraction. The modelling predicted relative peripheral myopia in emmetropic eyes in both horizontal and vertical visual fields. Along the horizontal visual field, the modelling predicted slight increases in relative peripheral hyperopia with increase in myopia that were less than those of the experimental results of Atchison et al (2005b). Along the vertical visual field, the modelling predicted little change in refraction, compared with the relative peripheral myopia of the experimental results for a range of refractions (Figure 2:9).

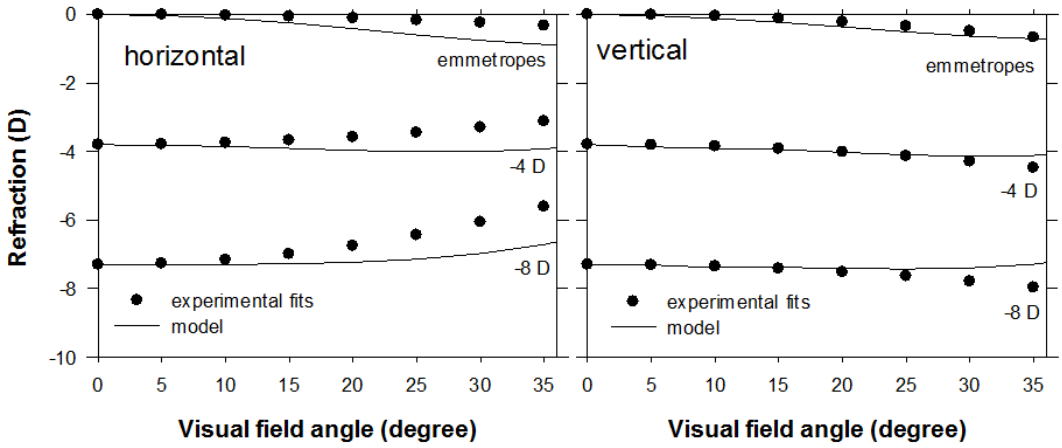

Figure 2:9: Mean refraction in a) horizontal and b) vertical visual fields, as a function of angle for measured data fits (Atchison et al., 2006) and theoretical data (Atchison, 2006) for emmetropia, 4 D myopia and 8 D myopia. For the experimental results, quadratic fitting coefficients are used. The quadratic fitting co-efficients along horizontal and vertical meridians are given by $H = -0.000206x - 0.000270$ and $V = -0.000048x - 0.000694$, respectively, where x is central refraction in dioptres, with units of D/degrees^2.

2.4.2.4 Relative peripheral refraction and progression of myopia

To determine whether emmetropes should be accepted for pilot training because of the risk that they would develop myopia, Hoogerheide et al. (1971) reported changes in peripheral refraction in 214 pilots and compared these with patterns of peripheral refraction.

The emmetropes and hyperopes who developed myopia was disproportionately represented by those with the type I refractive profile. 17/26 (65%) who developed myopia were of type I, while 118/121 (97%) who did not develop myopia were of type IV or type V. The proportions of each type that went on to develop myopia were 17/36 of type I (47%), 3/43 type II (7%), 3/14 type III (21%), 3/112 (3%) type IV, and 0/9 (0%) type V. Stone and Flitcroft (2004), and Wallman and Winawer (2004) drew attention to this work, beginning a period of interest that peripheral optics might influence development of myopia either through the peripheral refraction pattern or through the retinal shape.

It is generally understood that Hoogerheide et al. measured peripheral refraction before monitoring changes in central refraction, but recently and well after the commencement of this PhD study, it was explained that the peripheral refraction

was most likely measured after, rather than before, the pilots did or did not, develop myopia (Rosén et al., 2012). Thus, it is unlikely that the study provides evidence that peripheral refraction patterns are predictive of myopia development and progression.

Mutti et al. (2000) measured peripheral refraction at 30° in the nasal visual field in 820 children aged between 5 to 15 years. Following Ferree et al., they described ocular shape on the basis of relative peripheral refraction at this position. Relative peripheral hyperopia of +0.80 ± 1.29 D was measured in myopic children and interpreted as indicating prolate shape. Relative peripheral myopia of –0.41 ± 0.75 D was measured in emmetropic children and interpreted as indicating near spherical or oblate shape, and relative peripheral myopia of –1.09 ± 1.02 D was measured for hyperopic children and interpreted as indicating oblate shape. Since then, many studies have made inferences of shape based on peripheral refraction.

Mutti et al. followed their research cohort for a decade investigating peripheral refraction. Mutti et al. (2007) reported rapid changes in relative peripheral refraction in the myopic direction before the onset of myopia, although as noted by Charman and Radhakrishnan (2010) progression towards myopia began before relative peripheral refraction became markedly hypermetropic. However, their recent results (Mutti et al., 2011) suggest that relative peripheral hyperopia had little consistent influence on the risk of myopia onset, with a mean annual progression of myopia of −0.024 D per 1 D of relative peripheral hyperopia.

Sng et al. (2011) performed a one year longitudinal study on central and peripheral refraction along the horizontal visual field at ±15º and ±30º in Chinese Singaporean children aged 7 ± 3 years. At baseline, the peripheral refraction patterns in children who became or did not become myopic were similar. The children who were myopic at baseline or who became myopic had relative peripheral hyperopia at the follow up, while children who did not become myopic retained a relative peripheral myopia. Shifts in spherical equivalent refraction after 1 year in the 'became myopic group' were −1.51 ± 0.63 D at centre and −1.08 ± 0.70 D and −1.06 ± 0.64 D at temporal and nasal 30º visual field, respectively. Similar findings were reported recently by Lee and Cho (2013). These results indicate that relative peripheral hyperopia might not be an essential risk factor in development of myopia.

2.4.2.5 Advancements in instrumentation for peripheral refraction

Commercially available instruments measuring central refraction have been modified for peripheral refraction measurements. These modifications include the rotation of eye or head or the instrument itself for different angles. The latter is an advantage because it reduces the time required for data acquisition.

Tabernero and Schaeffel (2009a, b, 2011) introduced two versions of a device to measure the peripheral refraction using a scanning hot mirror with a custom-designed infrared photoretinoscope. A rectangular hot scanning mirror placed in front of eyes was rotated using two stepping motors (one translating, other rotating) to project the infrared light from the photoretinoscope into the eye at different horizontal angles. The second version gave 0.4° per step resolution, and enabled 225 points to be measured over a ± 45° field in about 4 seconds.

Jaeken et al. (2011) built a fast scanning peripheral Hartmann-Shack wave-front sensor that measured the off-axis wave-front aberrations out to ± 40º horizontal visual field in 1.8 seconds with an angular resolution of 1°. The subject has an open field of view without any moving elements in the line-of-sight and the head is kept in place by a head-chin rest. A motorised stage with a maximum speed of 90°/second rotated the scanning sensor at the centre of rotation in the pupil plane so that distance between the pupil plane of the eye and the sensor was maintained at all angles.

The "Eye Mapper" of Fedtke et al. (2011, 2012) uses the Shack Hartmann principle for measuring central and peripheral refractions of the eye. It consists of 33 stationary mirrors and one scanning mirror with 11 individual beam paths, allowing rapid peripheral refraction measurements in 10° steps across the visual field (−50° to +50°) within 0.45 seconds. It can be rotated to test different visual field meridians. Fedtke et al. compared the measurements between two contact lenses having different peripheral powers and showed the ability of the EyeMapper to detect the differences. They found good agreement with a conventional aberrometer and an auto-refractor for a model eye.

2.4.2.6 Animal studies related to peripheral retina

Results from animal experiments provide compelling evidence for the role of peripheral retina in the development of myopia (Smith et al., 2005, 2007, 2010, Smith, 2011, Huang et al., 2011). Smith et al. (2005) performed studies on infant (1 to 3 weeks) rhesus monkeys using ring diffusers that had either 4 or 8 mm central apertures to allow 24° or 37° of unrestricted central vision, respectively. Over about 14 weeks, these monkeys developed significantly less hyperopia/more myopia (+0.03 ± 2.39 D) than those of control monkeys (+2.39 ± 0.92 D). Ablating the central 10° diameter of the retina around the fovea in one eye of 7 treated infant monkeys did not alter the recovery from induced refractive errors when the diffusers were removed. This is supported by another study from the same group (Smith et al., 2007) that investigated whether an intact fovea is essential for normal emmetropization and for the development of form-deprivation myopia. They found that foveal ablation did not influence emmetropization in monkeys that were allowed unrestricted vision and did not prevent axial myopia in monkeys that wore a diffuser. Huang et al. (2011) found that form-deprivation altered central and peripheral refractions out to ± 45º along the horizontal meridian, but this was not influenced by foveal ablation.

Smith et al. (2010) assessed ocular shape using magnetic resonance imaging on 8 infant rhesus monkeys (3 weeks old) to determine the effect of optical defocus on refractive development. Wide-field, executive type bifocal lenses were edged and fitted in the goggles so that the transition between near and far segments of the lens was oriented vertically. The nasal and temporal segments of the lens had refractive powers of −3.00 D and 0.00 D, respectively, imposing −3.00 D hyperopic defocus in the nasal visual field alone. Myopia occurred in the nasal hemi-field with corresponding increased vitreous length in the temporal half of the globe. For 6 infants reared with full field monocular −3.00 D lenses, central myopia developed with symmetrical relative peripheral hyperopia and less oblate eye shapes. Similar results (opposite trend) were seen with +3.00 D myopic defocus (Smith et al., 2013).

These results suggest the importance of peripheral retina in the development of myopia. However, the recent findings mentioned in section 2.4.2.4 suggest, that in humans, the peripheral refraction pattern is largely a consequence of, rather than a determinant of myopia. Given that both the eye's optics and the retinal shape contribute to the peripheral refraction, it is possible that the retinal shape, possibly

through biomechanical factors, might be a determinant for the development of myopia rather than peripheral refraction.

2.4.2.7 Interventions to correct myopia

Most theories and investigations of myopia development have been concerned with the growth response to defocus signals corresponding to foveal vision, but Wallman and Winawer (2004) indicated that the defocus signal at periphery should be stronger than the centre simply because there are more neurons in the retinal periphery, and that relative peripheral hyperopia at the periphery may stimulate the eye to grow even if the eye is myopic at the centre. As reviewed by Norton and Siegwart (1995), data from several species suggest that axial length is regulated within the eye itself and involves direct communication from the retina to the sclera.

Peripheral refraction with conventional single vision spectacles

Conventional single vision lenses were identified to cause significant increase in relative peripheral hyperopia in moderate or high myopes along the horizontal visual field (Lin et al., 2010, Backhouse et al., 2012, Kang et al., 2012). Figure 2:10 shows a possible schema of central and peripheral refraction leading to an increase in myopia. Figure 2:10a shows peripheral hyperopic defocus in an emmetropic eye which might stimulate the ocular growth and cause myopia as shown in Figure 2:10b (dashed line). Correction with single vision lens places the peripheral image behind the retina again (Figure 2:10c) which might stimulate yet further growth of the eye.

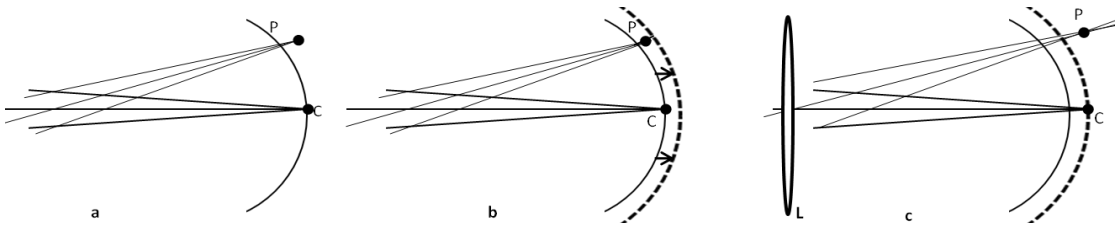

Figure 2:10: Possible scenario for the development of myopia: (a) peripheral focus P behind steep retina in an emmetropic eye with central focus at C, (b) growth of eye to become myopic (c) spectacle correction L causes the peripheral focus P to again be behind the retina and repeat the cycle. Based on Atchison et al. (2005a).

Development of new therapeutic anti-myopia lenses

'Anti-myopia' lenses are available to counteract relative peripheral hyperopia with the intention of slowing ocular elongation. They contain a central zone for the correction of central myopia surrounded by a peripheral therapeutic zone to slow the eye growth (Martinez et al., 2011). The commercial anti-myopia lens types in Asia are the ''Myovision'' lenses (Zeiss) and the "Myopilux Pro" (Essilor) varifocal design lenses (Elliott, 2011).

Numerous studies have investigated the effect of both bifocal and multifocal spectacle lenses on myopic progression in children (Cheng et al., 2011). Bifocal and progressive addition lenses slow the axial elongation of eye compared to single vision lenses, thereby reducing the progression of myopia (Leung and Brown, 1999, Gwiazda et al., 2003, Hasebe et al., 2008, Cheng et al., 2010).

Sankaridurg et al. (2010) performed a clinical trial in 201 myopic children using 3 types (I, II and III) of anti-myopia lenses manufactured by Carl Zeiss Vision designed to reduce relative peripheral hyperopia. Lens type I was a rotationally symmetrical design with a 20 mm clear central diameter surrounded by a progressively increasing positive power with a maximum spherical equivalent of +1.00 D relative peripheral power. Lens type II was a rotationally symmetrical design, with 14 mm clear central diameter with a more steeply ramped zone of increasing positive power than type I. A maximum spherical equivalent of +2.00 D relative peripheral power was achieved 25 mm from its centre. Lens type III was an asymmetric design with a clear aperture of 10 mm either side of centre horizontally and 10 mm inferiorly providing clear vision during convergence and down gaze. The design was optimised to reduce the astigmatism in the horizontal meridian while attaining a positive additional peripheral power of 1.90 D 25 mm from centre. A lens type IV was a conventional single vision design included as a control. After one year of wearing period no significance differences were found in rate of progression between anti-myopia lens wearing children and the control children. However, a small but significant reduction in myopia progression was noticed with type III lenses in a subgroup containing younger participants with a parental history of myopia.

A related study was performed by the same group in 45 Chinese children aged 7 to 14 years using contact lenses (CIBA VISION) that reduced relative peripheral hyperopia (Sankaridurg et al., 2011). The 9 mm treatment zone had a clear central zone of 1.5 mm semi-chord, followed by a zone of progressively increasing power of lens to reach a relative positive power of +1.00 D at 2 mm semi-chord and +2.00 D at the edge.

The relative peripheral refraction measurements at 20º, 30º and 40º in nasal and temporal visual fields and central axial length were compared to those of a standard spectacles wearing group after 1 year of treatment. The contact lenses produced greater reduction in the peripheral refraction in nasal field than the temporal field. Greater relative peripheral hyperopia was associated with greater progression of central myopia. They found 34% less progression of myopia in the contact lens group than the spectacle group after 1 year (−0.84 ± 0.47 D Vs. −0.54 ± 0.37 D) with axial length changes of 0.24 ± 0.17 mm for the contact lens group and 0.39 ± 0.19 mm for the spectacle group indicating considerable, predictable effects on peripheral refraction.

2.4.2.8 Measurements of eye shape

The eye is situated inside an orbit composed of seven bones. Although the eye occupies only about one-fifth of the adult human orbit (Schultz, 1940, Bron et al., 1997), it is possible that the size and morphology of the orbit may have a role in ocular growth during emmetropization. However, Chau et al. (2004) failed to show a significant relationship between eye size and orbital volume, and Cummings et al. (2012) indicated that there was an association between eye growth during the pre-natal stage but not post-natally.

The majority of the myopia imaging studies assessed the eye shape rather than retinal shape. Eye shape can be investigated by imaging techniques such as X-rays and computerized tomography (Deller et al., 1947, Zhou et al., 1998, Song et al., 2007), ultrasonography (Vohra and Good, 2000, Fledelius and Goldschmidt, 2010) and magnetic resonance imaging (Chen et al., 1992, Cheng et al., 1992, Miller et al., 2004, Atchison et al., 2004, 2005a, Singh et al., 2006, Moriyama et al., 2011, Lim et al., 2011, Ishii et al., 2011, Lim et al., 2013). The results from several studies of eye

shape are given in Table 2.2. The mean increases in axial length with increase in myopia for adult eyes are 0.33 mm/D and 0.35 mm/D according to Deller et al. (1947) and Atchison et al. (2004), which are in good agreement with studies of axial length in adults using other methods. Eye shape in these studies was mainly a comparison of one or both of height H and width W of the eye with the length L. The dimensions were not measured consistently across studies, for example some studies use the outer eye while others use the inner retina, but this does not affect the rate at which dimensions change with alteration in refraction. The results are expressed in different ways, but apart from Cheng et al. (1992) the studies found greater increase in length than in height and/or width with increase in myopia. Deller et al. (1947) found changes in L, H and W with changes in refraction in the approximate ratio 2:1:1, while Atchison et al. (2004) obtained the ratio 3:2:1 (in the midst of considerable intersubject variation). Two studies found no significant differences between eye shapes in emmetropia and hyperopia, but hyperopia was small in one study (Deller et al., 1947) and its range was not specified in the other (Zhou et al., 1998).

Some studies referred to the eye shape in terms of ellipsoids, using prolate and oblate to describe the situation where the ratio L/H (or/and L/W) is greater than and less than one, respectively (Singh et al., 2006, Moriyama et al., 2011, Lim et al., 2011), whereas Zhou et al. (1998) used the terms "long oval-shaped" and "cross oval-shaped" and Moriyama et al. (2011) used the terms "cylindrical" and "barrel". Using R_x, R_y and R_z instead of W, H and L and using equations (2), (3) and (6) shows that these ratios are just the eccentricities e for prolate ellipses. Ishii et al. (2011) considered that the use of a single metric was insufficient to describe eye shape and proposed the use of "elliptic Fourier" descriptors. Two of these, "width expansion" and "posterior length" terms, were strongly correlated with the L/H ratio and seemed to give useful information, although it is doubtful that these are any more suitable than providing the lengths.

Atchison et al. (2004) considered that approximately a quarter of their myopic participants fitted each of the global expansion and axial elongation models, described in Figure 2:3, exclusively. When considering height, the proportions shifted slightly in favour of the global expansion model (30% v. 26%) and while

considering width, the proportions shifted in favour of the axial elongation model (18% vs. 47%).

Measurements of retinal shape

Retinal shape can be determined by the methods mentioned in the previous section, e.g. magnetic resonance imaging (Chen et al., 1992, Atchison et al., 2005a, Gilmartin et al., 2011, Gilmartin et al., 2013). It can also be determined by indirect optical methods that are based on peripheral refraction (Dunne et al., 1987, 1995, Logan et al., 2004) and partial coherence interferometry (Schmid, 2003a, 2003b, 2011, Mallen and Kashyap, 2007, Atchison and Charman, 2011, Ehsaei et al., 2012, Faria-Ribeiro et al., 2013, Ding et al., 2013). Results using these techniques are summarised in Table 2.2.

Magnetic resonance imaging (MRI) is probably the best way of assessing retinal shape (Atchison et al., 2005a). MRI is superior to computerized x-ray tomography in terms of image quality but has disadvantages of high cost ($500/scan), long testing time (2-3 mins/image) and low resolution (approximately 0.15 mm) (Duong, 2011) and hence magnetic resonance imaging is not used extensively in research.

Following their 2004 paper, Atchison et al. (2005a) described retinal shape as asymmetric, decentred and tilted ellipsoids using equation (1). An example of this analysis is given in Figure 2:11. The mean ellipsoid of emmetropes had an oblate retinal shape (steepening towards equator) with greater width and height than length (R_z =10.04 ± 0.49 mm, R_x =11.40 ± 0.47 mm, R_y =11.18 ± 0.50 mm). With increase in myopia, the retinas became less oblate with more elongation in length (0.16 mm/D) than in height (0.09 mm/D) and width (0.04 mm/D), but few myopes had retinal shapes that were prolate. There was significant increase in vertex curvature with myopia (0.64 m^{-1}/D) along the horizontal plane, but not along the vertical plane. Fitting equations were:

$$c_{xv}\ (mm^{-1}) = -77.639 + 0.636SR$$

$$Q_x = +0.279 + 0.028SR$$

$$c_{yv}\ (mm^{-1}) = -78.691 - 0.019SR$$

$Q_y = +0.258 + 0.018SR$

where *SR* is the spectacle refraction. Also of note is that the mean retinal ellipsoid was tilted by 11.5° degrees about the vertical axis towards the nose, the retina vertex was decentred relative to the visual axis by $x = -2.28 + 0.055\ SR$ (to the nasal side) and there was an "anterior segment" from the anterior cornea to the front of the ellipsoids of approximately 3.0 mm that was not affected by refraction.

Similar to Atchison et al. (2005a), Gilmartin et al.'s MRI study (2013) found oblate retinal shapes in both myopes and emmetropes and with myopes having less oblateness. They proposed that a spherical retinal shape may act as a biomechanical limitation to further myopic axial elongation.

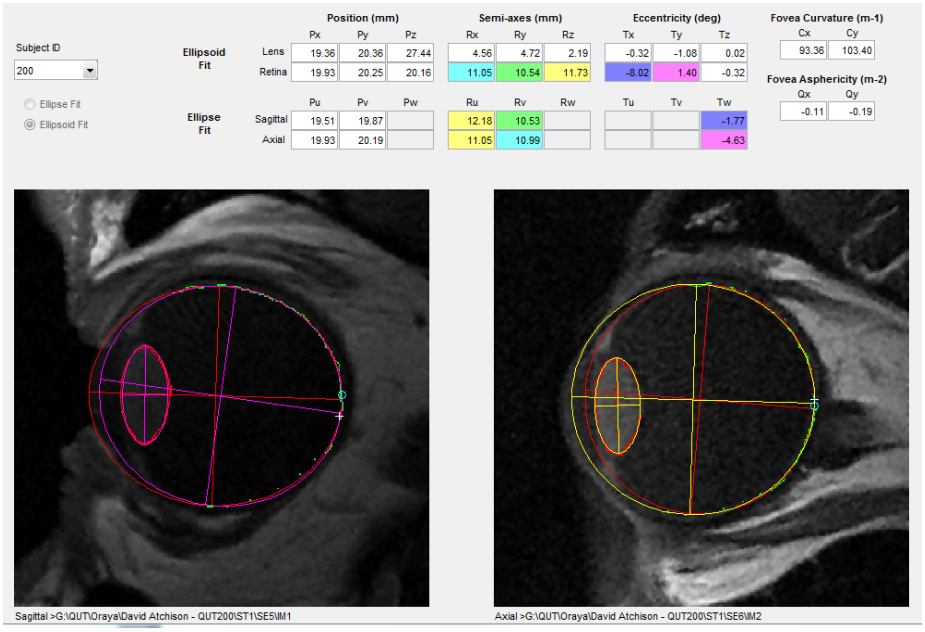

Figure 2:11: Processing of sagittal (left) and transverse axial (right) magnetic resonance images for one subject with –2.5 D refraction. Note that this subject has negative retinal asphericities, unlike most participants in the Atchison et al. (2005a) study.

Dunne's method

Dunne (1987, 1995) developed an algorithm to determine the retinal shape. Model eyes were generated, using a method devised by Bennett (1988) and modified by Royston et al. (1989), comprising a corneal surface, two lens surfaces and the retina, using measurements of corneal curvature, lens thickness, anterior chamber

depth, vitreous depth, and peripheral refraction. In this method, the curvatures of the lens surfaces are selected so that the ratio of the surface curvatures matches those of the lens in the Gullstrand-Emsley model eye. Dunne determined theoretical peripheral refractions at each field angle using sagittal and tangential ray-tracing (see section 2.4.2.2). The corneal surface was treated as an ellipse and its asphericity was adjusted so that the calculated peripheral astigmatism matched the measured peripheral astigmatism at any field angle. The retinal curvature was altered until the theoretical sagittal refraction matched the measured sagittal refraction. When this procedure was completed for a number of positions, the retinal shape was estimated by fitting an ellipse.

Logan et al. (2004) used Dunne's method to estimate the retinal shape in the transverse axial section of eyes for white and Chinese isomyopes and anisomyopes. They measured the ratio of the transverse chord diameter of the retina, at the maximum angles tested, to the axial length. This was found to be smaller in the more myopic eye of anisomyopes, and for right eyes, to become smaller as myopia increased in the Chinese eyes only. Reduction in the ratio was interpreted as a more prolate shape of the retina, but this parameter requires further investigation.

Partial coherence interferometry

Partial coherence interferometry compares the optical path lengths of two beams, one of which is reflected from the cornea and the other which travels into the eye and gets reflected at one of the surfaces. Because the source (diode laser or super luminescent diode) has a wide bandwidth of wavelengths compared with a laser, and consequentially a short coherence length, a strong interference signal occurs only when the optical path lengths are similar rather than when optical path lengths differ by multiples of wavelengths. One commercial instrument, the Carl Zeiss IOLMaster, provides only the total axial length (anterior chamber depth is provided by an optical method) while the newer Haag-Streit Lenstar provides internal lengths. The IOLMaster uses a single index within the eye (1.3549), but Haag-Streit does not indicate what is done for the Lenstar. Partial coherence interferometry is now used to obtain both on and off axis optical lengths. Unlike ultrasound it is non invasive, and measurements are quicker and more repeatable. PCI provides better resolution, 0.01

to 0.02 mm than ultrasound (0.10 mm) and MRI (0.15 mm) (Kimura et al., 2007, Lam et al., 2001).

Schmid (2003a, 2003b, 2011) developed his own partial coherence interferometer. He measured corneal to retinal lengths both axially and in the periphery at a maximum of 20° from fixation and gave a measure of retinal steepness by subtracting the central length from the peripheral length (relative peripheral eye length, *RPEL* = peripheral *EL* – central *EL*), with the interpretation that the more negative the *RPEL*, the steeper the retina. Because of the small angles used, this is probably a measure of foveal radius of curvature and surface tilt. *RPEL* was more negative ("steeper") for myopic than for emmetropic and hypermetropic children (Schmid, 2003a, 2003b), and myopic shifts over two years correlated significantly with *RPEL* at 20° nasal field with steeper retinas accompanied by more myopic shifts than flatter retinas (Schmid, 2011).

Mallen and Kashyap (2007) used the IOLMaster with an external attachment containing a beam-splitter, goniometer and a Maltese cross target that allowed the measurements of peripheral eye lengths. With similar attachments, Ehsaei et al. (2012) and Faria-Ribeiro et al. (2013) found more negative *RPEL* and naso-temporal asymmetry of *RPEL* in myopes (progressing myopes > non progressing myopes) than in emmetropes. Two studies found a correlation between *RPEL* and relative peripheral refraction (more negative *RPEL* with more relative peripheral hyperopia) in the horizontal visual field (Faria-Ribeiro et al., 2013, Orr et al., 2013). This method could be extended to giving estimates of vertex radius of curvature and asphericity.

The optical methods might have inaccuracies unless compensation is made for the deviation of off axis beams within the eye (the bending of light within the eye). As it has been applied to determining retinal shape, partial coherence interferometry suffers from optical distortions. Firstly, little account has been taken of the different refractive indices in the eye's media; as mentioned earlier the IOLMaster uses a constant refractive index to convert from optical path lengths to distances, and it is not clear what procedure is used by the Haag-Streit Lenstar. Secondly, no allowance has been made for deviation of beams inside the eye.

Theoretical investigations of the partial coherence interferometry technique indicated that it can give reasonably accurate results for retinal shape (Atchison and

Charman, 2011, Cameron et al., 2013). An improved method would make allowance for deviation of beams inside the eye using other biometric parameters (e.g. corneal topography, internal distances, lens surfaces from Scheimpflug photography or phakometry and lens gradient index from magnetic resonance imaging) and should be verified by a direct technique such as magnetic resonance imaging.

Table 2.2 Summary of studies of eye shape and retinal shape

Authors	Technique	Procedure	Participants	Results	Distances measured*
Deller et al. (1947) #	Radiography from X-rays – subjective responses	Slit beam transversed the eye perpendicular to the dimension measured. Exposure marked on film	11 Hyp, 19 E, 15 My Adults	E : similar *L, H, W*; Hyp similar *L, H, W* As My↑, increase in *L, H, W* in approx ratio 2:1:1	
Vohra & Good (2000) #	B-scan ultrasonography	Transverse axial	100 eyes classified by axial length. Most high My	ΔL:ΔW > 3	
Fledelius & Goldschmidt (2010) #	B-scan ultrasonography	Transverse axial	61 eyes/31 unilateral and bilateral high My > 50 years	"Regular" and "irregular" shapes Mean *L*/*W* 1.07 – range 0.92 to 1.36 Irregular shaped eyes had highest My and high *L*/*W*	
Zhou et al. (1998) #	Computerized X-ray tomography	Transverse axial section	33 Hyp, 76 E, 141 My (255 eyes/131 adults)	*L*/*W* for My > *L*/*W* for E > *L*/*W* for Hyp *L*/*W* ↑ as My↑	Not clear. *L* measured through optic nerve
Song et al. (2007) #	Computerized x-Ray tomography	Transverse axial and coronal sections	406 eyes/354 children < 20 years	Emmetropes similar *L, H, W* Myopia AL > *H, W*	*L* from posterior cornea
Cheng et al. (1992) #	Magnetic resonance imaging	Eye coil, transverse axial and coronal sections	8 Hyp, 6 E, 7 My	*W* > *L, H* Little change in shape with refraction	Outer dimensions
Chen et al. (1992) $	magnetic resonance imaging	Eye coil, transverse axial and coronal sections	3 Hyp, 4E, 4 My	Posterior retina more prolate in shape for My than E and Hyp in transverse axial section	
Miller et al. (2004) #	magnetic resonance imaging	Transverse axial section	9 Hyp, 32 E, 37 My	As My↑, ΔL > ΔW	

Atchison et al. (2004) #	magnetic resonance imaging	Eye coil, transverse axial and sagittal sections	22 E, 66 My young adults	As My↑, increase in *L, H, W* in approx ratio 3: 2: 1	
Atchison et al. (2005a) $	magnetic resonance imaging	Per Atchison et al. 2004 Retina shape determined from posterior 240°. 3D shapes obtained from sections, with rotations, decentration and asymmetry	Per Atchison et al. 2004	As My↑, increase in *L, H, W* of posterior retina in approx ratio 3: 2: 1 Oblate shape retinas in most eyes, but less so as My↑ Steepening of vertex curvature in transverse axial section, but not sagittal section	
Singh et al. (2006) $	magnetic resonance imaging	Head coil 3D images determined from 2D transverse axial images Ocular shape described qualitatively by colour coding	7 young adults with a range of refractions	Considerable variations in eye shape between participants of similar refractive errors.	
Moriyama et al. (2011) #	magnetic resonance imaging	Head coil Section not stated 3D images determined from series of 2D slices	20 E, 8 unilateral high myopes, 36 bilateral high myopes	Posterior staphyloma in several high myopic participants. Some had exaggerated posterior retinal oblate shapes (termed "barrel") and others had pronounced prolate shapes (termed "cylindrical")	Outer dimensions
Lim et al. (2011) #	magnetic resonance imaging	Head coil 3D images determined from series of 2D transverse axial slices	134 eyes/67 6 year old Singaporean Chinese boys	For non-My, as refraction less hyperopic: *L*↑, *H*↑, *W*↑ (unadjusted for height) For My, as My↑: *L*↑ but no change *H, W* (unadjusted for height). Conclusion: My eyes axially elongated	Outer dimensions
Ishii et al. (2011) #	magnetic resonance imaging	Head coil 3D images determined from 2D transverse axial images. Analysis of horizontal section Shape given by "Elliptic Fourier" descriptors	105 children, 1 month to 19 years old	"Width expansion" term PC1 strongly positively correlated with "oblateness" given by 1 –*L* / (2**W*) and with spherical equivalent refraction. "posterior length term" PC2 negatively correlated with oblateness Summary: Hard to made firm conclusion with regards eye shape and refraction as confounding effect of age	*L* measured from post corneal
Gilmartin et al. (2011) #$	magnetic resonance imaging	Head coil 3D images Determined semi-distances	31 E, 35 My young adults	Most retinas have oblate shapes, but less so for My than for E At half axial length, (*H* for My)/(*H* for E) = 1.02 and	

		from visual axis at 17%, 52.5% and 72.50% of axial length		(*W* for My)/(*W* for E) = 1.01 Above results suggest predominately axial expansion in both horizontal and vertical meridians	
Lim et al. (2013) #	magnetic resonance imaging	Head coil 3D images determined from 2D transverse axial slices Eye shape was assessed qualitatively from 3D models, and quantitatively from *L, W, H*	346 eyes of 173 newborn children (5 to 17 days)	Oblateness was calculated as 1 _ (AL/width) or 1 _ (AL/height) 294 eyes, 85% and 163 eyes, 47% had prolate eye shape using width and height, respectively.	*L* measured from post corneal
Gilmartin et al. (2013) $	magnetic resonance imaging	Head coil Transverse axial, sagittal and coronal sections	27 E, 28 My	Oblate shape of vitreous in most eyes, but less so as My↑	
Logan et al (2004) $	Dunne's method (1995)	Transverse axial section Peripheral refraction to ±35° Transverse chord diameter *TCD* (width at maximum angles) compared with *L*	56 isometropes and anisomyopes (> 2 D), white and Taiwanese-Chinese	*TCD*/*L* smaller in the more My eye *TCD*/*L*↓ as My↑ in Chinese eyes only Smaller *TCD*/*L* interpreted as more prolate shape	
Schmid (2003 a, b) $	partial coherence interferometry	Retinal steepness based on comparing lengths along different meridians to ±20°. *RPEL* = peripheral *L* – central *L*, steeper as more negative	23 Hyp, 23 E, 17 My 7-15 years	*RPEL* steeper in My than E, Hyp *RPEL* significantly related to refractive error group at 15° nasal and superior visual fields	
Schmid (2011) $	partial coherence interferometry	Retinal steepness per Schmid 2003a,b	140 7-11 year children, 92 available at two year follow-up	Myopic shifts over two years correlated significantly with *RPEL* at 20° nasal field (steeper retinas give more myopic shift)	
Mallen & Kashyap (2007) $	partial coherence interferometry	Modification of commercial instrument, *PEL*s measured by using	1 E and 2 My	Retinal asymmetry Evidence of temporal-nasal retinal asymmetry	

		external setup for showing targets Horizontal and vertical fields to ±40°			
Atchison & Charman (2011) $	partial coherence interferometry	Theoretical		In model eyes, reasonably accurate measure of retinal shape when incident beam normal to cornea without taking into account light bending within eye.	
Ehsaei et al. (2012) $	partial coherence interferometry	Modification of commercial instrument, PELs measured by using external setup for showing targets Horizontal and vertical fields to ±30°	27 E and 52 My	*RPEL* steeper (more negative) in My than E temporal-nasal retinal asymmetry greater in My than E	
Faria-Ribero et al. (2013) $	partial coherence interferometry	PELs measured by using external setup for showing targets Horizontal fields out to ±30°	30 non progressing My 32 Progressing My	*RPEL* steeper (more negative) in progressing My than in non progressing My Steeper *RPEL* associated with more relative peripheral hyperopia	
(Ding et al., 2013) $	partial coherence interferometry	PELs measured by using paper strips that were placed on lateral apertures if instrument Only at ±40° horizontal field	104 Monozygotic (27 E, 61 My) and 54 Dizygotic adolescent twin pairs (10 E, 27 My)	Suggests influence of genetics on *PEL* and *RPEL* Temporal-nasal retinal asymmetry in both Mono and Dizygotic twins	

Most technical details omitted. It is understood that *L* for My> *L* for E > *L* for *H*, as is found for all relevant studies and this is not covered

*Information included if length is not anterior cornea to inner retina or height and width are not measured between inner retinas

eye shape; $ retinal shape, E - emmetropes, My - myopes, Hyp – hyperopes; *L* - length, *H* - height, *W* – width; ↑ increases; ↓ decreases

2.5 RATIONALE OF THE STUDY

Studies of peripheral refraction and the retinal shape suggest that the peripheral retina may be important for myopia onset and progression. This literature review has described how patterns of retinal expansion during the development of myopia contribute to changing patterns of peripheral refraction, and how the pre-existing retinal shape might be a contributor to the development of myopia.

Retinal shape can be confused with the more nebulous concept of eye shape. As an example, an eye shape may be described as prolate because the length is longer than the width and/or height, but the corresponding retinal shape might be oblate. It is important to emphasise that eye shape and retinal shape are not the same and merely describing an eye shape as being prolate or oblate is insufficient without some understanding of the parameters contributing to this. Retinal shape has been measured independent of optical methods using magnetic resonance imaging. This is expensive, available mainly in hospitals and takes considerable time. Although indirect or optical methods are fast and cheap, their accuracy is not understood. Partial coherence interferometry has been used to determine retinal shape but there are some assumptions in its use, such as refractive index used to convert from optical path lengths to distances, and deviation of beams inside the eye, and it has not been assessed for accuracy against magnetic resonance imaging. For further work on retinal shape, determining the validity of these alternatives to magnetic resonance techniques is required.

This study refines and evaluates a simple method of determining retinal shape in terms of ellipsoids using off-axis partial coherence interferometry (PCI) and validates this method by comparing the data with magnetic resonance imaging. In this research project the simple PCI method will be used to measure retinal shape in different population groups, with varying refractive errors, and in isomyopes and anisomyopes for whom presumably the confounding influence of differences in genetic background and environmental influences are avoided. I will contribute an important assessment device with applications for understanding myopia development risk and likely optical treatment effectiveness that will benefit to people at risk of myopia development.

Chapter 3- Research Design and Pilot Studies

This chapter includes the information about ethics approval, inclusion/exclusion criteria, statistics analysis, preliminary pilot experiments and various instruments/techniques/protocols used for estimation of retinal shape.

3.1 ETHICS

This research involved 'low risk' experiments. According to the Queensland University of Technology Ethical Conduct in Human Research guidelines, research is 'low risk' where the only foreseeable risk is one of discomfort, which can involve body and/or mind. All instruments used in the experiments were non-contact. Appropriate training, assessment, and inductions were undertaken at the Institute of Health and Biomedical Innovation. A health and safety research risk assessment was carried out as part of the ethics application. The study followed the tenets of the declaration of Helsinki and was approved by the Human Research Ethics Committee of the Queensland University of Technology (1100001176) and the University of Queensland (2012000175). The nature of experimental procedures was explained to participants and written informed consent was obtained before taking measurements (Appendix 1).

3.2 INCLUSION AND EXCLUSION CRITERIA

Criteria for the assessment of participant eligibility were same for all main experiments and were assessed using routine clinical tests. Tests included eye and general history, visual acuity measurement under normal room illumination with Bailey-Lovie LogMAR visual acuity chart, refraction, slit lamp biomicroscopy, tonometry and undilated fundus examination. To minimise a potential confounding effect of age, the age of participants was limited to 18 to 30 years. Participants had best corrected visual acuity better than or equal to 6/6 (LogMAR 0.0) with astigmatism $\leq \pm 1.50$ D. Myopes had stable refractions based on their reports of

having unchanged spectacle prescriptions in the previous two years. To assess the risk of angle closure glaucoma following pupil dilation, intraocular pressure and the depth of anterior chamber periphery were measured. Only participants with no to negligible risk were included, i.e. intraocular pressure was limited to ≤ 21 mm Hg and anterior chamber depth to ≥ Grade 3 (Van Herrick's grading system). Individuals having any evidence or previous history of any ocular disease were excluded from participation.

3.3 PARTICIPANTS

Based on the research aims, the project had three main experiments. A total of 108 healthy young adults aged 18-30 years (mean ± SD: 23.8 ± 3.6 years, range 18 to 30 years) were recruited. The distributions of participants for the three experiments were:

- Experiment 1 (chapter 4): Validation of partial coherence interferometry for estimating retinal shape (n=58)
- Experiment 2 (chapter 5): Retinal shape in different racial groups (n=94)
- Experiment 3 (chapter 6): Retinal shape in iso- and aniso-myopes (n=21)

All participants who were in Experiment 1 were included in Experiment 2 and a subset from Experiments 1 and 2 participated in Experiment 3.

Only right eyes were tested in Experiments 1 and 2, whereas data from both eyes of participants were used in Experiment 3.

Forty percent (n = 42) of the participants were males and sixty percent (n = 64) were females. All participants (50 emmetropes and 56 myopes) were university students based in Queensland and their spherical equivalent refraction ranged from +0.75 to –8.15 D (mean ± SD: –1.77 ± 2.17 D). Myopia was defined as a spherical equivalent refraction (M) of ≤ −0.75 D and emmetropia as > −0.75 D to +0.75 D. Further specific information regarding participant characteristics for each experiment is described in the relevant chapters.

Two pilot experiments (sections 3.5.5.2 and 3.5.5.3) involved a small number of participants, some of whom were not involved in the main experiments.

3.4 STATISTICAL ANALYSIS

Data analysis was performed with SigmaPlot Version 12 (Systat Software, San Jose, CA) and IBM SPSS Statistics Version 21 (IBM SPSS Statistics, Armonk, NY). Statistical significance was set at $p < 0.05$.

Parametric tests were performed to determine the statistical significance of results between the groups (Student independent t test for two independent groups and paired t test for two different groups). SigmaPlot software checked automatically for the normality of the data by applying the Shapiro-Wilk test, and whenever data were not normally distributed the Wilcoxon Signed Rank Test was used.

Analysis of Variance (ANOVA) was performed to determine the differences in results when multiple parameters had to be considered such as race, refraction and visual field meridian. As applicable, post-hoc t-tests with Bonferroni correction were used to determine the significance of differences between races (East Asians, Caucasians and South Asians).

Bland-Altman plots were used to determine the agreement between two methods or conditions. Bland-Altman analysis provides an XY scatter plot in which the difference of the methods/conditions is on the Y-axis and the average of the two methods is on the X-axis. The mean of the differences and its 95% Limits of Agreement (LoA) were used to interpret the agreement.

Simple linear regressions were applied to find the association between spherical equivalent refraction and various parameters such as equivalent refractive index, lens surface radius of curvature, the highest order-coefficients of peripheral refraction component fits, relative peripheral eye lengths and retinal shape estimates. Analysis of covariance (ANCOVA) was performed to test the significance of slopes between races and between isomyopes and anisomyopes.

3.5 INSTRUMENTS AND TECHNIQUES

Standard clinical techniques included corneal topography with Medmont E300 and Oculus Pentacam, complete axial length and other axial intraocular length measurements of corneal thickness, anterior chamber depth and lens thickness (Pentacam, Lenstar). Specialised techniques included phakometry (custom-built instrument), peripheral refraction (Shin-Nippon SRW 5000 auto-refractor) and peripheral eye lengths (Lenstar). A subset of participants underwent magnetic resonance imaging (MRI).

3.5.1 VIDEOKERATOSCOPE

The Medmont E300 (Figure 3:1) is a computer-assisted videokeratoscope that works on the Placido-disk principle, providing topographical information from the anterior corneal surface. It quantifies corneal topography through analysing the corneal reflection of 32-Placido rings illuminated by red light-emitting diodes fitted into a conic structure. Position, size and spacing of these rings in the images determine the corneal shape. Closer rings indicate steeper corneas, and hence larger refractive power. The instrument software uses an ‘arc step method’ to analyse reconstruct topographical maps from upto 15120 measurement points. There are four different maps of corneal topography: axial power, tangential power, elevation height and refractive power. Together they provide a comprehensive description of the anterior corneal surface.

The instrument has an auto-focus mechanism that incorporates a range-finder to determine the distance from the corneal apex to the instrument’s camera and captures images only when good focus and alignment are attained. The participants sat comfortably in front of the instrument and fixated the centre of the ring target inside the cone-shaped head of the instrument. A series of images were captured, and each image taken was given a score by the software according to stability, completeness, focusing, and alignment of the ring pattern. The captured image was accepted only when the score was above 95 out of 100, as suggested in the instrument manual.

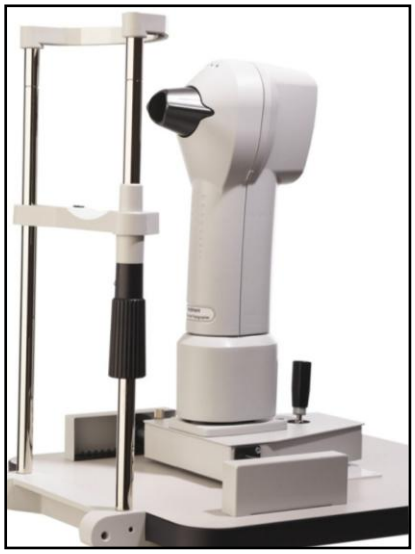

Figure 3:1: Medmont corneal topographer.

Small-cone Placido disc topographers have a shorter working distance (eliminate the shadows caused by nose or brow) and project a greater number of rings onto the cornea than large-cone topographers. Tang et al. (2000) reported that the Medmont E300 video-keratoscope can measure aspheric surfaces accurately. According to Cho et al. (2002), it provides highly accurate and repeatable results in less time with the larger measurement diameter (9 to 11 mm) than other video-keratometers (8 to 9 mm) because of its small Placido system.

3.5.2 PENTACAM

The Oculus Pentacam (Figure 3:2) uses a rotating Scheimpflug camera to provide a three–dimensional scan of the anterior segment of the eye. The Scheimpflug camera is a modification of a slit-lamp camera, with a modified geometry to improve depth of focus. In a Scheimpflug camera, the slit beam, camera lens, and CCD sensor intersect in a line where a cross-section of the eye appears in focus. By using a rotating Scheimpflug camera system, the Pentacam performs 12 to 50 two-dimensional single captures of the anterior segment of the eye, which can be converted to a three-dimensional model for analysis. From combined scans of different sections, information regarding the anterior and posterior corneal topography, corneal pachymetry, anterior chamber depth angle, and lens density can

be evaluated. The high depth-of-focus and the high resolution of the Scheimpflug image make it possible to detect small changes in the shape of the cornea and the lens.

Figure 3:2: Pentacam corneal topographer.

Studies have shown that this method has good repeatability in measuring central corneal thickness, corneal curvature, anterior chamber depth and lens density (Shankar et al., 2008, Barkana et al., 2005). In this study, the Pentacam was used to measure the cornea anterior and posterior radii of curvature, which were used in calculation of lens radii of curvature, lens equivalent refractive index and in estimating retinal shape estimates (section 3.5.7).

3.5.3 PHAKOMETER

Phakometry uses Purkinje images to assess the biometry of the lens. Illumination of an eye by a source results in four main Purkinje images formed by reflections from the anterior surface of the cornea (P1), posterior surface of the cornea (P2), anterior surface of the lens (P3) and the posterior surface of the lens (P4). In an unaccommodated eye, P3 is approximately twice the size of P1, while P4 is inverted and slightly smaller than P1. P1, P2 and P4 are formed near the pupil plane while P3 lies in the vitreous humour. The sizes of P3 and P4 relative to that of P1 are used to determine lens surface radii of curvature and lens equivalent index.

A custom-built phakometer was mounted on a 450 mm x 300 mm movable optical table over a base with a forehead and chin rest for easy alignment and steady positioning of the head during measurements (Figure 3:3). Rather than having a single spot source, in order to make images distinguishable and locatable when they are partially obscured by the pupil, the source was a semicircular ring of thirteen infrared LEDs (890 nm, Osram, SFH 487) angled 20° inwards and 70 -76 mm from the cornea. Images were captured by an IR-enhanced CCD camera (PixeLINK) provided with a 55 mm focal length telecentric lens (Edmund optics) focused at a distance of 260 mm.

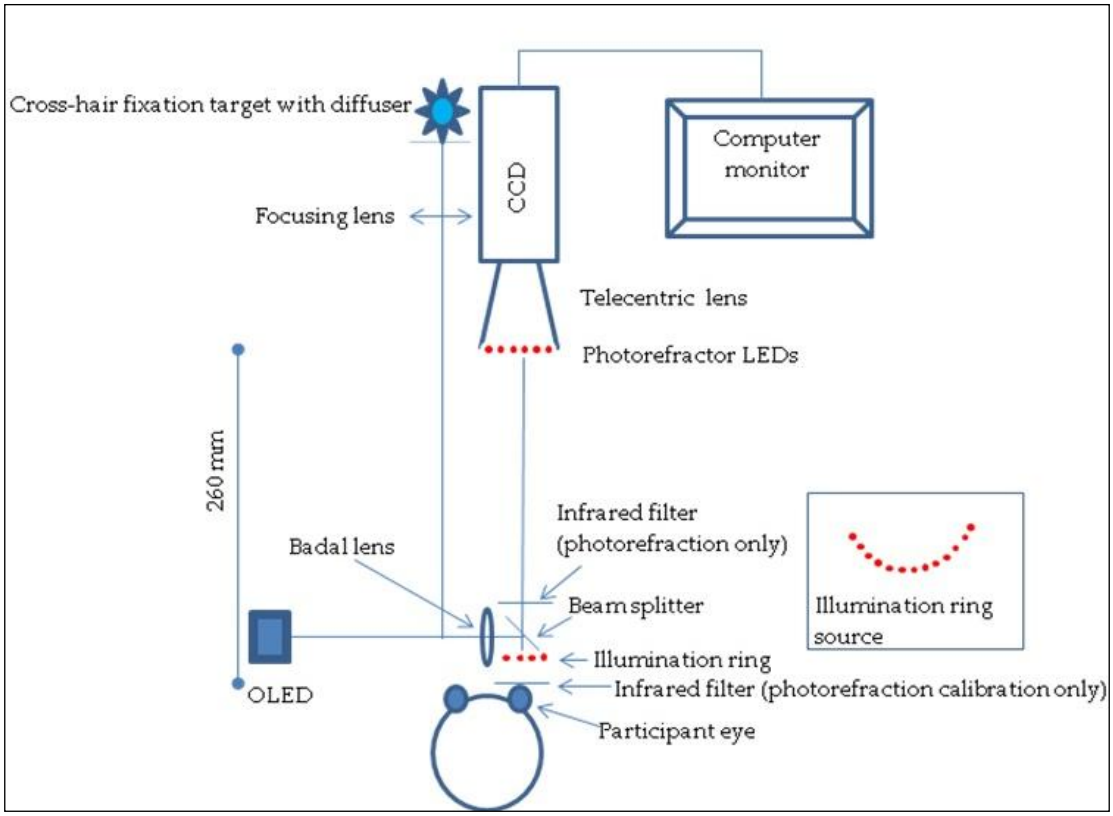

Figure 3:3: Schematic diagram of phakometer optical system having a CCD camera with telecentric lens for capturing images. Purkinje images are formed of the illumination ring source. The OLED displays the fixation targets through the beam splitter (Figure adapted from Adnan's unpublished PhD thesis).

An OLED, with viewing area 12.78 mm x 9.00 mm, dimensions 19.8 mm x 15.2 mm x 5.1 mm, and pixel pitch 15 µm controlled by computer, presented fixation targets across ±2.68˚ horizontal and ±1.99˚ vertical ranges at nine positions. The

targets were viewed through a 100 mm focal length Badal lens, which allowed a refraction range of −8 to +3 D. When the Purkinje image P1 was in focus at the camera, the pupil was at the second focal point of the lens.

The optical axis of the camera-lens was aligned to the central spot target (5^{th}) on the OLED screen. Participants were aligned when they fixated at the central fixation target of the OLED and the pupil of the eye was imaged in the centre of the camera, as viewed on the computer screen. Measurements were taken in the dark. P1 and P4 were clearly visible, but P3 was more difficult to view. The instrument was first moved so that P3 was in best focus, and then moved again to get the best possible combination of P1, P3 and P4, at which time the eye image was captured. On rotating the eye to fixate all of the OLED targets in turn, other images were captured, and the combined information about positions of the Purkinje images could be used to determine kappa, lens tilt, and lens decentration; although such measurements were obtained from a few participants, they are not reported here.

The setup also had a photo-refractor that consisted of fourteen 890 nm LEDs mounted in a custom-built knife-edge pattern in front of the lower half of the camera. This set up enabled recording of vertical luminance gradient pupillary images while the participant looked at the central fixation target (5th) of the OLED. The photo-refractor was not used for this project.

Custom-built software in MATLAB (Mathworks, Natick, MA) was written with three modes: fitting ellipses, a merit function to calculate lens biometry, and photorefraction to measure refraction/accommodation. The fitting ellipse mode fitted ellipses to the Purkinje images, to the pupil and to the limbus. It included an option to take the log of the image to enhance P3 detection. The sizes and centres of the Purkinje images, the pupil diameter, and the limbus diameter were determined (Figure 3:4). The Purkinje image positions could be referred to the pupil centre or to the cornea limbus centre. One millimetre on an image captured by the camera corresponded to 66.2 pixels on the CCD camera. Heights of P1, P3 and P4 were taken as the average of horizontal and vertical components of ellipses, averaged over 3 images.

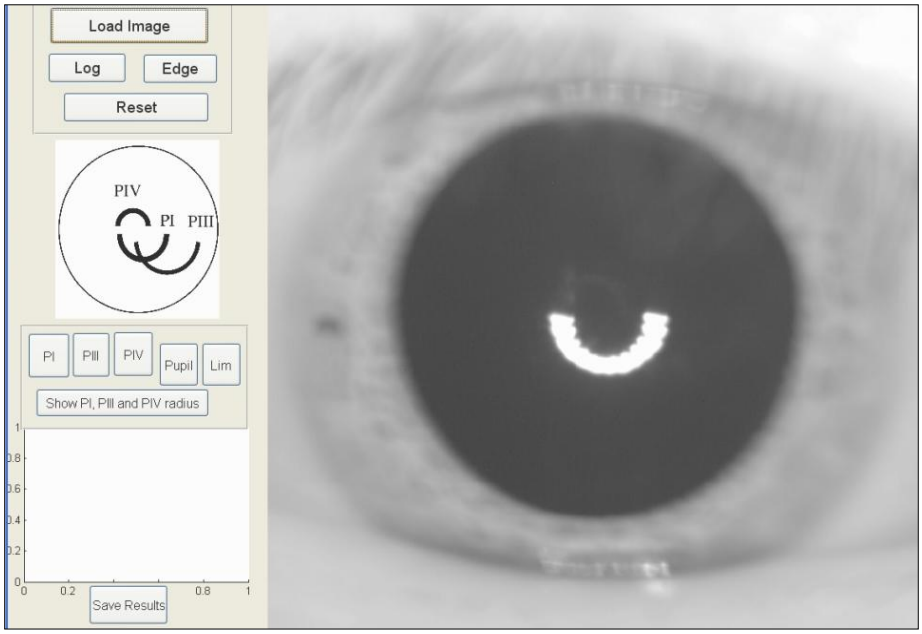

Figure 3:4: Ellipse fitting mode of the software.

The software's merit function mode estimates lens equivalent refractive index and radii of curvature from the following: Purkinje image heights, refraction (from Badal optometer setting), corneal radii of curvatures (average of anterior and posterior principal meridian from Pentacam), corneal thickness, anterior chamber depth, lens thickness, and vitreous length (200 µm added to correct from the inner limiting membrane to the retinal pigment epithelium - see section 3.5.7) (from Lenstar). A four refracting surface model eye is used. Refractive indices of the cornea, aqueous and vitreous at 555 nm are taken as those of the Gullstrand No 1 eye: 1.376, 1.336 and 1.336, respectively. Using the dispersion equations provided by Atchison & Smith (2005), refractive indices for the source of wavelength 890 nm are taken as 1.36822, 1.32829 and 1.32855, respectively.

The merit function *MF* has three components. The first component MF_1 is the square of the difference between the experimental vitreous length V_{exp} and the theoretical vitreous length V_{the} obtained through raytracing into the eye to the retina. The second and third components MF_2 and MF_3 are squares of the differences between the experimental image sizes h_{3exp} and h_{4exp} and their corresponding theoretical image sizes h_{3the} and h_{4the}. In brief,

$$MF = MF_1 + MF_2 + MF_3 = (V_{the} - V_{exp})^2 + (h_{3the} - h_{3exp})^2 + (h_{4the} - h_{4exp})^2 \qquad (12)$$

Recursive ray-tracing is continued until the merit function is reduced to a particular value or after a maximum number of cycles (2000) cycles.

Because the Lenstar uses a 820 nm wavelength, estimates of lens refractive index were converted from 890 nm to 820 nm. From the equations for the different ocular media given by Atchison & Smith (2005), a linear relationship between the lens indices at the two wavelengths is

$$n_{L820} = 1.0027 n_{L890} - 0.0026 \quad (13)$$

Lens equivalent power F_e was calculated from

$$F_e = F_{L1} + F_{L2} - (t_L/n_L) F_{L1}F_{L2} \quad (14)$$

where n_L is lens refractive index, t_L is lens thickness, and F_{L1} and F_{L2} are the front and back surface powers determined from

$$F_{L1} = (n_L - n_a)/r_{L1},\ F_{L2} = (n_v - n_L)/r_{L2} \quad (15)$$

where r_{L1} and r_{L2} are the lens radii of curvature and n_a and n_v are refractive indices of the aqueous and vitreous, respectively.

3.5.4 PERIPHERAL REFRACTION - AUTO-REFRACTOR

A Shin-Nippon auto-refractor SRW 5000 was used to measure refraction. The instrument uses the image size principle in which the sizes of the retinal image and its external image of an annular target are linearly related to the refraction (Atchison, 2009). Analysis of shape and dimensions of the final image determines the refraction. An open-field of view through a large beam-splitter provides the flexibility for the participants to view targets at a large range of positions relative to the axis of the instrument, and thus allow off-axis (peripheral) refraction measurement. Its use for peripheral refraction has been found to give results in good agreement with those for a Canon R-1 auto-refractor and a Hartmann-Shack instrument (Atchison, 2003).

The Shin Nippon SRW-5000 has a range of ±22.00 D sphere and ±10 D cylinder in steps of 0.125 D for power and 1˚ for cylindrical axis. Vertex distance can be altered to 0, 10, 12, 13.5, 15 or 16.5 mm. Measurements were obtained using 12 mm for all participants.

Before each recording session, the instrument was carefully aligned with the on-axis fixation target by ensuring that the centre of the red-square, seen by the participant when the instrument was turned on, coincided with the external target. This matched the optical axis of the instrument to the line-of-sight. The instrument monitor provides an image of a ring graticule that gives the instrument axis, the corneal reflection from a ring of LEDs and the participant's pupil. The instrument was moved by a joystick, transversely so that the centre of the pupil coincided with the graticule and anterio-posteriorly so the corneal reflection was sharply focused. For large fixation angles, the complete corneal reflection was not in focus at one time and the best overall focus was selected.

Refraction data (sphere *Sph*, cylinder *Cyl* and axis θ) are displayed on the monitor. An interface was used to export the refraction data to a personal computer via an RS-232 port. Custom built software converted these into power vector components (Thibos et al., 1997)

$$M = Sph + \frac{Cyl}{2} \tag{16}$$

$$J_{180} = -\left(\frac{Cyl}{2}\right) sin2\theta \tag{17}$$

$$J_{45} = -\left(\frac{Cyl}{2}\right) cos2\theta \tag{18}$$

and displayed these components in an Excel spread sheet.

Peripheral refraction measurements were taken at 14 positions along the horizontal visual field out to ±35º and at 12 positions along the vertical visual field out to ±30º in 5º intervals (Figure 3:5). For measurements along the horizontal visual field, participants rotated their eyes to fixate black 4 cm x 4 cm crosses, stroke width 3 mm, on a wall 3 m from the eye. For the higher myopes, fixation was aided by bright LEDs. The instrument's mirror was not big enough to encompass the necessary range of angles along the vertical meridian; and accordingly targets were placed on a vertical wall 1.67 m to the side of the participant and viewed through a 45º inclined beam-splitter between the eye and instrument. This short fixation distance was not considered to be a problem as measurements along both horizontal and vertical fields were obtained after the participants were cyclopleged with 1% tropicamide.

The beam-splitter did not affect on-axis refraction for a model eye (mean ± SD of 5 measurements for M with and without mirror –5.75 ± 0.12 D and –5.75 ± 0.25 D, respectively) or for human volunteers (mean difference ± SD for three participants: ΔM:–0.06 ± 0.22 D, ΔJ_{180} = +0.04 ± 0.14 D and ΔJ_{45} +0.02 ± 0.17 D).

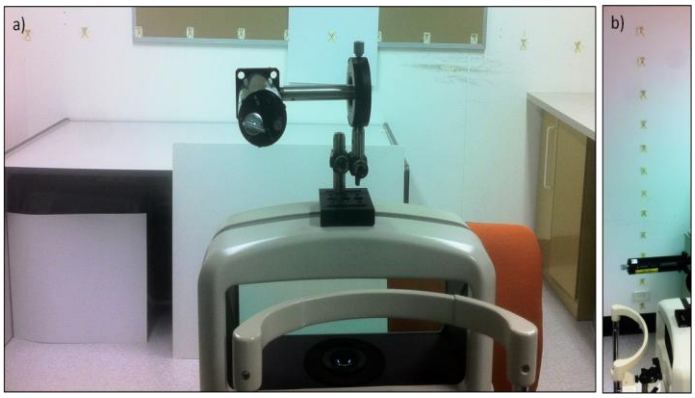

Figure 3:5: Shin-Nippon SRW 5000 auto-refractor setup for measuring central and peripheral refraction. Target placement for a) horizontal and b) vertical visual fields. An external attachment with laser light was fixed to the top of the instrument to show targets to myopic participants.

To investigate the influence of the mirror on peripheral refraction, measurement was taken along the horizontal visual field from 3 participants without and with the mirror (the horizontal field was used because it was not possible to obtain measurements along the vertical field without the mirror). Figure 3:6 shows two sets of measurements for M, J_{180} and $J_{45.}$ The measurements obtained with and without mirror were not significantly different for three participants ($p > 0.05$).

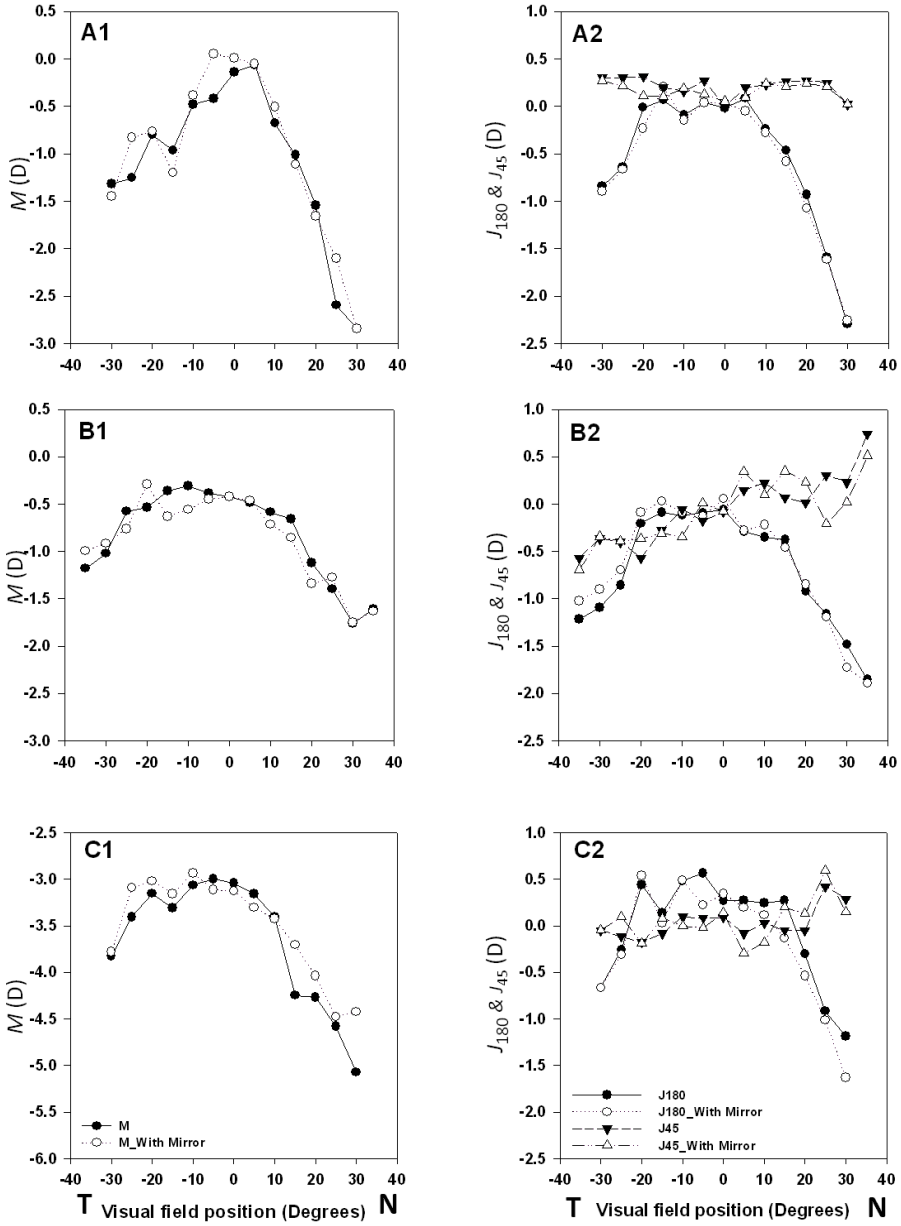

Figure 3:6: Comparison of peripheral horizontal field refraction without and with partial mirror for participants A, B and C. Graphs A1, B1 and C1 show spherical equivalent refraction and A2, B2 and C2 show astigmatic components (T = temporal and N = nasal).

3.5.5 PARTIAL COHERENCE INTERFEROMETRY

A light field is called coherent when there is a fixed phase relationship between the electric field values either at different locations or at different times.

Interference is an optical effect that occurs when two or more waves superimpose to form a resultant wave whose amplitude is the vector summation of the individual waves at each field point.

Two well-known commercial partial coherence interferometry instruments for measuring eye lengths are the IOLMaster (IOLMaster *V5*, Carl-Zeiss Meditec AG Jena, Germany) and Lenstar (Lenstar LS900, Haag Streit, Bern, Switzerland). There are also two recent instruments, the Nidek Optical Biometer AL-Scan and the Topcon ALADDIN biometer, about which little information is available. Unlike ocular ultrasound they are non-invasive and measurements are quicker and more repeatable. The IOLMaster and Lenstar instruments provide better resolution (0.01-0.02 mm) than ultrasound (0.10 mm) and magnetic resonance imaging (0.15 mm) (Kimura et al., 2007, Lam et al., 2001). They contain Michelson interferometers to create partial coherence and to compare the optical path lengths of two beams, one of which is reflected from a reference mirror on a moveable stage and the other which travels into the eye and is reflected from one or more surfaces (anterior and posterior corneal surface, anterior and posterior lens surface, retina, and choroid).

Figure 3:7 is a representation of the IOLMaster. Infrared radiation with a short coherence length is emitted by a laser diode. This incident beam radiation splits into two equal coaxial beams at a partially reflecting mirror B1, with one beam reflected by movable mirror M1 and the other beam by stationary mirror M2. These beams enter the eye where reflections take place at the anterior cornea (C) and the retinal pigment epithelium (RPE) interfaces. After leaving the eye, they are reflected from beam-splitter B2 onto photo detector PTD. The displacement d of mirror M1 is related to signals detected at the photo-detector, thus resulting in determination of the optical path length L in the eye. Interference between different components takes place when the optical path length difference is smaller than the coherence length of 160 µm. From modelling, the theoretical relationship to estimate the geometrical length L from the optical path length OPL for an emmetropic eye is:

$$L = OPL/1.3459 \quad (19)$$

where 1.3549 is the mean *group* refractive index at 780 nm (Haigis et al., 2000). Group refractive index is the ratio of the vacuum velocity to the group velocity in a medium. It is related to the group velocity rather than to the phase velocity in the medium. The phase velocity is the rate at which the phase of a wave propagates in a medium, while the group velocity is the rate at which the envelope wave (overall wave shape amplitude) moves through that medium.

In the instrument, a calibration is used to match the axial length measured by ultrasonography, where the distance between anterior cornea and inner limiting membrane is measured:

$$L = (OPL/1.3549 - 1.3033)/0.957 \quad (20)$$

or

$$L = 0.7711*OPL - 1.3617 \quad (21)$$

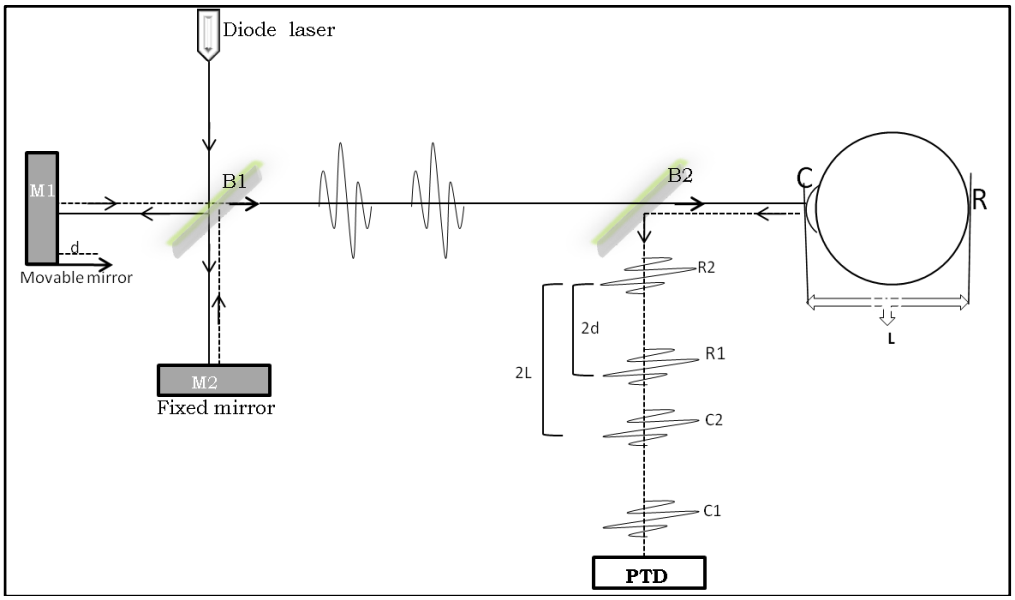

Figure 3:7: Schematic representation of IOLMaster. Based on Haigis et al. (2000).

The IOLMaster contains a diode laser producing infrared radiation centred at approximately 780 nm, and the Lenstar contains a super luminescent diode producing infrared radiation centred at approximately 820 nm. These sources have

wide bandwidths with corresponding short coherence length so that strong interference signals occurs only when the optical path lengths are similar rather than differing by multiples of wavelengths. The IOLMaster uses the partial coherence interferometry principle only for axial length measurements.

The Lenstar is more complex than the IOLMaster and uses 4 interferometers to recognise the signal from posterior cornea, anterior lens, posterior lens and retinal pigment epithelium. The instrument is formed mainly of a time domain optical coherence tomographer (TD-OCT) and a spectral domain optical coherence tomographer (SD-OCT) which shares a broadband light source of short coherence length. The instrument uses a moveable rotating mirror to travel certain physical distances corresponding to optical distances inside the eye. To pass over the vitreous humour, the instrument uses a comb of a transparent material of known refractive index n to increase the path length in the reference arm. In addition, the SD-OCT uses a grating to acquire multiple scans simultaneously. Corneal, anterior chamber and lens thicknesses are measured, together with lens and corneal topographies (although the latter is under sampled) using the OCT in addition to the use of two light emitting diodes in different meridians (up to 4 meridians) (Waelti and Schmid, 1999). The manufacturer does not indicate what refractive index or indices are used, but it is intended to give similar axial lengths to the IOLMaster (Read et al., 2011). It is not known whether this average index is used for the other media or whether they have their own indices. An experiment was conducted to investigate this.

3.5.5.1 Refractive index investigation

Methods

Axial lengths of several model eyes were determined using both an IOLMaster and a Lenstar. An overall group refractive index n_{ave} for the Lenstar was estimated by comparing these lengths and taking into account difference in wavelengths for the instruments.

Using the A-scan screen in the Lenstar Graphical User Interface (GUI), each ocular boundary of a real eye was shifted in small steps (Figure 3:8). This caused different changes in the geometrical lengths on either side of the boundary. The change in one medium's thickness was plotted against the change in the other

medium's thickness to give a linear curve with a negative slope (Figure 3:9). As the changes made by shifting boundaries were only to calculated biometric information and were not influenced by the eye which has been used, only one eye was necessary. Assuming that the optical path lengths changed equally as the boundary was moved, this slope *m* was the ratio of the two media refractive indices:

$$m = \Delta x_2/\Delta x_1 = -n_1/n_2 \quad (22)$$

where Δx_i is change in physical thickness of medium i with group refractive index n_i.

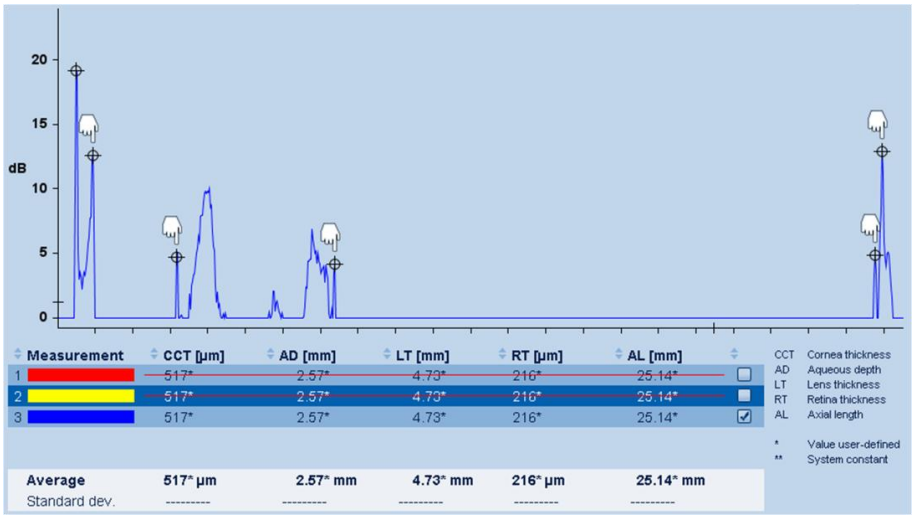

Figure 3:8: A sample A-scan screen from the Lenstar graphical user interface with hands pointing towards all the peaks that can be redefined by the user. The six peaks indicated by "⊕" represent (left-to-right) the reflections from anterior cornea, posterior cornea, anterior lens, posterior lens, internal limiting membrane and retinal pigment epithelium.

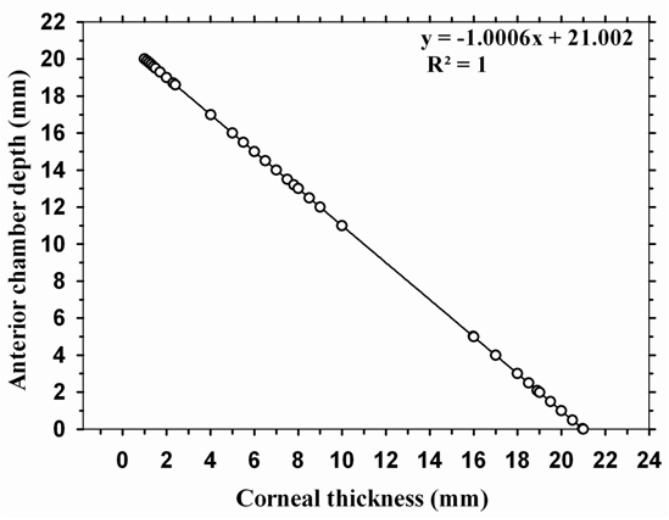

Figure 3:9: Anterior chamber depth (geometrical) as a function of corneal thickness (geometrical) while sliding the posterior corneal boundary, thus equally varying their optical path lengths. The slope represents the ratio of the assumed group refractive indices of the two media. The slope is influenced only by refractive indices assumed in the calculations, and is independent of what eye is being used.

The ratio between the average group refractive index of the eye and that of the lens was taken by moving peaks to expand the lens to cover the whole length of the eye, and comparing the thickness of the lens to the axial length reading given by the GUI. The ratio between the indices for lens and aqueous was acquired by sliding the anterior surface of the lens. Similarly, the ratio between the indices for the aqueous and the cornea was achieved by sliding the posterior surface of the cornea.

The indices were compared with indices found in schematic eyes. The refractive indices in these eyes were corrected from 555 nm to 820 nm using two approaches. In the 'water scaling' approach, chromatic dispersion similar to water at 20°C (Daimon and Masumura, 2007) was assumed. The refractive index at 820 nm is

$$n_{820} = n_{555} \times n_{820,water}/n_{555,water} \quad (23)$$

where $n_{820,water}$ and $n_{555,water}$ are the phase refractive indices of water at 820 and 555 nm, respectively.

As the indices in this equation are phase indices applicable to single rays, n_{820} was converted to a group index applicable to wave bundles using

$$n_g(\lambda) = n_p(\lambda) - \lambda \frac{dn_p}{d\lambda} \quad (24)$$

where $n_g(\lambda)$ and $n_p(\lambda)$ are group and phase indices at wavelength λ.

In the 'Atchison & Smith' approach (2005), Cauchy dispersion formulae of ocular media were used. These formulae apply for the phase indices of the Gullstrand No. 1 eye, and, as necessary, scaling was used:

$$n_{820} = n_{555} \times n_{820,Gull}/n_{555,Gull} \quad (25)$$

where $n_{820,\mathrm{Gull}}$ and $n_{555,\mathrm{Gull}}$ are the phase refractive indices of Gullstrand model eye at 820 and 555 nm, respectively.

Conversions from phase indices to group indices were made using Equation (24).

Table 3.1 shows the group refractive indices of the Gullstrand No. 1 eye and the Le Grand full theoretical eye according to the two approaches. These schematic eyes were chosen because their lens refractive indices are at the lower and higher ends of a range of schematic eyes. The indices for the Gullstrand eye lens, which has a shell structure of a high index nucleus surrounded by a lower index cortex, are based on its average phase index of 1.3994 at $555\ nm$. For the Le Grand eye, as for most paraxial schematic eyes, the gradient index of the lens has been replaced by an "equivalent index" which is higher than the index at any point in the lens in order to give the correct power. The 'water scaling' approach gives indices that are 0.0001 to 0.0015 higher than the 'Atchison & Smith' approach.

Table 3.1: Group refractive indices of Gullstrand No. 1 and Le Grand schematic eyes at 820 nm.

Eye model/approach	Cornea	Aqueous	Lens	Vitreous
Gullstrand/water scaling	1.3834	1.3435	1.4066	1.3434
Le Grand/water scaling	1.3844	1.3449	1.4271	1.3434
Gullstrand/Atchison & Smith	1.3823	1.3423	1.4063	1.3419
Le Grand/Atchison & Smith	1.3834	1.3437	1.4270	1.3419

Results

The IOLMaster and Lenstar instruments produced the same estimates of axial length of physical model eyes to within ± 0.01 mm. It follows that the average refractive index assumed by the Lenstar can be estimated from the IOLMaster refractive index, accounting for the difference in source wavelength. Multiplying the average group theoretical refractive index n_{IOL} used in the IOLMaster equation (19) by the ratio of group indices of water at 820 nm and 780 nm, n_{ave} for the Lenstar was estimated as:

$$n_{ave} = n_{IOL} \times \frac{n_{820,waterg}}{n_{780,waterg}} = 1.3549 \times \frac{1.3421}{1.3429} = 1.3540 \qquad (26)$$

where $n_{820,waterg}$ and $n_{555,waterg}$ are the group refractive indices of water at 820 and 555 nm, respectively.

Table 3.2 shows both the ratios between the group refractive indices of ocular media, obtained by sliding boundaries in the Lenstar GUI, and the estimated group refractive indices using 1.3540 for n_{ave}. The Lenstar does not measure the vitreous length, but it could be calculated by subtracting all geometrical thicknesses from axial length. As an effect, the refractive index of the vitreous is equivalent to n_{ave}.

Table 3.2: Estimated effective refractive indices of ocular media used by the Lenstar GUI.

Ocular medium	Ratio	Estimated effective refractive index
Lens	$n_L/n_{ave} = 1.0450$	$1.0450 \times 1.3540 = 1.4149$
Aqueous	$n_{AQ}/n_L = 0.9475$	$0.9475 \times 1.4149 = 1.3406$
Cornea	$n_C/n_{AQ} = 0.9994$	$0.9994 \times 1.3406 = 1.3398$

Using Table 3.1 and Table 3.2, the ratios of estimated group refractive indices of the Lenstar and those of the schematic eyes were determined (Table 3.3). For the cornea, the estimated indices differ considerably by approximately 3.2% from schematic eye indices. For the aqueous the estimated indices differ by only 0.1-0.3% from the schematic eye indices: no distance correction is needed. For the lens, estimated refractive indices vary by –0.9% to +0.6% from schematic eye indices. An accurate value for group refractive index in visible light is about 1.410 for lenses of

young adult eyes, corresponding to 1.417 group index at 820 nm. This suggests the Lenstar underestimates lens group refractive index by 0.15%, corresponding to distance overestimation of less than 0.01 mm in 4 mm lenses. As 0.01 mm is the resolution limit for the lens, no distance correction is needed.

Table 3.3: Ratio of estimated group refractive indices of Lenstar and those of schematic eyes at 820 nm.

Eye model/approach	Cornea	Aqueous	Lens
Gullstrand/water scaling	0.9685	0.9978	1.0059
Le Grand/water scaling	0.9678	0.9968	0.9915
Gullstrand/Atchison & Smith	0.9693	0.9987	1.0061
Le Grand/ Atchison & Smith	0.9685	0.9977	0.9915

Recent communication with Haag Streit via Designs for Vision, its supplier in Australia, provided a template that shows "air thicknesses" that are converted to geometric lengths. The following export codes are used for deriving air thicknesses: {AIRAL}, {AIRCCT}, {AIRACD} and {AIRLT} for axial length, corneal thickness, anterior chamber depth and lens thickness, respectively. The "air thickness" was considered as a mean group optical path length. Refractive indices were determined using this template from a database of about 5000 measurements. For each medium, there is a linear equation relating thickness L and optical path length OPL:

Axial length (mm) : $OPL = 1.2866L + 1.9587$ $R^2 = 1.000$ (27)

Corneal thickness (μm) : $OPL = 1.3447L + 0.0654$ $R^2 = 0.9999$ (28)

Ant. chamber depth (mm): $OPL = 1.3444L + 0.1331$ $R^2 = 0.9999$ (29)

Lens thickness (mm) : $OPL = 1.4187L + 0.0002$ $R^2 = 0.9999$ (30)

The equations obtained with GUI are comparable to those obtained here with "air thickness" except that the latter showed an offset in each case, indicating that the

"refractive index" will depend on the thickness. The ratio of *OPL* to geometric thickness decreases as thickness increases (Figure 3:10). For the lens and cornea, the off-set is negligible and is probably noise due to the measurement precision. In the case of the anterior chamber depth there is a considerable off-set of 0.13 mm.

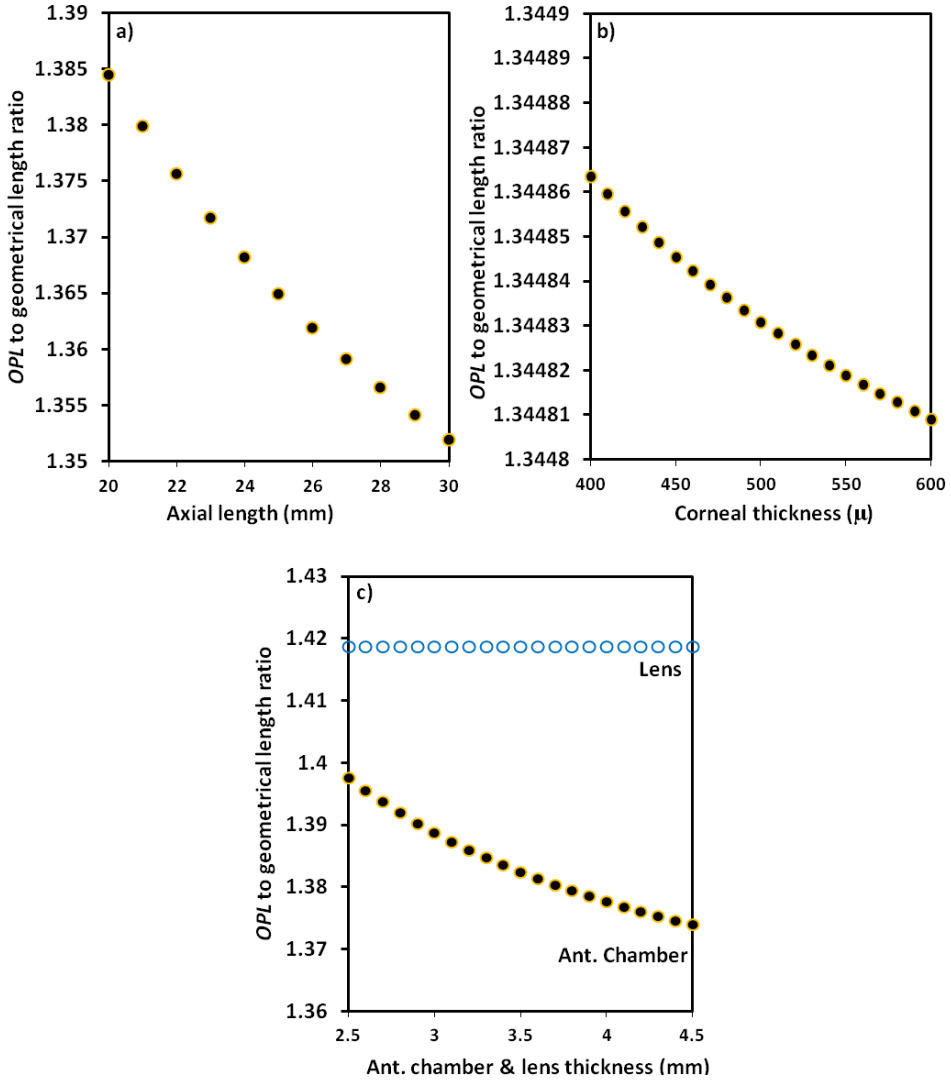

Figure 3:10: Ratios of *OPL* to geometrical length derived from equations (27) to (30) for a) axial length, b) corneal thickness, c) anterior chamber depth (bottom) and lens (top).

Discussion

Based on this work, it is clear in the operation of the Lenstar that different group refractive indices are assigned to different media in the eye. The equations used by Haag-Streit appear to give appropriate group indices for the aqueous and lens, but the value for the cornea (1.3447) is much too low and the values for the axial length appear to be too high (the value of 1.354 is not attained till a length of 29 mm). Because of these anomalies, it is difficult to be confident that the equations are converting from *real* optical path lengths to geometrical thicknesses. The understanding of the measurements of optical path length within the instrument is limited, such as what calibrations might be needed to convert measurements to real optical path lengths. It must be borne in mind that the axial length calibration of the IOLMaster, given by equation (20) was to ensure that it gave similar results to ultrasonography, and the Lenstar calibration was to ensure that it gave similar results to the IOLMaster rather than emphasis on accuracy in its own right.

Accordingly, in the modelling to determine retinal shape (section 3.5.7), I believe that the best approach is to adopt the geometrical thicknesses as given by the instrument and to use refractive indices based on suitable schematic eyes as modified for different wavelengths according to the equations provided by Atchison & Smith (2005).

In this regard, it should be noted that Faria-Ribeiro et al. (2014) estimated errors of axial length of the IOLMaster caused by variations in lens thicknesses. They used the group refractive indices used by Hitzenberger (1991) and Haigis et al. (2000) except that for axial length they used the theoretical equation (19) rather than equation (20) based on calibration against ultrasonography. Errors were within ±0.10 mm across a wide range of axial lengths and lens thicknesses (Figure 3:11a), but would have been much higher if the calibration equation had been used (Figure 3:11b).

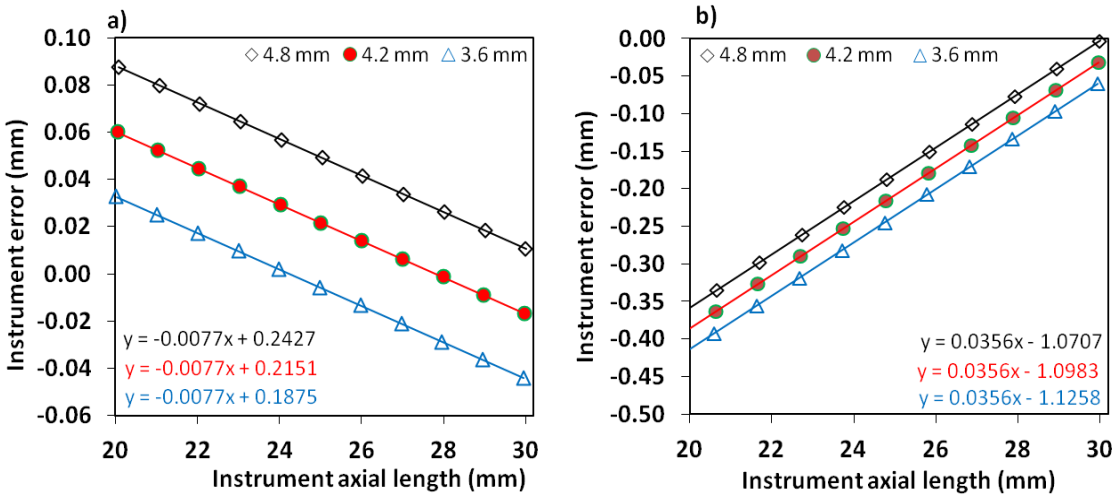

Figure 3:11: Theoretical error of the IOLMaster as a function of instrument axial length for different lens thicknesses using a) equation (19), and b) equation (20). Based on Faria-Ribeiro et al. (2014).

In conclusion, the Lenstar biometer uses different refractive indices for different ocular media. Some of the refractive indices, such as that for the cornea, are not physiological, and it is likely that the calibrations in the instrument correspond to instrument-specific corrections and not the *real* optical path lengths.

3.5.5.2 Preliminary Experiment 1: Repeatability and comparison of partial coherence interferometry instruments for measuring peripheral eye lengths

A few studies have used partial coherence interferometry for measuring peripheral eye lengths, but no study has investigated repeatabilities and agreement of the instruments. As both instruments were available, repeatabilities and agreement of the instruments were evaluated in a preliminary experiment.

Measurement of peripheral eye lengths

A total of 7 healthy adults, consisting of 2 emmetropes (< ±0.75 D) and 5 myopes (−0.75 D to −6.25 D), with the age range 23 to 57 years (mean age 35 ± 11 years) having best corrected visual acuity of 6/6 or better were recruited. After dilating the pupil with 1 drop each of 1.0% tropicamide and 2.5% phenylephrine,

central and peripheral eye lengths were recorded using the IOLMaster V5 and Lenstar LS 900.

Peripheral eye length measurements were obtained by using an external attachment, similar to that of Mallen and Kashyap (2007), containing a goniometer, a 50/50 beam-splitter (50% transmission/50% reflection), a Maltese cross fixation target placed at focal length of a Badal lens (+33.3 D) simulating optical infinity, and an LED source (Figure 3:12). The Maltese cross was aligned with the instrument fixation axis for on-axis measurements. The goniometer was moved over the base rail (movement along X, Y and Z axes), until the Maltese cross target could be seen at all positions of goniometer rotation, thus ensuring that the effective position about which the target rotated corresponded with the centre-of-rotation of the eye. For the horizontal visual field, the attachment was fixed to the top of chinrest frame of the IOLMaster or Lenstar instrument using a pair of right-angle retort clamps, while for the vertical visual field, the attachment was to the side frame of the chin rest.

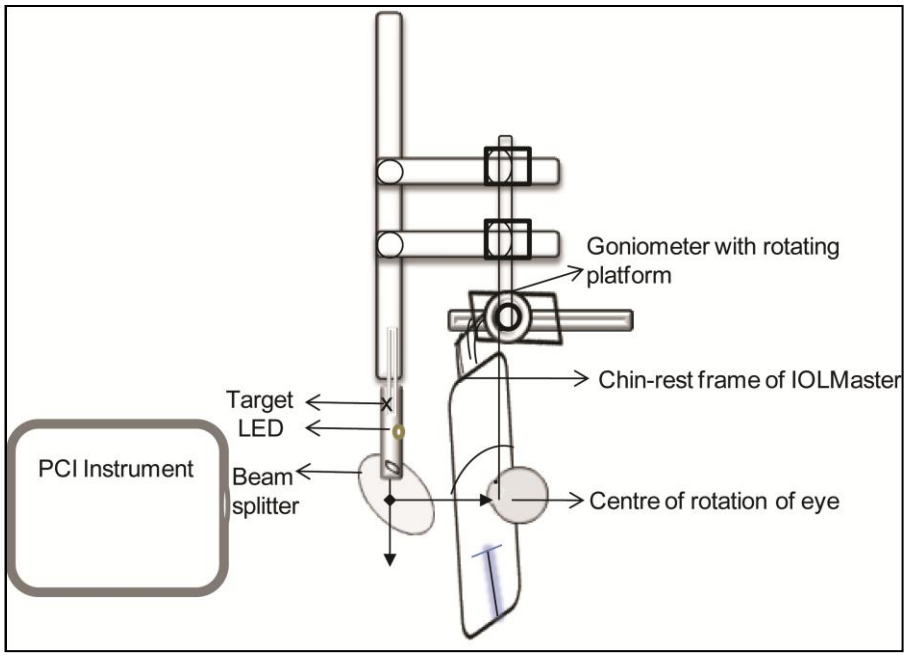

Figure 3:12: The PCI instrument's external attachment that show targets in the peripheral visual field in order to measure peripheral eye lengths.

Translation of the front of the eye upon rotation required realignment of the pupil along the instrument axis. Participants were asked to blink completely before each measurement to stabilize tear film. The alignment mire was maintained in clear

focus, and it moved towards the pupil margin as the field angle increased. A minimum of four consecutive measurements were recorded at each position and their mean was calculated. Eye length measurements with IOLMaster were interpreted (accepted or rejected) by the investigator based on the signal-to-noise ratios (SNR) and the appearance of graphs. The values which had SNR below 2.0 were rejected as per the manufacturer guidelines. The Lenstar does not show any SNR but uses a proprietary intelligent detection system that enables the instrument to take measurements only when the eye is stable. If the patient blinks or loses fixation, the measurements are automatically rejected and measures resume when the participant's fixation improves. When the eye was not aligned properly, an error symbol was displayed adjacent to the value and these measurements were deleted.

The effect of the beam-splitter was assessed by sets of five measurements for a model eye and a human eye. Using the Lenstar calibration eye model, axial length was 23.80 ± 0.00 mm with or without the beam-splitter for both instruments. For the human eye and for the Lenstar, axial length was 23.35 ± 0.00 mm with or without the beam-splitter and intraocular distances were not affected significantly by the beam splitter (screenshot of measurements is shown in Figure 3:13).

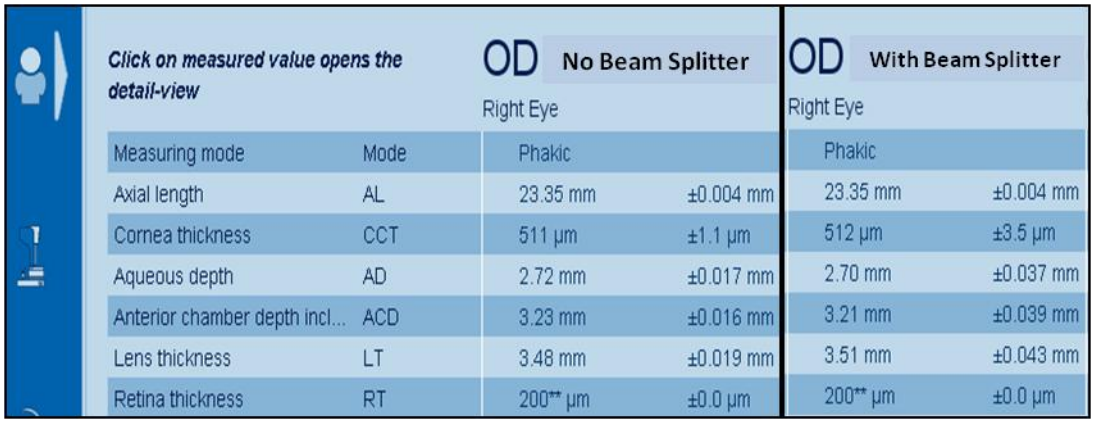

Figure 3:13: Screenshot of measurements with and without beam-splitter.

Data collection

The eye lengths were determined in 5º steps out to 30º along the nasal visual field, out to 35º along the temporal visual field, and out to ±30º along the vertical visual field. Measurements were not possible any further because the edge of the iris obstructed the passage of the beam. All the measurements were performed by the same investigator and collected from right eyes except for one participant for whom the left eye was used. For right eyes, rotation to the right side corresponded to the nasal visual field denoted with (+) sign (temporal retina) and rotation to the left side corresponded to the temporal visual field denoted with (–) sign (nasal retina). Similarly, upward rotation corresponded to the inferior visual field denoted with (–) sign (superior retina) and downward rotation corresponded to the superior visual field denoted with (+) sign (inferior retina).

For inter-sessional reliability determination, measurements were obtained at two different sessions (different days for 4 participants and the same day for 3 participants). The order of instruments in a session was assigned randomly. Measurements were recorded along the horizontal visual field (temporal to nasal) followed by the measurements along the vertical visual field (superior to inferior). The average time to obtain a measurement set was 45 minutes for the IOLMaster and 60 minutes for the Lenstar.

Analysis

For determining intra-sessional repeatability for each instrument, each participant/session/visual field position was represented by the standard deviation of the first 4 measurements. The intra-sessional repeatability was given by the mean of these standard deviations across 7 participants, 2 sessions and visual field positions (14 for the horizontal visual field and 13 for the vertical visual field).

For determining inter-sessional repeatability for each instrument, each participant/visual field position was represented by the difference between the mean values of the two sessions. The inter-sessional repeatability was given by the standard deviation of these differences across participants and visual field positions.

For determining the agreement between the two instruments, each participant/visual field position was represented by the mean difference between

instruments across the two sessions. The agreement was given by the mean and the standard deviation of the differences across participants and visual field positions.

One weakness about the above approach is that multiple positions from each participant are treated as independent observations. Bland and Altman (2007) have a method for investigating agreement between methods with multiple observations for individual participants. This can be applied here, treating different peripheral positions as if they are different observations for which the underlying quantity is varying. As compared to considering each position for a participant as independent, the standard deviations (or 95% prediction limits) increase by ≤2% for intra-sessional, inter-sessional and inter-instrument analyses, which is small and can be ignored.

In addition to the above analyses, repeated-measures analyses of variance (ANOVA) were conducted on eye lengths with participants as the repeated measures. A first ANOVA was conducted for intra-sessional standard deviations, with session (session 1, session 2), instrument (IOLMaster, Lenstar) and visual field position as within-participant factors. A second ANOVA was conducted for absolute inter-sessional differences, with instrument and visual field position as within-participant factors. A third ANOVA was conducted for differences between instruments, with session and visual field position as within-participant factors. These three ANOVAs were conducted for the horizontal and vertical visual fields separately and for combined data; as results were similar for the three approaches, only results for the combined data are mentioned.

Results

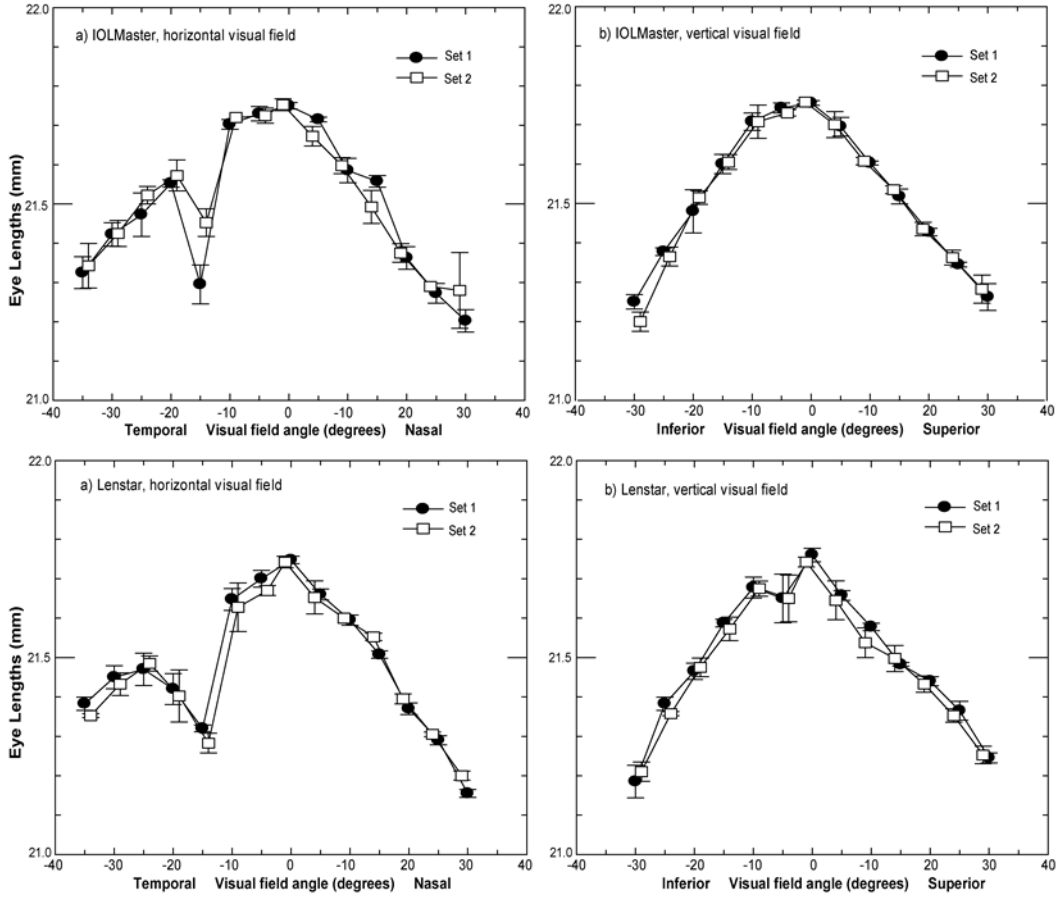

Figure 3:14: Repeatability of eye length measurements:for one subject for: IOLMaster along a) horizontal and b) vertical visual fields; Lenstar along c) horizontal and d) vertical visual fields. Error bars are intra-sessional standard deviations.

For the IOLMaster, the intra-sessional repeatabilities were 0.04 ± 0.04 mm along the horizontal and vertical visual fields. Corresponding results for the Lenstar were 0.02 ± 0.02 mm along both the horizontal and vertical visual fields. The difference between the two instruments was significant in the corresponding ANOVA ($F_{1, 6} = 19.1$, $p = 0.005$).

The IOLMaster and the Lenstar had intra-sessional standard deviations of 0.02 and 0.01 mm, respectively, at the centre of the visual field. The standard deviations were greater away from the centre, with maximum values for the IOLMaster of 0.07 mm (at 20º, 25º temporal and 10º, 30º superior field positions) and for the Lenstar of 0.06 mm (at 15º temporal field position corresponding to the optic disc). The

increased intra-sessional variation away from the centre was supported by the significant effect of visual field position ($F_{26, 156} = 4.2$, $p < 0.001$).

Figure 3:15 shows Bland-Altman plots of inter-sessional repeatability. Different symbols are given for different participants. The inter-sessional repeatabilities for the IOLMaster for the horizontal and vertical visual fields were ±0.11 and ±0.08 mm, respectively; corresponding repeatabilities for the Lenstar were ±0.05 and ±0.04 mm. The difference between the two instruments was marginally significant in the corresponding ANOVA ($F_{1,6} = 5.8$, $p = 0.05$).

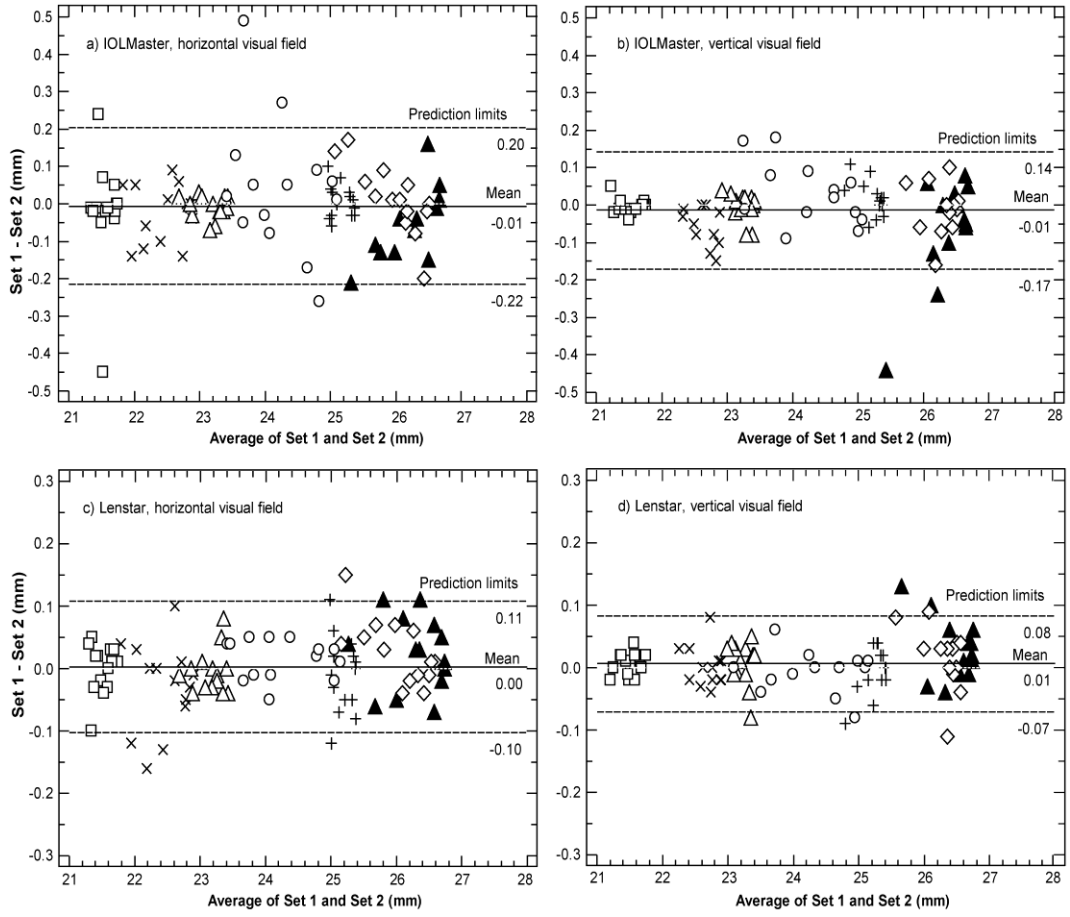

Figure 3:15: Bland-Altman plots of inter-sessional repeatability of eye length: IOLMaster along a) horizontal and b) vertical visual fields; Lenstar along c) horizontal and d) vertical visual fields. Different symbols represent data of different participants, with 14 points and 13 points for each participant along horizontal and vertical fields, respectively. The mean differences and the 95% prediction limits are shown by straight lines.

The inter-sessional repeatability increased from the centre towards the peripheral visual field for both the IOLMaster and the Lenstar. Both instruments had repeatabilities of 0.03 mm at the centre of the field, increasing for the IOLMaster to approximately 0.20 mm (15º temporal, 30º temporal and 30º superior field positions) and increasing for the Lenstar to approximately 0.08 mm (15º temporal and 20º-30º nasal field positions). The increased inter-sessional variation away from the centre was supported by the significant effect of visual field position ($F_{26,156}$ = 2.4, p <0.001).

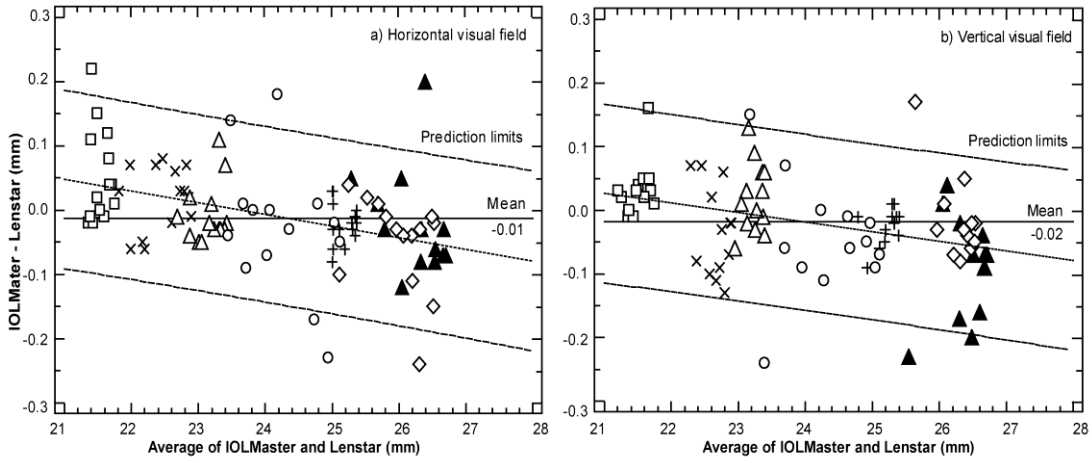

Figure 3:16: Bland-Altman plots of agreement of eye lengths between IOLMaster and Lenstar along a) horizontal and b) vertical visual fields. Different symbols are given for different participants, with 14 points and 13 points for each participant along horizontal and vertical fields, respectively. The mean differences and the 95% prediction limits are shown by straight lines. The dotted lines show regressions: horizontal visual field slope –0.0177 (R^2 = 0.17, n = 98, p <0.001); vertical visual field –0.0153, (R^2 = 0.14, n =91, p <0.001). When regressions were repeated based on mean values for each participant (n = 7), similar slopes were obtained, but that for the vertical visual field was marginally significant (p = 0.07).

Figure 3:16 shows Bland-Altman plots of agreement between the two instruments. As for Figure 3:15, different symbols are given for different participants. The agreements between the instruments were 0.01 mm and 0.02 mm for the horizontal and visual fields, respectively, with standard deviations of ±0.07

mm for both visual fields. These results indicate that the instruments are in good agreement. The differences between the two instruments varied from 0.02 mm at the centre of the visual field to 0.04 mm along the horizontal field (5º, 10º, 25º nasal and 30º temporal), and 0.06 mm along the vertical field (30º inferior), but there was no statistically significant difference between the instruments at any field position and analysis of variance did not show an effect of field position ($F_{26, 156} = 1.0$, $p = 0.47$). For one participant (square boxes on left of plots) the IOLMaster had greater measures than the Lenstar for most positions while for another participant (filled triangles on right side of plots) the reverse was the case. In both these participants, the variation (one instrument greater or lesser) is noticed only at the temporal visual field and was irregular (greater difference at 15º and 20º than at extreme 30º visual field), but did not show any systematic constant steep increase or decrease in pattern.

The differences between the instruments change significantly with axial length, with the Lenstar giving larger measurements of axial length than the IOLMaster for longer eyes; the slopes in Figure 3:16 are approximately –0.016 ($p < 0.001$).

Discussion

For measuring peripheral eye lengths along the horizontal and vertical visual fields, an assessment was made for intra-sessional and inter-sessional repeatability of IOLMaster and Lenstar (partial coherence interferometry instruments) and the agreement between the instruments. Intra-sessional repeatability was 0.04 mm for the IOLMaster and 0.02 mm for the Lenstar. Inter-sessional repeatabilities were ±0.11 and ±0.08 mm for the IOLMaster for the horizontal and vertical visual fields, respectively; corresponding repeatabilities for the Lenstar were 0.05 and 0.04 mm. Repeatabilities worsened away from fixation. Agreements between the instruments were good at 0.01 ± 0.07 mm and 0.02 ± 0.07 mm for the horizontal and vertical visual fields, respectively, with no significant influence of visual field position; but the lengths with the Lenstar became greater than those with the IOLMaster as axial length increased (rate about 0.016 mm/mm).

The intra-sessional and inter-sessional repeatabilities of both instruments were excellent. The latter is particularly of note as the external device had to be re-attached before each session with each instrument, and the relative peripheral eye

length at extreme visual field positions ranged between 0.3 mm and 2.1 mm for participants. The smaller (better) intra-session repeatability with Lenstar compared to IOLMaster may be partly due to a difference in the recording method as each Lenstar measurement is the average of 16 scans. Also, the Lenstar had the better inter-sessional repeatability. Quantification was made based on the direct relation between the axial length and refraction (0.3 mm = 1.0 D), with the consideration that it is clinically important to detect change of 0.07 mm (corresponding to 0.25 D). The SD's for IOLMaster and Lenstar (intra-session repeatability) 0.05 mm and 0.02 mm corresponds to about 0.15 D and 0.06 D change in refraction, and Lenstar's repeatability SD values corresponding to about 0.15 D. Since these instruments identify less than the clinically important difference (0.07 mm = 0.25 D), this is considered an excellent agreement. Likewise, the differences between the two instruments varied from 0.02 mm at the centre to maxima of 0.04 mm and 0.06 mm along the horizontal and the vertical field, corresponding to about 0.15 and 0.20 D change in refraction and accordingly were considered in good agreement.

The on-axis intra-sessional repeatability of 0.02 mm is better than 0.04 mm as reported by Santodomingo et al. (2002), while the 0.01 mm for the Lenstar is at the lower end of 0.01 to 0.04 mm repeatabilities in other studies (Buckhurst et al., 2009, Cruysberg et al., 2010, Shammas and Hoffer, 2012, Rohrer et al., 2009, Bjelos Roncevic et al., 2011). In the only previous investigation of off-axis repeatability with the Lenstar, for 5 positions along the horizontal field, Schulle and Berntsen (2013) reported repeatabilities of 0.03 to 0.05 mm, similar to those obtained here.

The on-axis inter-sessional repeatabilities of 0.03 mm for both instruments are within the 0.02 to 0.04 mm range reported for the IOLMaster (McDaniel and Mutti, 2002, Sheng et al., 2004, Kimura et al., 2007) and poorer than 0.01mm reported for the Lenstar (Buckhurst et al., 2009, Shammas and Hoffer, 2012), but similar to that reported by Schulle and Berntsen.The latter reported repeatabilities of 0.025 and 0.06 mm at two off-axis positions, similar to those obtained here.

The measurements became greater for the Lenstar than for the IOLMaster with increase in eye length (0.016 mm/mm). I analysed the results of three studies of on-axis length (Rohrer et al., 2009, Buckhurst et al., 2009, Salouti et al., 2011, Zhao et al., 2013) (personal communications) and confirmed this trend only for the study of Buckhurst et al. for which the slope was 0.010 mm/mm.

Several studies have already reported the excellent agreement between the instruments for on-axis length measurements. Mean differences were reported as 0.00 to 0.04 mm, with some studies, but not others, finding significant differences (Buckhurst et al., 2009, Holzer et al., 2009, Rohrer et al., 2009, Salouti et al., 2011). As axial length change directly changes the refractive error (0.30 mm = 1D), the agreements of ±0.07 mm are equivalent to approximately ±0.25 D. This implies that both these instruments are capable of identifying the clinically significant changes which is the important to detect in myopia research.

The ease of peripheral measurements was similar for the two instruments. The average time to obtain a measurement set, including the adjustments of the external attachment, was 40 minutes for the IOLMaster and 50 minutes for the Lenstar. This difference is partly because of the different technology used by the instruments. The Lenstar uses a proprietary "intelligent detection system" that enables the instrument to takes measurements only when the eye is stable - if the patient blinks or loses fixation, the instrument waits until the patient's fixation returns. The IOLMaster does not consider eye movement and displays the reading immediately with the investigator accepting or rejecting readings based on the signal-to-noise ratio.

Conclusion

Good agreement between IOLMaster and Lenstar for central and peripheral eye length measurements along both horizontal and vertical visual fields indicates that the instruments can be used interchangeably for measuring central and peripheral eye lengths. While the present preliminary experiment has not established the validity of using peripheral eye length measurements for determining retinal shape, it does show that such measurements with two commercial partial coherence interferometers are similar and repeatable. Because the Lenstar showed better intra-sessional and inter-sessional repeatability compared to IOLMaster, it was used for the rest of the experiments. Validation of Lenstar for estimating retinal shape is described under Chapter 4.

3.5.5.3 Preliminary Experiment 2: Influence of eye rotation on peripheral eye length measurement

Using eye rotation when measuring peripheral refraction leads to concern about whether the rotation could influence results through pressure exerted by eyelids or extra-ocular muscles. Ferree et al. (1931, 1932) and Seidemann et al. (2002) reported that eye rotation could shift refraction myopically by up to 2.50 D and 0.75 D, respectively, but Radhakrishnan & Charman (2008) and Mathur et al. (2009b) did not find significant differences between eye and no-eye rotation conditions.

Similarly to the case of peripheral refraction, the issue of rotating the eye to measure peripheral eye length arises. Since the partial coherence interferometry methods offer high resolution (0.01 mm), and can therefore detect small changes in eye length, any change in eye shape due to extra-ocular muscle effect should be larger than the noise level. Bayramlar et al.'s (1999) finding of increased axial elongation during convergence under cycloplegia supports Greene's (1980) theory that oblique muscle contraction can influence axial elongation. A recent study by Ghosh et al. (2012) found that the eye elongates in downward gaze due to gravity. As convergence, accommodation and downward gaze shift of the eye may increase axial length, it is important to determine effects of eye rotation on peripheral eye lengths.

Macfadden et al. (2007) claimed significant effects of eye rotation on peripheral eye length measurements along the horizontal visual field using the IOLMaster, but they did not mention the duration of rotation to cause these results. The targets were attached to the instrument and were moved to achieve the alignment, and this may have affected comparisons between eye rotating and non-eye rotating conditions.

This preliminary experiment aims to determine whether the eye rotation approach for measuring peripheral eye lengths is valid. Measurements of peripheral eye length were compared when the eye or the head was rotated in emmetropes and myopes along both horizontal and vertical visual fields.

Data collection

Twenty-three healthy young adults were recruited, consisting of 11 emmetropes (spherical equivalent within ±0.75 D) and 12 myopes (−0.75 D to −6.00 D). Mean age was 25 ± 3 years and mean refraction was −1.25 ± 1.75 D. Participants had best corrected visual acuity of 6/6 or better and astigmatism <0.75 D. Horizontal field measurement was done for all participants and vertical field measurement was done for a subset of 8 participants (4 emmetropes, 4 myopes).

Central and peripheral eye lengths were measured with the Haag Streit Lenstar LS 900 biometer as it shows good repeatability for peripheral eye lengths as reported in section: 3.4.5.1) (Schulle and Berntsen, 2013, Verkicharla et al., 2013).

Measurements were made from right eye of all participants with the left eye occluded. Eye lengths were determined at the following visual field positions: 0^{o}, (–)30° temporal, (+)30º nasal, (+)25º superior and (–)25º inferior. Smaller angles were used vertically than horizontally because of physical limitations in the no-eye rotation condition for the vertical visual field. Measurements at (–)30º inferior required lifting the instrument more than 10 cm from the provided table, and then tilting the instrument backwards. Since the distance between the instrument and the eye must be kept at 68 mm, the participants had to lean forward. Measurements at (+)30º superior were obstructed by the frontal orbital bone.

Visual field position 0º was always tested first, followed by the positive angles and then by the negative angles.

There were two different experimental conditions: eye rotation and no-eye rotation. For the eye rotation condition, participants rotated their eyes with the head aligned along the instrument axis and fixated a Maltese cross target at optical infinity provided through an attachment described above. Measurements were obtained by following the same procedure that was described in section 3.4.5.1.

For the no-eye rotation condition along the horizontal visual field meridian, participants rotated their head with the eye remaining fixed relative to the head (Figure 3:17). A separate chin rest frame was made for this purpose and a bite bar was mounted on to a rotation stage. The attachment described above was slid horizontally so that the participant saw the complete target at the angle of interest.

For the no-eye rotation condition along the vertical visual field, the instrument rather than the head was rotated. The rotation of the instrument involved an angle inclination assessment device and the participant's bite bar was moved up and down to match the centre of rotation of the eye to the instrument axis. All the participants maintained fixation on the target, which was directly ahead (Figure 3:18).

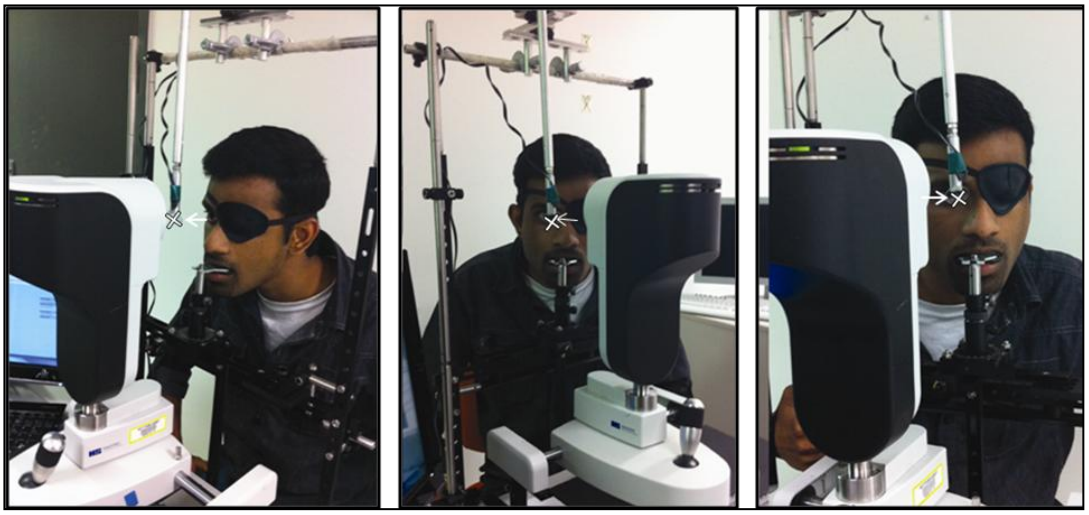

Figure 3:17: Setup for the no-eye rotation condition along the horizontal visual field : (left) participant looking straight ahead, (middle) head rotation to the right (+30° nasal field), and (right) head rotation to the left (–30° temporal field). White arrows point to the Maltese cross target in front of the eye.

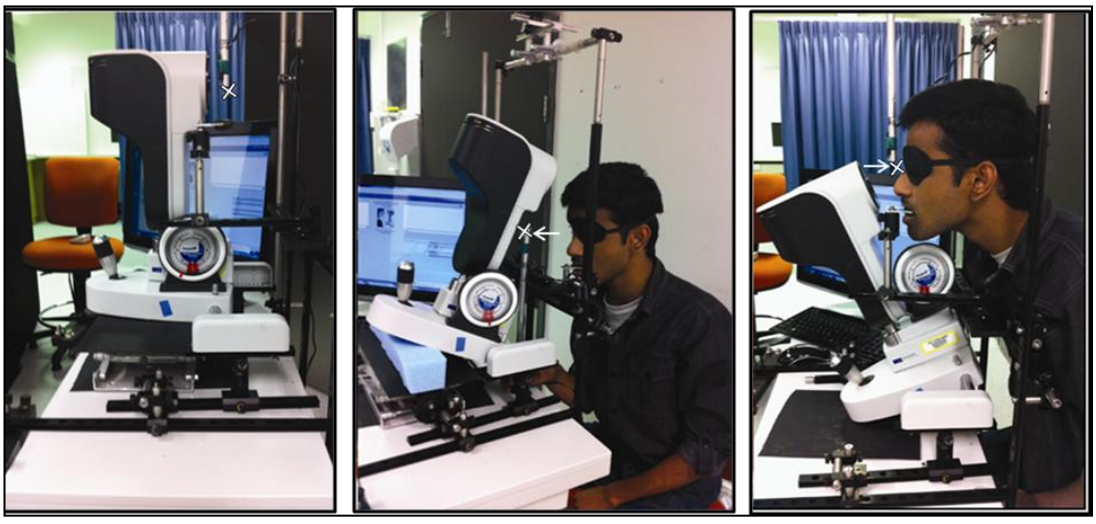

Figure 3:18: Setup and instrument position for the no-eye rotation condition along the vertical visual field: (left) instrument setup for participant looking straight ahead, (middle) forward tilt of the instrument (+25° superior field), and (right) backward tilt of the instrument (–25° inferior field). White arrows point to the Maltese cross target in front of the eye.

Measurements commenced 20 minutes after pupil dilation with 1% tropicamide. At least three consecutive measurements were recorded with both the conditions at each position, with each measurement taking less than 10 seconds. After measurements with the eye rotation condition, a "rest" of 30 minutes was given before proceeding to the no-eye rotation condition.

The influence of the duration of maintaining eye position on peripheral eye lengths was assessed by recording measurements at 0, 60, 120, 180 and 210 seconds after eye rotation in six participants (4 myopes and 2 emmetropes). Measurements were obtained at ±30° along both horizontal and vertical visual fields, unlike in the no-eye-rotation condition above where measurements were obtained at ±25° in the vertical field due to physical limitations. The fixation was maintained steadily by all participants for the entire duration of 210 seconds and was monitored by the examiner. After 210 seconds of eye rotation towards positive angle, a "rest" of at-least 15 minutes was given to all participants to avoid any systematic bias before proceeding to the measurements of negative angle. During the "rest" period, participants looked at a distant wall.

Analysis

For determining influence of eye rotation on peripheral eye lengths, a repeated measures analysis of variance (ANOVA) was performed for each visual field meridian using measurements from the two conditions and two positions. The Wilcoxon Signed Rank Test was used to determine the significance of the duration following eye rotation ($\pm 30^{o}$ along both horizontal and vertical visual fields) on peripheral eye lengths. A significance criterion of $p < 0.05$ was used for all tests.

Results

Figure 3:19 and Figure 3:20 show the differences in eye length measurement between the eye rotation and no-eye rotation conditions for each participant along the horizontal and vertical meridians. There are no obvious different patterns between the two groups.

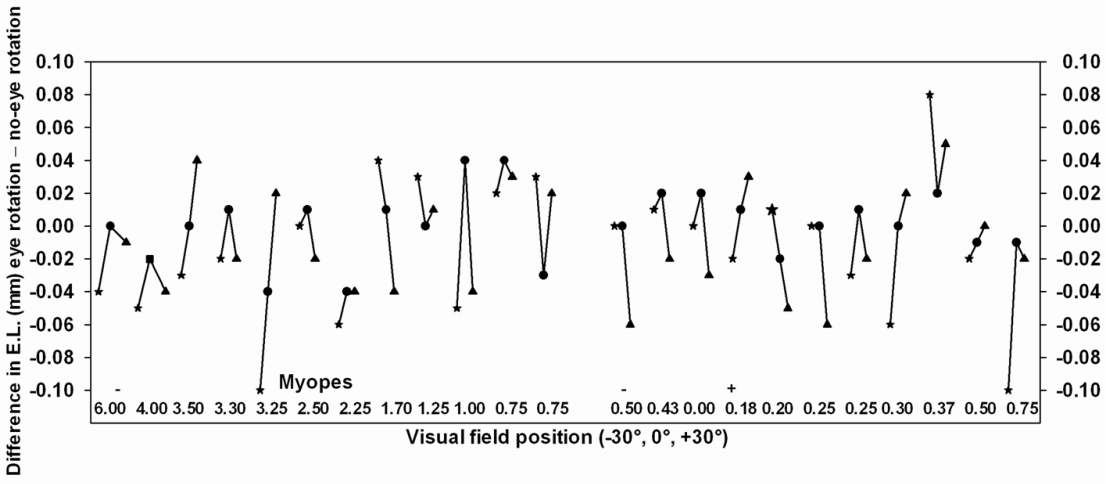

Figure 3:19: Differences in eye length measurements (mm) between the eye rotation and no-eye rotation conditions for each participant at three horizontal visual field positions (-30º, 0º, 30º in this order).

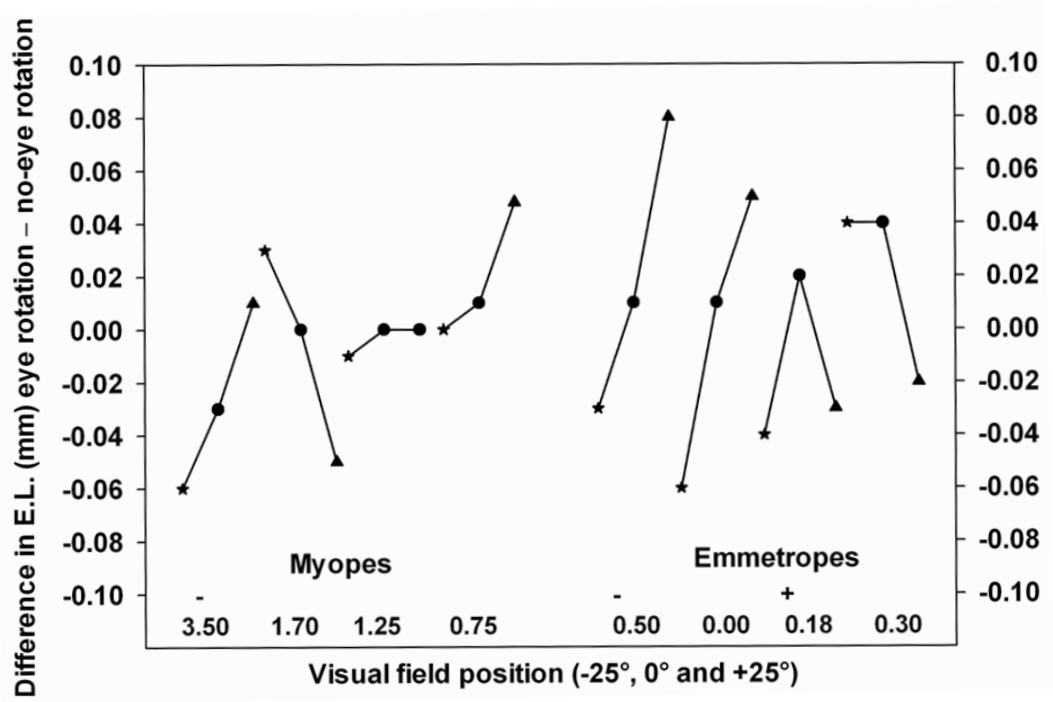

Figure 3:20: Differences in eye length measurements (mm) between the eye rotation and no-eye rotation conditions for each participant at three vertical visual field positions (-25º, 0º, 25º in this order).

Analysis of variance showed no difference in peripheral eye lengths between the conditions along the vertical meridian ($F_{1, 7} = 0.155$, $p = 0.705$). There was a statistically significant difference between the conditions along the horizontal

meridian ($F_{1, 22}$= 4.85, p = 0.038), but the differences were not significant at individual positions (p ≥ 0.10, paired t-tests).This is supported by Figure 3:21, which shows the group (myopes, emmetropes and total) differences in peripheral eye lengths between conditions. Mean differences ±95% confidence interval limits along the horizontal field were –0.016 ± 0.018 mm (–30º) and –0.011 ± 0.013 mm (+30º); corresponding values along the vertical field were –0.016 ± 0.026 mm (–25º) and 0.011 ± 0.031 mm (+25º), respectively. The differences were not significant at any visual field position in emmetropes, myopes or the total group.

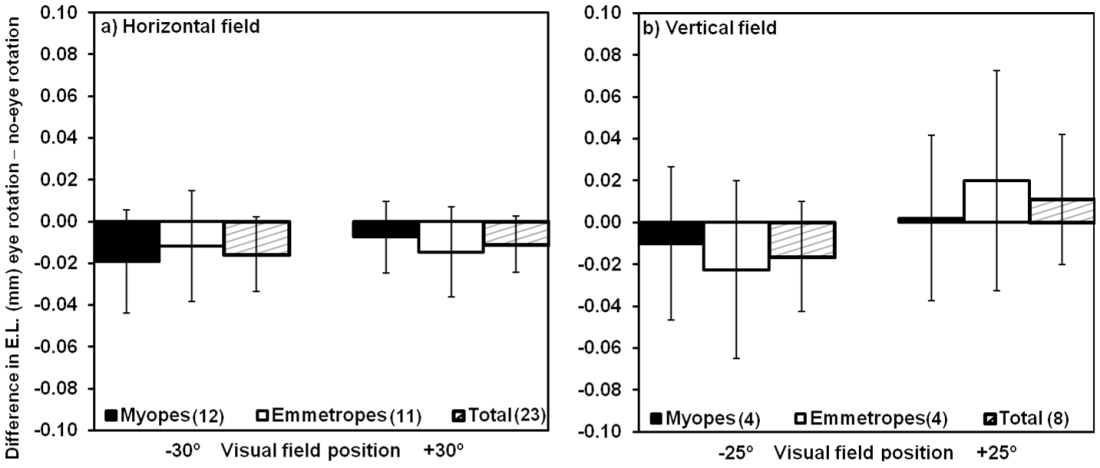

Figure 3:21: Mean differences of eye length measurements between eye rotation and no-eye rotation conditions along the a) horizontal (±30º) and b) vertical visual fields (±25º). These are shown for myopes, emmetropes and all participants. Error bars represent 95% confidence intervals of means.

Figure 3:22 shows the influence of time after eye rotation on peripheral eye length for six participants (4 myopes and 2 emmetropes). There was no significant change in peripheral eye lengths after 210 seconds at any visual field position (p > 0.05).

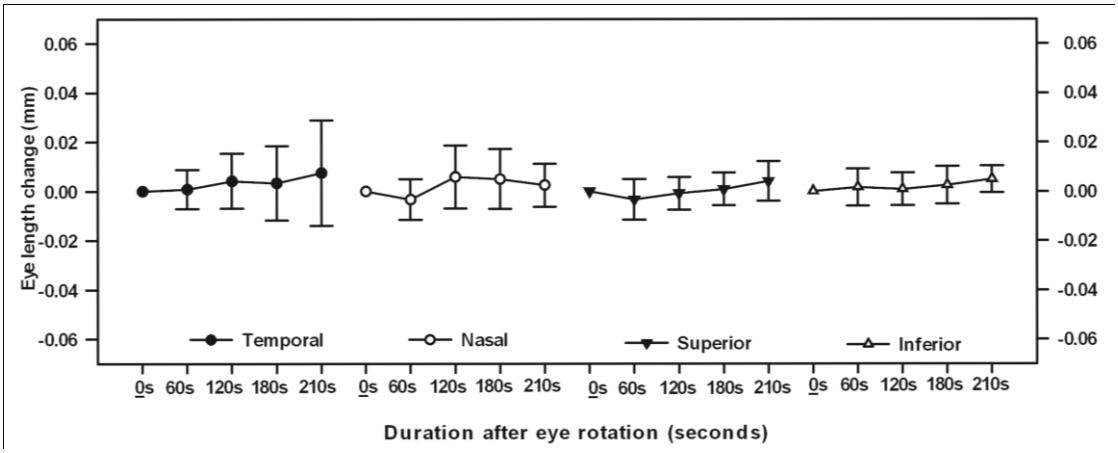

Figure 3:22: Mean changes in peripheral eye length measurements from 6 participants in four visual field positions with the eye held rotated relative to the head for 210 seconds. Error bars are standard deviations.

Discussion

This experiment investigated differences in peripheral eye length measurements between eye rotation and head rotation conditions using the Lenstar along horizontal and vertical visual fields out to 30° and 25°, respectively, from the straight ahead position. The conditions were not significantly different along the vertical visual field. The conditions were significantly different along the horizontal visual field, although not at individual 30° temporal and 30° nasal positions. Furthermore the 95% limits of agreement between the two conditions across the (±30º) horizontal (–0.013 ± 0.077 mm) and (±25º) vertical field (–0.003 ± 0.091 mm) were within the 95% repeatability limits previously found for the instrument (±0.10 mm) across a range of visual field positions (see section 3.4.5.1) (Verkicharla et al., 2013).

To give some context to the measurement differences, the effect of an error of −0.016 ± 0.018 mm was determined, corresponding to 95% confidence limits of the differences between the two conditions at –30° horizontal, might have on retinal shape estimates. A simple model was used consisting of a corneal surface with radius of curvature of 7.8 mm, backed by a medium of refractive index of 1.333 and a retina with a radius of curvature of −12 mm and placed 24 mm behind the cornea. A peripheral ray was directed towards the centre of curvature of the cornea, with deviations likely to occur at a lens being ignored. Based on this single angle, the estimated retinal radius of curvature of a spherical retina would be −11.94 ± 0.08

mm, and the estimated asphericity (*Q*) without modifying the radius of curvature would be +0.04 ± 0.05 (Atchison, 2006). These errors are of small magnitude.

Statistical power was low. A power analysis comparing the two conditions using G*power software (p = 0.05, power = 0.80) indicates that 46 to 135 participants are necessary to obtain significance for the mean differences obtained at the different visual field positions. Considering that the difference between the two conditions is small and does not influence retinal shape results, the study was not conducted on the mentioned sample as the time required for this was not warranted.

Radhakrishnan & Charman (2008) and Mathur et al. (2009b) did not find any influence of eye rotation on peripheral refraction along the horizontal meridian for either emmetropic or myopic groups. This does not eliminate the possibility of change at oblique directions, with Ehrlich (1987) finding 0.29 D transient myopic shift in central refraction after a prolonged (2 hours) binocular task at 20 cm distance and Ghosh et al. (2012) finding increase in central axial length (0.018 mm) in combined downward and inward gaze. Radhakrishnan & Charman (2008) also investigated the effect of prolonged oblique viewing (150 seconds) on peripheral refraction and did not find any effect, which fits the finding that peripheral eye length did not change even after holding the eye in rotated positions for 210 seconds.

Conclusion

The differences in measurement between the eye rotation and no-eye rotation conditions were sufficiently small that either condition could be used to estimate retinal shape from peripheral eye lengths, at least out to the angles that were used here. Accordingly, I used the eye rotation approach for the experiments to be described in the next chapters.

3.5.6 MAGNETIC RESONANCE IMAGING

Magnetic resonance imaging (MRI) is most commonly used as a medical imaging technique in radiology to visualise the internal structure and functions of human body parts (Edelman et al., 2006). MRI can also image any plane (or a 3D volume) and can provide both anatomical and functional information. Although the image resolution obtained through MRI is relatively poor compared with other radiographic techniques such as X-ray, and computerised tomography , it gives better contrast between the different soft tissues of the body (Scherzinger and Hendee, 1985).

An MRI machine uses a powerful static magnetic field to align the magnetisation of hydrogen nuclei in the body (because they are charged and possess spin angular momentum, they behave like little magnets) and radio-frequency fields to systematically alter the alignment of this magnetisation. Hydrogen nuclei present in the body are predominantly in the form of water (H_2O) and fat molecules. Because the nuclei are subjected to a magnetic field and absorb radiation at resonance, the method is also called Nuclear Magnetic Resonance Imaging. When a radiofrequency pulse is applied, atoms absorb some of the pulse's energy, which tips the nuclear magnetisation away from the static magnetic field direction. When the radio frequency pulse is turned off, the hydrogen atoms release absorbed energy, giving rise to a detectable signal which decays with time as the nuclear magnetisation relaxes back to equilibrium. This signal is detected by a radio frequency coil or antenna that transforms the signal into electrical current, which is then used to construct the image of a slice (or set of slices) of the scanned area. The nuclear magnetisation can be divided into two components: a ‘longitudinal’ component which increases exponentially with a characteristic time known as T1 as the component of magnetisation parallel to the static magnetic field returns to equilibrium and a ‘transverse’ component which decreases exponentially with a characteristic time known as T2 as the components of magnetisation perpendicular to the static magnetic field decay to zero. Based on its origin, the longitudinal time T1 is called spin-lattice relaxation time and the transverse time T2 as spin-spin relaxation time. Different tissues, because of their different chemical constitutions and different physical states, will have different relaxation times. Images can be weighted in favour of T1 or T2. For example, to create a T2-weighted image one has

to wait for different amounts of magnetisation to decay before measuring the MR signal by changing the echo time (TE). T1 weighted images cause fat to appear bright and water to appear dark and vice versa with the T2 weighted images. In contrast to T1-weighted MRI, T2-weighted MRI illustrates internal eye shape by high-contrast delineation of the vitreous-retina interface. Therefore, in this project T2-weighted MRI was used.

In order to generate an image, the NMR signals must be spatially encoded. This is achieved by application of pulsed magnetic field gradients that are applied either before signal detection ('phase encoding') or during signal detection ('frequency encoding').

3.5.6.1 Image acquisition parameters

MRI has a relatively slow acquisition rate which makes the images prone to motion artefacts/noise and it has limited resolution in comparison with optical techniques. The relationship between the MR signal and the image noise present is expressed as the signal-to-noise ratio (SNR). Mathematically, the SNR is the ratio of the signal intensity measured in a region of interest and the standard deviation of the signal intensity in a region outside the area of interest. There are several factors affecting SNR (Redpath, 1998): transmit and receive radio frequency coil (RF coil), voxel size, slice thickness and receiver bandwidth, field of view (FOV), size of the matrix, number of acquisitions, scan time, repetition time (TR) and echo time (TE). One way to improve SNR in MRI is to place the receiver coil as close as possible to the part of the anatomy to be imaged. For this reason, a small 'surface coil' as the detector coil was used in this study and placed as close as possible to the subject's eye.

An MR image consists of a two dimensional matrix of pixels. Each pixel provides information on a corresponding three-dimensional volume element, termed a 'voxel'. The larger the voxel size, larger the number of spins inside it, so the signal is directly proportional to the voxel size within a tissue of uniform spin density. The two main factors determining resolution are the field of view (FOV) and the matrix size. Large matrices can incorporate more picture elements that improve the image resolution but the small pixel size decreases SNR. When matrix size is held constant,

the field of view (FOV) determines the size of the pixels/voxels (Weishaupt et al., 2003).

Pixel size = FOV (mm)/matrix size

To achieve optimal image resolution, very thin slices with a high SNR are required. However, thinner slices imply smaller voxels and are therefore associated with more noise, and so the SNR decreases. The poorer SNR of thin slices can be compensated to some extent by increasing the number of acquisitions or by a longer repletion time TR, the time period between the beginning of a *pulse sequence* and the beginning of the succeeding pulse sequence. The echo time (TE) is the echo time between successive excitation pulses to the echo maximum.

Receiver bandwidth is the range of frequencies collected by an MR system. A wide receiver bandwidth enables faster data acquisition and minimises artefacts, but reduces SNR as more noise is included.

Another limiting factor is the image acquisition/scan time, which increases with the matrix size. Number of excitations (NEX) or number of signal averages (NSA) denotes how many times a signal from a given slice is measured. SNR improves as the NEX increases (in proportion to the square root of the NEX), but scan time increases linearly with the NEX.

Considering the effect of various parameters on SNR, resolution and scan time, particular improvement in imaging is not possible without compromise in any other parameter (Table 3.4).

Table 3.4: Effects of different parameters on SNR, resolution and scan time.

Parameter	SNR	Resolution	Scan time
Increasing slice thickness	Increases	Decreases	Decreases
Increasing FOV	Increases	Decreases	Increases
Increasing matrix size	Decreases	Increases	Increases
Increasing TR	Increases		Increases
Increasing TE	Decreases		Increases
Increasing NEX	Increases		Increases
Increasing magnetic field strength	Increases		
Increasing receiver bandwidth	Decreases		
Employing local coils	Increases		

3.5.6.2 Imaging protocol

Magnetic resonance imaging was undertaken at the University of Queensland Centre for Advanced Imaging with a Siemens Trio 3.0 Tesla (Siemens Magnetom Trio), whole-body clinical magnetic resonance scanning system using a standard Siemens 4.0 cm receive only radiofrequency surface coil positioned over the eye following a procedure based on that used by Atchison et al. (2005). In preliminary experiments, results obtained with the 4.0 cm surface coil were compared against eye images acquired with a Siemens 32-channel phased-array head coil. Although the head coil allowed both eyes to be imaged, the surface coil yielded superior signal to noise and image resolution.

Procedures adhered strictly to the NHMRC guidelines and a checklist (standard survey form) was used to select suitable participants and to screen for items that cannot be taken into the magnetic field. Persons with heart pacemakers, bionic implants or other metallic implants that might cause localised heating or degrade image quality were excluded. Female subjects were requested not to wear eye make-up on the day of the examination, in order to reduce susceptibility artefacts. All imaging was carried out under the supervision of a qualified MR Radiologist.

Scanning was performed with participants lying supine. The target was a white cross 1.3 cm × 1.3 cm, stroke width 0.5 mm on a black background, projected onto a translucent screen mounted in the end of the magnet bore at a viewing distance of 0.93 metres (a+b in Figure 3:23). Participants looked upwards to view the target through an adjustable mirror (M) mounted at 45º to the vertical (fixed tilt). The position of the mirror was adjusted manually backwards and forwards to get the eye in the right position, i.e. corneal surface of the eye directly below the centre of the mirror as shown in Figure 3:23.

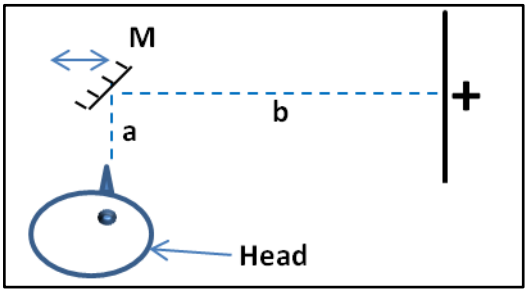

Figure 3:23: Setup for showing target inside MRI instrument.

The surface coil was taped over the participant's right eye so that the view of the target was not obstructed. A thin self-adhesive felt spacer cut to fit the coil provided separation from the skin of the patient. To optimise imaging, care was taken to ensure that the surface coil stayed close to the eye (Figure 3:24). To ensure minimum eye movement, the participant's non-tested eye was occluded with an eye patch. Heads of the subjects were immobilised with appropriate padding and they were asked to focus and fixate on the target image and to minimise blinking during data acquisition. Between acquisitions they were advised to close their eyes and blink freely in order to renew the tear film.

For myopes requiring correction < –1.00D, trial lenses on top of the 20 mm thick coil were used to provide a clear target. The distance between the eye and correcting lenses was estimated to be approximately 25 mm, and this was used as a basis for determining lens power. Participants were advised to restrict blinking while keeping the eye as still as possible and focused on the cross.

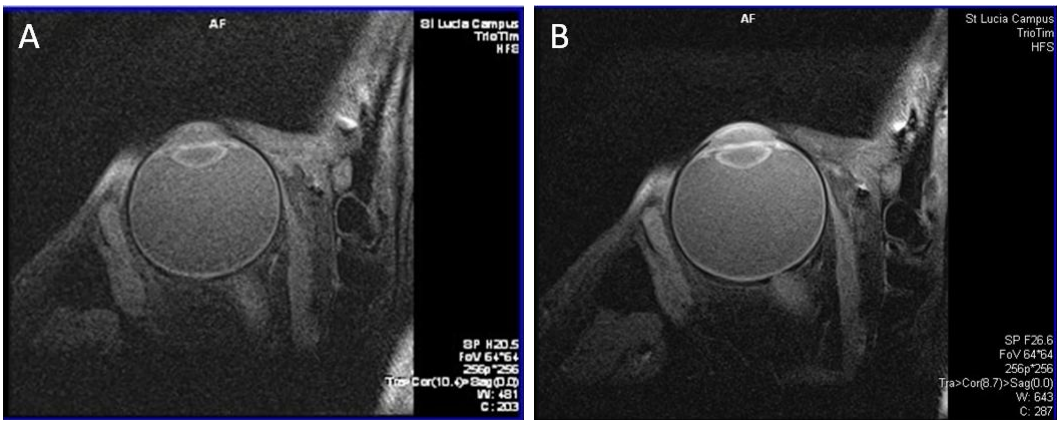

Figure 3:24: Effect of coil position on SNR. a) Poor SNR due to bad positioning of the coil, b) improved SNR when placed close to the eye.

Sagittal and transverse-axial 2-dimensional images were acquired using a multi slice turbo spin-echo (TSE) imaging sequence and 3-dimensional images using a Half-Fourier-Acquisition Single-Shot Turbo Spin-Echo (HASTE) sequence. A transverse axial single slice multi-spin echo sequence was also used to acquire T2 map data for determining the refractive index distribution through the crystalline lens (Jones et al., 2005). The cross section through the eye was displayed on a computer monitor.

Two radiofrequency pulses, one excitation (90) and one refocussing (180) pulse, generates a spin echo. The basic difference between conventional spin-echo, turbo spin-echo, and HASTE sequences is the use of multiple-echo sequences. K-space is the Fourier transform of the MR image measured. Conventional spin-echo sequences acquire one echo that contains information relating to only one line of K-space data, for each TR interval. Fast spin-echo sequences use a number of additional 180° pulses (known as the echo-train length) to produce additional spin echoes that represents more lines of K-space data for each TR interval. The HASTE sequence is a single-shot version of fast spin-echo in which a half-Fourier acquisition is used to allow acquisition of slightly greater than one half the K-space data during one TR interval. This reduces the number of 'phase-encoding' steps by nearly a factor of two, further reducing overall image acquisition times and making HASTE relatively resistant to magnetic susceptibility and motion artefacts.

Pilot testing was performed to determine the extent to which image artefacts arise from the various parameters and an optimised protocol was followed through the experiments/data collection Table 3.5. The standard imaging protocol started with fast localiser scans (also known as scout or survey images) obtained in three orthogonal planes in few seconds. A localiser scan determines where the imaging slices should be placed to image the anatomical structures of interest. Multi-slice fast spin echo (FSE) images (64 mm FOV; 256 × 256 matrix; 2mm slice thickness (no gaps); TR = 4000; TE=16; echo train length 12, imaging time 128 s) in both axial and sagittal planes were acquired. Following this, a T2-weighted HASTE sequence to generate 3D isotropic images of the eye with 0.5 mm cubic voxels (128 × 128 × 64 matrix; TR = 2500; TE=56; imaging time 4 min) was employed. Finally, a single slice axial multi-echo spin echo sequence (64 mm FOV; 256 × 256 matrix; 2 mm slice thickness; TR = 2000; 4 echos: TE=12.5/25/37.5/50; imaging time 4.5 min) was used to acquire data for calculating the refractive index distribution through the lens. The slice was placed through the symmetry axis of the lens, using the centre slice from the sagittal FSE images for positioning.

A diverging lens was then placed over the eye in order to stimulate accommodation (5D) and the subject was asked once again to focus on the target image. The sagittal FSE and multi-echo spin echo images were repeated with accommodation.

Images obtained from series 6 Spin Echo to determine refractive index distribution and from series 8-9 with accommodation were not used as part of this thesis.

Table 3.5: Imaging protocol

	Type	Orient.	Slice Thick	No. Slices	Slice Space	FOV	Matrix	TR	TE	FAT SAT	No. Avg	Image Time
1 & 2	Localisers											
3	TSE (ETL=12)	Axial	2 mm	15	Nil	64 mm	256×256	4000	16	Y	1	2min 8s
4	TSE (ETL=12)	Sagittal	2 mm	15	Nil	64 mm	256×256	4000	16	Y	1	2min 8s
5	3D HASTE	Axial	0.5 mm	64	Nil	64 mm	128×128	2500	56	Y	2	4min 2s
6	Spin Echo	Axial	2 mm	1	N/A	64 mm	256×256	2000	12.5/25/37.5/50 ms	Y	1	4min 32s
7	Localiser											
8	TSE (ETL=12)	Sagittal	2 mm	15	Nil	64 mm	256×256	4000	16	y	1	2min 8s
9	Spin Echo	Axial	2 mm	1	N/A	64 mm	256×256	2000	12.5/25/37.5/50 ms	Y	1	4min 32s

3.5.6.3 MRI image analysis

MRI data were analysed using custom written MATLAB® (Mathworks, Natick, MA) software. An analysis hierarchy pipeline is shown as a flowchart in Figure 3:25. The major steps were:

1. Image alignment to get the eye parallel to the z-axis,
2. Retina segmentation to extract retina boundaries, and
3. Data fitting to estimate the vertex radius of curvature and asphericity.

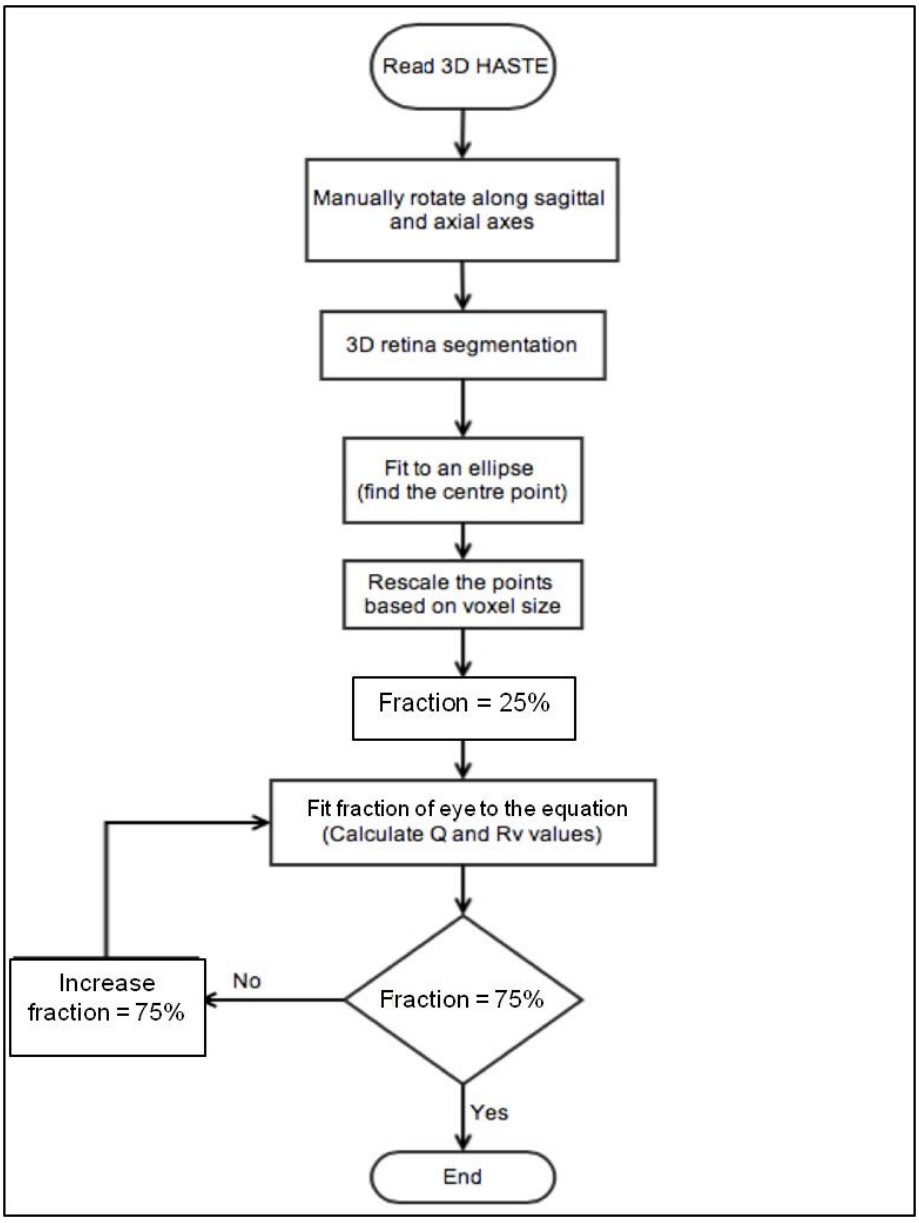

Figure 3:25: Data processing pipeline for MRI.

Image alignment

It was not possible to identify the fovea, because of insufficient resolution of the MRI images. Images were aligned to the estimated foveal position by rotating them in two phases.

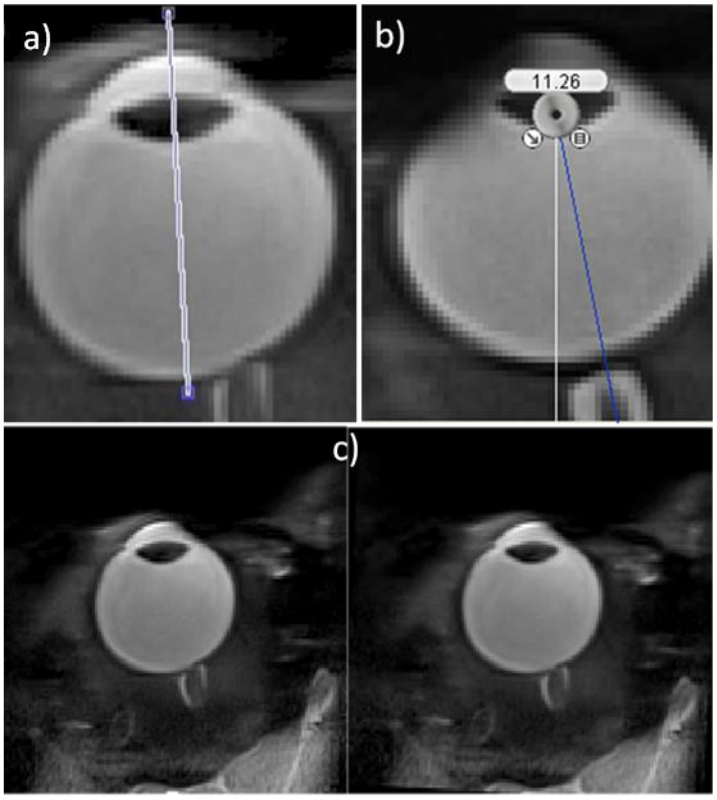

Figure 3:26: Image rotation in a) step 1 towards optical axis, b) step 2 rotation from optical axis to approximate visual axis, and c) comparing before (left) and after rotation (right).

In the first phase, the sagittal and axial views of the 3D HASTE were rotated. In the sagittal view, a line passing through the estimated centres of curvatures of the cornea and lens, and to the retina, was drawn. Based on the posterior pole of the lens (near posterior nodal point of eye) an image was rotated so that this "optical axis" was aligned vertically. Each slice of the image was rotated using a bi-cubic interpolation technique. The rotated data were transferred to the "transverse axial" view and the same procedure was repeated for horizontal alignment (Figure 3:26a).

In the second phase, using the axial view, the HASTE image was rotated from the optical axis to the approximate visual axis. The optic nerve should be approximately 15º nasal to the fovea, with the optical axis lying between them. The optic nerve was visible in all images and the angle subtended between the optic nerve centre and the optical axis at the posterior nodal point (back of the lens) was determined for 20 participants using a 'screen protractor' (Figure 3:26b). The values ranged from 11.25º to 11.75º (average 11.5º). Thus, the fovea was taken to be 3.5º from the optical axis. Accordingly, all images were rotated an additional 3.5º for analyses relative to the visual axis (Figure 3:26c).

Retina segmentation

The retinal boundary was segmented in each slice and the results were incorporated in a 3D matrix. To segment the retina, a Canny edge detection algorithm with large threshold value was applied using the MATLAB Image Processing Toolbox. The edge detection routine picks up the transition between voxels that are purely vitreous to those that are solely in the sclera. The dimensions of the (cubic) voxels in 3D HASTE images are 0.5 mm. Since the retina and choroid are ~0.2 mm thick, edge voxel extend from the vitreous, through the retina and choroid and into the sclera. The edges found are therefore most likely to be approximately mid-way between the vitreous/retinal boundary and the choroid/sclera boundary.

The retinal boundary was separated from the rest of the detected edges by applying morphological filters about the approximate size and shape of retina (any small object having boundary voxels less than 100 was removed). Additionally, advanced segmentation technique, "active contour" was applied when low contrast to noise ratio or other artefacts limited the conventional edge detection accuracy. The active contour method uses an initial curve and tries to minimise the total gradient of the curve.

In order to decrease the influence of partial volume effects, the retina was segmented in all three planes (axial, sagittal and coronal). All the acquired boundary points concatenated to build a big N×3 matrix in the coordinate system, where N

denotes the number of segmented voxels. Figure 3:27 shows the steps followed in segmentation.

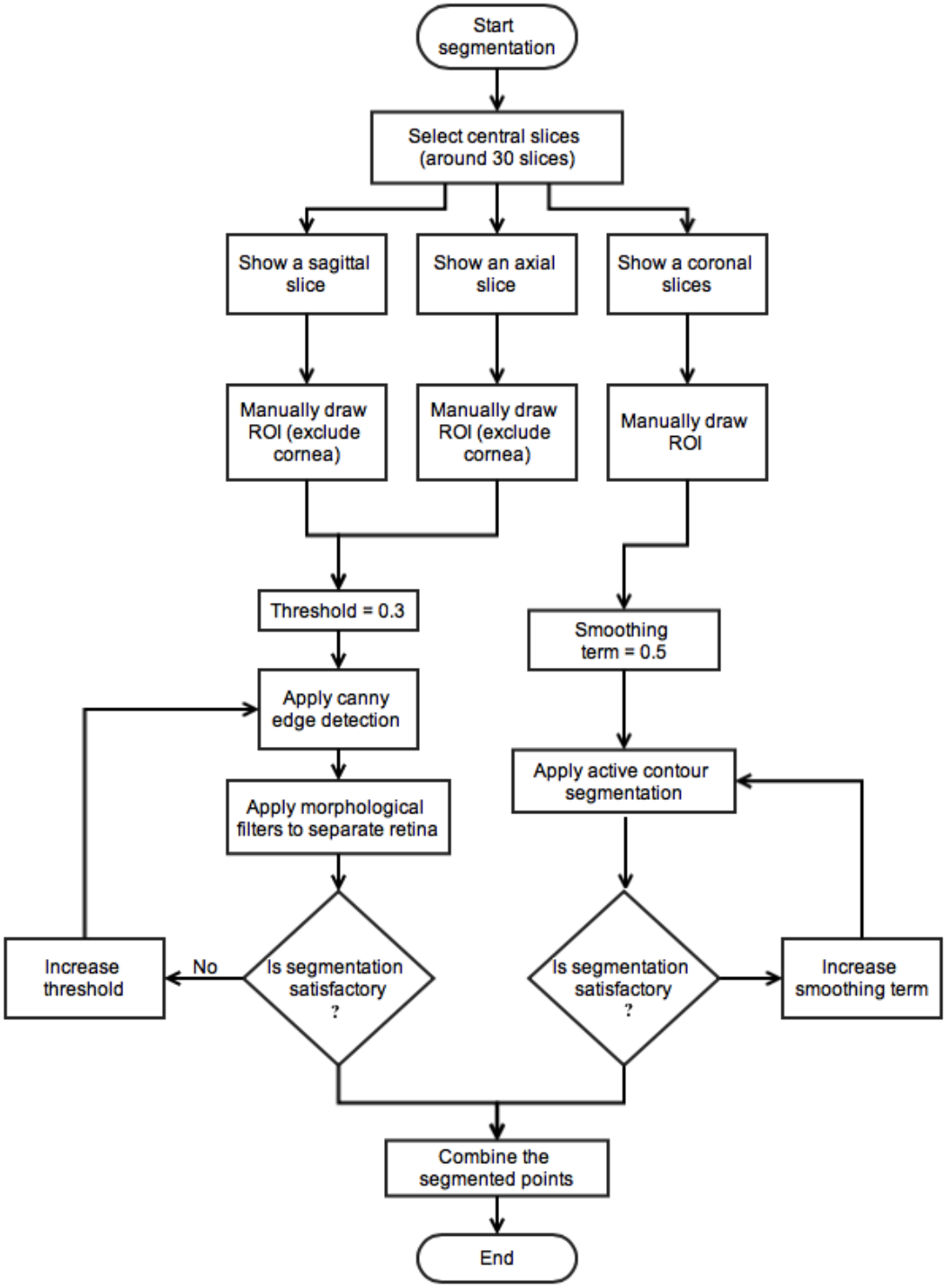

Figure 3:27: Image segmentation pipeline for MRI.

Data Fitting

The coordinates of the back of the eye were found by exploring the extreme point in the slice that contains the central plane of the eye. The transformation vector was calculated by subtracting the coordinate vector, representing the back of the eye, from that representing the origin of the coordinate system (0, 0, 0). The biggest area inside the retina was picked as the centre slice. This was used to find the reference point (the lowest point in the segmented image). Before data fitting, the centre slice, centre point, and back reference point were "sanity-checked" by visual inspection to ensure they were chosen sensibly without outlier voxels (Figure 3:28a) and a 3D reconstruction of the eye was shown for the same purpose (Figure 3:28b). Such outliers occur when the edge detection algorithm identifies other signal sources (e.g. muscles) mistakenly as the retinal boundary.

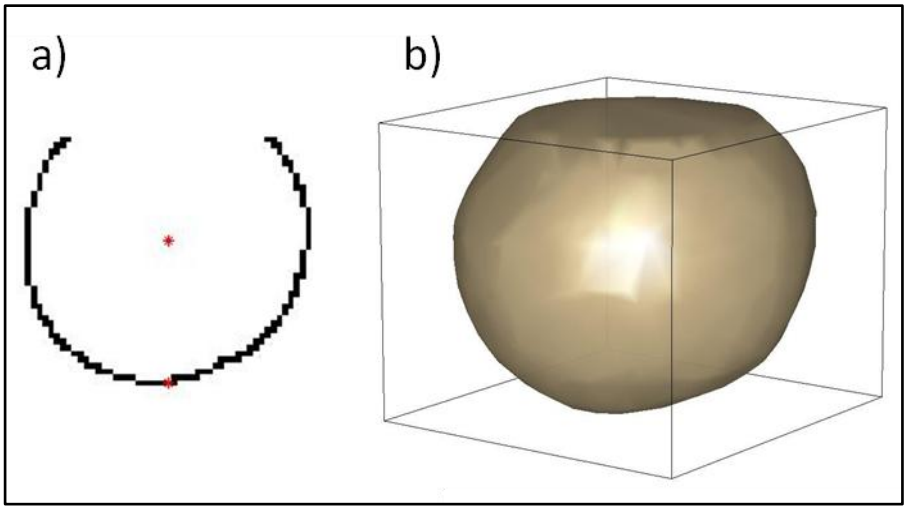

Figure 3:28: Sanity checking in MRI processing. a) Centre point and the point representing the back of the eye. b) Shape of the eye.

The vertex radius of curvature and asphericity were determined for 11 different fractions of the eye (F) ranging from F=25% to F=75% in 5% steps. To determine the vertex radius of curvature and asphericity of the desired fraction, the centre point of the eye (i.e centre point of the ellipse) was calculated by fitting the segmented boundary points of the retina to an ellipsoid and the desired fraction was extracted by masking the unwanted area. All the selected voxels were arranged into an N×3 matrix, representing the retinal points and the data were fitted to the equation:

$$C_x^2X^2 + C_y^2Y^2 + C_z^2Z^2 - 2C_zZ = 0 \quad (31)$$

which is equivalent to equation (7), with $C_x = 1/R_x$; $C_y = 1/R_y$ and $C_z = 1/R_z$. Using these, vertex radius of curvatures $R_{xv} = R_x^2/R_z$ and $R_{yv} = R_y^2/R_z$ and asphericities $Q_x = R^2_x/R^2_z - 1$ and $Q_y = R^2_y/R^2_z - 1$ in the XZ and YZ planes, respectively, were determined (equations (8-11) in section 2.4.2.1).

The percentage was defined from the reference point. For example it was 100% when the results were obtained from the reference point to the top most point (complete eye). Figure 3:29 shows the smallest and biggest fractions of the eye that have been used for determining the retinal shape estimates with MRI. The 100% in angular notation equals 180º about the centre point of the eye on each side of the axis and 50% means 90º out of 180º. The coefficient of determination (R^2), the square of the correlation between the co-ordinates and their fitted values were used to evaluate the goodness of fit.

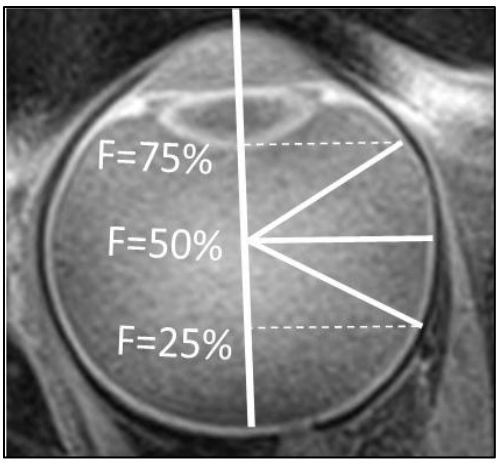

Figure 3:29: Fractions of eye (F) used to determine retinal shape estimates with MRI, the maximum being 75% and the minimum being 25%. Angle subtended at centre of eye for various fractions are show in Table 3.6.

Area (% fraction) can be converted to angles from

Area of sphere = $4\pi R^2$ (where R is radius of circle) (32)

Area covered by angle $\theta_1 = 4\pi R^2[1 - \cos(\theta_1/2)]$ (33)

For example, to find the angle associated with 25% of the area of the eye, the area of the retina, equations (32) and (33) gives $\theta_1 = 2.094$ radians or 120º. Table 3.6 shows

the angle θ_1 (as defined in Figure 3:30) which corresponds to any given fraction of the eye.

Table 3.6: Angle subtended at the centre of the eye in degrees (θ_1 in Figure 3:30) corresponding to % fraction of the eye.

Fraction %	θ_1 (degrees)
25%	120
30%	132.8
35%	145.1
40%	156.9
45%	168.5
50%	180
55%	191.5
60%	203.1
65%	214.9
70%	227.2
75%	240

To get the best comparison between MRI and PCI -derived retinal shapes, it is desirable to compare similar regions. PCI eye length measurements were obtained out to ±35º (central 70º), where this angle is referenced to the centre of curvature of the cornea which is conveniently close to the posterior nodal point and posterior lens vertex. With reference to Figure 3:30, the tangents of the angles θ_1 and θ_2 subtended at the centre of the eye and posterior nodal point, respectively, to give the same retinal region are related to the corresponding distances by

$$\theta_1 = 2\tan^{-1}[l_2/l_1 \tan(\theta_2/2)] \qquad (34)$$

where the distance l_2 for the PCI data is approximately related to the axial length L by

$$l_2 = L - 7.8 \qquad (35)$$

For 60 participants, θ_1 was estimated to range from 116º to 136º (mean ± SD = 124º ± 5º) for θ_2 = 70º. From equation (33), this corresponds to a retinal area of 27%. This is about the minimum fraction of the eye that was analysed with MRI (25%).

MRI data corresponding to less than 35% resulted in noise in a few data sets because the fitting ran up against the lower bound of 0.01 mm^{-1} that was placed on C_z. The decision was made to use 35% of the MRI data for the comparison with PCI.

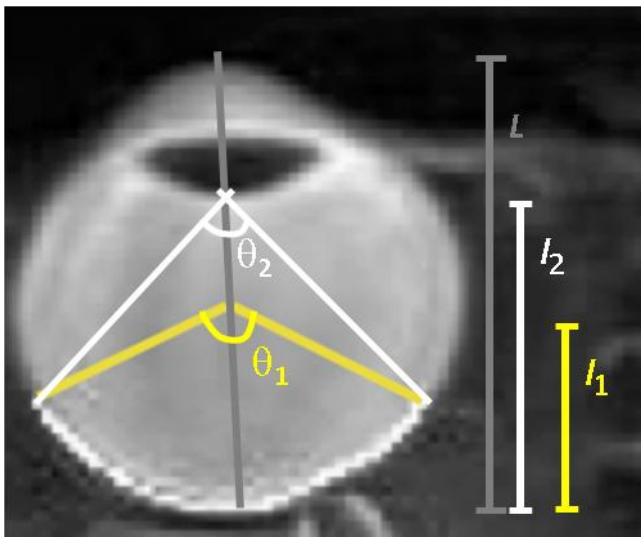

Figure 3:30: Angles and distances to calculate similar regions with PCI and MRI . θ_1 and θ_2 are the angles subtended approximately at the centre of eye (MRI) and at the posterior lens vertex (PCI), l_1 and l_2 are the corresponding distances, and L is the axial length of the eye obtained from the Lenstar.

3.5.7 OPTICAL MODELLING FOR RETINAL SHAPE ESTIMATION

Development of retinal shape estimation involved modelling which was done in three Stages of increasing sophistication (Stages 1, 2, and 3 to be described below), with the expectation that the retinal shape estimation would improve at each successive Stage. Each Stage used the central and peripheral eye lengths measured with the Lenstar. The Lenstar determines the position of the retinal epithelium, and to match with the IOLMaster its default axial length is determined by subtracting 200 μm assumed to be the distance from the retinal pigment epithelium (RPE) to the internal limiting membrane (ILM). Although the user interface allows the ILM to be accurately located in most cases, I have added the 200 μm to the axial length determination. This is because the position of the photoreceptors, rather than the internal limiting membrane, is important when considering visual function and

because the positions obtained with MRI are likely to be closer to the RPE than to the ILM (section 3.5.6.3).

The Le Grand full theoretical eye consisting of anterior and posterior surfaces for the cornea and lens was used as the basic eye model (Table 3.7). Using the assumption that the Lenstar beams strike the anterior cornea normally, rays were direct towards the point on the axis corresponding to the sagittal centre of curvature of this surface. Ray-tracing was done into the eye to estimate retinal co-ordinates. Using a solver template in Excel, these were fitted to a conic equation

$$f = \frac{c(x - x_0)^2}{1 + \sqrt{1 - (1 + Q)c^2(x - x_0)^2}} - \frac{cx_0^2}{1 + \sqrt{1 - (1 + Q)c^2 x_0^2}} \qquad (36)$$

where c is the vertex curvature of the retina, Q is asphericity, x is measured values along the X-axis (or Y-axis where appropriate) and x_0 is an offset so that the fovea has co-ordinates (0, 0).

A column of theoretically predicted values was created by setting the initial values of the variables in the fitting equation. The difference between the predicted and real value was squared and summed over all data points (SS). The Solver was set to manipulate the values of the formula variables to achieve the minimum of SS, thus plotting the best fit to those points. To measure the strength of a linear association between the real and the predicted variables, the Pearson correlation coefficient (R) was calculated between the predicted and real coordinates provided in two columns and then squared (R^2).

In Stage 2 modelling, for the fit to resemble the way MRI fits were done, analysis was repeated with $x_0 = 0$. The retinal shape estimates of R_v and Q were not significantly different between the cases where $x_0 = 0$ and $x_0 \neq 0$ ($p > 0.05$), so Stage 2 and 3 analyses were done only with $x_0 = 0$.

Apart from the three Stages of PCI, retinal shape was also estimated using Dunne's method which is based on peripheral refraction (see section 2.4.2.8 and below). Equation (36) was used for fitting with $x_0 \neq 0$. x_0 values across horizontal and vertical meridians and for all participants ranged from –0.97 to 0.82 (mean ± SD: –0.13 ± 0.33 degrees). Considering that the x_0 values were small and of little consequence, re-analysis with $x_0 = 0$ was not done.

The fits obtained with PCI and Dunne's method were compared with the fit obtained from magnetic resonance imagery (sections 4.4 and 4.5). See section 3.5.8 for a refinement of the comparison. The retinal region for Dunne's method would approximately match that for PCI, that is, 27%.

Table 3.7: Parameters of Le Grand full theoretical eye

Medium	n	R (mm)	D (mm)	Surface power (D)
Air	1			
		7.8		48.346
Cornea	1.3771		0.55	
		6.5		–6.108
Aqueous	1.3374		3.05	
		10.2		8.098
Lens	1.42		4.00	
		–6		14.000
Vitreous	1.336		16.59655	
Axial length			24.19655	

Stage 1 uncustomised without deviation

The beam incident on the eye model was assumed to be undeviated. The only part of the Le Grand eye that was used was the anterior corneal surface (spherical with radius of curvature of 7.8 mm). Equations to determine the retinal co-ordinates relative to the fovea for a ray subtending an angle θ to the axis were based on the treatment of Atchison and Charman (2011). Relevant parameters are given in Figure 3:31.

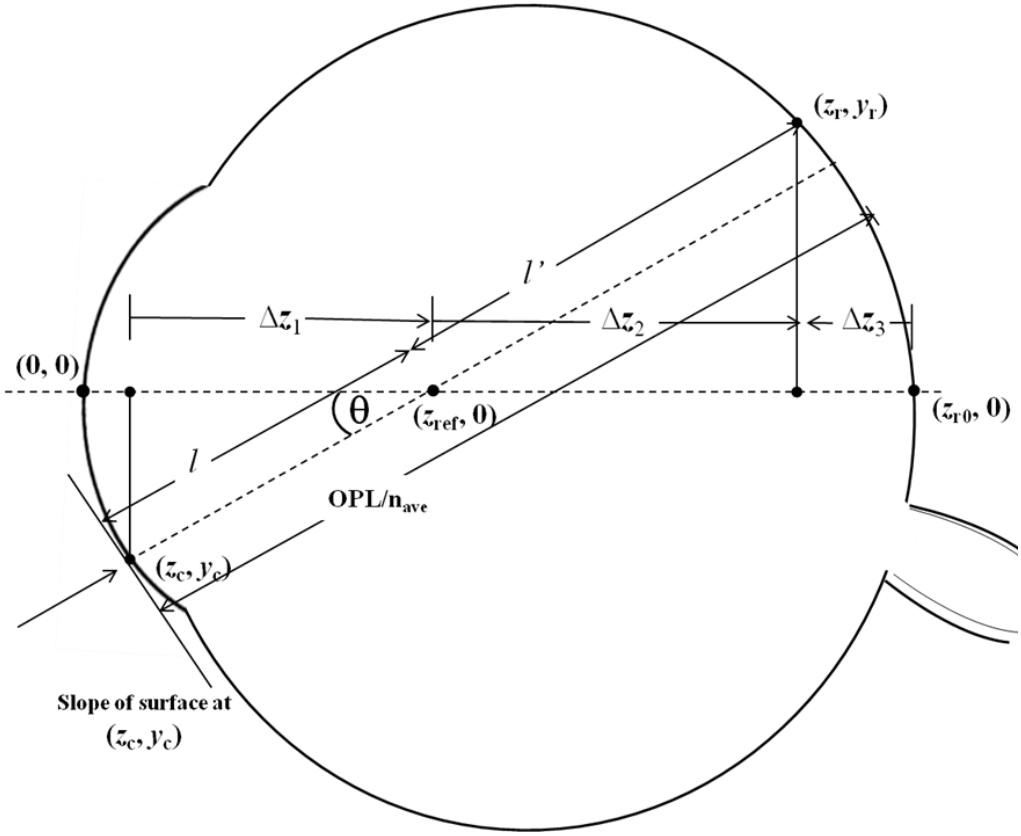

Figure 3:31: Parameters used for determination of retinal co-ordinates in Stage 1 modelling.

Considering the y-z section, the equation for cornea surface points (z_c, y_c) is given by

$$y_c^2 + (1 + Q_c)z_c^2 - 2z_c r_{cv} = 0 \quad (37)$$

where r_{cv} is the vertex radius of curvature and Q_c is asphericity. A solution for z_c in terms of θ is

$$z_c = r_{cv}\frac{1+\tan^2\theta(1+Q_c) - \sqrt{1+\tan^2\theta(1+Q_c)}}{(1+Q_c)[1+\tan^2\theta(1+Q_c)]} \quad (38)$$

while y_c is given by

$$y_c = \sqrt{[2z_c r_{cv} - (1 + Q_c)z_c^2]} \quad (39)$$

The distance of the normal from the surface point to the reference point on the axis is the sagittal radius of curvature r_s given by

$$r_s = \sqrt{(r_{cv}^2 - Q_c y_c^2)} \quad (40)$$

The distance from the corneal vertex to the reference centre z_{ref} is given by

$$z_{ref} = r_s\cos\theta + z_c \quad (41)$$

The distance from the axial point, corresponding to the sag of the anterior cornea, to the reference centre, is

$$\Delta z_1 = z_{ref} - z_c \quad (42)$$

The distance of the assumed raypath before the reference point is

$$l = \sqrt{\Delta z_1^2 + y_c^2} \quad (43)$$

The distance of the assumed raypath *l*' after the reference point is related to *l*, the total optical path length *OPL*, and the average refractive index n_{ave} by

$$l' = OPL/n_{ave} - l \quad (44)$$

The axial and height components of the retinal position corresponding to *l*' are

$$\Delta z_2 = l'\cos\theta \qquad y_r = l'\sin\theta \quad (45)$$

Where y_r is the determined retinal co-ordinate for height. The determined horizontal position of the retinal co-ordinate, relative to the on-axis retinal position (z_{rv}, 0) is

$$\Delta z_3 = -(z_{rv} - z_{ref} - \Delta z_2) \quad (46)$$

Here z_{rv} is given by pathlength OPL_0/n_{ave}, where OPL_0 is the on-axis optical pathlength.

Simplification is possible for a spherical cornea ($Q_c = 0$) in the present case. As the Lenstar gives eye length measurements, ignoring the refractive indices of the ocular media and conversion to optical path lengths, the equations (37) to (46) can be replaced by the following equations

$$y_r = (PEL - r_{cv})\sin\theta \quad (47)$$

$$\Delta z_3 = r_{cv}(1 - \cos\theta) + PEL\cos\theta - AL \quad (48)$$

where *AL* and *PEL* and are the on-axis and off-axis eye lengths.

Stage 2 uncustomised with deviation

No customisation of the Le Grand full theoretical eye was used (as for Stage 1), but deviation was allowed to occur at surfaces except at the anterior cornea. Relevant parameters are given in Figure 3:32.

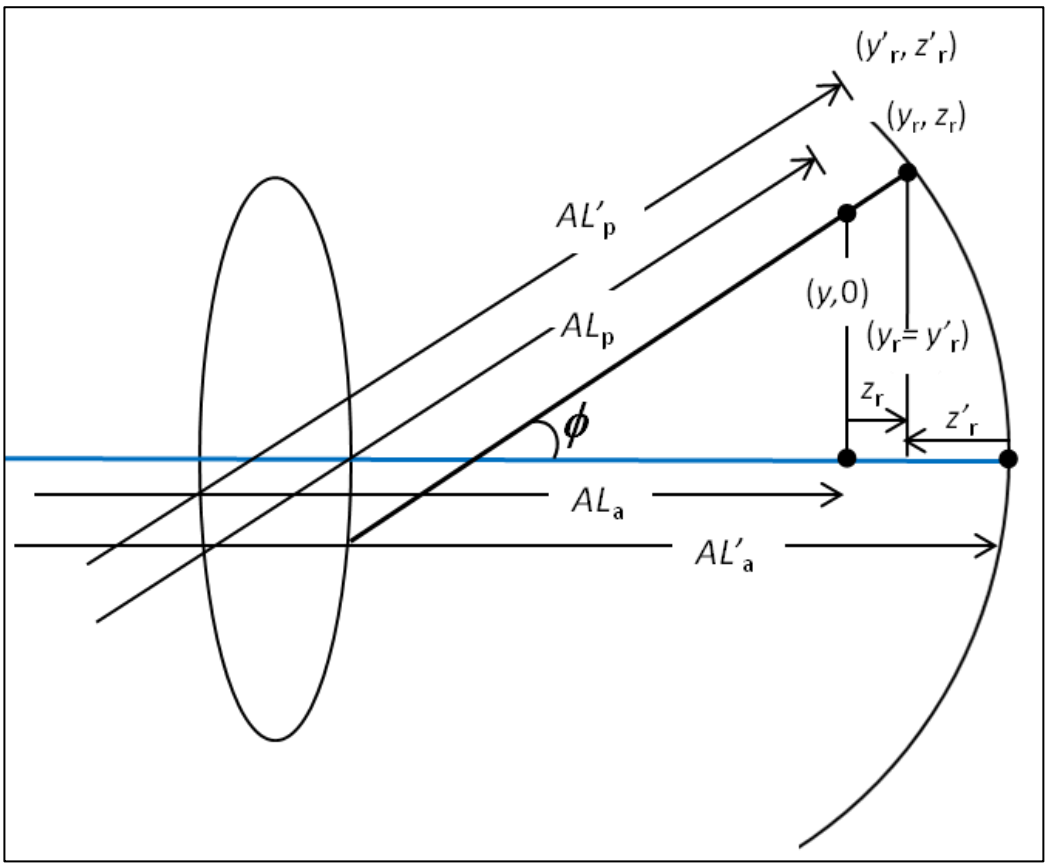

Figure 3:32: Parameters used for determination of retinal co-ordinates in Stage 2 modelling.

Raytracing was done using the optical design program Zemax (version 10.0, July, 2011). As the Lenstar operates at 820 nm, the refractive indices in Table 3.7 for the visible are inappropriate. Assuming that these apply at 555 nm and using Table 5 of Atchison and Smith (2005) with appropriate scaling, the refractive indices at 820 nm are n_{corn} 1.3707, n_{aq} 1.3312, n_{lens} 1.4134, and n_{vitr} 1.3298. Note that these are phase indices and are lower than the corresponding group indices given in Table 3.1.

The first surface was a small stop, corresponding to the centre of curvature of the cornea, followed by the anterior surface of the cornea at –7.8 mm from the stop,

and then the other refracting surfaces. For each object angle, raytracing was done through the stop centre, with variation in position of a flat retina, until retinal co-ordinates corresponded to measured peripheral eye lengths.

For an object angle θ and for a Le Grand model eye with axial length AL_a and a flat retina, in Zemax, peripheral length AL_p, image angle ϕ and retinal co-ordinates (y, 0) were determined by ray-tracing.

For an eye with measured peripheral length AL'_p, the retinal co-ordinates (y_r, z_r) are

$$(y_r, z_r) = (y + (AL'_p - AL_p)\sin\phi,\ 0 + (AL'_p - AL_p)\cos\phi) \quad (49)$$

If the central axial length is measured as AL'_a rather than the AL_a, of the basic eye model, the retinal co-ordinate changed to new retinal co-ordinates (y_r', z_r'),

$$(y_r', z_r') = (y_r, z_r - (AL'_a - AL_a))$$

$$= (y + (AL'_p - AL_p)\sin\phi,\ (AL'_p - AL_p)\cos\phi - (AL'_a - AL_a)) \quad (50)$$

Stage 3 customised

Many Le Grand full schematic eye components were replaced with individual eye data: the anterior corneal topography (average of four images imported from Medmont corneal topography), the posterior cornea radius of curvature (from Pentacam topography, spherical surface used by averaging across the meridians), anterior and posterior lens radii of curvatures (phakometry), equivalent lens refractive index (phakometry), and intra-ocular axial distances within the eye (Lenstar).

It was assumed that the on-axis measurement with the Lenstar corresponded with the corneal topographic axis and thus images were not tilted or decentred. A custom built MATLAB (Mathworks) program in combination with Zemax was used to produce a variable corneal "sagittal centre of curvature" as the stop and first surface to ensure no deviation at the first surface. This used calculation of the surface slope at various positions on the surface.

The MATLAB program read the measurements of anterior corneal topography taken using Medmont and created a mean Grid sag surface. After loading the anterior

corneal surface as a Grid sag surface, the rest of the model was created in Zemax from participant data. A chief ray was traced from a distant object in the field to an aperture (1st surface, diameter 2 mm) and then to the anterior corneal surface (Grid sag surface). The (negative) distance of the anterior cornea from the stop was altered in a loop until the difference between the cosine of the field angle and the Z cosine of the ray at the surface was ≤ 0.0001. Relevant parameters are given in Figure 3:33.

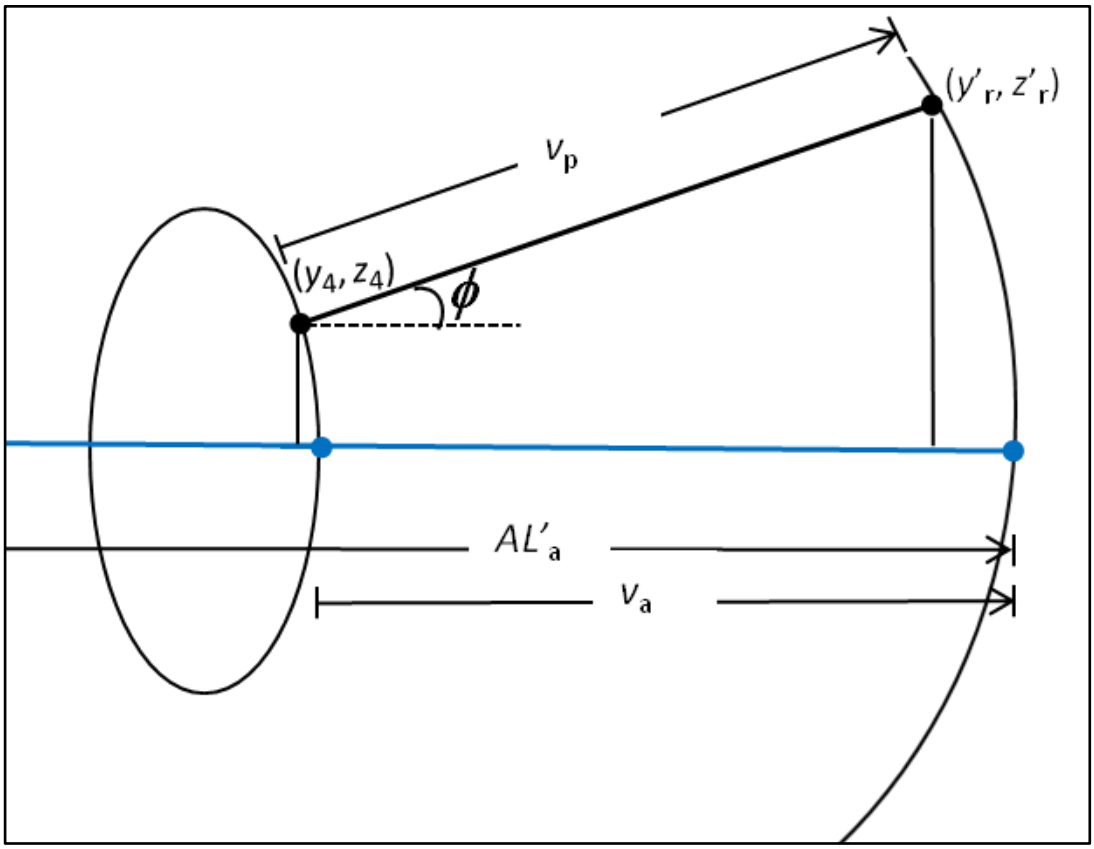

Figure 3:33: Parameters used for determination of retinal co-ordinates in Stage 3 modelling.

The on-axis vitreous length is estimated as

$$v_a = AL'_a - (CCT_a + ACD_a + LT_a)$$

where AL'_a is the on-axis length as in Stage 2 and CCT_a, ACD_a and LT_a are on-axis distances within the cornea, anterior chamber and lens.

The peripheral vitreous length is estimated as

$$v_p = AL'_p - (CCT_p + ACD_p + LT_p)$$

where AL'_p is the peripheral length as in Stage 2 and CCT_p, ACD_p and LT_p are peripheral distances within the cornea, anterior chamber and lens.

Using the image space angle ϕ, the off-axis retinal co-ordinates (y_r', z_r') are given by

$$z_r' = v_p \cos\phi + z_4 - v_a \quad (51)$$

$$y_r' = y_4 + v_p \sin\phi \quad (52)$$

where (z_4, y_4) are the co-ordinates of the chief ray at the posterior lens surface (relative to its vertex).

As a check, using a 7.8 mm spherical corneal surface (Le Grand model eye) as a Grid sag surface gave the same results as for Stage 2.

Dunne's method

Dunne's method has been described in section 2.4.2.8. A version of a program kindly provided by Dr. Dunne was revised to apply the method.

Essentially, this method modifies a three surface model eye according to measured internal ocular distances and the anterior corneal radius of curvature. Out-of-the-eye ray-tracing was done at each visual field angle for the meridian of interest. The corneal asphericity for each visual field angle is manipulated until the peripheral astigmatism matched its measurement for a retina with a (–)12 mm radius of curvature. Retinal radius of curvature for each angle, and consequently retinal co-ordinate intersection with the chief ray, were altered until the sagittal refraction matched its measurement (refraction at right angles to the visual field meridian). Equation (36) was applied to the set of retinal co-ordinates to obtain a conic fit.

Some other points in the procedure will be mentioned. From the radii of curvature along the principal meridians of the anterior cornea, the sagittal refraction components (along the vertical/horizontal meridian for the horizontal/vertical field) were modified to compensate for any on-axis astigmatism. The Gullstrand-Emsley eye indices, rather than those of the Le Grand eye used for PCI, were retained: 4/3 for the aqueous and vitreous and 1.416 for the lens. As mentioned in section 2.4.2.8,

the curvatures of the lens surfaces were selected to give the correct refraction while their ratio matched those of the lens in the Gullstrand-Emsley model eye.

3.5.8 COMPARISON OF RETINAL SHAPE ESTIMATES

The retinal shape was estimated in terms of vertex radius of curvature and asphericity along horizontal and vertical meridians using MRI and PCI methods as described in section 3.5.6.3 and 3.5.7.

The vertex radius of curvature (R_v) and asphericity (Q) result from fitting an aspheric surface to a number of points on the retina. These parameters are not independent of each other; for example a positive change in Q can compensate for a positive change in R_v. In addition, both MRI and PCI methods of retinal shape estimation differ in many aspects like the resolution, data acquisition and analysis, and as the data are obtained from same participants, it is important to have a common tool to compare R_v and Q together. For this reason, the estimated parameters along each meridian were combined to form a "surface shape". Substituting values for c ($1/R_v$) and Q in equation (36), retinal surface shapes for each participant along both meridians obtained from PCI and MRI methods were re-constructed in MATLAB. A similar method is used in optics to determine the surface accuracy i.e. the measurement of the deviation between the actual shape and the intended shape of an optical surface (Christophe, 1971). The comparison was made by taking the average of point-by-point height differences between the two surfaces over a fixed distance of 15.6 mm (15.6 mm = 7.8 mm either side from peak/centre or absolute maximum height of the curve) and giving this as a percentage of the sagittal heights across the distance:

$$Percentage\ difference = \frac{\frac{\sum_{i=1}^{n}\left|z_{i,PCI}-z_{i,MRI}\right|}{N}}{0.5\times(sag_{PCI}+sag_{MRI})}\times 100\% \qquad (53)$$

where $z_{i,PCI}$ and $z_{i,MRI}$ are the z-coordinates for the ith point using the PCI and MRI fits, respectively. sag_{PCI} and sag_{MRI} are the sagittal heights of the PCI and MRI fits, respectively, and N is the number of sampled points (1561). Figure 3:34 shows the surface shape comparisons for one participant.

Considering that it is more appropriate to compare surface shapes rather than comparing vertex radius of curvature and asphericity separately, conclusions on agreement of retinal shape estimates between MRI and PCI in Chapter 4 were based on this approach.

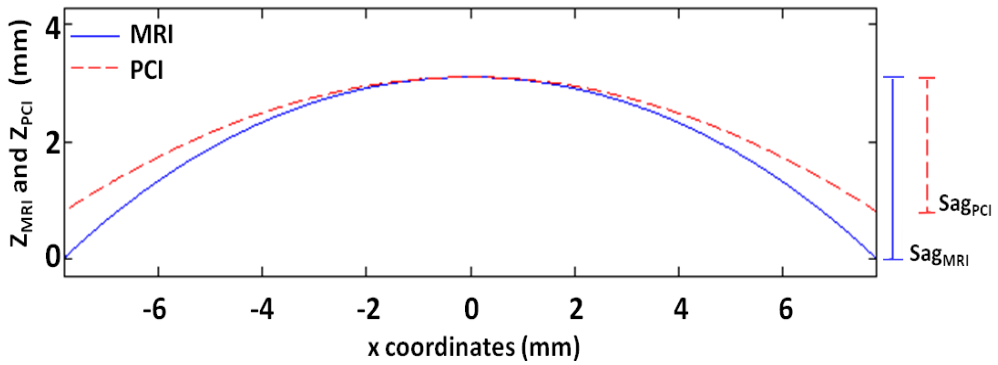

Figure 3:34: Retinal surface shapes for MRI and PCI for one participant. The blue solid line and the red dotted lines represent MRI and PCI methods, respectively.

The percentage difference approach does not indicate if one surface shape is consistently flatter than another. Therefore, the areas under the surface shapes were compared. To determine areas, the region under surface shape was divided into multiple narrow rectangles, of width 0.01 mm, whose areas were added. The two surface shapes started from the same vertex and the areas under the two surface shapes were calculated with reference to the surface shape that had the greatest sag. For example, in Figure 3:34 the reference is the MRI surface shape (blue solid line) and the area under the flatter PCI surface shape (red dotted line) is greater than the area under the MRI surface shape.

Chapter 4- Validation of Partial Coherence Interferometry Instrument for Estimating Retinal Shape

Magnetic resonance imaging (MRI) is considered as a standard for estimating retinal shape because it images the physical dimensions of retina/eye. Partial coherence interferometry has been used to determine retinal shape but there are some assumptions in its use, such as the refractive index used to convert from optical path lengths to distances and deviation of beams inside the eye, and it has not been assessed for accuracy against MRI.

This chapter describes a validation experiment, where comparisons were made for retinal shape estimates determined from partial coherence interferometry and magnetic resonance imaging to address the first thesis aim: "to determine the reliability of a simple method of determining retinal shape using off-axis partial coherence interferometry, and to validate this method by comparing the results to that of magnetic resonance imaging" and its associated hypothesis 1: "retinal shape can be accurately predicted by measuring off-axis eye lengths with a commercial partial coherence interferometry instrument". The aim was partly addressed in section 3.5.5 where the repeatability of PCI instruments was assessed. There it was decided to use the Lenstar with eye rotation to change fixation, because the instrument demonstrated excellent intra and inter-sessional reliability (section 3.5.5.2) and eye rotations did not influence measurements (section 3.5.5.3).

The chapter is divided into 6 sections. Section 4.1 is an overview of methods. Section 4.2 describes the influence of image rotation of MRI images on retinal shape estimates. The images obtained from MRI had poor resolution and it was not possible to identify the fovea. To align the images to the estimated foveal position, all the images were rotated during the analysis in two phases as described in section 3.5.6.3. Section 4.3 gives estimates of lens equivalent refractive index and radii of curvature to be used in Stage 3 modelling of retinal shape estimation. Although strictly these are not needed in this chapter, the section provides useful information on how these parameters are related to refraction. Section 4.4 and 4.5 shows the

comparison of retinal shape estimates between MRI and PCI, and between MRI and Dunne's method. For PCI, the three Stages described in section 3.5.7 will be used. Section 4.6 presents the conclusion as to the best method to be used for estimating retinal shape.

4.1 METHOD

Ninety-four participants were recruited, but MRI was performed only on a subset of sixty participants (30 emmetropes, M = +0.75 D to −0.62 D and 30 myopes, M = –1.25 D to −8.25 D). The mean age of these sixty participants was 22.5 ± 3.1 years with a range of 18 to 28 years; there was no significant difference between ages of emmetropic and myopic participants (p = 0.76). Peripheral eye lengths, peripheral refraction and magnetic resonance imaging (MRI) were obtained according to the protocols given in sections 3.5.5.2, 3.5.4 and 3.5.6.2, respectively.

From peripheral eye length measurements, estimates of vertex radius of curvature (R_{xv} and R_{yv}) and asphericity (Q_x and Q_y) were determined in the three Stages of increasing sophistication described in section 3.5.7. From peripheral refraction, retinal shape estimates were made using Dunne's method described in sections 2.4.2.8 and 3.5.7.

Agreement of retinal shape estimates between the methods was shown by Bland and Altman plots with the mean difference in results and the 95% limits of agreement (LoA). Paired *t*-tests were conducted to determine the significance of mean differences. The parameters R_v and Q along each meridian were combined to form a "surface shape" and agreements between MRI and PCI and between MRI and Dunne's methods were given as percentage differences between surface shapes and as the ratios of areas under the surface shapes (section 3.5.8).

4.2 INFLUENCE OF IMAGE ROTATION ON RETINAL SHAPE ESTIMATES

The images obtained from MRI had poor resolution (0.5 mm) and it was not possible to identify the fovea. To align the images to the estimated foveal position, all the images were rotated during the analysis in two phases as described in section 3.5.6.3. In phase 1, the retinal shape was estimated with reference to the optical axis and in second phase it was re-referenced to the visual axis. Here the effect of re-referencing to visual axis on retinal shape is investigated.

Figure 4.1 shows Bland-Altman plots of vertex radius of curvature for the two phases. For the horizontal meridian, the 95% limits of agreement were –0.36 to +0.48 mm and the mean difference between the phases was +0.06 ± 0.05 mm 95% CIs ($p = 0.02$). For the vertical meridian, the 95% limits of agreement were –0.52 to +0.28 mm and the mean difference between the phases was –0.12 ± 0.05 mm 95% CIs ($p < 0.001$).

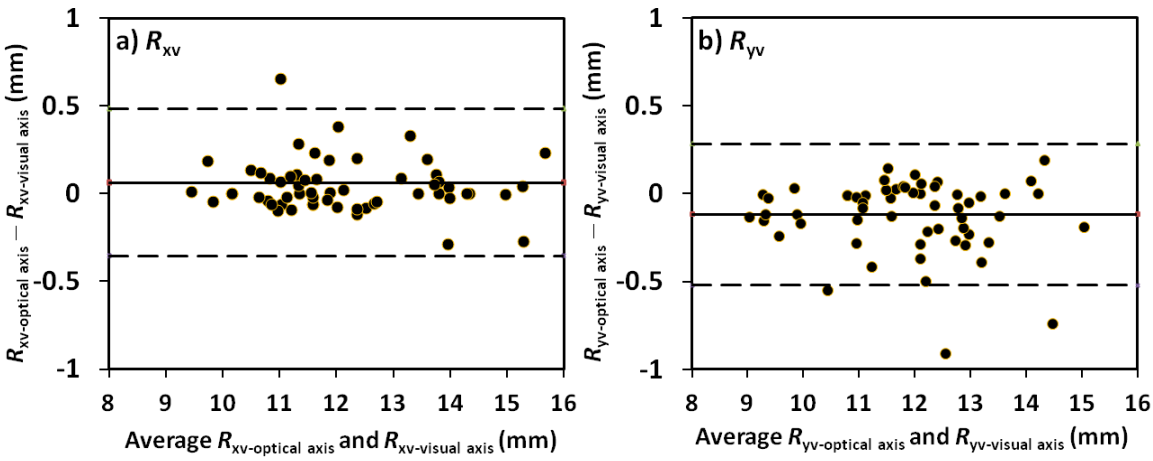

Figure 4:1: Bland-Altman plots of agreement of vertex radii of curvatures between optical axis and visual axis along a) horizontal and b) vertical meridians. The mean difference is shown by the bold line and the 95% limits of agreement are shown by dashed lines.

Figure 4:2 shows Bland-Altman plots of asphericity for the two phases. For the horizontal meridian, the 95% limits of agreement were –0.06 to +0.05 and the mean difference between the phases was –0.01 ± 0.01 95% CIs (p = 0.07). For the vertical meridian, the 95% limits of agreement were –0.12 to +0.07 and the mean difference between the phases was –0.02 ± 0.01 95% CIs (p < 0.001).

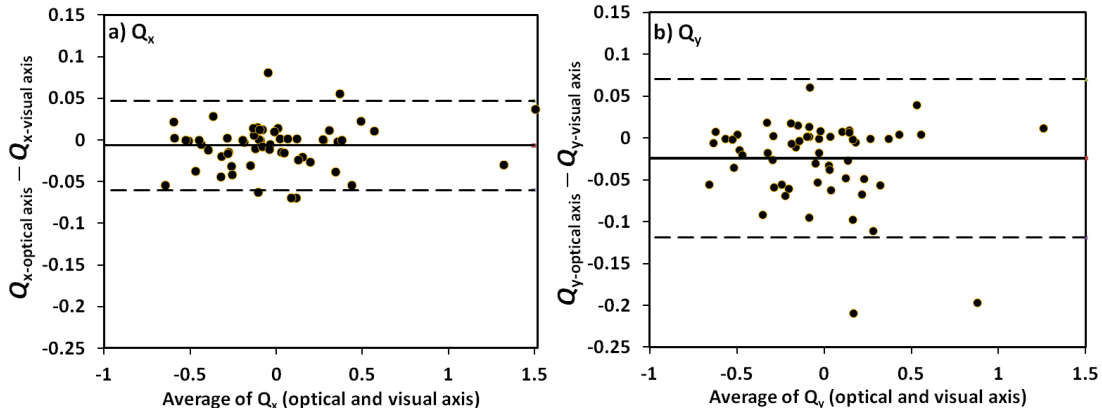

Figure 4:2: Bland-Altman plots of agreement of asphericities between optical axis and visual axis along a) horizontal and b) vertical meridians. The mean difference is shown by the bold line and the 95% limits of agreement are shown by dashed lines.

The goodness of fits (R^2) to the retinal shapes did not change significantly with re-referencing. Mean ± SD of R^2 that were obtained with optical axis as a reference were 0.94 ± 0.04 with a range 0.73 to 0.98. Corresponding values with the visual axis as a reference were 0.93 ± 0.06, with a range 0.68 to 0.98. The mean difference ± SD of R^2 between the two phases was 0.02 ± 0.05. Two participants had R^2 values less than 0.8 and were not included in this analysis.

Although the re-referencing gave significant changes in three of the shape components (R_{xv}, R_{yv} and Q_y), changes were generally small. Furthermore, for the vertical meridian the changes in R_{yv} and Q_y tended to balance.

4.3 PHAKOMETRY

Equivalent refractive index and anterior and posterior lens radii of curvature of lens were obtained from 94 participants, including the 60 participants used for the PCI-MRI and PCI-Dunne's method comparisons in the next section, with the custom built phakometer using the procedure described in section 3.5.3. These parameters were used in Stage 3 modelling (section 3.5.7).

Results for equivalent refractive index, anterior radius of curvature, posterior radius of curvature and lens equivalent power are shown as a function of spherical equivalent refraction in Figure 4:3, 4:4a, 4:4b, and 4:5, respectively. There was no significant trend for any parameter. The refractive index ranged from 1.401 to 1.455 with a mean ± SD of 1.431 ± 0.01, the anterior radius of curvature ranged from 9.1 to 12.6 mm with a mean ± SD of 10.9 ± 0.7 mm, and the posterior radius of curvature ranged from –5.1 to –8.8 mm with a mean ± SD of –6.7 ± 0.7 mm. The equivalent lens power was calculated from the other parameters using equations (14) and (15); the equivalent lens power ranged from 14.5 to 26.6 D with a mean ± SD of 21.6 ± 2.3 D.

Table 4.1 shows mean ± SD for each of the parameters in different races. There were no significant differences between races ($p > 0.05$).

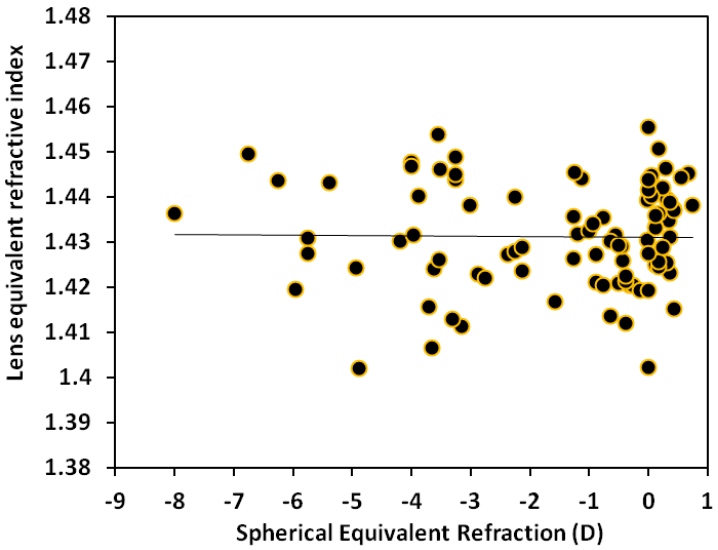

Figure 4:3: Relationship between lens equivalent refractive index at 820 nm and spherical equivalent refraction for 94 participants. Linear regression fit: $y = –0.0001x + 1.431$, $R^2 = 0.001$, $p = 0.88$.

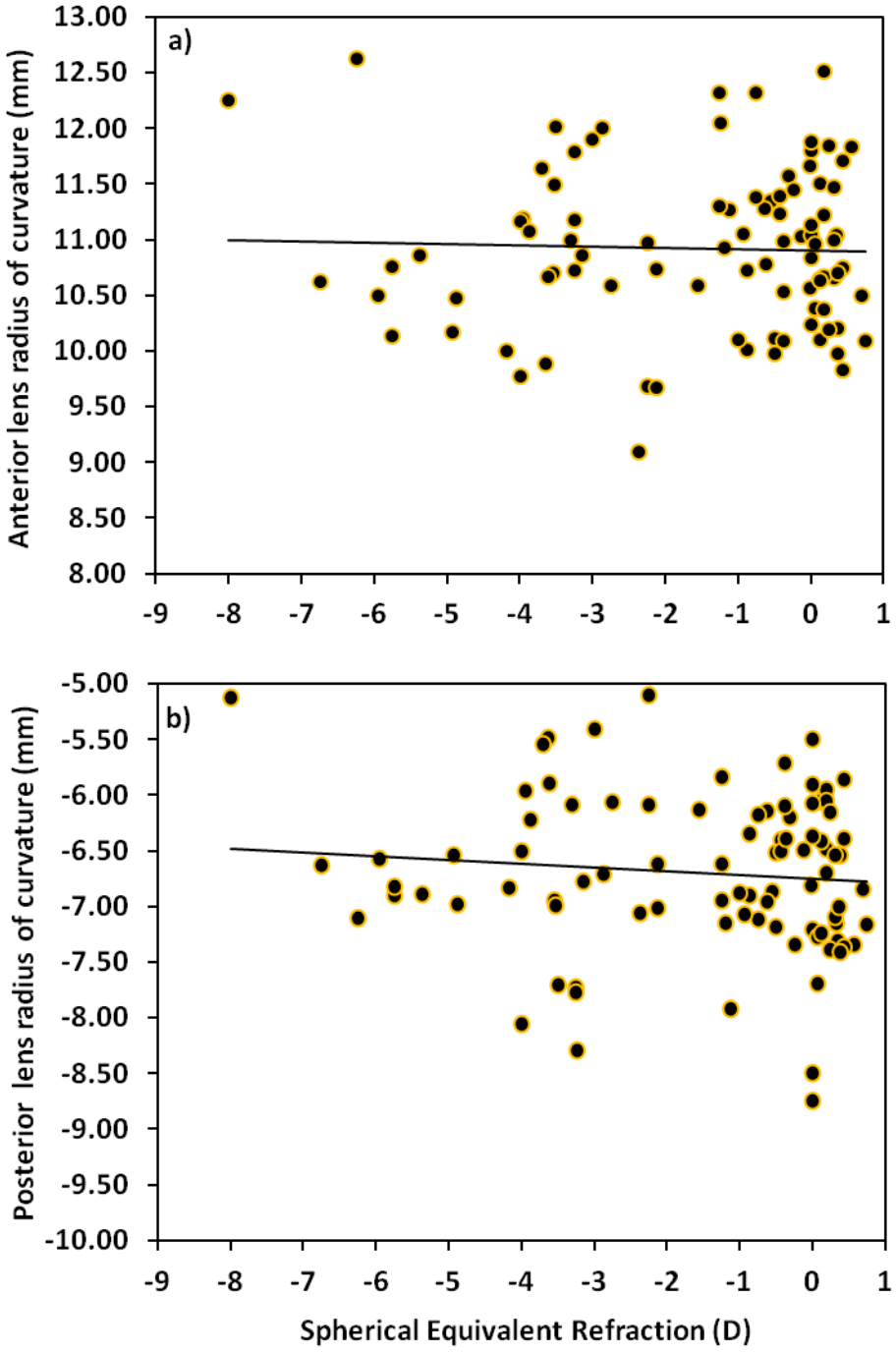

Figure 4:4: Relationship between a) anterior lens radius of curvature, and b) posterior lens radius of curvature, with spherical equivalent refraction. Linear regression fits: anterior lens radius of curvature $y = -0.011x + 10.91$, $R^2 = 0.001$, $p = 0.34$; posterior lens radius of curvature $y = -0.034x - 6.75$, $R^2 = 0.009$, $p = 0.19$.

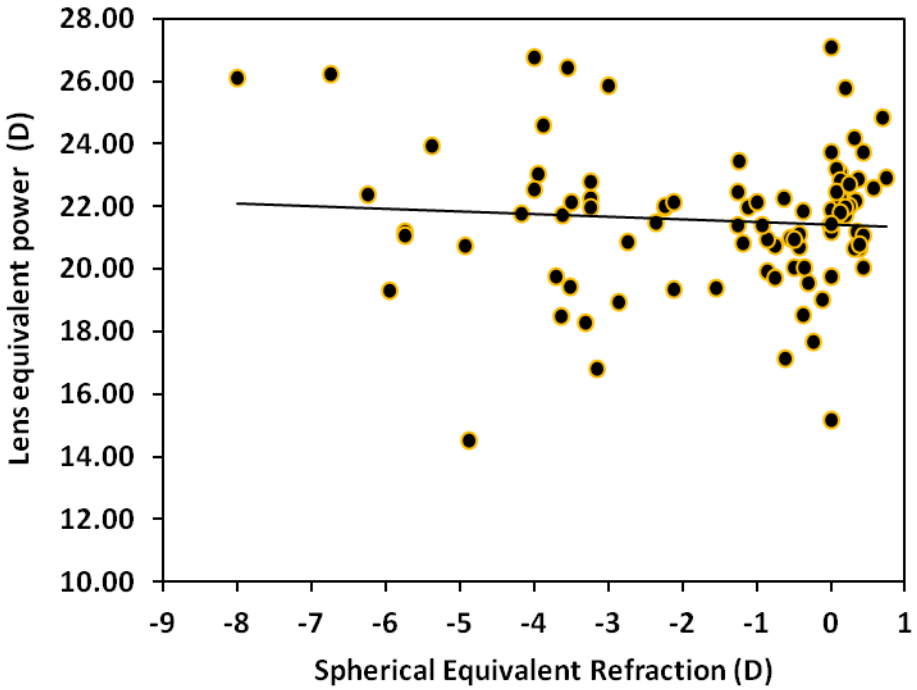

Figure 4:5: Relationship between lens equivalent refractive index at 820 nm and spherical equivalent refraction. Linear regression fit: $y = -0.083x + 21.42$, $R^2 = 0.006$, $p = 0.63$.

Table 4.1: Lens parameters in different racial groups. Data are mean ± SD.

Race	Anterior radius of curvature (mm)	Posterior radius of curvature (mm)	Equivalent refractive index	Equivalent power (D)
East Asians	+10.82 ± 0.75	–6.66 ± 0.66	1.431 ± 0.012	+21.83 ± 2.53
Caucasians	+11.01 ± 0.71	–6.74 ± 0.79	1.431 ± 0.011	+21.34 ± 1.91
South Asians	+11.05 ± 0.76	–6.54 ± 0.67	1.429 ± 0.011	+21.37 ± 1.90

4.4 RETINAL SHAPE COMPARISION - MRI VS. PCI

Figure 4:6 shows mean ± SD of the retinal coordinates derived from the three Stages of modelling from 58 participants along the horizontal and vertical meridians. The Z retinal coordinates became more negative and the X/Y coordinates shifted laterally with increasing level of sophistication from Stage 1 to 2, such that there was little change in mean retinal steepness. Stages 2 and 3 have similar values.

Figure 4:7a-d shows frequencies of the ratios of areas under the surface shapes for Stage 1 and Stage 2 (Stage 1/Stage 2) and for Stage 2 and Stage 3 (Stage 2/Stage 3). Stage 1 gave larger areas (flatter shapes) than Stage 2 along horizontal and vertical meridians, in 59% and 48% of the participants, respectively, with only 3% and 17% showing smaller areas (steeper shapes) in Stage 1 (Figures 4:7a, b). Stage 2 gave larger areas (flatter shapes) than Stage 3 in 67% of participants along both meridians with only 16% and 22% showing smaller areas in Stage 2 (Figures 4:7c, d). Mean ± SD of ratios of areas under surface shape for Stage 1 and Stage 2 along horizontal and vertical meridians are 1.00 ± 0.02 and 1.00 ± 0.04, respectively; and the corresponding ratios for Stage 2 and Stage 3 are 1.02 ± 0.05 and 1.00 ± 0.06.

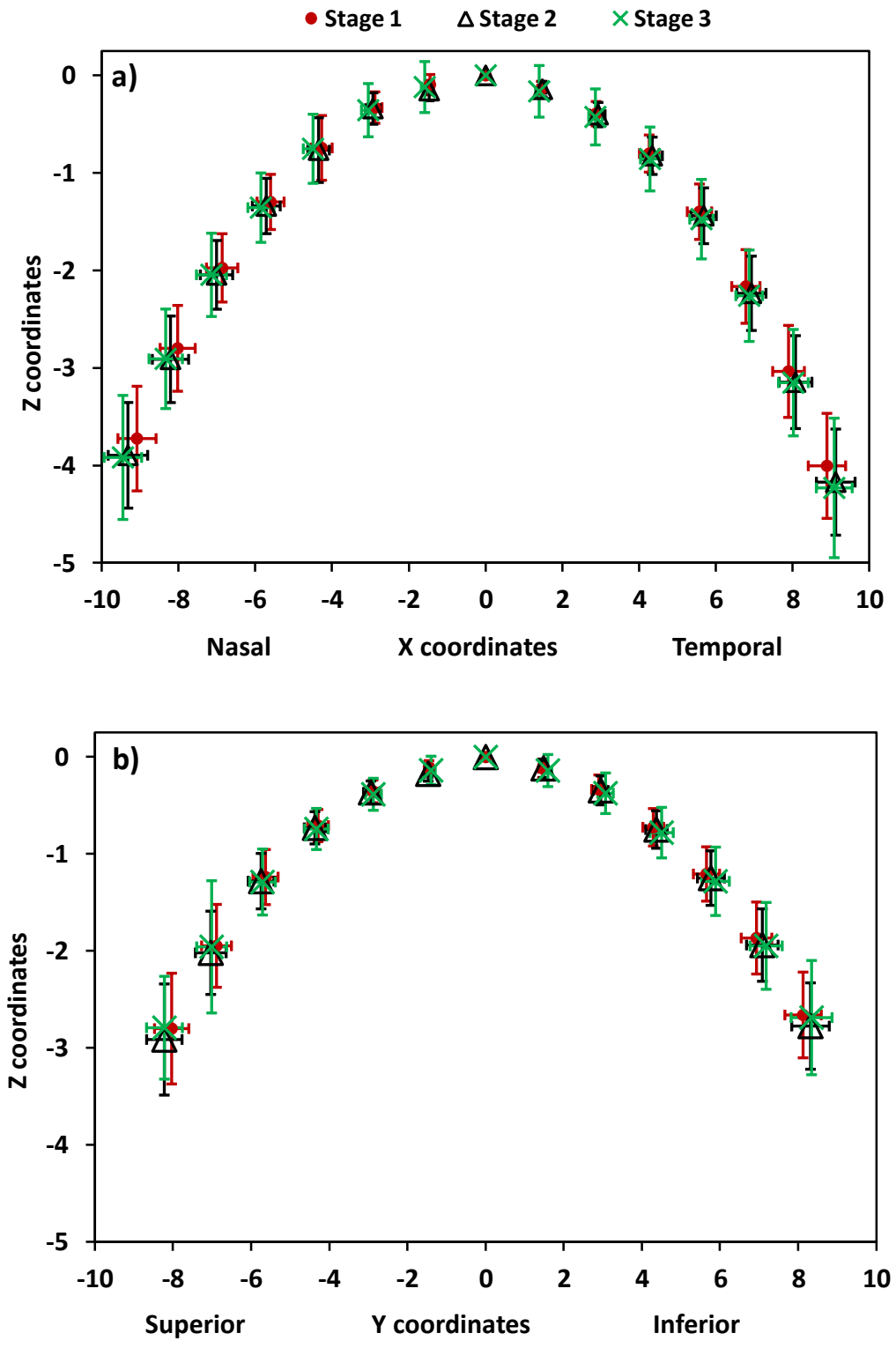

Figure 4:6: Retinal coordinates in the three Stages of increasing sophistication[1] along a) the horizontal meridian, and b) the vertical meridian. Horizontal and vertical error bars represent SD for Z and X/Y coordinates, respectively.

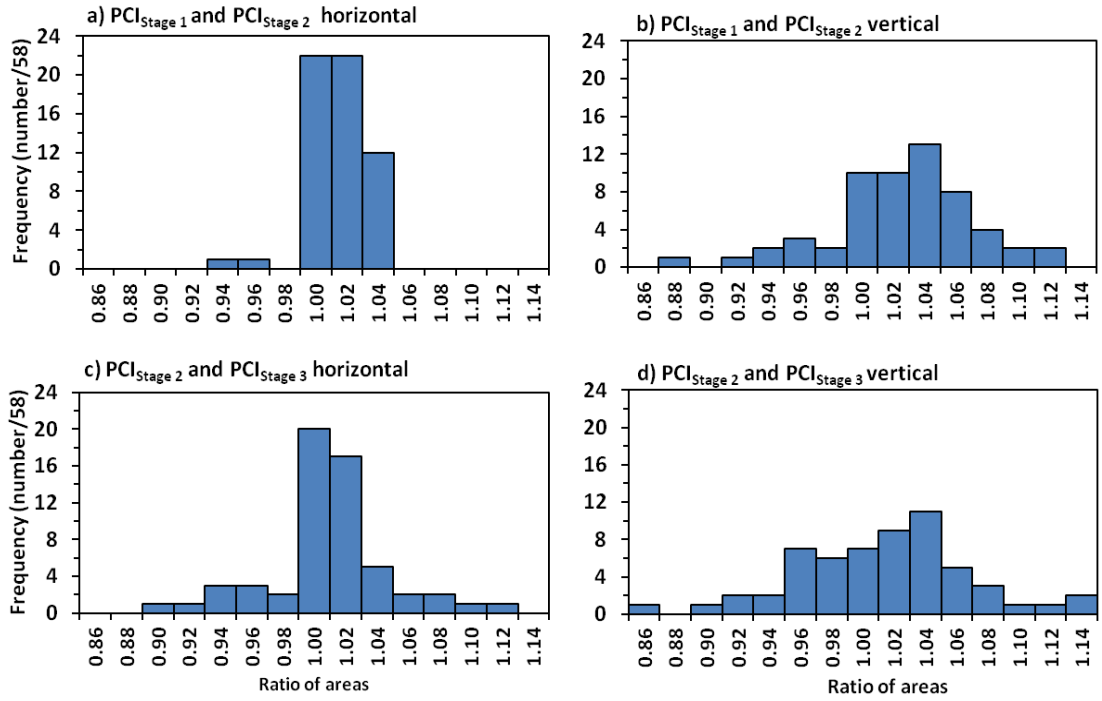

Figure 4:7: Frequency of participants against ratio of areas under the "surface shapes" for PCI Stages 1 and 2 ($PCI_{Stage\ 1}$/$PCI_{Stage\ 2}$) along a) horizontal and b) vertical meridians, and for PCI Stages 2 and 3 ($PCI_{Stage\ 2}$/$PCI_{Stage\ 3}$) along c) horizontal and vertical meridians.

Figure 4:8a-d, Figure 4:9a-d and Figure 4:10a-d show Bland-Altman plots of agreement of vertex radius of curvature (a, b) and asphericity (c, d) between the MRI and the 3 Stages of the PCI method. The plots indicate better agreement of retinal shape estimates along the horizontal meridian than along the vertical meridian. Although both the vertex radius of curvature and the asphericity plots show negative correlation, this does not yield any conclusions as the parameters are not independent. The mean ± 95% LoA of the corresponding plots are shown in

Table 4.2. The comparison of retinal shape estimates of all three Stages of PCI method with MRI showed similar means ± 95% LoA and also similar trend in Bland-Altman plots. Paired *t* test comparing the retinal shape estimates (R_{xv}, R_{yv}, Q_x and Q_y) between MRI and three Stages of PCI showed statistical significant differences between MRI and Stage 3 for R_{xv}, Q_x and Q_y, but not between MRI and either Stage 1 or Stage 2. R_{yv} was significantly different between MRI and all three Stages of PCI.

Figure 4:8e, 4:9e and 4:10e show the percentage difference in agreement between MRI and the three Stages of PCI. Mean ± 95% CI of the difference of

agreement along the horizontal meridian were 3.8 ± 0.7%, 3.7 ± 0.6% and 3.5 ± 0.6% for Stages 1, 2, and 3, respectively; corresponding values for the vertical meridian were 5.6 ± 0.9%, 6.2 ± 1.1% and 6.2 ± 1.0%.

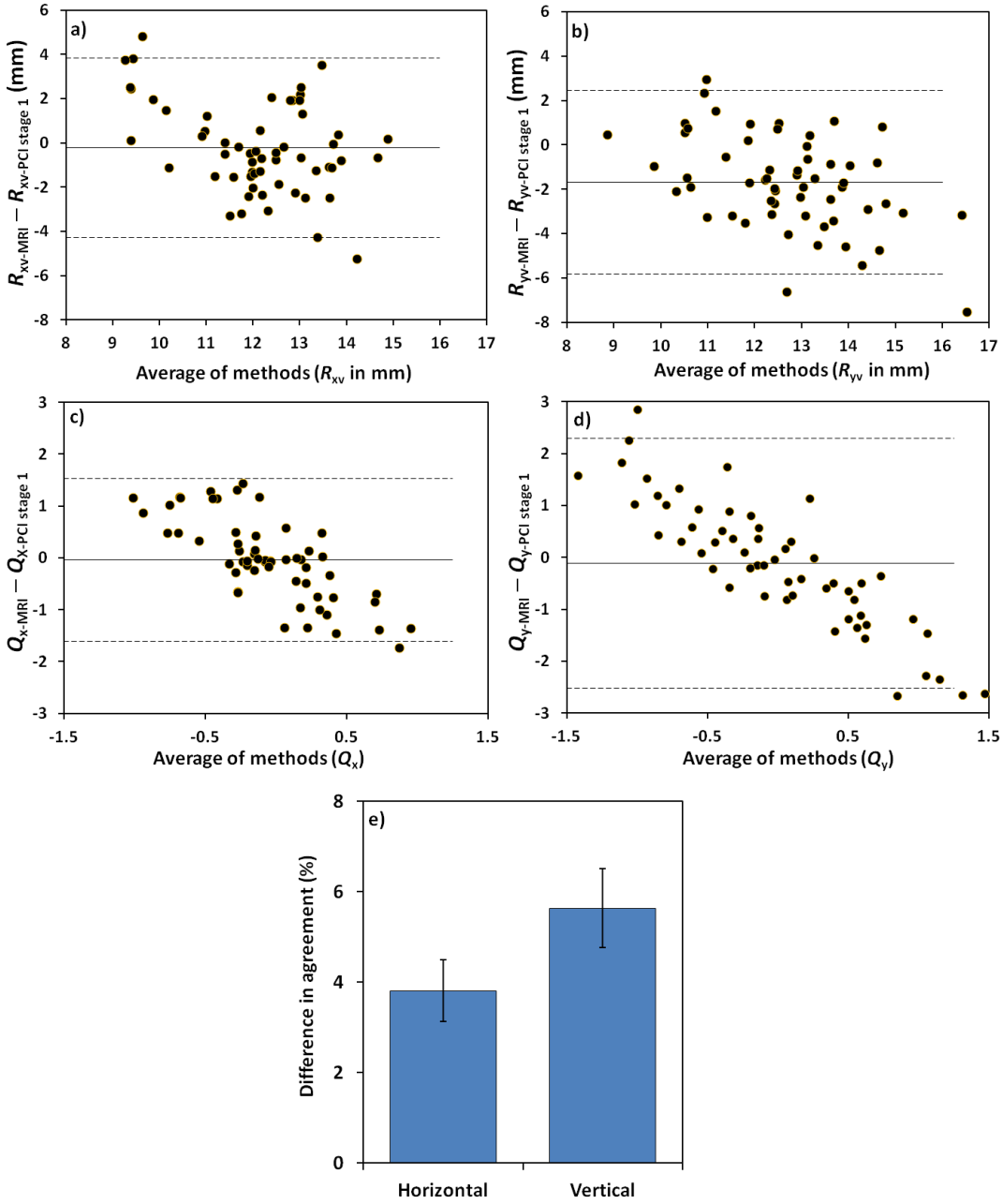

Figure 4:8: Agreement of retinal shape estimates between MRI and $PCI_{Stage\ 1}$: vertex radii of curvature along a) horizontal and b) vertical visual fields; asphericities along c) horizontal and d) vertical visual fields. Mean differences are shown by the bold line and the 95% limits of agreement are shown by dashed lines; e) mean difference in agreement of retinal surface estimates between the two methods. Error bars indicate 95% confidence intervals of the mean.

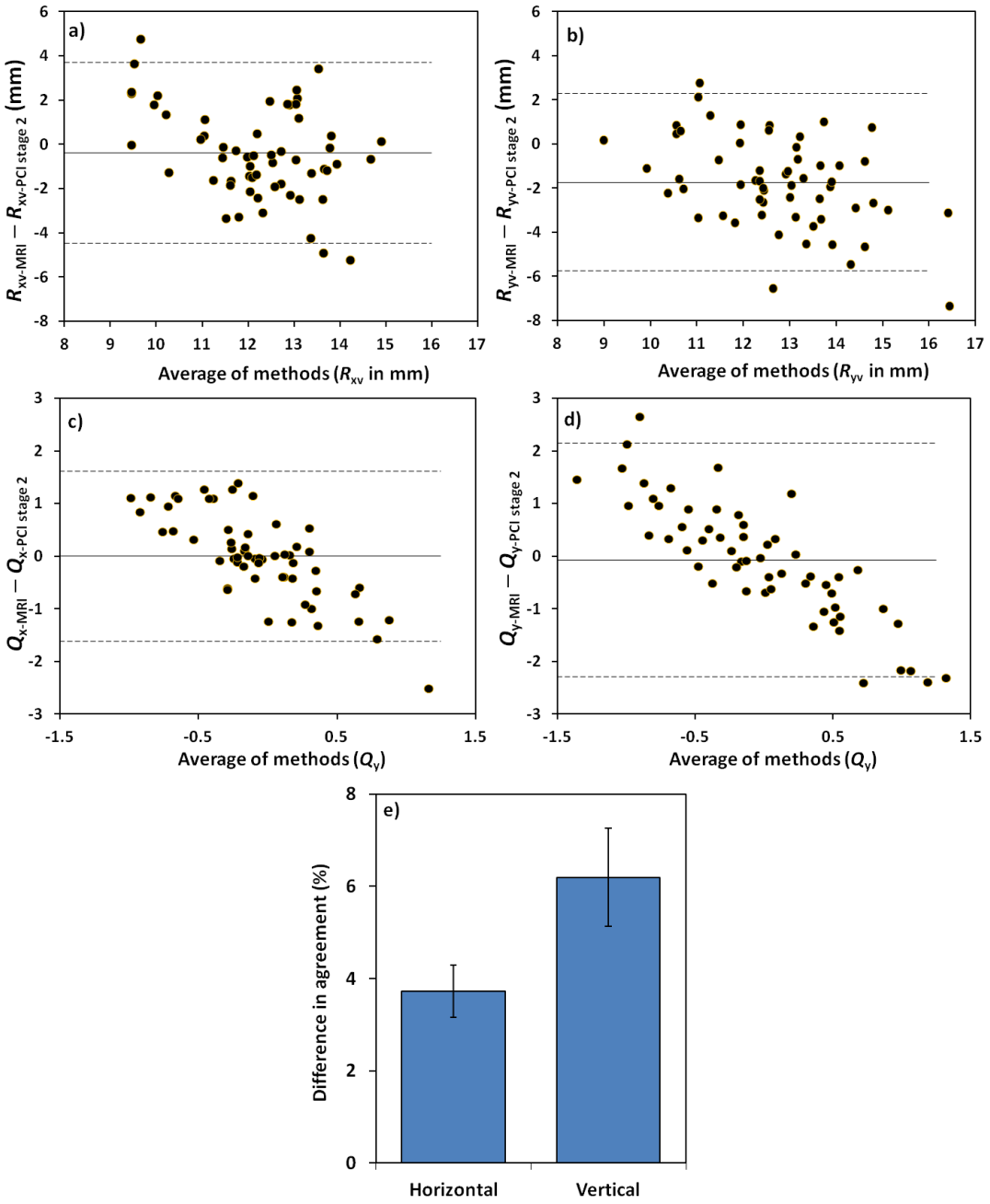

Figure 4:9: Agreement of retinal shape estimates between MRI and $PCI_{Stage\ 2}$. Other details are as for Figure 4:8.

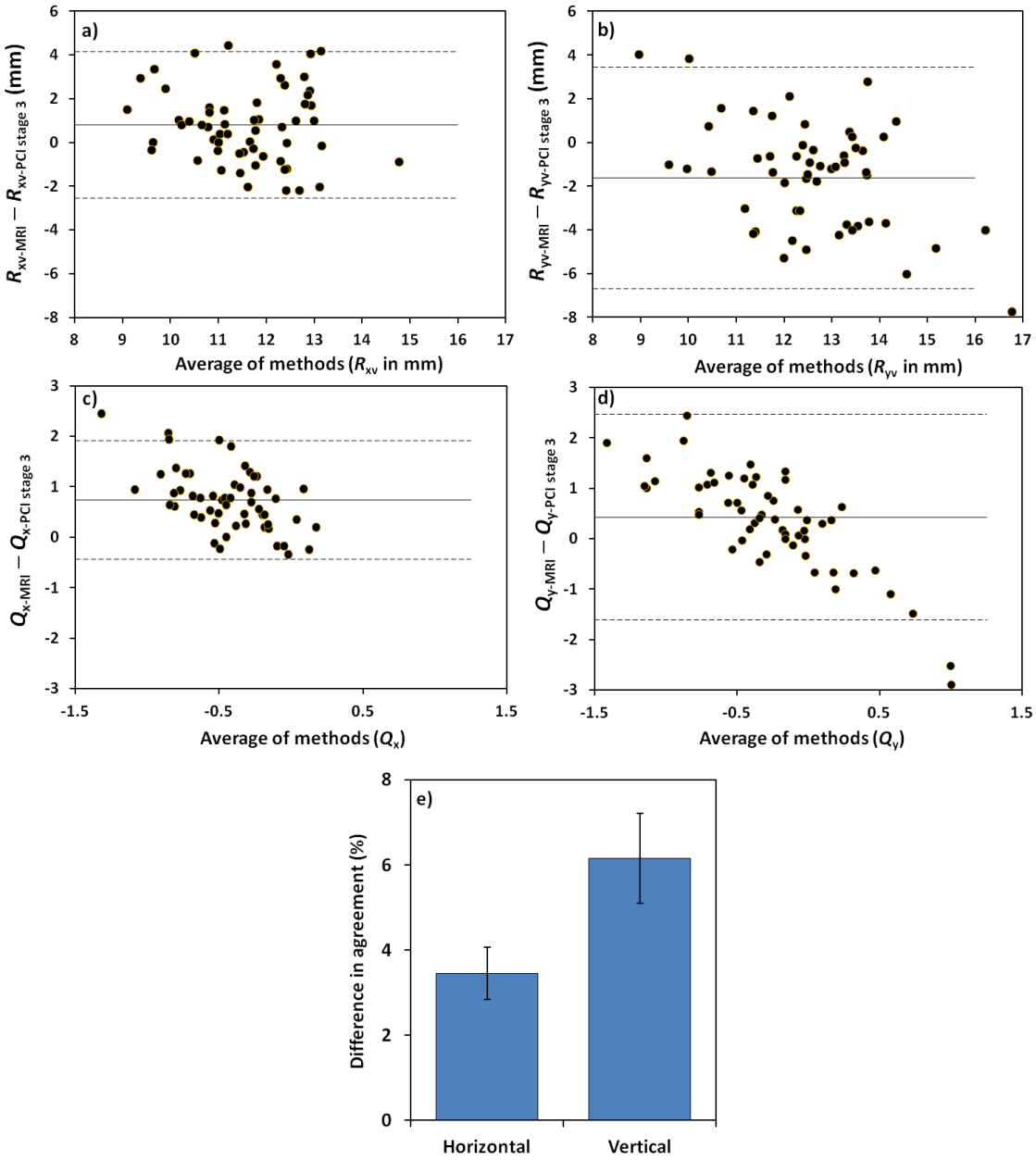

Figure 4:10: Agreement of retinal shape estimates between MRI and $PCI_{Stage\ 3}$. Other details are as for Figure 4:8.

Table 4.2: Agreement for retinal shape estimates between MRI and three Stages of PCI . Data are mean ± 95% limits of agreement. * $p < 0.05$.

Estimate	MRI - $PCI_{Stage\ 1}$	MRI - $PCI_{Stage\ 2}$	MRI - $PCI_{Stage\ 3}$
R_{xv}	–0.2 ± 4.1	–0.4 ± 4.1	+0.8 ± 3.4*
Q_x	–0.04 ± 1.57	–0.00 ± 1.62	+0.74 ± 1.17*
R_{yv}	–1.7 ± 4.1*	–1.7 ± 4.0*	–1.6 ± 5.1*
Q_y	–0.11 ± 2.41	–0.07 ± 2.22	+0.43 ± 2.04*

Figure 4:11(a-f) shows frequencies of the ratios of areas under the surface shapes for MRI with the different PCI Stages. Along both horizontal and vertical meridians, all three Stages of PCI generally had larger areas (flatter shapes) than MRI. For the horizontal meridian, Stages 1, 2 and 3 of PCI had larger areas than MRI in 60%, 60% and 45% of cases, respectively (Figures 4:11a, c and e). For the vertical meridian this was even more pronounced with all of the PCI Stages having larger areas than MRI in at least 60% of cases (Figure 4:11b, d and f). Mean ± SD of ratio of areas under surface shapes between Stage 1, 2, 3, in order, and MRI along the horizontal meridian were 1.01 ± 0.06, 1.01 ± 0.06, 0.99 ± 0.06; corresponding ratios for vertical meridian were 1.05 ± 0.06, 1.06 ± 0.08, 1.06 ± 0.08.

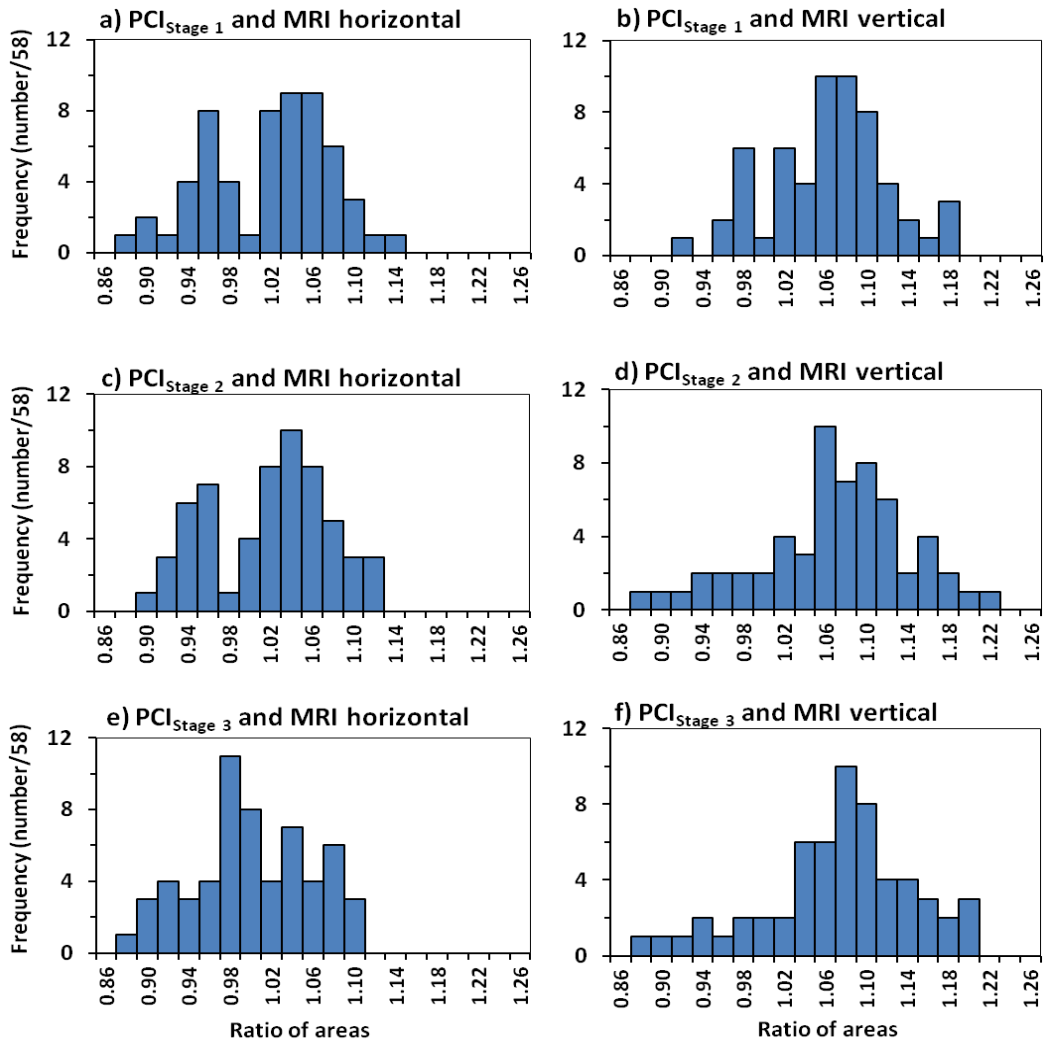

Figure 4:11: Frequency of participants against ratio of area under the "surface shapes" for PCI Stage 1 and MRI ($PCI_{Stage\ 1}$/MRI) along a) horizontal and b) vertical meridians, for PCI Stage 2 and MRI($PCI_{Stage\ 2}$/MRI) along c) horizontal and d) vertical meridians, and for PCI Stage 3 and MRI ($PCI_{Stage\ 3}$/MRI) along e) horizontal and f) vertical meridians.

The uncertainty of retinal shape estimates with MRI was determined by taking into consideration that the dimensions of the voxels in 3D HASTE images were 0.5 mm. A simple model with a spherical retinal surface having a radius of curvature of 12 mm over a distance of 15.6 mm (15.6 mm = 7.8 mm either side from peak/centre) was used to determine surface coordinates using equation (34). The distance of 7.8 mm, smaller than the smallest radius of curvature in the data set of 58 participants (8.5 mm) was chosen to maintain a 1:1 relationship between Y and Z coordinates. Otherwise, for a larger distance, each Y-coordinate will have more than one Z-coordinate corresponding to it.

Figure 4:12 shows three fits where the blue curve assumes the points at the centre of MRI voxels for both the centre and edge of the curve, the green curve assumes the upper edge of the voxel at the centre of the curve and the lower edge of the voxel at the edges of the curve, and the red curve assumes the opposite to the green curve. The green and red curves were repositioned to have the same vertex as the one passing through the centre of the voxel (blue curve). Pushing the central point up by 0.25 mm and the edges down by same amount (green curve) and smoothing the curve between them after repositioning produced R_v = 8.36 mm, Q = –1.51 with the Solver template (section 3.5.7). Pushing the central point down and the edges up (red curve) produced R_v = 17.18 mm with Q = 2.96. Comparing these values using equation (53) gives the difference in agreement (uncertainty) between two curves of 14.1%. Fitting the coordinates to a best circle (Q = 0) gave R_{Eq} = 10.27 (green curve) and 14.67 (red curve) with uncertainty of 12%.

The estimates above assume the voxel counts as edge voxels that form the retinal boundary (for the edge/boundary detection algorithm, edge voxels are between vitreous and sclera) irrespective of the amount of the voxel enclosed inside it. As the edge detection algorithm has a thresholding condition, this assumption only gives the maximum possible differences that could occur in retinal shape due to the partial volume effect on MRI. Therefore, the percentages above are exaggerations of the uncertainty in the most extreme cases (from 0% - 100% of the voxels filled).

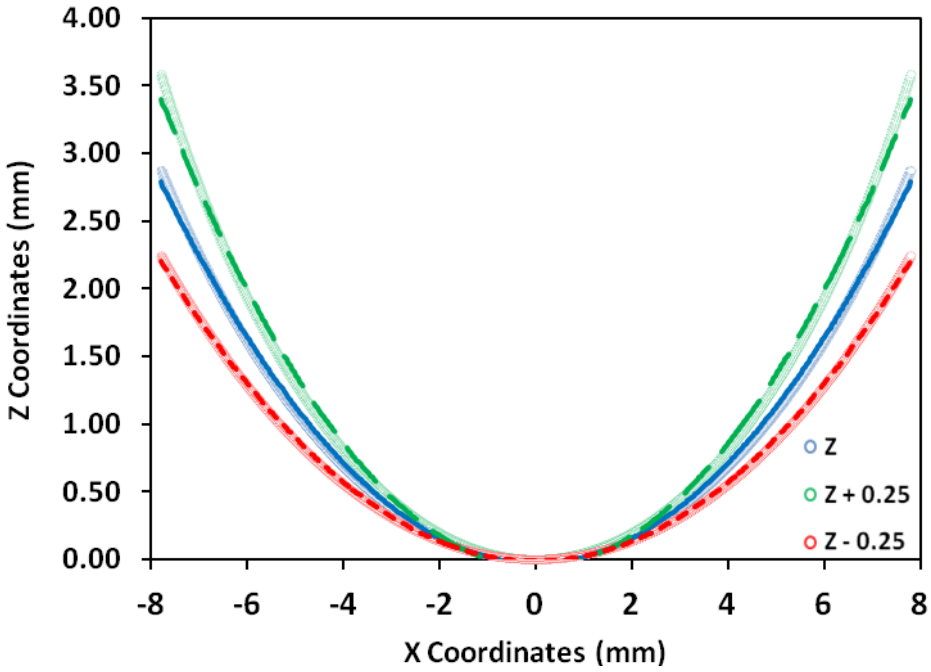

Figure 4:12: Retinal surface coordinates determined points corresponding to centre of voxel for both the centre and edge of the curve (blue) and at the opposite extremes of the 0.5 mm voxels (green: Z +0.25 indicates upper edge of voxel at centre and lower edge of the voxel at the edge of curve, and red: Z –0.25 indicates lower edge of voxel at centre and upper edge of the voxel at the edge of the curve).

Summary

In several cases there were significantly different estimates for both R_v and Q between PCI and MRI, but it was clear often that there was compensation such as a positive change in Q, in one method, relative to the other, compensating for a positive change in R_v. Therefore, as a better approach for comparing MRI and PCI, these parameters were combined to form a "surface shape".

All three PCI Stages showed similar ranges of percentage difference with MRI. Estimates along the horizontal (< 4%) and vertical meridian (<7%) were smaller than the theoretical uncertainty of MRI (12-14%). For the majority of participants, area under surface shape with all three Stages of PCI was larger (flatter shapes) than the MRI along both meridians, but with the differences being relatively less along the horizontal than along the vertical meridian.

4.5 RETINAL SHAPE COMPARISION - MRI VS. DUNNE'S METHOD

Retinal coordinates were determined using Dunne's method (section 3.5.7). The retinal coordinates were fitted to equation (36) to estimate retinal shape.

Figure 4:13 shows Bland-Altman plots of agreement between MRI and Dunne's method for vertex radius of curvature (a, b) and asphericity (c, d) along horizontal and vertical field meridians. Mean difference ± 95% LoA for vertex radius of curvature and asphericity along the horizontal meridian were –1.7 ± 4.3 mm and –0.15 ± 2.18, respectively; corresponding values along the vertical meridian were –3.1 ± 5.6 mm and –0.60 ± 3.46. The two methods gave significantly different results for all parameters except for asphericity Q_x along the vertical meridian ($p = 0.15$).

Figure 4:13e shows differences in agreement between the two methods, with mean ± 95% CI of 6.0 ± 1.2% (horizontal) and 8.9 ± 1.1% (vertical). These are about 1.5 times the differences in agreement between MRI and any of the PCI Stages.

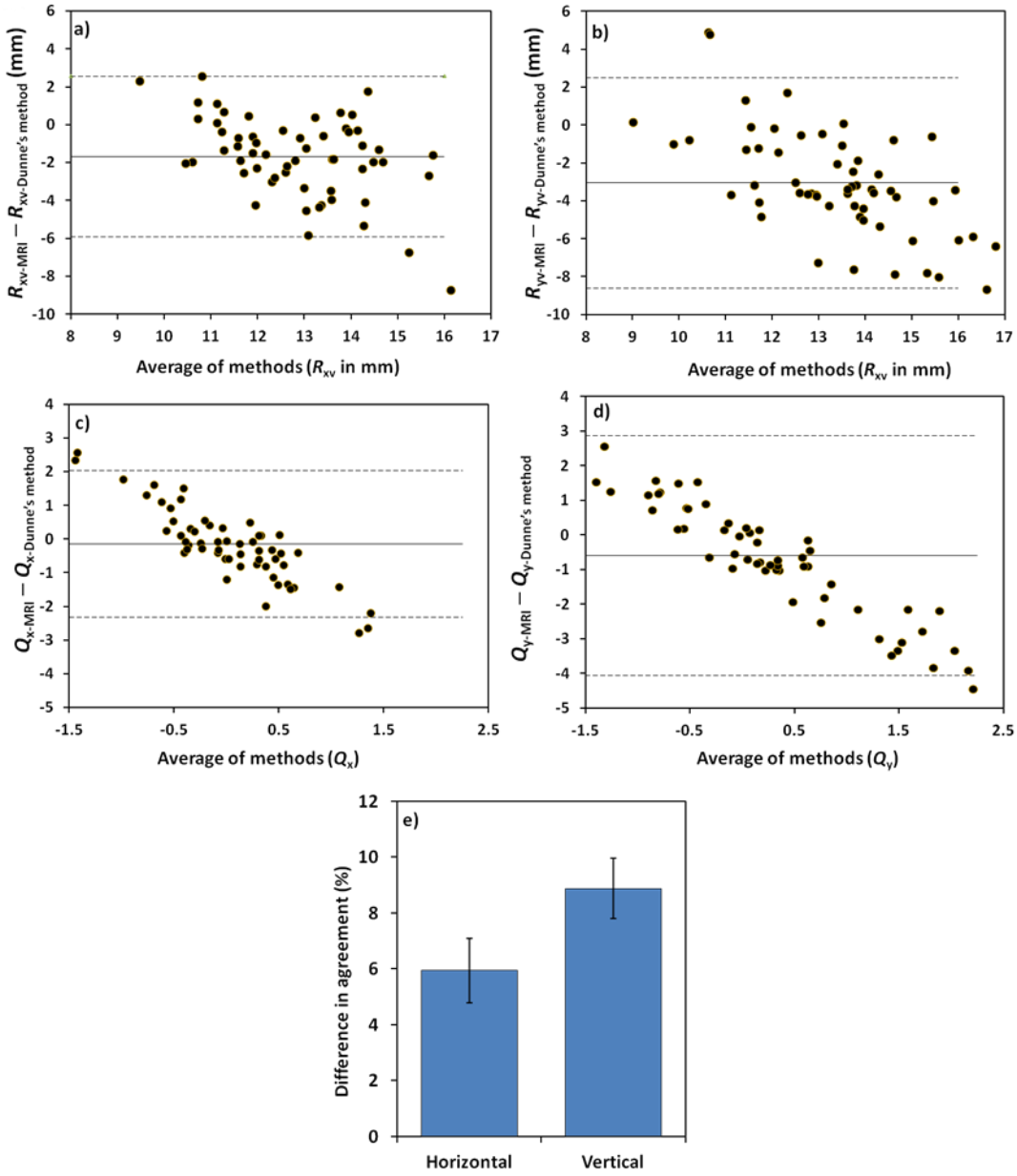

Figure 4:13: Agreement of retinal shape estimates between MRI and Dunne's method:Other details are as for Figure 4:8.

Figure 4.14 shows frequencies of the ratios of areas under the surface shapes for MRI and Dunne's method. Along both horizontal and vertical meridians, areas under surface shapes with Dunne's method were larger (flatter shapes) than MRI PCI in 80% of participants.

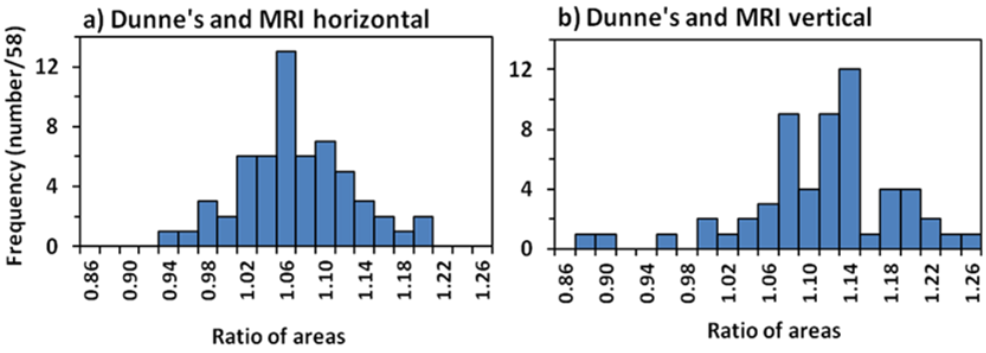

Figure 4.14 Frequency of participants against ratio of area under the "surface shapes" between Dunne's method and MRI: (Dunne//MRI) along a) horizontal and b) vertical meridians.

4.6 CONCLUSION

This study compared retinal shape estimates between MRI and PCI and between MRI and Dunne's method. In several cases there were significantly different estimates for both R_v and Q between the methods, but it was clear often that there was compensation such as a positive change in Q, in one method, relative to the other, compensating for a positive change in R_v. Therefore, a better approach to comparing MRI and PCI would be to combine these parameters to form a "surface shape". The results show good agreement (within the theoretical uncertainty of MRI of 12-14%) between MRI and all three Stages of PCI (4% along horizontal meridian and 6% error along the vertical meridian), but not as good between MRI and Dunne's method (6% along the horizontal meridian and 9% along the vertical meridian). Thus, all the PCI Stages would appear to give better estimates of retinal shape than Dunne's method. It is possible that the Dunne's method would provide improved agreement with MRI results with a different model or different iterative method.

For the majority of participants, all three Stages of the PCI method and the Dunne's method gave flatter estimates of retinal shape than did MRI, with the differences being smaller along the horizontal than along the vertical meridian. This variation between the MRI and other methods could be due in part to the large voxel size of the MRI images (0.5 mm) which influences the edge detection routine used in determining retinal shape estimates as it picks up the transition between voxels that are purely vitreous to those that are solely in the sclera. The differences could be attributed to thresholding used for picking the retinal boundary and the partial volume effect which indicates that if the voxel imaged was less than twice the 'full

width at half maximum resolution' in X-, Y- and Z-dimensions, the resultant activity in the region was underestimated. Another possible reason for differences between the MRI and other methods could be due to the comparison of retinal shapes involving different percentages of retinal area such as 35% for MRI, and 27% for PCI (section 3.5.6) and Dunne's method (section 3.5.7). As mentioned in section 3.5.6.3, because of the low sampling of MRI, fitting to any retinal area smaller than 35% resulted in too much noise, and therefore 35% fits were chosen despite the area mismatch between methods.

The reason for better agreement between MRI and the other two methods for the horizontal meridian than for the vertical meridian is not known, but might be related to a different sampling with PCI and Dunne's method (±35º in 5º steps: 15 points along horizontal meridian; ±30º in 5º steps: 13 points along vertical meridian).

It is likely that the three Stages of the PCI method give similar results because the assumption that the infrared beam is directed normal to the anterior cornea is reasonable and that the normals pass close to the nodal points of the eye so that the deviation within the eye is small. In Atchison and Charman's (2011) theoretical work using variations on the Gullstrand number 1 eye, they found that Stage 1 was highly accurate out to at least ±40°.

For the PCI method, the Stage 1 analysis was a very simple method assuming the parameters of the Le Grand model eye and ignoring light deviation within the eye. Beam incident on the eye model was assumed to be undeviated which might lead to inaccurate results in presence of irregular corneas, refractive myopia or index myopia. Although Stage 3 involves more sophisticated analysis (including aspheric cornea, lens radius of curvatures and equivalent refractive index) than other Stages, it takes considerable time. The results for intermediate Stage 2 analysis that used model eye parameters along with peripheral eye lengths from real eyes were similar to those of the most sophisticated Stage 3, and *therefore this simpler, yet accurate and efficient level of analysis (Stage 2) is recommended for retinal shape estimation*.

This study validated PCI against MRI for estimating retinal shape, thus addressing the first aim of the thesis, and supports its associated hypothesis that retinal shape can be accurately predicted by measuring off-axis eye lengths with a commercial PCI. The Experiments 2 and 3 that involved retinal shape estimation in chapters 5 and 6 used the Stage 2 analysis.

Chapter 5- Retinal Shape in Different Racial Groups

Race appears to be associated with myopiogenesis, with East Asians showing high myopia prevalence both inside and outside Asia (section 2.2). Considering structural variations in the eye, it is possible that retinal shapes are different between races. This chapter investigates how retinal shape alters with race using the $PCI_{Stage\ 2}$ method. It addresses the second aim: "to use the validated method to measure retinal shape in East Asian, South Asian and Caucasian emmetropes and myopes to determine how retinal shape and peripheral refraction are related in eyes of people with different racial backgrounds" and tests the associated hypothesis 2: "there are differences in retinal shapes among different racial groups" and the associated hypothesis 3: "there are meridional (vertical and horizontal) variations in retinal shape".

This chapter is divided into 5 sections. Section 5.1 is an overview of methods. Section 5.2, 5.3 and 5.4 investigate the influence of meridian and race on peripheral refraction, peripheral eye lengths and retinal shape, respectively. Section 5.5 gives the conclusions of the chapter.

5.1 PARTICIPANTS

Participants indicated racial group based on their ancestry in the 'participant demographic/information sheet'. Based on the Australian Standard Classification of Cultural and Ethnic Groups (ABS, 2011), participants were classified as

- East Asians (EA): people from China, Malaysia, Korea and Singapore with Chinese ancestry,
- South Asians (SA): people from India, Pakistan and Sri Lanka with Indian ancestry, and
- Caucasians (CA): people from Australia, Germany and Netherlands with Caucasian ancestry.

Ninety-four participants, aged between 18 to 30 years and with spherical equivalent refraction between +0.75D to −5.50 D, were divided into two refraction groups of emmetropes (49) and myopes (45) based on central spherical equivalent refraction. Considering the time involvement in data collection and the sophisticated analysis for determining retinal shape estimates, sample size in this study was compromised. The participants were mostly undergraduate students living in the Australian state of Queensland. Because of sampling bias due to selection of participants from a single region, they may not be completely representative of East Asians, Caucasians and South Asians. Therefore, the interpretation or comparison of these results with other studies is made with caution. Table 5.1 has racial group characteristics.

Table 5.1: Racial group characteristics. Emm = emmetropes, Myo = myopes

Race	Emm	*M* (mean ± SD) Dioptres	Myo	*M* (mean ± SD) Dioptres	Total	Age (mean ± SD) years
EA	14	0.01 ± 0.1	22	–2.75 ± 1.39 (–0.82 to –5.25 D)	36	22.7 ± 3.6
CA	25	0.01 ± 0.08	15	–3.06 ± 1.01 (–0.82 to –4.17 D)	40	23.5 ± 3.4
SA	10	–0.07 ± 0.13	8	–2.19 ± 1.16 (–0.82 to –4.00 D)	18	24.7 ± 2.5
Total	49	–0.01 ± 0.38	45	–2.75 ± 1.25	94	23.7 ± 3.5

There is a possibility that results might be influenced by gender and axial length. Average central axial lengths are greater in males than in females of similar refraction (Shufelt et al., 2005, Atchison et al., 2008, Iyamu et al., 2011, Yin et al., 2012). Variations in axial length between races was identified with the tendency for East Asians to have longer axial lengths than other races (Ip et al., 2007a, Tariq et al., 2010, Lee et al., 2013). Therefore, appropriate distribution of participants based on gender in each racial group is important for meaningful comparisons. Table 5.2 shows the distribution of males and females and their mean axial lengths for the refraction/racial group combinations. As expected, males had greater axial lengths

than females in all three races. There were considerably more females than males in the East Asian and Caucasian groups (65% and 72%, respectively), while the reverse was the case for the smaller South Asian group (33%). The mean axial length differences between the three races were not statistically significant (independent sample t-tests: EA vs. CA, p = 0.98; EA vs. SA, p = 0.20; CA vs. SA, p = 0.20). It was not considered that gender and axial length needed to be taken into account for the study. Certainly, a much larger scale study could be conducted to consider the effect of gender on retinal shape.

Table 5.2: Axial length (mm) according to gender in different races

	Emmetropes				Myopes			
Race	**Males**		**Females**		**Males**		**Females**	
East Asians	24.46 ± 0.49	5	23.35± 0.57	9	25.04 ± 1.13	5	24.69 ± 0.64	17
Caucasians	24.09 ± 0.60	9	23.69 ± 0.61	16	25.66 ± 0.21	5	24.94 ± 0.58	10
South Asians	23.60 ± 0.69	7	23.12 ± 0.59	3	24.61 ± 1.01	5	24.57 ± 1.08	3
Total		**21**		**28**		**15**		**30**

5.2 PERIPHERAL REFRACTION

Method

Peripheral refraction was obtained with the Shin-Nippon auto refractor using the procedure described in section 3.5.4. Relative peripheral refraction (*RPR*) was determined by subtracting central refraction from refractions obtained at different visual field angles (*RPR* = peripheral *M* – central *M*).

M, *RPR*, J_{180}, and J_{45} were plotted as a function of visual field position. For *M*, *RPR* and J_{180} data, second order polynomial fits were applied for each participant:

$$y = ax^2 + bx + c \quad (54)$$

and for J_{45} data, first order linear fits were applied for each participant:

$$y = bx + c \quad (55)$$

where *x* was the visual field angle in degrees and was taken as being positive for both nasal and superior visual fields. Data corresponding to the optic disc (15º temporal field) were not included in analysis.

Two-way ANOVAs were conducted on the highest order coefficients for *RPR*, J_{180}, and J_{45} separately, with race (EA/CA/SA) and refraction group (myopes/emmetropes) as between-subject factors and visual field meridian (horizontal/vertical) as a within-subject factor. For analysis with J_{180}, signs for horizontal data were changed to match them with vertical data. Post-hoc t-tests with Bonferroni correction were used to compare results between races. To investigate if peripheral refraction components and *RPR* were affected by myopia magnitude, linear regressions were determined for the highest order coefficients as functions of central *M*. Analysis of covariance (ANCOVA) was performed to test the significance of slopes between races.

Results

Figure 5:1 shows mean *M* along horizontal and vertical field meridians as a function of visual field angle in different racial groups for both emmetropes and myopes. It includes second order polynomial fits for which the coefficients are given in Table 5.3.

The patterns were different along the horizontal and vertical meridians (ANOVA of *RPR* for coefficient "a" in equation (54): $F_{1, 176} = 17.9$, $p < 0.001$). Refraction group and race did not significantly affect the "a" coefficient of *RPR* ($F_{1, 176} = 1.11$, $p = 0.29$ and $F_{2, 176} = 2.97$, $p = 0.06$, respectively), although race was close to being significant. Along the horizontal meridian emmetropes exhibited slight relative peripheral myopia, which in myopes changed to relative peripheral hyperopia (Figure 5:1a), and along the vertical meridian both emmetropes and myopes showed relative peripheral myopia which was greater in the emmetropes than in myopes (Figure 5:1b). The linear regressions showed that, along both the horizontal and vertical meridians, the slope of coefficient "a" per dioptre of central *M* was most negative for Caucasians followed by East Asians and South Asians (Figure 5:2a and b). The slopes were significantly different between the races in the ANCOVA along the horizontal ($F_{2, 88} = 12.1$, $p < 0.001$) but not along the vertical

meridian ($F_{2, 88} = 0.44$, $p = 0.65$), and post hoc testing did not show significant pair-wise comparisons.

Figure 5:3 shows mean J_{180} along the horizontal and vertical field meridians as a function of visual field angle in different racial groups for both emmetropes and myopes. It includes second order polynomial fits for which the coefficients are given in Table 5.3.

The patterns were similar along the horizontal and vertical meridians, but the field affected coefficient significantly ($F_{1, 176} = 42.2$, $p < 0.001$) with steeper fits along the vertical meridian (0.0012 ± 0.004 D/degrees^2) than along the horizontal meridian (0.0009 ± 0.002 D/degrees^2). Refraction group and race did not affect the "a" coefficient significantly ($F_{1, 176} = 1.52$, $p = 0.22$ and $F_{2, 176} = 1.38$, $p = 0.25$, respectively). The linear regressions show that the absolute slope of coefficient "a" per dioptre of central *M* was greater for South Asians than for the other races (Figure 5:4a and b). The slopes were not significantly different between the races in the ANCOVAs ($F_{2, 88} = 2.43$, $p = 0.09$, horizontal meridian; $F_{2, 88} = 2.33$, $p = 0.10$, vertical meridian).

Figure 5:5 shows J_{45} along the meridians as a function of visual field angle in different racial groups for both emmetropes and myopes. It includes linear polynomial fits for which the coefficients are given in Table 5.3.

The patterns were similar along the horizontal and vertical meridians, but the field affected coefficient "b" in equation (55) significantly ($F_{1, 176} = 15.9$, $p < 0.001$) with steeper fits along the vertical than along the horizontal meridian. Race, but not refraction group, affected the "b" coefficient significantly ($F_{2, 176} = 6.39$, $p = 0.002$ and $F_{1, 176} = 1.76$, $p = 0.19$, respectively). Post hoc testing showed that Caucasians had significantly higher coefficients than East Asians (mean ± SD: $+0.008 \pm 0.008$ D/degree vs. 0.005 ± 0.006, $p = 0.02$). The linear regressions show that the slopes of coefficient "b" per dioptre of central *M* were not significant for any of the races (Figure 5.6 a and b) nor between the races in the corresponding ANCOVA ($F_{2, 88} = 1.09$, $p = 0.34$, horizontal meridian; $F_{2, 88} = 3.51$, $p = 0.06$, vertical meridian).

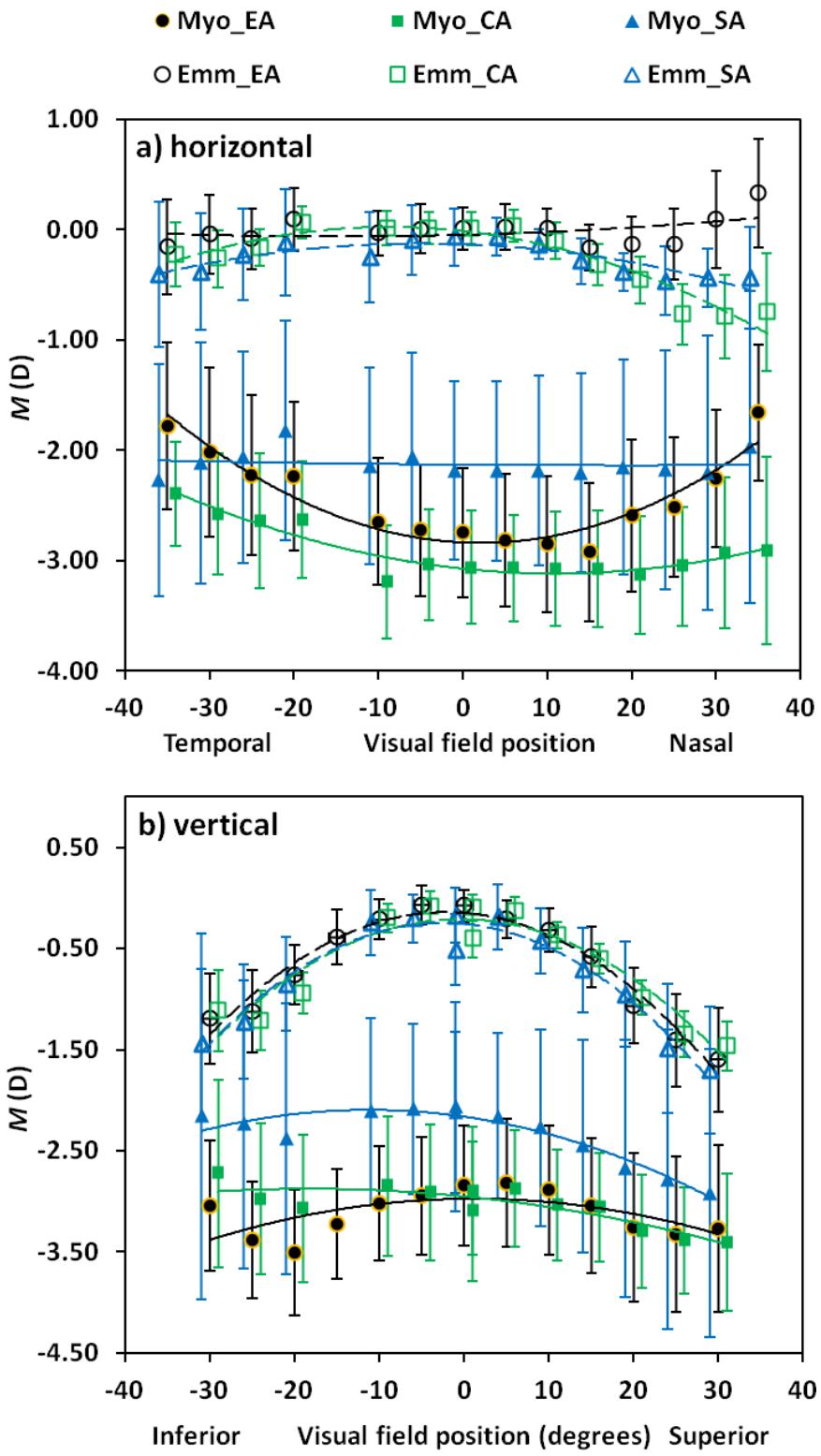

Figure 5:1: Mean spherical equivalent refraction *M* along a) horizontal and b) vertical visual field meridians in different racial groups for emmetropes and myopes . Error bars indicate 95% confidence intervals of mean. Plots are staggered horizontally to make them more legible.

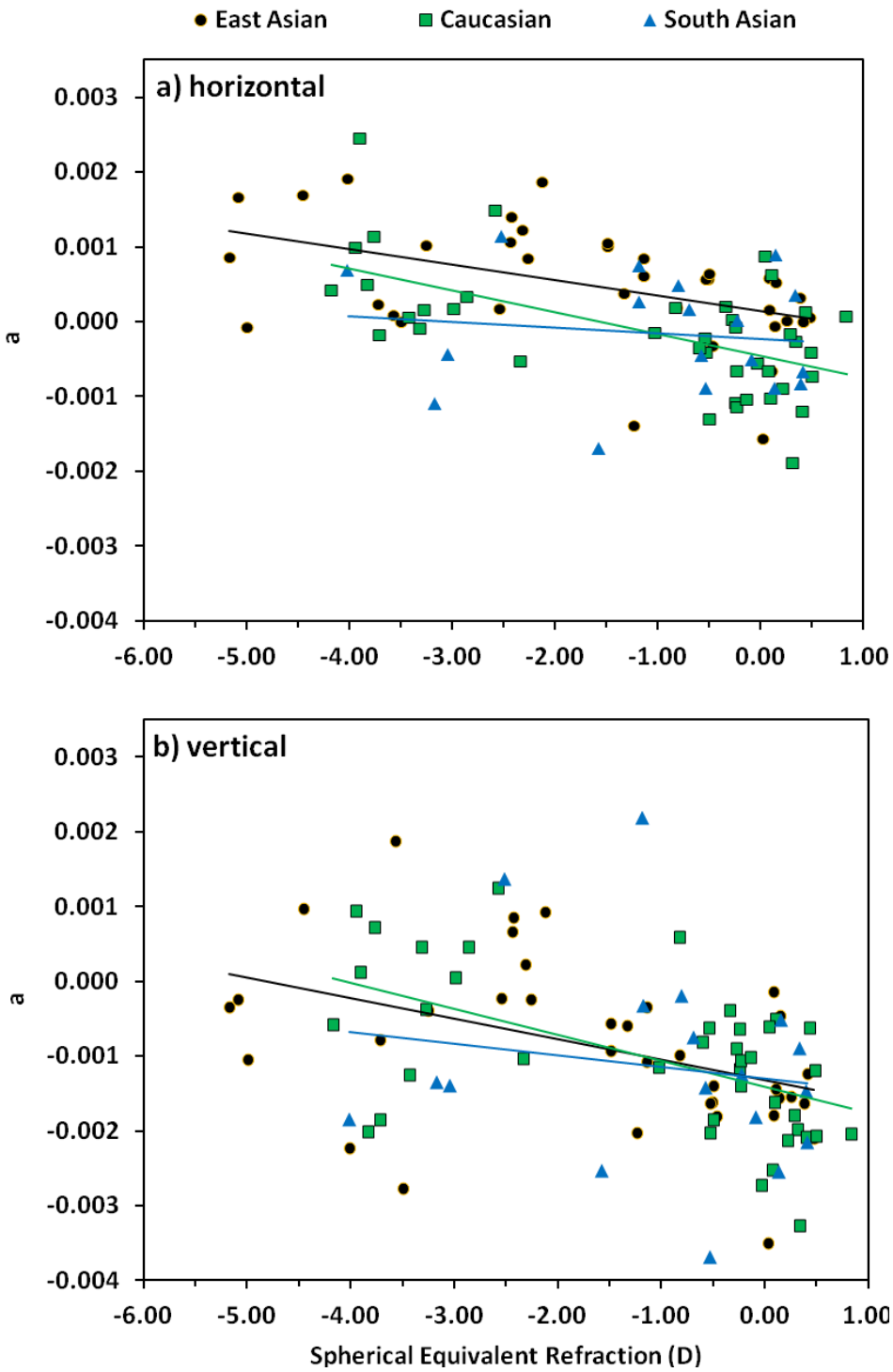

Figure 5:2: Coefficients 'a' of the polynomial fits of *RPR* along a) horizontal and b) vertical visual field meridians for each participant from different races as a function of central spherical equivalent refraction. Linear regressions for the horizontal meridian are EA: $y = –0.0002x + 0.0001$, $R^2 = 0.21$, $p = 0.004$; CA: $y = –0.0003x – 0.0005$, $R^2 = 0.34$, $p < 0.001$; SA: $y = –0.00008x – 0.0002$, $R^2 = 0.02$, $p = 0.61$. Linear regression for the vertical meridian are EA: $y = –0.0003x – 0.0013$, $R^2 = 0.18$, $p = 0.009$; CA: $y = –0.0004x – 0.0014$, $R^2 = 0.29$, $p < 0.001$; SA: $y = –0.0002x – 0.0013$, $R^2 = 0.02$, $p = 0.54$.

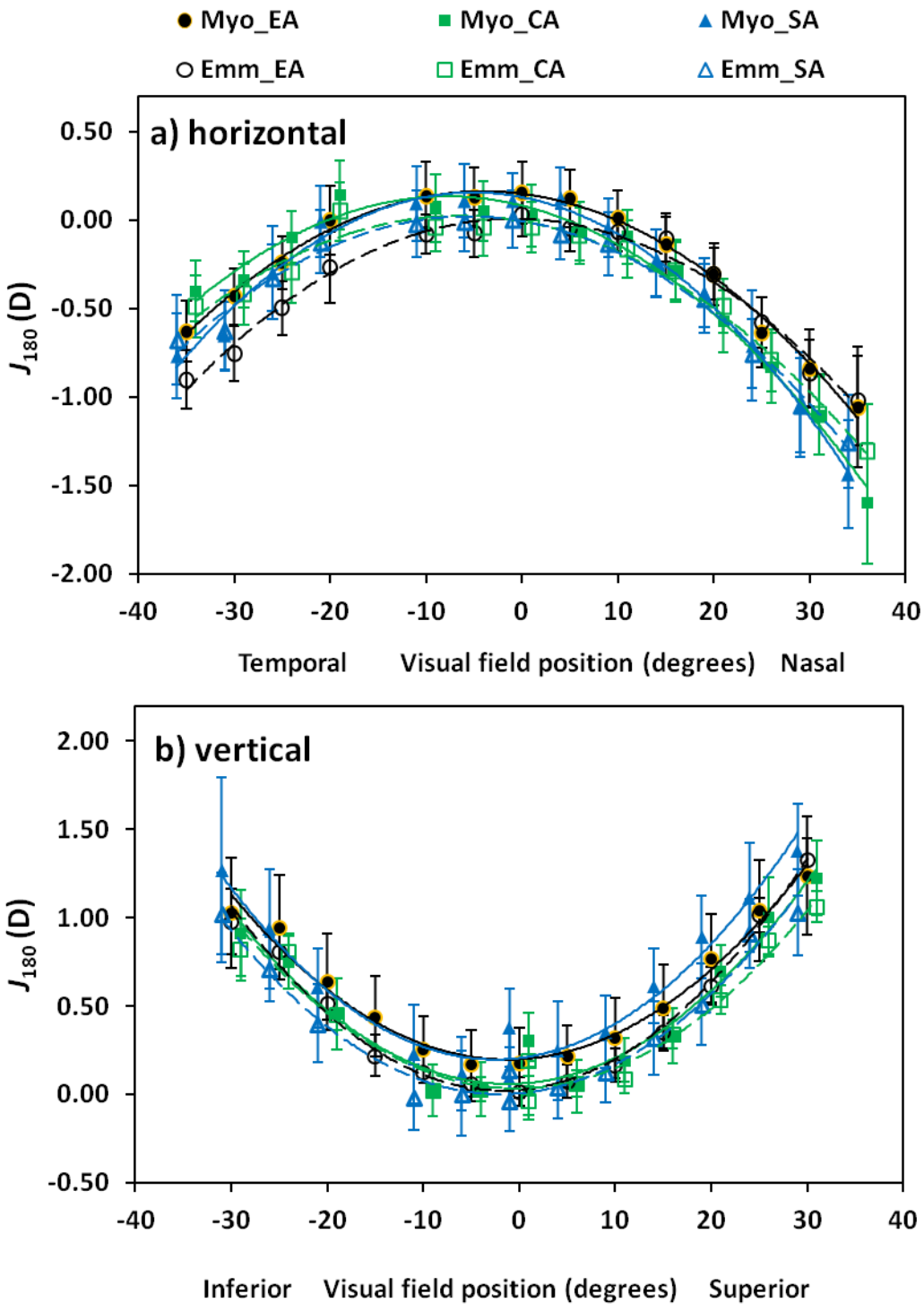

Figure 5:3: Mean J_{180} astigmatism along a) horizontal and b) vertical visual field meridians in different racial groups for emmetropes and myopes . Error bars indicate 95% confidence intervals of mean. Plots are staggered horizontally to make them more legible.

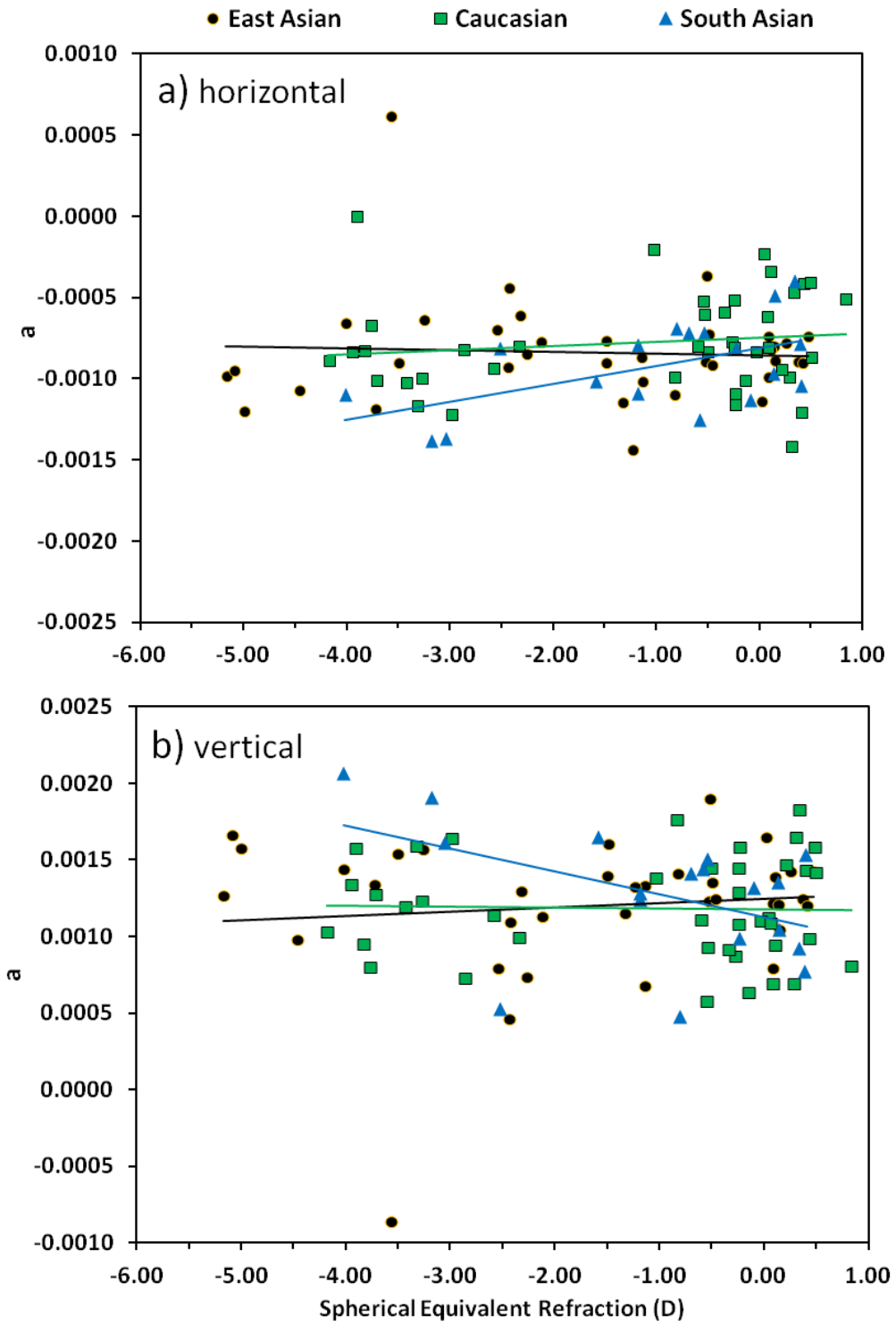

Figure 5:4: Coefficients 'a' of the polynomial fits of J_{180} astigmatism along a) horizontal and b) vertical visual field meridians for each participant from different races as a function of central spherical equivalent refraction. Linear regressions for the horizontal meridian are EA: $y = -0.00001x - 0.0009$, $R^2 = 0.01$, p = 0.55; CA: $y = +0.00002x - 0.0008$, $R^2 = 0.02$, p = 0.11; SA: $y = +0.0001x - 0.001$, $R^2 = 0.29$, p = 0.02. Linear regressions for the vertical meridian are EA: $y = +0.00003x + 0.001$, $R^2 = 0.01$, p = 0.53; CA: $y = -0.0001x + 0.0011$, $R^2 = 0.01$, p = 0.87; SA: $y = -0.0002x + 0.001$, $R^2 = 0.22$, p = 0.049.

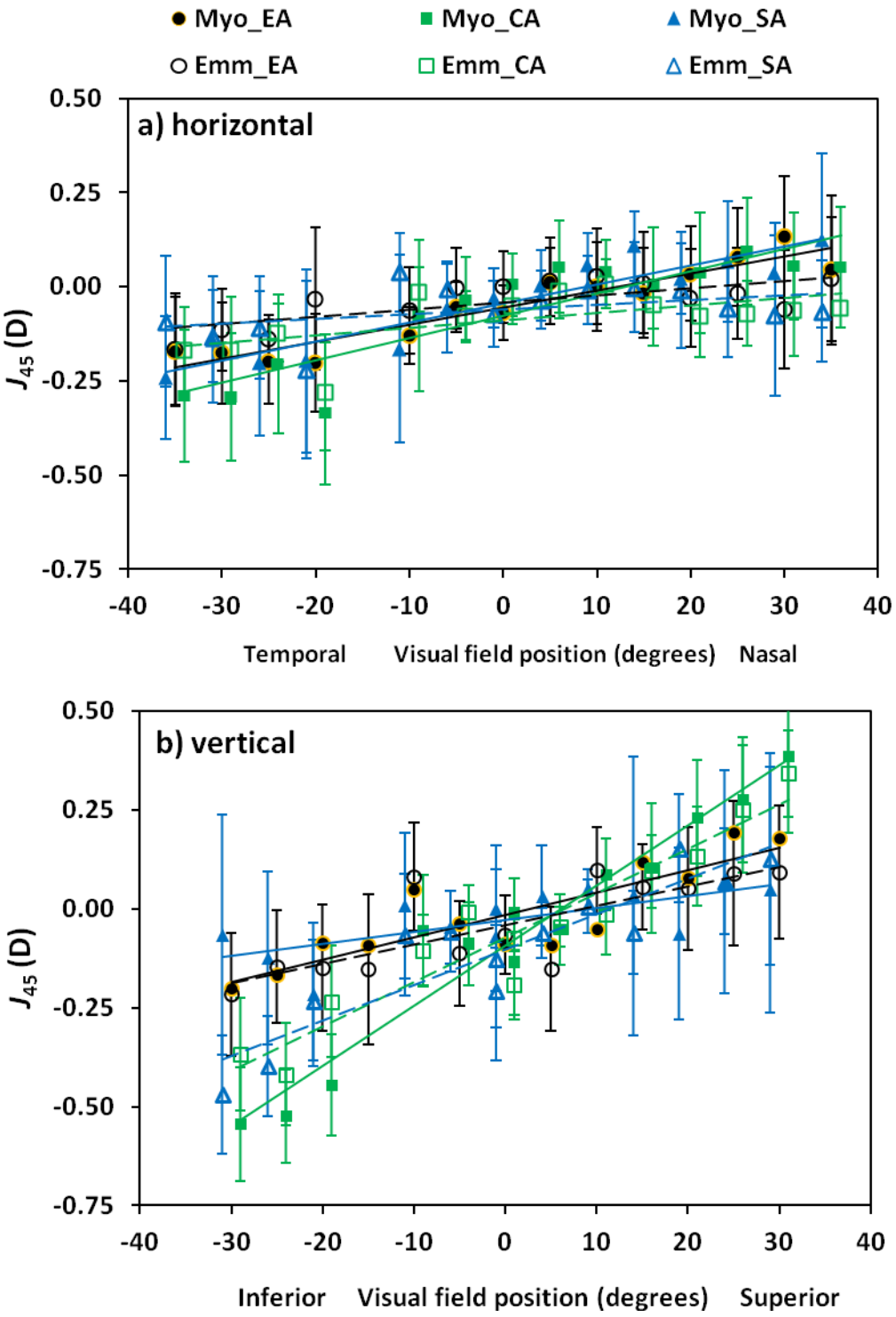

Figure 5:5: Mean J_{45} astigmatism along a) horizontal and b) vertical visual field meridians in different racial groups for emmetropes and myopes. Error bars indicate 95% confidence intervals of mean. Plots are staggered horizontally to make them more legible.

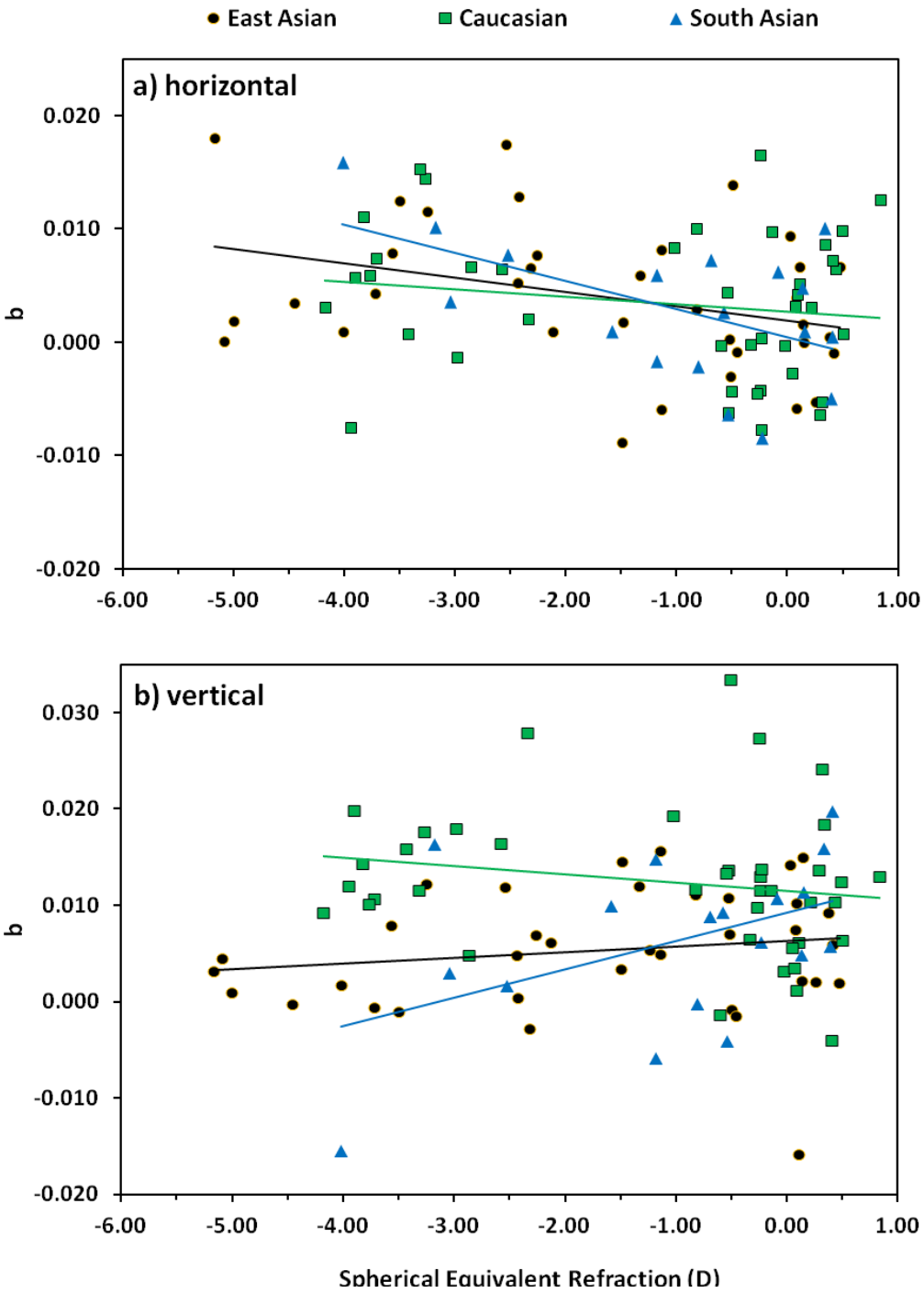

Figure 5:6: Coefficients 'b' of the linear fits of J_{45} astigmatism along a) horizontal and b) vertical visual field meridians for each participant from different races as a function of central spherical equivalent refraction. Linear regressions for the horizontal meridian are EA: $y = –0.0013x + 0.0019$, $R^2 = 0.12$, $p = 0.07$; CA: $y = –0.0007x + 0.0027$, $R^2 = 0.03$, $p = 0.24$; SA: $y = –0.0025x + 0.0004$, $R^2 = 0.28$, $p = 0.07$. Linear regressions for the vertical meridian are EA: $y = +0.0006x + 0.0063$, $R^2 = 0.03$, $p = 0.34$; CA: $y = –0.0008x + 0.011$, $R^2 = 0.03$, $p = 0.25$; SA: $y = +0.0029x + 0.0092$, $R^2 = 0.20$, $p = 0.06$.

Table 5.3: Polynomial fit coefficients for *M*, *RPR*, J_{180} and J_{45} along horizontal and vertical field meridians for each racial group (EA = East Asian, CA = Caucasian, SA = South Asian) and refractive group (E = Emmetrope, M = Myope).

	Race	E/M	Horizontal				Vertical		
			a	**b**	**c**		**a**	**b**	**c**
M	EA	E	–0.00002	+0.00049	–0.03		–0.00156	–0.00658	–0.15
		M	+0.00078	–0.00397	–2.82		–0.00042	+0.00094	–2.98
	CA	E	–0.00048	–0.00938	–0.02		–0.00148	–0.00427	–0.17
		M	+0.00036	–0.00726	–3.08		–0.00024	–0.00801	–2.96
	SA	E	–0.00028	–0.00208	–0.13		–0.00165	–0.00466	–0.20
		M	+0.00001	–0.00058	–2.14		–0.00051	–0.01103	–2.16
RPR	EA	E	–0.00002	+0.00066	–0.04		–0.00156	–0.00658	–0.07
		M	+0.00073	–0.00430	–0.06		–0.00042	+0.00094	–0.13
	CA	E	–0.00048	–0.00938	–0.03		–0.00148	–0.00427	–0.08
		M	+0.00036	–0.00726	–0.01		–0.00024	–0.00801	–0.06
	SA	E	–0.00028	–0.00208	–0.06		–0.00165	–0.00466	–0.03
		M	+0.00001	–0.00058	+0.05		–0.00051	–0.01103	–0.05
J_{180}	EA	E	–0.00083	–0.00132	+0.01		+0.00131	+0.00442	+0.03
		M	–0.00084	–0.00677	+0.15		+0.00113	+0.00286	+0.20
	CA	E	–0.00075	–0.01111	–0.01		+0.00115	+0.00298	+0.01
		M	–0.00086	–0.01512	+0.07		+0.00124	+0.00500	+0.03
	SA	E	–0.00083	–0.00772	+0.01		+0.00123	+0.00261	–0.03
		M	–0.00103	–0.00842	+0.14		+0.00134	+0.00416	+0.16
J_{45}	EA	E		+0.00192	–0.04			+0.00443	–0.02
		M		+0.00403	–0.01			+0.00581	+0.01
	CA	E		+0.00200	–0.09			+0.01109	–0.05
		M		+0.00591	–0.07			+0.01463	–0.06
	SA	E		+0.00124	–0.06			+0.00884	–0.10
		M		+0.00449	–0.05			+0.00324	–0.05

Discussion

Generally, the results support previous investigations concerning patterns in the horizontal and vertical field meridians and how these are associated with central refraction:

There was negative *RPR* (relative peripheral myopia) in both meridians for emmetropes, but this became positive (relative peripheral hyperopia) in myopes along the horizontal meridian only (Atchison et al., 2006, Berntsen et al., 2010).

Peripheral J_{45} was 2-3 times larger along the vertical than along the horizontal meridian, but was not affected by refraction (Atchison et al., 2006).

Peripheral J_{180} was greater and had less variability than *RPR*, and was greater along the vertical than along the horizontal meridian, but I note that Atchison et al. (2006) found similar results in the two meridians.

The results show effects of race on peripheral refraction:

Caucasians developed positive *RPR* (relative peripheral hyperopia) with increased myopia at greater rates than for the other races along the horizontal meridian.

Peripheral J_{180} along both horizontal and vertical fields increased with myopia for South Asians only.

There was a trend for East Asians to have greater relative peripheral hyperopia than other races along the horizontal meridian (Figure 5:1a), but this was not quite significant. Logan et al. (2004) did not find such a trend, but Kang et al. (2010) found that moderate myopic East Asians had greater relative peripheral hyperopia than did moderate myopic Caucasians in the temporal visual field. Because the differences in significance of race between this study and that for Kang et al. may be at least in part due to differences in analysis, I performed a similar ANOVA analysis as Kang et al. (2010). I did a repeated-measures ANOVA on the horizontal *RPR* data at ±30 degrees with race (EA, CA only) and refractive group (emmetropes, low and moderate myopia categories as selected by Kang et al.) as between-subject factors. Race was indeed a significant influence on relative refraction pattern ($F_{2, 69} = 5.3$, p =

0.03), but there was no interaction between race and refraction group ($F_{2, 69} = 0.7$, $p = 0.53$).

Caucasians had significantly higher "b" coefficients for J_{45} than did East Asians. Peripheral refraction profiles in South Asians and the differences in peripheral refraction profiles of races along the vertical meridian have not been reported before.

5.3 PERIPHERAL EYE LENGTHS

Method

Peripheral eye length measurements were obtained with the Lenstar using the procedure described in section 3.5.5. Relative peripheral eye length (*RPEL*) was determined by subtracting central axial length from the eye length obtained at different visual field angles:

RPEL = peripheral *EL* – central *EL*

RPEL was plotted as a function of visual field position. Data corresponding to the approximate optic disc position (15º temporal field) were not included in analysis. Second order polynomial fits were applied for each participant as for peripheral refraction (section 5.1, equation (54)).

Two-way ANOVAs were conducted on the highest order coefficient "a" with race (EA/CA/SA) and refraction group (myopes/emmetropes) as between-subject factors and visual field meridian (horizontal/vertical) as a within-subject factor. Post hoc t-tests with Bonferroni correction were used to compare between races.

To investigate if *RPEL* was affected by myopia magnitude, linear regressions were determined for the coefficients as function of central *M*. Analysis of covariance (ANCOVA) was performed to test the significance of slopes between races.

Results

Figure 5:7 shows mean relative peripheral eye lengths along horizontal and vertical fields as a function of visual field angle in different racial groups for both emmetropes and myopes. It includes polynomial fits, for which the coefficients are

given in Table 5.4. The patterns were affected significantly by all factors (ANOVAs for coefficient "a" were: $F_{1,176}$ (meridian) = 17.9, $p < 0.001$; $F_{1,176}$ (refraction) = 85.5, $p < 0.001$; $F_{2,176} = 3.4$ (race), $p = 0.04$). All plots showed negative *RPEL*, but with higher values along the horizontal than along the vertical field and with higher values for myopes than for emmetropes. More negative coefficients were found in East Asians (mean ± SD: –0.0009 ± 0.0004 mm/degree^2) than in Caucasians (–0.0005 ± 0.0004) and South Asians (–0.0006 ± 0.0004), with all post-hoc comparisons except for Caucasians with Asians being significant; this racial variation was attributable solely to differences along the horizontal meridian.

The linear regressions showed that the slope of coefficient "a" per dioptre of central *M* was greater for the vertical than for the horizontal meridian (Figure 5:8) and were not significantly different between the races in the corresponding ANCOVAs ($F_{2,88} = 0.24$, $p = 0.78$, horizontal meridian; $F_{2,88} = 0.38$, $p = 0.69$ vertical meridian).

Table 5.4: Polynomial fit coefficients for *RPEL* along horizontal and vertical field meridians for each racial group (EA = East Asian, CA = Caucasian, SA = South Asian) and refractive group (E = Emmetrope, M = Myope).

	Race	E/M	Horizontal				Vertical		
			a	**b**	**c**		**a**	**b**	**c**
RPEL	EA	E	–0.00075	–0.00462	–0.01		–0.00025	+0.00157	–0.04
		M	–0.00113	–0.00348	–0.04		–0.00080	–0.00299	–0.01
	CA	E	–0.00046	–0.00315	–0.02		–0.00023	–0.00132	–0.04
		M	–0.00087	–0.00507	–0.04		–0.00090	+0.00116	+0.00
	SA	E	–0.00315	–0.00365	–0.04		–0.00030	–0.00207	–0.04
		M	–0.00086	–0.00212	–0.06		–0.00079	–0.00582	–0.03

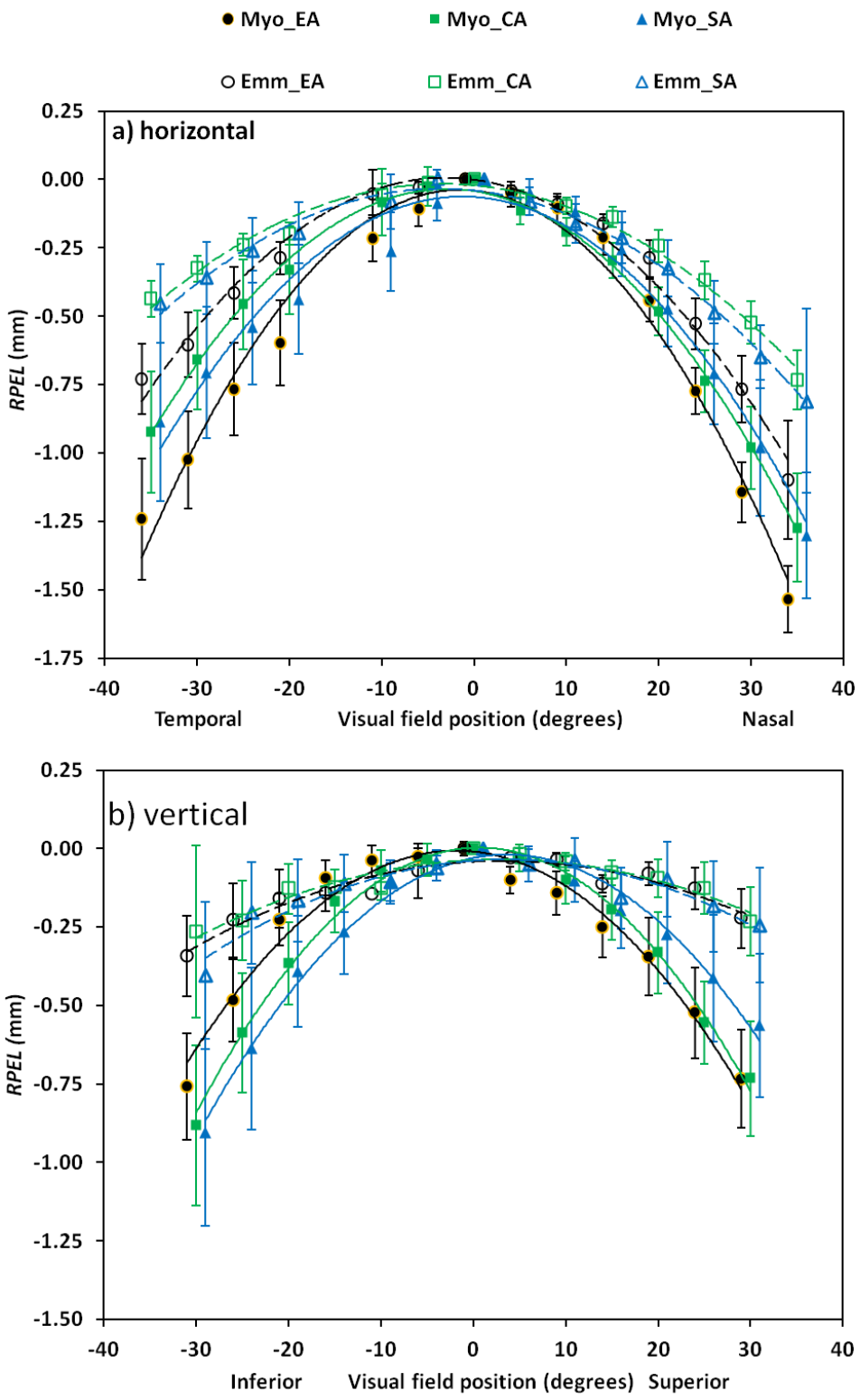

Figure 5:7: Mean *RPEL* along a) horizontal and b) vertical visual field meridians in different racial groups for both emmetropes and myopes. Error bars indicate 95% confidence intervals of mean. Plots are staggered horizontally to make them more legible.

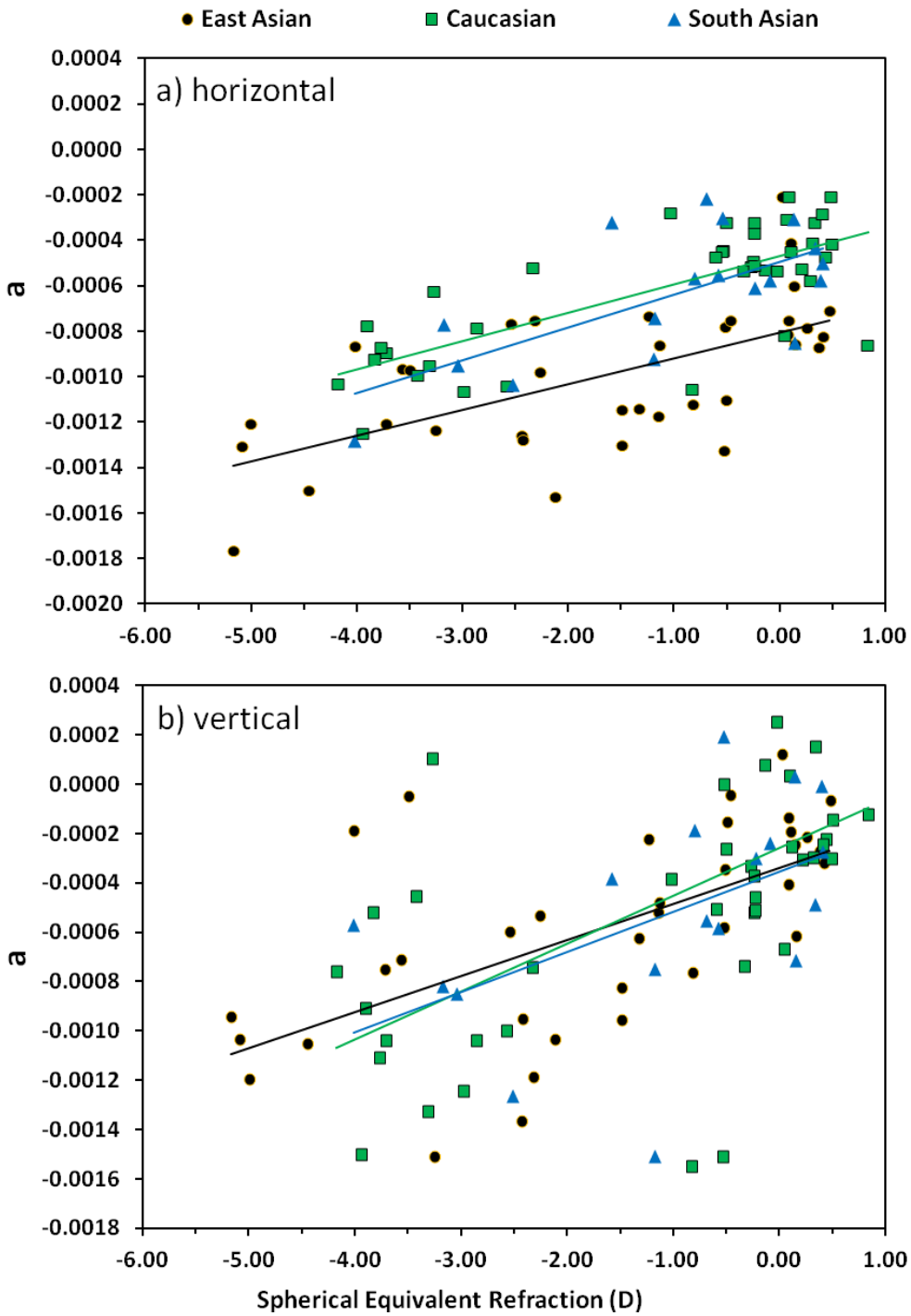

Figure 5:8: Coefficients 'a' of the polynomial fits of *RPEL* along a) horizontal and b) vertical visual field meridians in different racial groups as a function of central spherical equivalent refraction. Linear regressions for the horizontal meridian are EA: $y = +0.00011x - 0.00081$, $R^2 = 0.38$, $p < 0.001$; CA: $y = +0.00013x - 0.00047$, $R^2 = 0.55$, $p < 0.001$; SA: $y = +0.00014x - 0.00051$, $R^2 = 0.46$, $p < 0.001$. Linear regressions for the vertical meridian are EA: $y = +0.00015x - 0.0003$, $R^2 = 0.38$, $p < 0.001$; CA: $y = +0.00019x - 0.00030$, $R^2 = 0.33$, $p = 0.002$; SA: $y = +0.00016x - 0.00035$, $R^2 = 0.25$, $p = 0.03$.

Discussion

All participants had negative *RPEL*s, which became more negative as myopia increased in agreement with studies using a similar external attachment (Ehsaei et al., 2012, Faria-Ribeiro et al., 2013) and a custom built interferometer (Schmid, 2003a, 2003b). The *RPEL*s were more negative along the horizontal meridian than along the vertical meridian, but changed more rapidly along the vertical meridian as myopia increased.

The changes in *RPEL* with central refraction were consistent with the changes in relative peripheral refraction found in section 5.2 (more negative *RPEL* with more relative peripheral hyperopia). Two other studies found significant correlations between *RPEL* and relative peripheral refraction in the horizontal visual field (Faria-Ribeiro et al., 2013, Orr et al., 2013). Considering all our participants showed negative *RPEL*s, it is worth mentioning that the sign of *RPEL* alone does not indicate the shape of the retina nor the sign of relative peripheral refraction.

Concerning race, East Asians had more negative *RPEL*s than the other races along the horizontal meridian across a range of refractions. This is consistent with the non-significant tendency for East Asians to have more relative hyperopia than other races as found in section 5.2.

5.4 RETINAL SHAPE

Method

Retinal shape was estimated in terms of vertex radius of curvature and asphericity using the validated $PCI_{Stage\ 2}$ method described in section 3.5.7.

Mean ± 95% confidence interval limits of vertex radius of curvature and asphericity were determined in emmetropes and myopes of different races along horizontal and vertical field meridians.

Two-way ANOVAs were conducted on the vertex radius of curvature and asphericity separately with race (EA/CA/SA) and refraction group (myopes/emmetropes) as between-subject factors and visual field meridian (horizontal/vertical) as a within-subject factor. Post hoc t-tests with Bonferroni correction were used to compare between races.

To investigate if retinal shape estimates were affected by myopia magnitude, linear regressions were determined for vertex radius of curvature and asphericity plotted against central *M*. Analysis of covariance (ANCOVA) was performed to test the significance of slopes between races.

Results

Figure 5:9 shows the means ± SD of the retinal coordinates in the different racial groups. For the horizontal meridian, the retinas were steeper for the East Asians than for the other races (Figure 5:9a), but there were no racial trends for the vertical meridian (Figure 5:9b). The retinal coordinates along horizontal and vertical meridians in emmetropes and myopes are shown for each race separately in Figure 5:10a-f. The nasal-temporal and superior-inferior asymmetries occurred for all combinations of race and refraction groups.

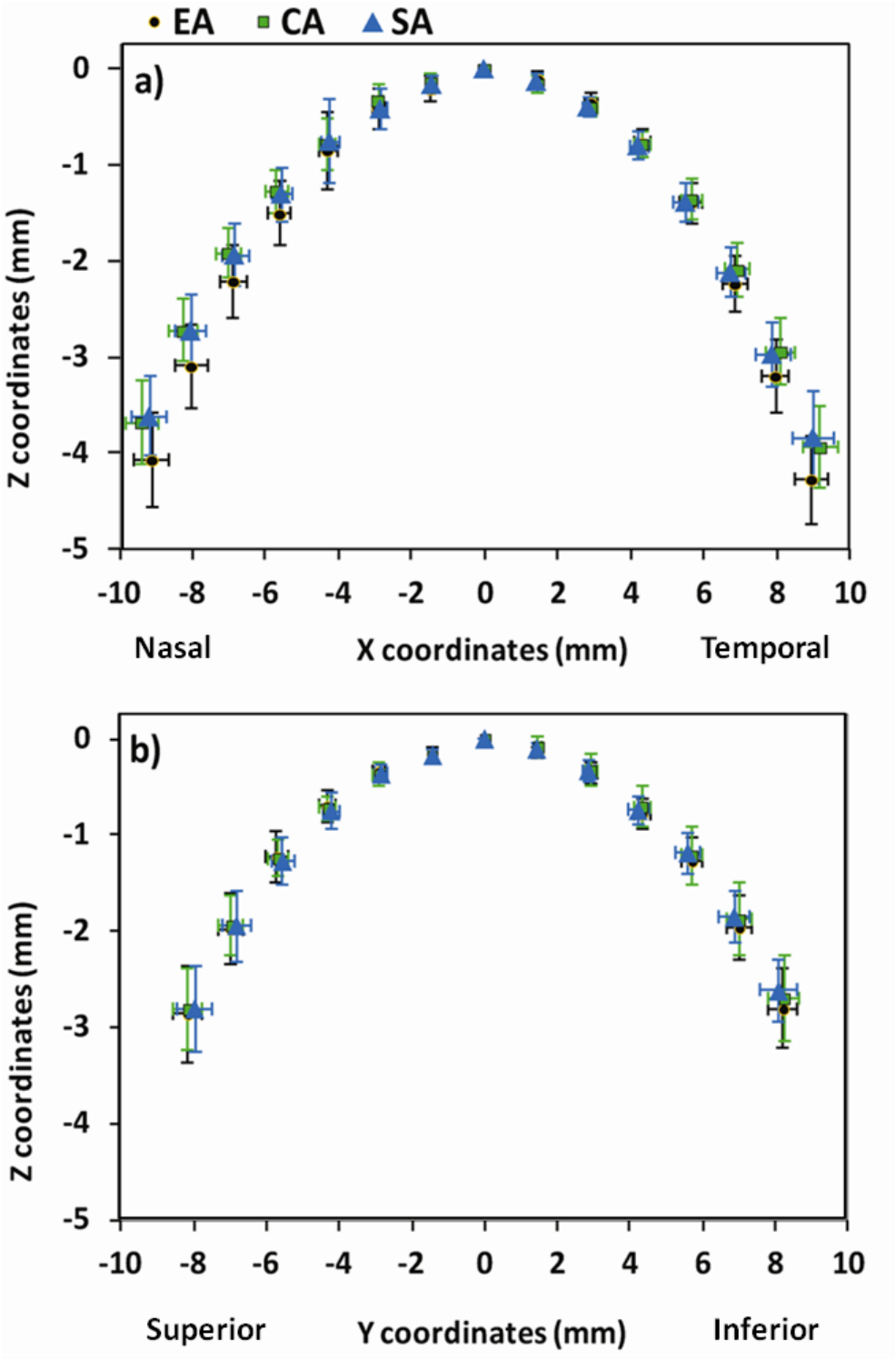

Figure 5:9: Retinal coordinates in the three races along a) horizontal and b) vertical field. Horizontal and vertical error bars represent standard deviations for Z and X/Y coordinates, respectively.

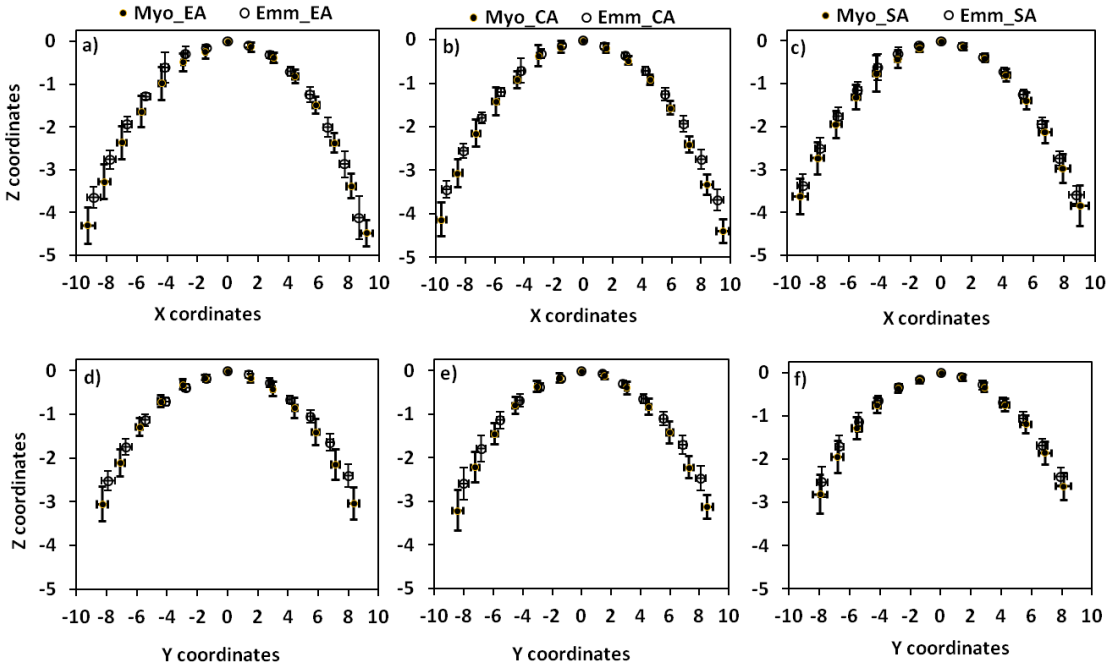

Figure 5:10: Retinal coordinates in emmetropes and myopes for EA, CA and SA along the horizontal meridian (a), b), c)) and along the vertical meridian (d), e), f)). Horizontal and vertical error bars represent standard deviations for Z and X/Y coordinates, respectively.

Figure 5:11a and b shows the means and their 95% confidence interval limits for vertex radius of curvature and asphericity, respectively, in different racial groups for both emmetropes and myopes along horizontal and vertical field meridians. Vertex radius of curvature was affected significantly by visual field meridian and refraction (ANOVA: $F_{1, 516}$ (meridian) = 14.6, $p < 0.001$; $F_{1,516}$ (refraction) = 9.5, $p = 0.002$) but not quite by race ($F_{2, 516} = 2.8$, $p = 0.06$). The vertex radii of curvature were smaller along the horizontal (mean ± SD: 11.8 ± 1.6 mm) than along the vertical meridian (13.0 ± 1.9 mm), with smaller radii of curvatures for myopes (11.8 ± 2.0 mm) than for emmetropes (12.9 ± 1.6 mm).

Although race did not show significant influence on vertex radius of curvature, there were significant interactions between field and race ($F_{2, 176} = 0.19$, $p = 0.02$). East Asians showed smaller vertex radii of curvature along horizontal (11.2 ± 0.51 mm) and vertical meridians (12.6 ± 0.6 mm) than Caucasians (12.3 ± 0.5 mm and 13.3 ± 0.7 mm), with the South Asians being intermediate (12.0 ± 0.70 mm and 12.8 ± 0.8 mm). There was statistical significance for the differences between East Asians and Caucasians for the horizontal meridian ($p < 0.001$).

The ANOVA did not show statistically significances with either visual field meridian, refraction group or race ($F_{1,\ 158}$ (meridian) = 2.13, p =0.15; $F_{1,158}$ (refraction) = 0.17, p = 0.68; $F_{2,158}$ (race) = 1.32, p = 0.27). The mean asphericities along horizontal and vertical meridians were –0.38 ± 0.17 and –0.19 ± 0.41 (East Asians), –0.51 ± 0.23 and –0.06 ± 0.41 (Caucasians) and –0.68 ± 0.29 and –0.51 ± 0.46 (South Asians). An interesting effect is the considerable, and of itself significant, difference between East Asian emmetropes and myopes along the vertical field.

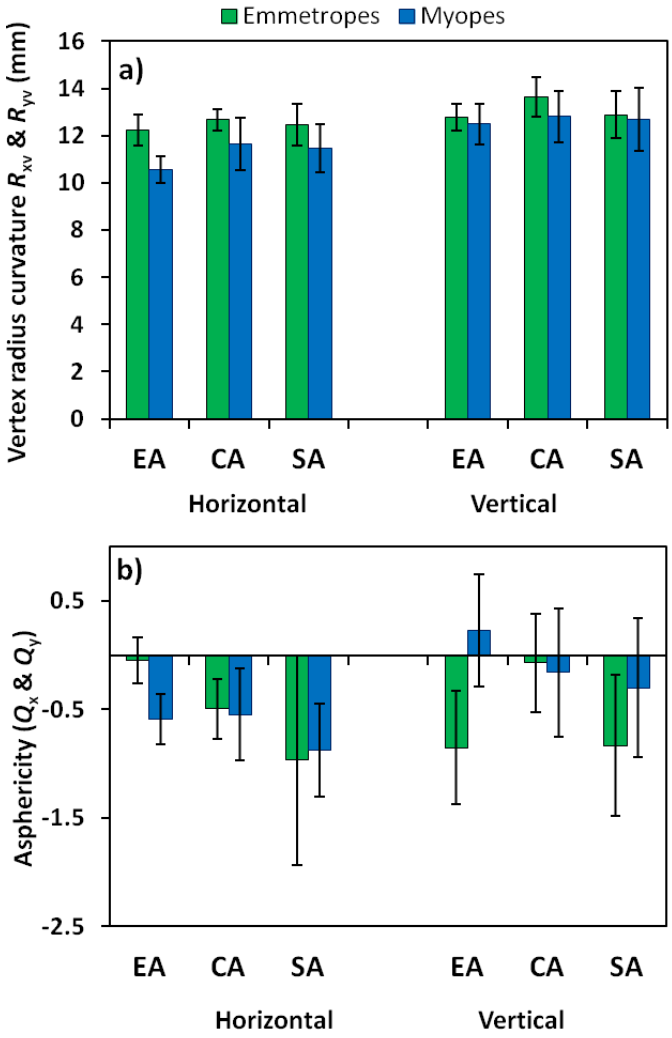

Figure 5:11: Mean retinal vertex radius of curvature a) and asphericity b), in emmetropes and myopes of different races along horizontal and vertical field meridians. Error bars indicate 95% confidence intervals of mean.

Figure 5:12 shows the linear regression of vertex radius of curvature and asphericity against central *M* along horizontal and vertical meridians. There is a

tendency for the vertex radius of curvature to decrease with increasing myopia along the horizontal meridian, and while the East Asians showed a significant slope (Table 5.5), the slopes were not significantly different between the races in the corresponding ANCOVA ($F_{2, 88} = 0.28$, $p = 0.76$). East Asians showed a significant slope for asphericity and the horizontal meridian (Table 5.4), but again the slopes were not significantly different between the races in the corresponding ANCOVA ($F_{2, 88} = 0.53$, $p = 0.59$).

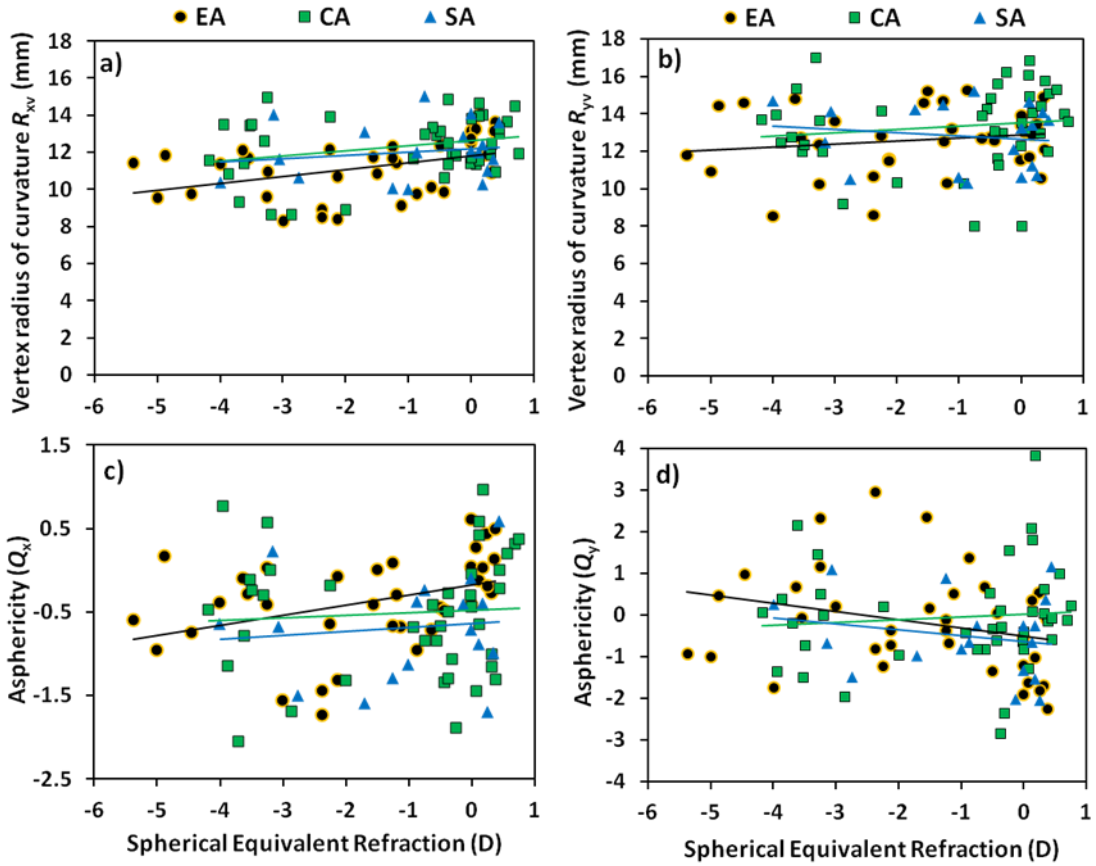

Figure 5:12: Retinal vertex radius of curvatures and asphericities of participants as a function of central spherical equivalent refraction: retinal radius of curvature along a) horizontal and b) vertical field meridians; asphericities along c) horizontal and d) vertical field meridians.

Table 5.5: Linear regression fit coefficients for retinal shape estimates along horizontal and vertical field meridians for each racial group (EA = East Asian, CA = Caucasian, SA = South Asian) as a function of central spherical equivalent refraction. The p values refer to the "a" co-efficient.

Race		Horizontal field meridian				Vertical field meridian		
		a	**b**	p		**a**	**b**	p
EA	R_{xv}	+0.377	+11.83	0.01	R_{yv}	+0.155	+12.86	0.36
	Q_x	+0.121	–0.18	0.02	Q_y	–0.196	–0.52	0.10
CA	R_{xv}	+0.268	+12.62	0.09	R_{yv}	+0.178	+13.54	0.40
	Q_x	+0.032	–0.48	0.66	Q_y	+0.065	+0.01	0.60
SA	R_{xv}	+0.177	+12.21	0.51	R_{yv}	–0.171	+12.63	0.56
	Q_x	+0.048	–0.64	0.66	Q_y	–0.142	–0.65	0.42

Figure 5:13 a-d compares the mean retinal surface shapes between the racial groups in emmetropes and myopes along horizontal and vertical meridians. East Asian emmetropes and myopes had steeper retinas than their Caucasian and South Asians counterparts except for emmetropia along the vertical meridian (Figure 5:13b). The mean percentage differences of retinal surface shape between East Asian emmetropes and Caucasian/South Asian emmetropes were 2.5% and < 1% along horizontal and vertical meridians, respectively. The differences were greater for myopia, with the corresponding differences being 4.6% and 1.8%.

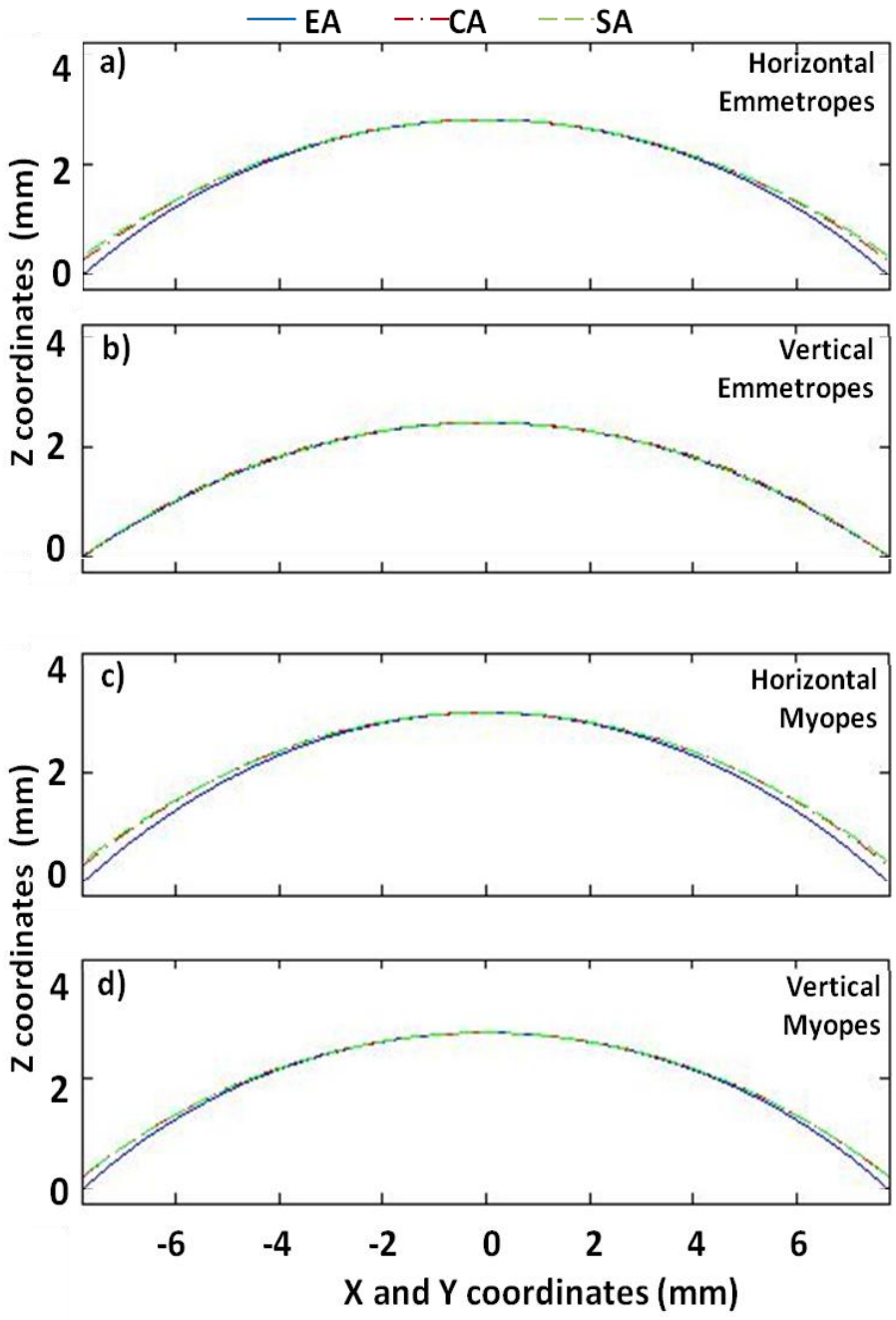

Figure 5:13: Retinal surface shape comparison between East Asians (EA), Caucasians (CA) and South Asians (SA) in emmetropes along a) horizontal and b) vertical meridians, and in myopes along c) horizontal and d) vertical meridian.

Discussion

Field meridian, refraction and race had significant effects on vertex radius of curvature but not on asphericity. The horizontal meridian had smaller radii of curvature than the vertical meridian (mean difference ± SD 1.1 ± 2.1 mm). The effects were not as strong for refraction: while emmetropes and myopes showed significant differences with the myopes having the smaller radii of curvature (mean difference 1.1 mm), most slopes of vertex radius of curvature as a function of refraction were not significant. East Asians had smaller radii of curvature than Caucasians (mean difference 1.0 mm). The steeper retinal shapes (smaller vertex radii of curvature) in East Asians than in other races was consistent with higher relative peripheral hyperopia (section 5.2) and more negative relative peripheral eye length (section 5.3).

The results of this study can be compared with three previous studies. Atchison et al. (2005a) determined retinal shapes with MRI for a young adult, largely Caucasian population. The radius of curvature became smaller along the horizontal, but not along the vertical meridian, as myopia increased, and the asphericity became less positive along both meridians as myopia increased. The current study showed a tendency for the vertex radius of curvature to decrease with increasing myopia along the horizontal meridian, but there was no trend for asphericity. There were considerable differences between the two studies, as Atchison et al. fitted conicoids to 240º degrees of the retina using MRI rather than the 132.5º degrees used here. Similar to Atchison et al. (2005a), Gilmartin et al.'s MRI study (2013) found oblate retinal shapes in both myopes and emmetropes and with myopes having less oblateness. Using Dunne's method, Logan et al. (2004) found differences in retinal coordinates between Caucasians and Chinese and found asymmetry of retinal shape changes from emmetropes to myopes that was higher for East Asians than Caucasians along the horizontal field. However, differences in asymmetry between refraction groups and races were not apparent in this study.

Models of region of retinal expansion (global, equatorial, posterior pole, and axial expansion) in myopia were introduced in section 2.4.2.2. It would be interesting to determine whether the retinal shapes of the three races follow the same model or follow different models. Unfortunately, as the measurements with PCI were

restricted to about 27% of the posterior eye as mentioned in section 3.5.6.3, this study cannot provide useful information about this.

Combining the results from this study with the high prevalence rates of myopia in East Asians suggests that steeper retinas are a risk factor for the myopia development. This requires confirmation by longitudinal studies.

5.5 CONCLUSION

Retinal shape was compared between three different races (East Asians, Caucasians and South Asians) in emmetropes and myopes along both horizontal and vertical meridians, thus addressing the second aim of the thesis: "to use the validated method to measure retinal shape in East Asian, South Asian and Caucasian myopes and emmetropes to determine how retinal shape and peripheral refraction are related in eyes of people with different racial backgrounds".

Peripheral refraction, peripheral eye lengths and retinal shapes were affected by meridian, refraction and racial group. East Asian myopes had greater relative peripheral hyperopia, more negative *RPEL*s and smaller vertex radius of curvature along both horizontal and vertical meridians than Caucasian myopes, while the South Asians were intermediate. Retinal shapes were steeper along the horizontal meridian than along the vertical meridian, in myopia than in emmetropia, and in East Asians than in Caucasians. These results support hypotheses 2 and 3 of the thesis that "there are differences in retinal shapes among different racial groups" and that "there are meridional variations in retinal shape".

Chapter 6- Retinal Shape in Isomyopes and Anisomyopes

As both eyes of an individual are exposed to the same visual (environmental) influences and the confounding influence of differences in genetic background are avoided, the anisomyopia condition may be useful for understanding the relationship between retinal shape and myopia. This chapter investigates if there are differences in retinal shape and peripheral refraction between two eyes of isomyopes and anisomyopes. As mentioned in section 2.4.1, I am not aware of any studies that have investigated whether the biometry or the structural properties of higher myopic eyes of anisomyopes are different from that of eyes of isomyopes with similar refraction, and this will also be investigated. The chapter addresses the third aim: "to determine how retinal shape and peripheral refraction vary between the two eyes of individuals with isomyopia and anisomyopia" and its associated hypothesis 4: "retinal shapes are different in isomyopic eyes and anisomyopic eyes of the same refraction".

This chapter is divided into 3 sections. Section 6.1 is an overview of methods. Sections 6.2 describes the differences in retinal shape (PCI_{Stage2} method) between the two eyes of isomyopes and anisomyopes and compares retinal shapes of myopic eyes of anisomyopic participants with isomyopic eyes of similar refraction. It includes differences in peripheral refraction between two eyes of isomyopes and anisomyopes. Section 6.3 gives the conclusions of the chapter.

6.1 METHOD

Here, twenty-one participants (12 isomyopes and 9 anisomyopes) were recruited. Anisomyopia was defined as the difference in *M* between two eyes of ≥ 1.00 D. As only isomyopes were included in the race comparison study of Chapter 5, ten isomyopic participants from that cohort were recruited for this study. Mean age of both isomyopes and anisomyopes was 23 ± 4 years with a range of 18 to 29 years. All participants had on-axis astigmatism of less than 1.50 D. Table 6.1 summarizes the characteristics of participants.

Peripheral refraction was obtained with the Shin-Nippon auto refractor using the procedure described in section 3.5.4. *RPR*, J_{180}, and J_{45} were plotted as a function of visual field position. For *RPR* and J_{180} data, second order polynomial fits were applied for each participant using equation (54) and for J_{45} data, first order linear fits were applied for each participant using equation (55).

Peripheral eye length measurements were obtained with the Lenstar, using the procedure described in section 3.5.5. Retinal shape was estimated in terms of vertex radius of curvature (R_{xv} and R_{yv}) and asphericity (Q_x and Q_y) using the $PCI_{Stage\ 2}$ method described in section 3.5.7. The R_v and Q parameters along each meridian were combined to form a "surface shape" using the procedure described in section 3.5.8. Differences between retinal shapes of the two eyes of participants were given as percentages (section 3.5.8).

I investigated how the higher myopic eyes of anisomyopic participants compare with isomyopic eyes of the same refraction. The retinal coordinates were fitted to a best sphere (Q = 0) to determine equivalent retinal radius of curvature (R_{Eq}) and were compared with a large isomyopic group of 60 eyes (combined right and left eyes of isomyopes in this experiment and all myopes from the previous experiment in Chapter 5). Because of small sample size (due to difficulty in finding participants with anisomyopia despite many recruitment advertisements) and unequal spread of participants across the range of refraction, R_{Eq} of isomyopic participants from three races were pooled together. This is a limitation of this study.

For peripheral refraction data, statistical significances between the two eyes of isomyopes and between two eyes (lower and higher myopic eyes) of anisomyopes were determined with paired t-tests. For retinal shape data R_{Eq}, analysis of covariance (ANCOVA) was performed to test the significance of differences in rate of change in R_{Eq} with refraction slopes between three groups: combined right and left eyes of isomyopes, the lower myopic eyes of anisomyopes, and the higher myopic eyes of anisomyopes.

Table 6.1: Characteristics of isomyopic and anisomyopic participants.

Condition	ID	M_R (D)	AL (mm)	M_L (D)	***AL*** (mm)	Age (years)	Gender	Race
ISO	SO	–1.00	23.52	–1.50	23.54	29	F	EA
ISO	AS	–4.00	25.19	–4.00	25.34	24	F	CA
ISO	JW	–3.75	25.9	–3.25	25.58	20	M	CA
ISO	JL	–6.00	26.73	–6.50	27.14	19	M	EA
ISO	NB	–1.25	23.13	–0.50	23.00	27	M	SA
ISO	JV	–3.00	25.66	–2.75	25.46	28	M	CA
ISO	PA	–1.25	24.11	–1.00	24.16	29	M	SA
ISO	SL	–2.00	25.29	–2.00	25.39	18	F	EA
ISO	SFL	–4.00	24.12	–3.50	24.13	22	F	EA
ISO	MG	–4.00	24.09	–4.50	24.28	24	F	CA
ISO	AR	–0.75	25.5	–1.25	25.49	24	F	CA
ISO	JK	–5.25	25.72	–5.00	25.69	20	F	EA
ANISO	PP	–3.50	23.11	–4.50	25.75	23	F	EA
ANISO	NT	–5.25	26.10	–2.75	25.22	20	F	EA
ANISO	LC	–3.75	24.5	–0.75	23.92	20	F	CA
ANISO	AL	–1.25	25.27	–4.25	26.32	19	F	EA
ANISO	YT	–3.25	25.12	–6.51	26.49	21	F	EA
ANISO	AA	–3.25	26.13	–5.25	27.27	24	F	CA
ANISO	THH	–5.00	25.11	–2.50	24.17	20	F	EA
ANISO	AK	–7.50	27.80	–6.25	27.67	29	M	SA
ANISO	QZ	–4.50	25.62	–3.00	25.11	27	M	EA

6.2 RESULTS

Peripheral refraction

Figure 6:1 to Figure 6:4 show relative peripheral refraction of the fellow eyes of both isomyopes and anisomyopes. For isomyopes, the fellow eyes had similar patterns with the coefficient "a" in equation (54) not being statistically significant different between the two eyes (p = 0.34, horizontal; p = 0.91, vertical). For anisomyopes along the horizontal meridian, the more myopic eyes clearly had more positive or less negative relative peripheral refraction in 7/9 cases and the "a" co-efficients were significantly different between the more and less myopic eyes (p = 0.02). Along the vertical meridian, the more myopic eyes clearly had more positive

or less negative relative peripheral refraction in 5/9 cases but the "a" co-efficients were not significantly different between the more and less myopic eyes (p = 0.11).

The astigmatic components had similar patterns for fellow eyes of both isomyopes or anisomyopes, with the differences between the more and less myopic eyes for "a" coefficients (J_{180}) and "b" co-efficients for (J_{45}) not being significantly different.

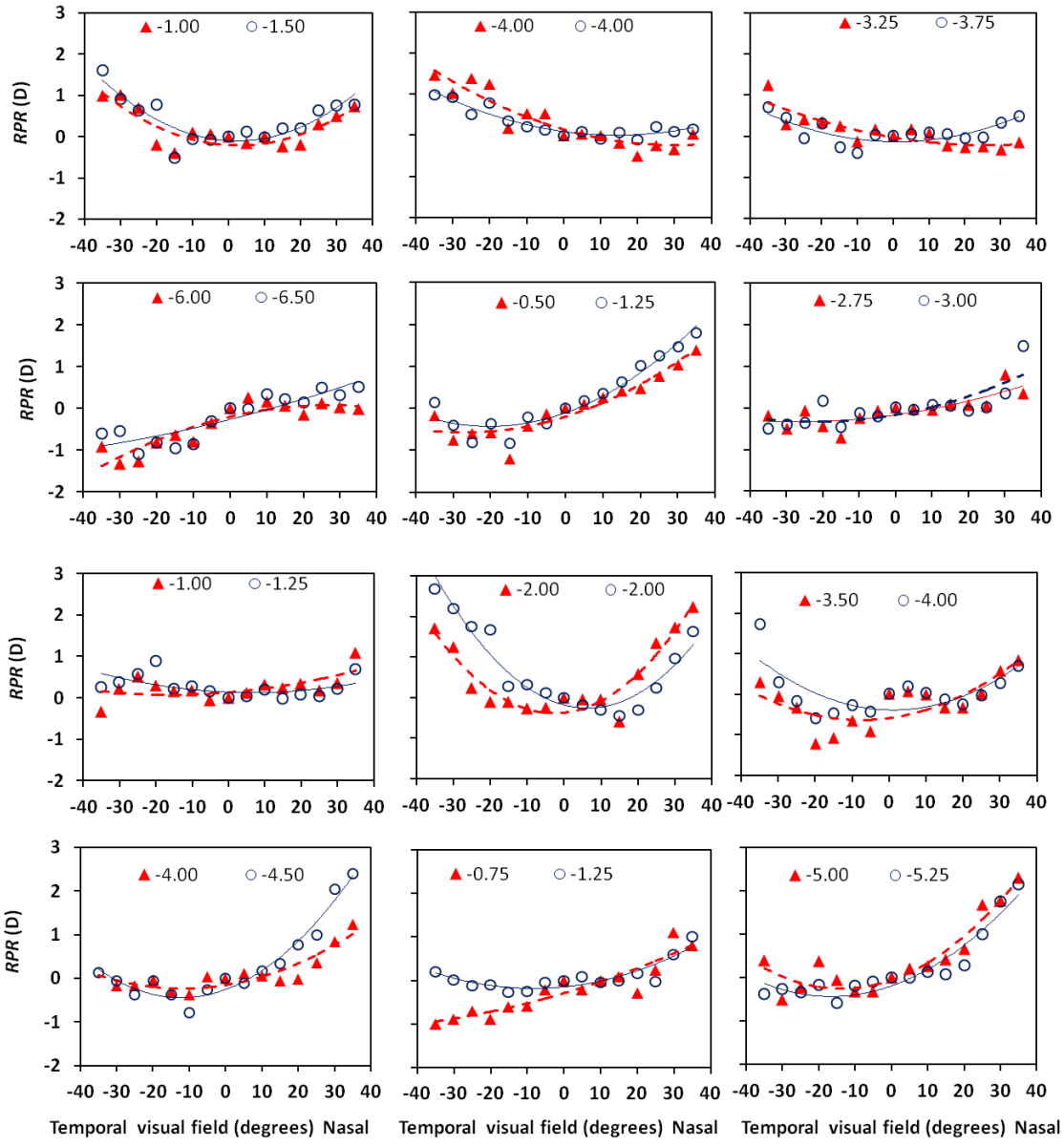

Figure 6:1: Relative peripheral refraction along the horizontal field meridian for fellow eyes of isomyopes (lower myopic eyes, red closed triangles and red dashed curves; higher myopic eyes, blue open circles and blue curves).

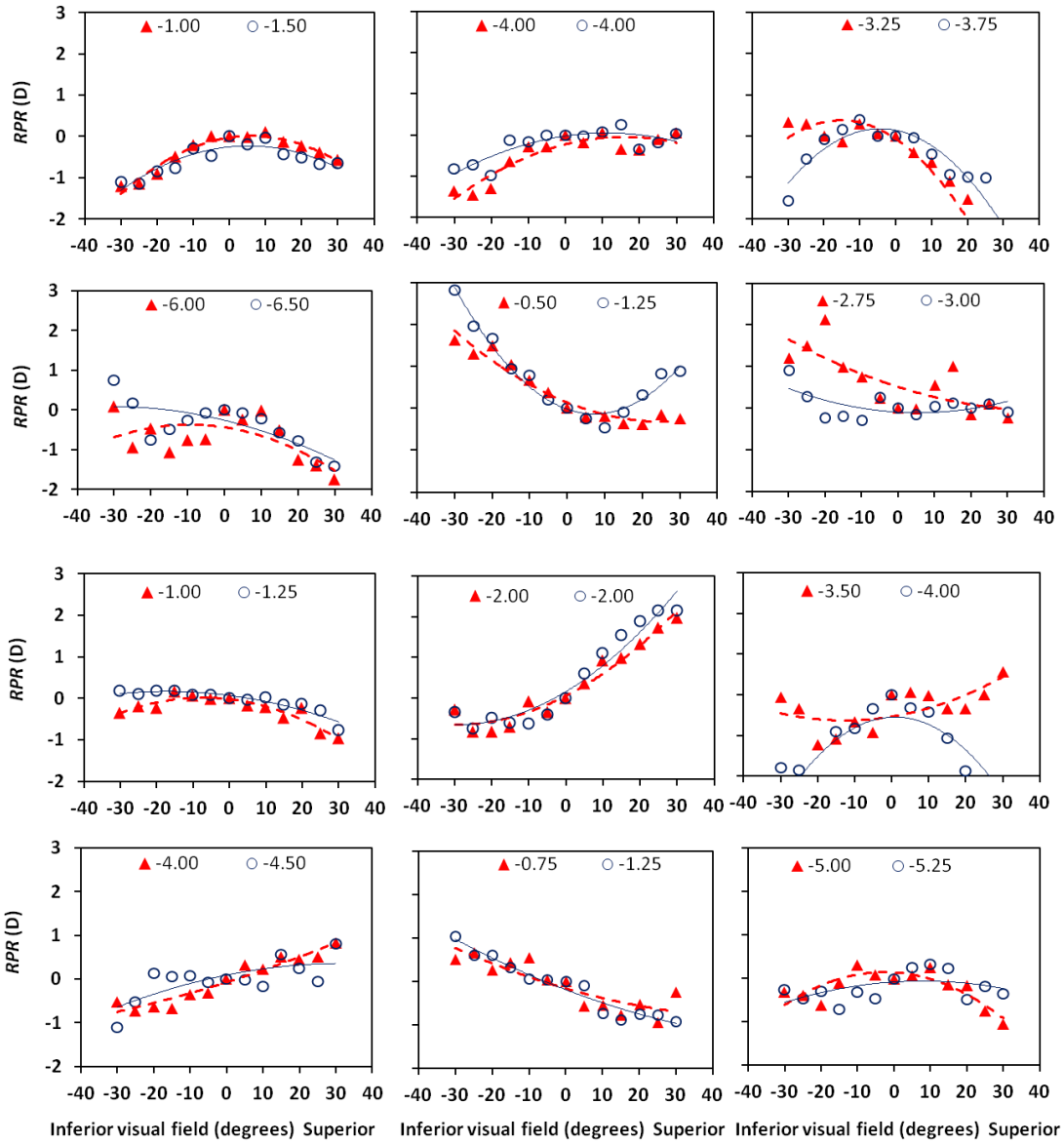

Figure 6:2: Relative peripheral refraction along the vertical field meridian for fellow eyes of isomyopes (lower myopic eyes, red closed triangles and red dashed curve; higher myopic eyes, open circles and blue curves).

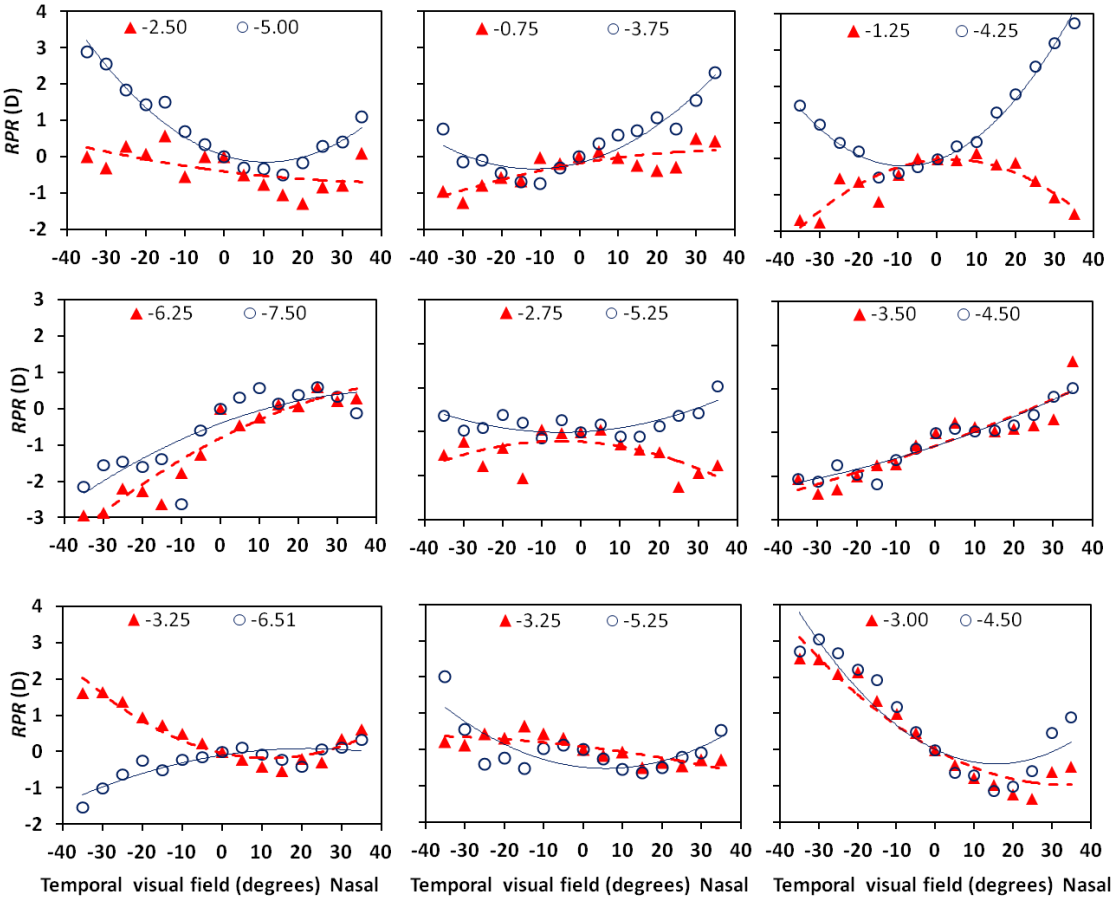

Figure 6:3: Relative peripheral refraction along the horizontal field meridian for fellow eyes of anisomyopes (lower myopic eyes, red closed triangles and red dashed curves; higher myopic eyes, open circles and blue curves).

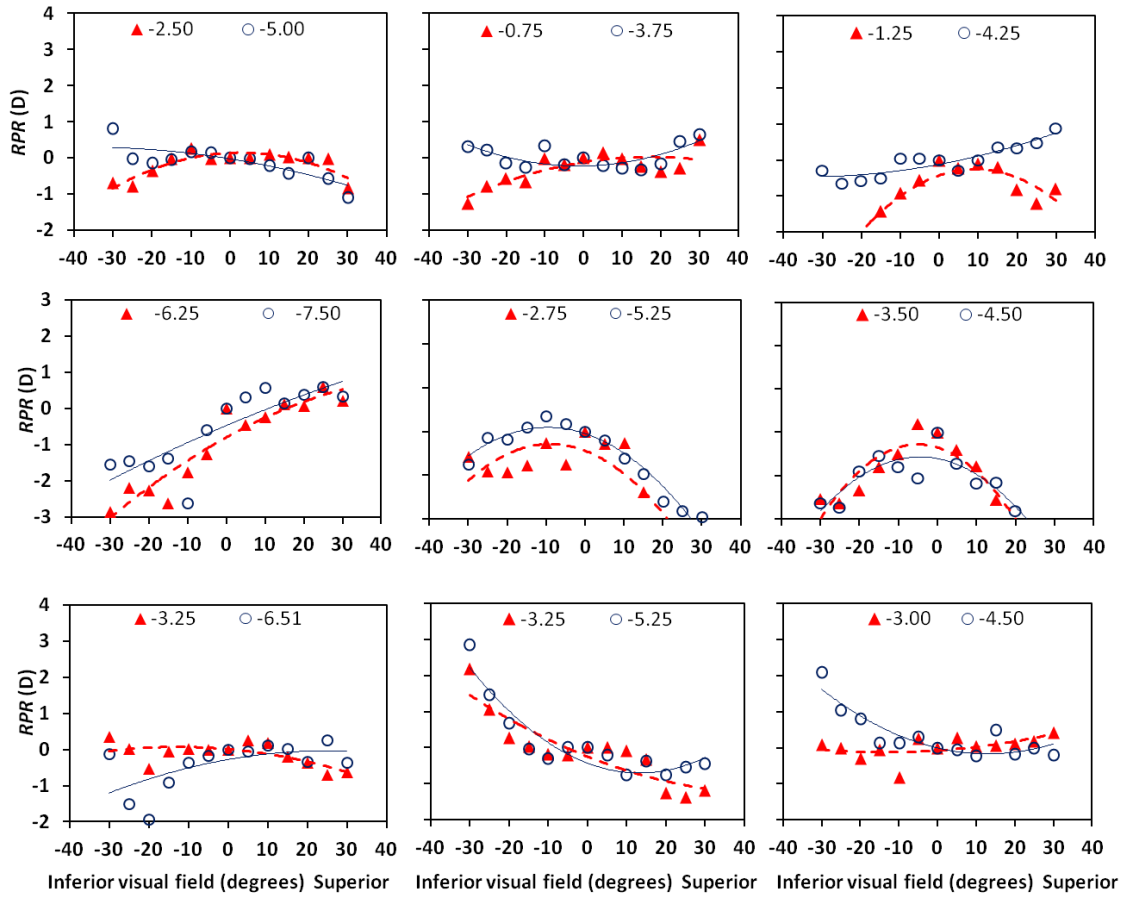

Figure 6:4: Relative peripheral refraction along the vertical field meridian for fellow eyes of anisomyopes (lower myopic eyes, red closed triangles and red dashed curves; higher myopic eyes, open circles and blue curves).

Retinal shape

Figure 6:5 shows the mean percentage difference in retinal shapes between the two eyes of both isomyopes and anisomyopes. For isometropes the fellow eyes had similar shapes (mean difference ± 95% CI 1.5 ± 0.5% horizontally, 2.7 ± 1.1% vertically). For anisometropes the fellow eyes had dissimilar shapes (mean difference 95% CI 5.1 ± 2.5% horizontally, 4.1 ± 2.4% vertically).

Figure 6:6 and Figure 6:7 show retinal shapes of fellow eyes of participants along horizontal and vertical meridians.

Figure 6:8 shows frequencies of the ratios of areas under the surface shapes for fellow eyes. Along both the horizontal and vertical meridians, isometropes had ratios close to unity of between 0.98 and 1.02. For anisomyopic participants, the higher

myopic eyes had steeper retinal shapes (lesser area) than the lower myopic eyes for 7 and 4 out of 9 participants along the horizontal and vertical meridians, respectively.

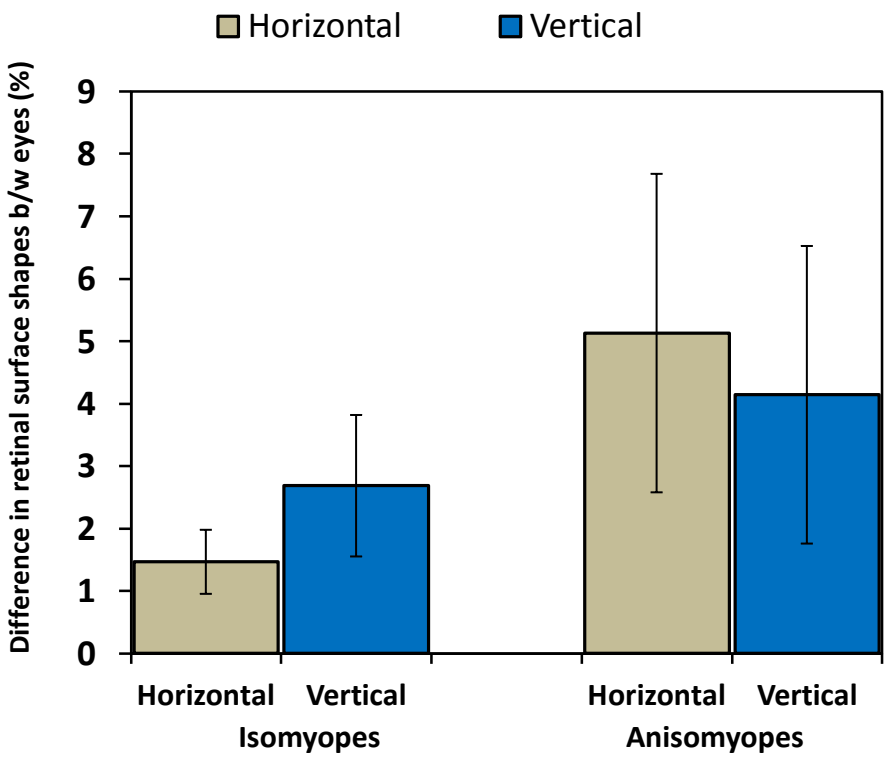

Figure 6:5: Mean percentage differences in retinal surface shapes between fellow eyes for horizontal and vertical meridians. Error bars indicate 95% confidence intervals of means.

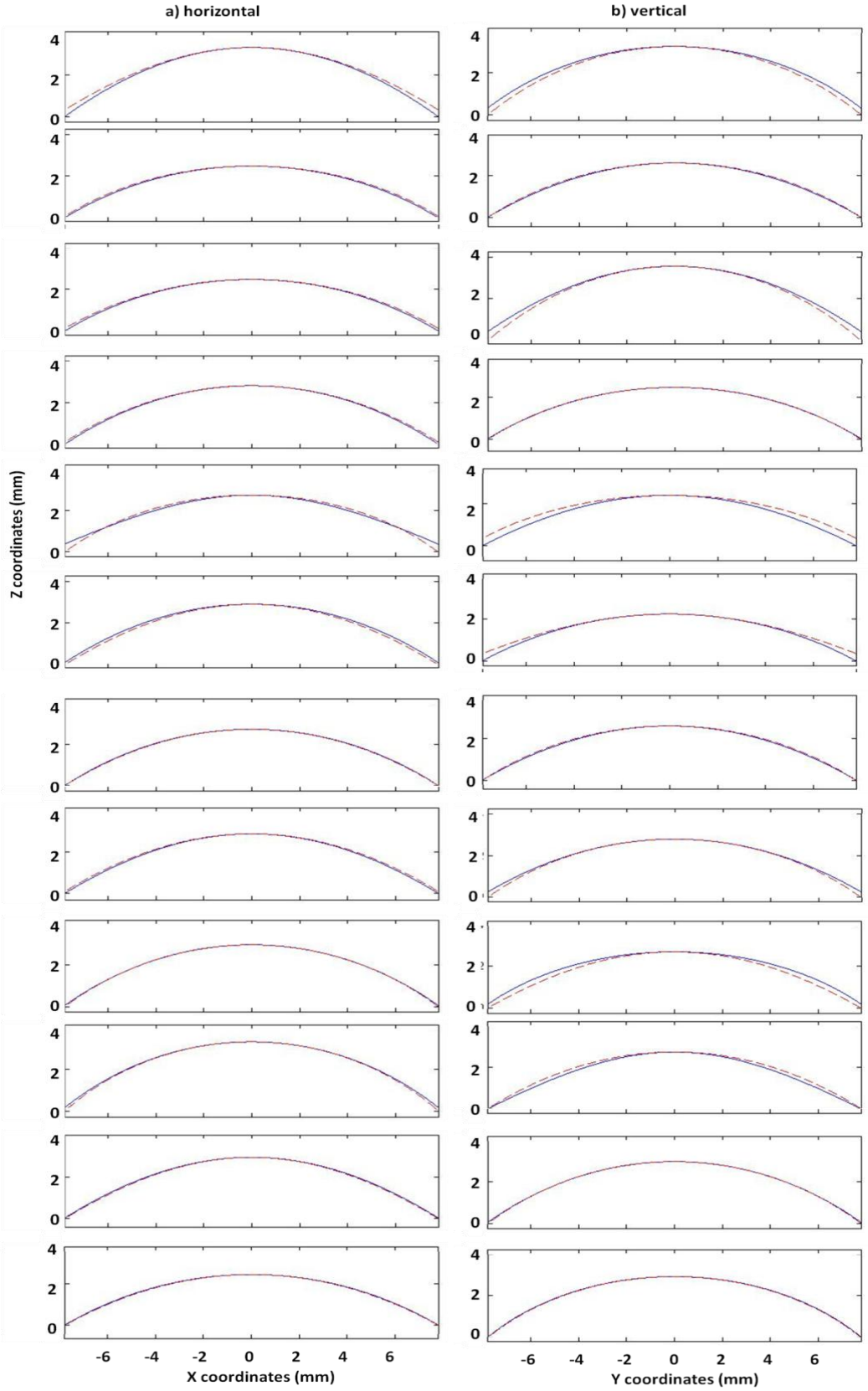

Figure 6:6: Retinal shapes of lower myopic eyes (red dashed curves) and higher myopic eyes (blue curves) of isomyopic participants for the horizontal and vertical meridians.

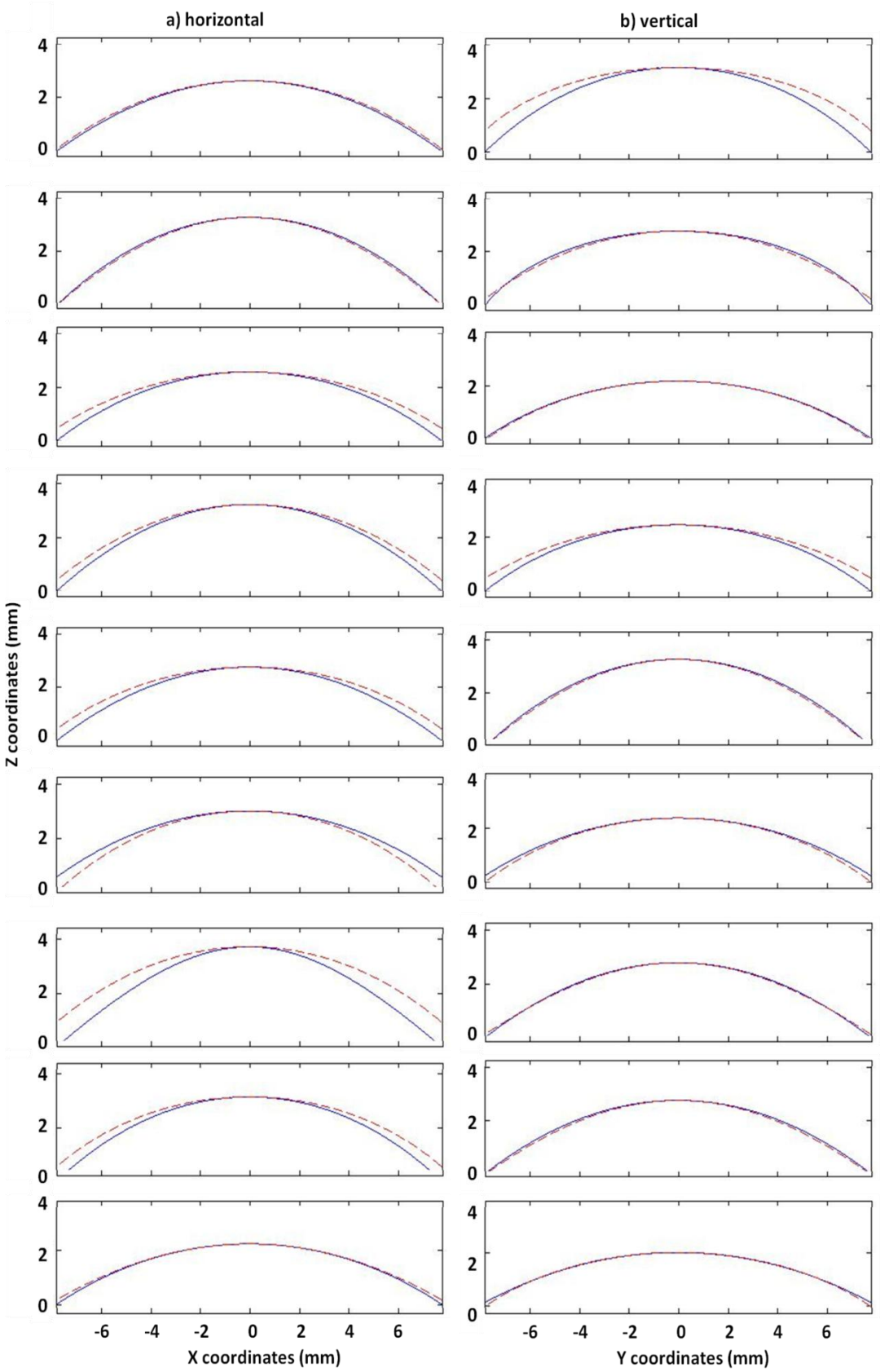

Figure 6:7: Retinal shapes of lower myopic eyes (red dashed curves) and higher myopic eyes (blue curves) of anisomyopic participants for the horizontal and vertical meridians

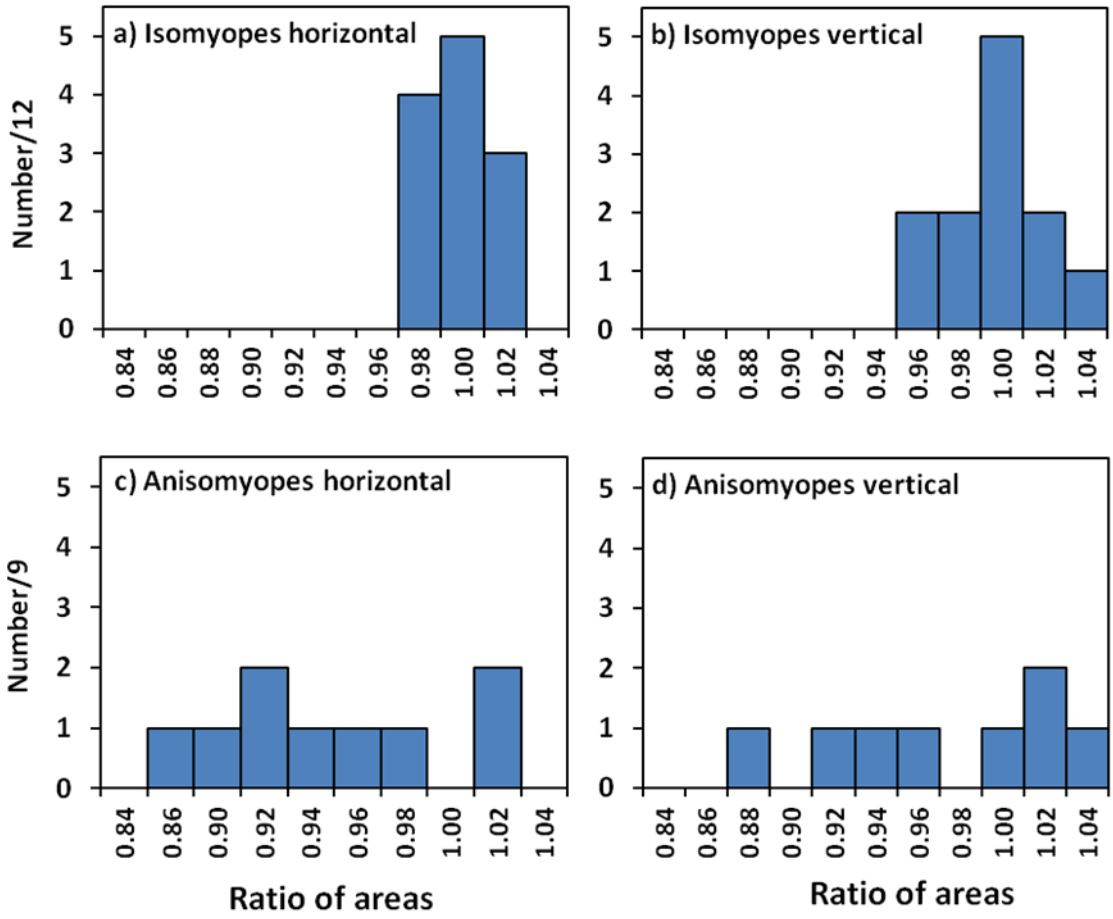

Figure 6:8: Frequency of participants against ratio of area under the "surface shapes" between fellow eyes of isomyopic participants (higher/lower myopic eye) along a) horizontal and b) vertical meridians, and of anisomyopic participants (higher/lower myopic eye) along c) horizontal and d) vertical meridians.

To investigate how the higher myopic eyes of anisomyopic participants compared with isomyopic eyes of similar refractions, retinal coordinates were fitted to a best sphere to determine the equivalent retinal radius of curvature (R_{Eq}) for each retina. The linear regressions of R_{Eq} against central M are shown in Figure 6:9 for three refraction groups: combined right and left eyes of isomyopes, the lower myopic eyes of anisomyopes, and the higher myopic eyes of anisomyopes. The slopes of the regressions are shown in Table 6.2; none were significantly different from zero ($p > 0.05$) and nor were they significantly different from each other (ANCOVA $F_{2, 71} = 2.71$ $p = 0.08$, horizontal meridian; ANCOVA $F_{2, 71} = 0.32$, $p = 0.72$, vertical meridian).

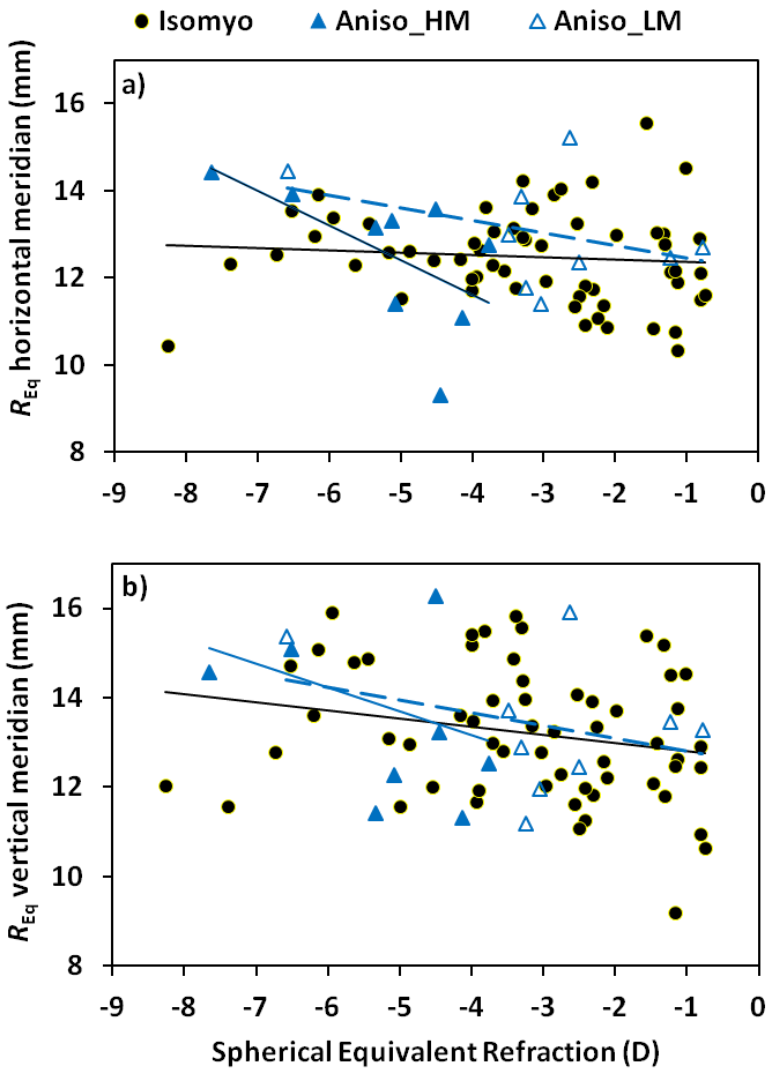

Figure 6:9: Retinal equivalent radius of curvature as a function of central spherical equivalent refraction along a) horizontal and b) vertical meridians. Groups are eyes of isomyopes (black closed circles and black solid lines), lower myopic eyes of anisometropes (blue empty triangles and blue dashed lines) and higher myopic eyes of anisometropes (filled blue triangles and blue solid lines).

Table 6.2: Linear regression fit coefficients for retinal equivalent radius of curvature R_{Eq} as a function of central spherical equivalent refraction along horizontal and vertical field meridians.

Refraction Group	Eye	Horizontal field meridian					Vertical field meridian			
		a	**b**	R^2	p		**a**	**b**	R^2	p
Isomyopes	R and L	–0.055	+12.31	0.01	0.47		–0.183	+12.62	0.05	0.10
Anisomyopes	lower	–0.286	+12.18	0.13	0.32		–0.285	+12.51	0.09	0.42
	higher	–0.796	+8.433	0.03	0.09		–0.532	+11.03	0.09	0.43

R and L = right and left eyes, lower = lower myopic eye, higher = higher myopic eye. The p values refer to the "a" co-efficients which are the slopes of the fits.

Discussion

For isomyopes, retinal surface shape and peripheral refractions were similar in fellow eyes. For anisomyopes, the high myopic eyes showed significantly steeper retinas and significantly more positive/less negative relative peripheral refraction along the horizontal meridian. Peripheral $J_{180\ \text{and}}\ J_{45}$ were not influenced by anisomyopia. The results support Logan et al. (2004), who used Dunne's method to estimate retinal shape along the horizontal meridian and found steeper shapes of the higher myopic eye than of the fellow eye of anisomyopes. They referred to the former as being more prolate which in the context of mathematical fitting may not be accurate (see section 2.4.2.1).

Previous studies investigating biomechanical, optical or structural properties in anisomyopic eyes did not compare the results of the higher myopic eyes with the isomyopic eyes of same refraction (Logan et al., 2004, Vincent et al., 2014). This was taken into account in this study by investigating whether the retina shapes of the more myopic eyes of anisometropes are different from those of isometropes with the same refractions. I did not find any evidence that this is the case, but it is possible that the limited anisomyope sample size (9) and pooling of data from different races prevented real differences being found.

6.3 CONCLUSION

Retinal shape and peripheral refraction were determined for the two eyes of isomyopes and anisomyopes, thus addressing the third aim of the thesis: "to determine how retinal shape and peripheral refraction vary between the two eyes of individuals with isomyopia and anisomyopia".

Retinal shapes and peripheral refraction were different between two eyes of anisomyopes but not generally of isomyopes. The higher myopic eyes of most anisomyopic participants had steeper retinas and more relative positive peripheral refraction than their fellow eyes along the horizontal meridian. However, there was no evidence that the higher myopic were different from isomyopic eyes with the same refraction. Because of small sample size and unequal spread of participants over wide range of refraction, the analysis involved pooling of participants from different races (EA, CA, SA). Therefore, the small sample size and a confounding

effect of race may have masked a true effect. Given the limitations of this experiment, it is more appropriate to put that hypothesis 4 of the thesis that “retinal shapes are different in isomyopic eyes and anisomyopic eyes of the same refraction” was not supported rather than to put that it was rejected.

Chapter 7- Discussion and Conclusion

7.1 SUMMARY

Myopia is an important health issue, being associated with ocular disease in later life (section 2.3). Accompanying increase in the prevalence of myopia in the past few decades have been many theories involving the role of various factors in myopia development and progression, with the intention of developing preventive strategies.

Most of the theories of myopia have been related to the central retina and the state of focus along the visual axis. Hoogerheide et al. (1971) reported different patterns of peripheral refraction in emmetropic and hyperopic trainee pilots who went on to develop myopia than in those who did not. Thirty years on, inspired by Hoogerheide et al., there was an explosion of both animal and human studies investigating the roles that the peripheral retina and peripheral vision might play in the development of myopia.

One aspect related to peripheral vision and peripheral optics is the shape of the retina, for which there are only a few studies. Retinal shape has been determined directly using magnetic resonance imaging (MRI) (section 2.4.2.8). This is a hospital based procedure, whose expense and considerable testing time making it difficult to be a part of myopic research, particularly for large scale clinical investigations. Additionally, its resolution is poor, thus making it difficult to detect small changes over a period of time. In the absence of a better or a simple method, retinal shape or overall eye shape have been inferred from indirect methods of peripheral refraction and partial coherence interferometry (PCI) based peripheral eye length measurements. There are some assumptions in the use of these methods and they have not been compared against MRI.

The purpose of this study was to develop and validate a PCI based method for estimating retinal shape, and then to use it to determine retinal shapes of different races and in anisomyopes. Three aims have been addressed with 4 associated hypotheses to be tested.

A summary of the results is as follows: PCI was used to measure peripheral (off-axis) eye lengths, combined with other measures and modelling. In Experiment 1, retinal shapes estimates using PCI with different modelling sophistications were compared with those obtained from MRI in 58 young adults. The most appropriate eye model involved a common schematic eye with ray deviation at surfaces but without customization of optical parameters. The validated method was used to compare retinal shapes in young adult Caucasians, East Asians and South Asians. Steeper retinas were found along the horizontal than along the vertical meridian, in myopes than in emmetropes, and in East Asian myopes than in Caucasian myopes. The method was also used to compare retinal shapes of the two eyes in isomyopes and anisomyopes. While the higher myopic eyes of anisomyopic participants had greater relative peripheral hyperopia and steeper retinas than their fellow eyes along the horizontal meridian, there was no evidence that these eyes had different retinal shapes than isomyopic eyes of same refraction. The variations in retinal shape between meridians, with refraction, and between races indicate that retinal shape may play a role in myopia development.

It should be mentioned that it has been shown recently that peripheral refraction in the Hoogerheide et al. study was most likely measured after, rather than before, pilots did or not develop myopia (Rosén et al., 2012), and thus it is unlikely that Hoogerheide et al. provided evidence that peripheral refractive patterns are predictive of myopia development. While there seems to have been a waning of interest in the role of the peripheral retina over the last couple of years, possibly in response to the Rosén et al. study, it should be borne in mind that the course of this thesis was set well before the revelation about the Hoogerheide et al. study was made.

7.2 VALIDATION OF PARTIAL COHERENCE INTERFEROMETRY INSTRUMENT FOR ESTIMATING RETINAL SHAPE

The first aim of this study was to determine the reliability of a simple method for determining retinal shape using off-axis partial coherence interferometry, and to validate this method by comparing the results with that of MRI. The associated hypothesis 1 was that retinal shape can be accurately predicted by measuring "off-axis eye lengths" with a commercial partial coherence interferometry instrument. The methodology was given in Chapter 3, including three preliminary investigations, and the main Experiment 1 was described in Chapter 4.

Two PCI instruments were candidates to be used in the main study, the Carl Zeiss IOLMaster and the Haag-Streit Lenstar. A device was developed that could be attached to either instrument. Its fixation target could be moved in an arc to provide peripheral visual angles to ±35° horizontally and ±30° vertically. The results from the first preliminary experiment (section 3.5.5.2) showed an excellent agreement between IOLMaster and Lenstar for peripheral eye length measurements (mean ± SD: 0.01 ± 0.07 mm for the horizontal and 0.02 ± 0.07 mm for the vertical visual fields, SDs corresponding to only 0.25 D) with the Lenstar showing better intra-session and inter-session repeatability than IOLMaster. The repeatabilities were similar to those reported in several on-axis studies and in one off-axis study. On the basis of this study, I decided to use the Lenstar. This work has been published (Verkicharla et al., 2013).

As mentioned above, peripheral visual field angles were obtained by rotating the eye relative to the instrument rather than more technically difficult method of rotating the instrument relative to the head. In a second preliminary experiment (section 3.5.5.3), I determined whether eye rotation would affect results, such as through pressure exerted by eyelids or extra-ocular muscles. The Lenstar was modified so that peripheral measurements could be obtained under both "eye rotation" and "no-eye rotation" conditions. Peripheral eye lengths were not significantly different between the two conditions along the vertical meridian. Whereas the peripheral eye lengths for the conditions were significantly different

along the horizontal meridian, they were not at individual positions and the differences were not important. The eye rotation approach did not change the measurements significantly even after holding the eye in rotated positions for 210 seconds. I concluded that the eye rotation approach to determine peripheral eye lengths was valid. This work has been published (Verkicharla et al., 2014).

There was one further preliminary investigation (section 3.5.5.1). The Lenstar instrument gives axial length and intraocular distances, except for the vitreous chamber depth which is obtained from the other distances, but does not indicate whether these distances use a common "refractive index" conversion from optical pathlengths to physical lengths, or whether there are separate conversions for each media. This was important for the modelling to be used with PCI to determine retinal shape. Using the Lenstar Graphical User Interface, it was observed that boundaries between media could be manipulated and opposite changes in optical path lengths on either side of the boundary could be introduced. Those ratios were combined with the overall eye refractive index to estimate separate refractive indices. Furthermore, Haag-Streit provided my research group with a template to obtain 'air thicknesses' to compare with physical distances. It became clear that the Lenstar uses different refractive indices for different ocular media. Some of the refractive indices, such as that for the cornea, are not physiological, and therefore, it is likely that the calibrations in the instrument correspond to instrument specific corrections and are not the *real* optical paths. The decision was made to trust the Lenstar provided distances, and to use refractive indices in modelling based on accepted schematic with a correction for the wavelength (820 nm) of the Lenstar.

Several procedures were required to obtain retinal shapes in terms of non-rotationally symmetric conicoids from MRI images (section 3.5.6).This included fits using 35% of the retinal area in order to be comparable with the region covered by PCI measurements. Modelling to obtain retinal shape from PCI was done in three levels of sophistication, all using variants of the Le Grand model eye (section 3.5.7). All modelling made the assumption that the beam from the instrument is incident normal to the anterior cornea. For Stage 1, deviation at surfaces was disregarded and no customisation was made. For Stage 2, deviation at surfaces occurred but no customization was made. For Stage 3, deviation at surfaces occurred, and the

following customisations were made: individual intraocular distances, anterior corneal topography, and a lens with parameters derived from Phakometry.

Following correction to the MRI based fits so that they were referenced to the fovea, the retinal shape estimates were compared between PCI and MRI in 58 participants. From Stage 1 to Stage 2, the retinal shape co-ordinates changed so that the Z co-ordinates (the sags) increased and the X/Y co-ordinates moved laterally, but such that there was little change in mean retinal steepness. The differences between Stages 2 and 3 were subtle.

Fitting conicoids (or conics) to surfaces gives two components of shape, the vertex radius of curvature R_v and asphericity Q, which are not independent. I had thought that these parameters could be used to make comparisons between MRI and PCI. In several cases there were significantly different estimates for both R_v and Q, but it was clear often that there was compensation such as a positive change in Q, in one method relative to the other, compensating for a positive change in R_v. I decided that a better approach to comparing MRI and PCI would be to combine these parameters to form a "surface shape", and to determine the differences between shape estimates (section 3.5.8).

The difference in retinal shape estimates between the MRI and PCI methods (<4% and <7% along horizontal and vertical field meridian) were within estimates of the uncertainty of MRI (12–14%), suggesting good agreement between the two methods for estimating retinal shape. For the majority of the participants, all three Stages of the PCI method gave slightly flatter estimates of retinal shape than did MRI, with the differences being smaller along the horizontal than along the vertical meridian.

In section 4.6, reasons for the differences between the different PCI Stages and between PCI and MRI were discussed. It is likely that the three Stages of the PCI method give similar results because the assumption that the infrared beam is directed normal to the anterior cornea is reasonable and furthermore than the normals to the cornea pass close to the nodal points of the eye so that the deviation within the eye is small. Differences between MRI and PCI might be attributed in part to thresholding and partial volume effects in MRI image processing, and the need to use bigger areas of the retina for the former so that the estimates were not overly affected by noise.

An alternate to the PCI based method of determining retinal shape is Dunne's method, which involves manipulating ocular parameters so that the peripheral refractions of model eyes match those of measurements (section 2.4.2.2 and 3.5.7). Retinal shape estimated with Dunne's method showed relatively poor agreement with MRI (6% along the horizontal meridian and 9% along the vertical meridian) compared with PCI (4% and 6% for horizontal and vertical), and the flatter estimates of retinal shape found with PCI were exacerbated with Dunne's method. It remains possible that Dunne's estimates provide better agreement with MRI with a different foundation model eye; this was not investigated further.

To conclude, there was good agreement between PCI based methods and MRI for estimating retinal shape. The hypothesis 1, that retinal shape can be accurately predicted by measuring "off-axis eye lengths" with a commercial partial coherence interferometry instrument, has been supported. As the relatively unsophisticated Stage 2 is easy to implement, and gave results similar to those of the customized Stage 3, it was used for the further investigations of retinal shape in the thesis.

7.3 RETINAL SHAPE IN DIFFERENT RACIAL GROUPS

The second aim of the study was to use the validated PCI method to estimate retinal shape in East Asian, South Asian and Caucasian emmetropes and myopes to determine how retinal shape and peripheral refraction are related in eyes of people with different racial backgrounds. The associated hypotheses 2 and 3 were "there are differences in retinal shapes among different racial groups" and "there are meridional (vertical and horizontal) variations in retinal shape". This involved 94 participants of East Asian, Caucasian and South Asian background and was given as Experiment 2 in Chapter 5.

The results support the hypotheses as all of peripheral refraction, peripheral eye length and retinal shape were significantly affected by meridian, refraction and racial group. More relative peripheral hyperopia, more negative relative peripheral eye lengths and steeper retinas were found along the horizontal than along the vertical meridian, in emmetropes than in myopes, and in East Asian myopes than in Caucasian myopes. There were interactions between meridian and refraction, with

the retina becoming steeper as myopia increased along the horizontal but not along the vertical meridian.

The conic fittings to the meridians showed smaller vertex radii of curvature for myopes than for emmetropes, and along the horizontal than along the vertical meridian, but there were no significant trends in asphericity with refraction or meridian, and thus retinas became steeper with increase in myopia over the retinal region investigated in the study (section 5.4). Many studies of peripheral refraction along the horizontal meridian have referred to either the retinal shape or eye shape becoming prolate as myopia increases. As technically the terms oblate and prolate refer to the asphericity of conics and conicoids (section 2.4.2.1 and the published paper Verkicharla et al. (2012)) with oblate shapes steepening away from the vertex and prolate shapes flattening away from the vertex, this study provides no evidence that this is the case. Over a much larger region of the retina, Atchison et al.'s (2005a) MRI study found that retinas of young adult became less oblate as myopia increased along both horizontal and vertical meridians, but with few retinas being prolate.

It would be interesting to investigate whether the retinal shapes of the three races follow the same model or follow different models of retinal expansion (section 2.4.2.2). As the measurements with PCI were limited to about 27% of the posterior eye, this study cannot provide information about this. Further investigation of the MRI derived retinal shapes over larger regions will later be undertaken for the participants used in this study.

The changing relative peripheral refraction pattern with refraction, with negative (myopic) relative peripheral refraction in both meridians for emmetropia becoming positive in myopia along the horizontal meridian but not the vertical meridian, agrees with previous studies (Atchison et al., 2006, Berntsen et al., 2010). Similarly the changing relative peripheral eye length with refraction, with negative relative peripheral eye length in emmetropia becoming yet more negative in myopia, supports previous studies (Ehsaei et al., 2012, Faria-Ribeiro et al., 2013, Schmid, 2003a, 2003b). The sign of relative peripheral eye length was always negative and therefore the sign alone does not indicate the shape of the retina or the sign of relative peripheral refraction.

The meridional, refraction and racial patterns of both relative peripheral refraction and relative peripheral eye length are consistent with those of retinal

shape, when the latter are restricted to considering overall flattening or steepening over the region of interest in this study. Accordingly, predictions regarding two of these can be made validly from patterns derived from one of the other two. That is, more positive (hyperopic) relative peripheral refraction predicts more negative peripheral eye lengths and steeper retinas, more negative peripheral eye lengths predict more positive relative peripheral refraction and steeper retinas, and steeper retinas (derived from peripheral eye lengths) predict more positive relative peripheral refraction. While other ocular parameters, such as anterior corneal shape, may contribute to the relationship between peripheral refraction and retinal shape, these would seem to have minor influences at most.

As the peripheral refraction and retinal shape in participants were not known before they developed myopia, we are not able to indicate whether one of relative peripheral hyperopic defocus or retinal shape drives the development/progression of myopia, or whether simply that both change as myopia develops. It is possible that the retinal shape, possibly through biomechanical factors, might be a determinant for the development of myopia rather than peripheral refraction. Steeper retinas in emmetropic East Asians than in emmetropic Caucasians may account for the higher tendency for myopia development and progression in the former. The results from this study can be related to the high prevalence rates in East Asians and indicate the possibility of steeper retinas being a risk factor for the myopia development, but this needs to be confirmed with longitudinal studies.

It is also interesting to speculate on the possible influence of meridian on development of myopia, as changes in peripheral refraction or retinal shape with increase in myopia are more marked along the horizontal than along the vertical meridian, a difference which may be mechanical in that there is much more space in the orbit around the eye vertically than there is horizontally. I note that many researchers have either not tested along the vertical meridian or have made speculations about the roles of peripheral refraction or retinal shape in myopia development while ignoring the findings for the vertical meridian such as found by Atchison et al. (2006) and Berntsen et al. (2010). It is possible the retinal system is more sensitive to signals for the horizontal than the vertical meridian.

7.4 RETINAL SHAPE IN ISOMYOPES AND ANISOMYOPES

The third aim of the study was to determine how retinal shape and peripheral refraction vary between the two eyes of individuals with isomyopia and anisomyopia. The associated hypothesis 4 was "retinal shapes are different in isomyopic eyes and anisomyopic eyes of the same refraction". This work involved 12 isomyopes and 9 anisomyopes (mean equivalent refraction difference between the fellow eyes ≥ 1.00 D) and was given as Experiment 3 in Chapter 6. I hoped that an investigation of anisomyopia might shed some light on myopia development, because it avoids the confounding effects of the environment and genetics.

The higher myopic eyes of most anisomyopic participants had steeper retinas and higher relative peripheral hyperopia than their fellow eyes along the horizontal meridian. Previous investigations of anisometropia did not investigate ocular biometric differences between anisomyopic and isomyopic eyes of same refraction (section 2.4.1). There were no significant differences in the retinal shape between anisomyopic and isomyopic eyes of same refraction. However, the small sample sizes and a confounding effect of race may have masked a true effect. It is more appropriate to say that the hypothesis was not supported rather than it was rejected. Further studies are required to investigate this hypothesis in a large sample.

7.5 FURTHER WORK

There are some additional investigations that can be conducted on the considerable ocular biometric data collected in this study. The parameters, such as anterior corneal shape, can be used to explore racial differences and to investigate their influence on peripheral refraction. For the latter, I suspect that the influences will be minor (section 7.3).

As mentioned in section 7.4, the anisomyopia investigation could be continued with a much larger participant group.

This study showed association between retinal shape and myopia, but not causation. It was a cross-sectional study in which the participant group consisted of young adult emmetropes and myopes, with refraction having stabilised in the latter. Further studies are recommended to investigate a role for retinal shape in myopiogenesis, including longitudinal studies involving children of different ethnicities and refraction (emmetropes, and stable and progressing myopes). For conducting the off-axis partial coherence interferometry method in children, the testing time of 12-14 minutes needs to be reduced to prevent fatigue and not to lengthen a testing protocol involving several tests. The method described here (section 3.5.5.2) requires manual adjustment of an attachment, and some automation should be considered.

Another possible instrumentation that can be used for determining retinal shape is optical coherence tomography, which is based on partial coherence interferometry. Although there are issues with optical distortion of the retinal images, this can be corrected potentially by using optically based algorithms (Kuo et al., 2013). Further studies using OCT images would benefit myopia research as they provide measurements in very short time.

References

ABS. 2011. Australian Bureau of Statistics: Australian Standard Classification of Cultural and Ethnic Groups. 1249.0 2nd ed.

Adhikari S, Paudel N, Adhikari P, Shrestha GS & Shrestha JB 2013. Screening preschool children for visual disorders: A pilot study. *Optometry and Visual Performance,* 1, 202-207.

Ahmed I, Mian S, Mudasir S & Andrabi KI 2008. Prevalence of myopia in students of Srinagar city of Kashmir, India. *International Journal of Health Sciences,* 2, 77-81.

Ames JA & Proctor CA 1921. Dioptrics of the eye. *Journal of the Optical Society of America,* 5, 22-83.

Anderson SJ, Mullen KT & Hess RF 1991. Human peripheral spatial resolution for achromatic and chromatic stimuli: limits imposed by optical and retinal factors. *The Journal of Physiology,* 442, 47-64.

Atchison DA 2003. Comparison of peripheral refractions determined by different instruments. *Optometry and Vision Science,* 80, 655-660.

Atchison DA 2006. Optical models for human myopic eyes. *Vision Research,* 46, 2236-2250.

Atchison DA 2009. Objective refraction. *In: Optometry: Science, techniques and clinical management.* 2nd ed: Butterworth-Heinemann.13, 203.

Atchison DA & Charman WN 2011. Can partial coherence interferometry be used to determine retinal shape? *Optometry and Vision Science,* 88, 601-607.

Atchison DA, Jones CE, Schmid KL, Pritchard N, Pope JM, et al. 2004. Eye shape in emmetropia and myopia. *Investigative Ophthalmology and Visual Science,* 45, 3380-3386.

Atchison DA, Markwell EL, Kasthurirangan S, Pope JM, Smith G, et al. 2008. Age-related changes in optical and biometric characteristics of emmetropic eyes. *Journal of Vision,* 8, 29 1-20.

Atchison DA, Pritchard N & Schmid KL 2006. Peripheral refraction along the horizontal and vertical visual fields in myopia. *Vision Research,* 46, 1450-1458.

Atchison DA, Pritchard N, Schmid KL, Scott DH, Jones CE, et al. 2005a. Shape of the retinal surface in emmetropia and myopia. *Investigative Ophthalmology and Visual Science,* 46, 2698-2707.

Atchison DA, Pritchard N, White SD & Griffiths AM 2005b. Influence of age on peripheral refraction. *Vision Research,* 45, 715-720.

Atchison DA & Smith G 2000. Optics of the human eye, *Butterworth-Heinemann,* 13-14.

Atchison DA & Smith G 2005. Chromatic dispersions of the ocular media of human eyes. *Journal of the Optical Society of America A,* 22, 29-37.

Backhouse S, Fox S, Ibrahim B & Phillips JR 2012. Peripheral refraction in myopia corrected with spectacles versus contact lenses. *Ophthalmic and Physiological Optics,* 32, 294-303.

Barkana Y, Gerber Y, Elbaz U, Schwartz S, Ken-Dror G, et al. 2005. Central corneal thickness measurement with the Pentacam Scheimpflug system, optical low-coherence reflectometry pachymeter, and ultrasound pachymetry. *Journal of Cataract and Refractive Surgery,* 31, 1729-1735.

Bayramlar H, Cekic O & Hepsen IF 1999. Does convergence, not accommodation, cause axial-length elongation at near? A biometric study in teens. *Ophthalmic Research,* 31, 304-308.

Bennett AG 1988. A method of determining the equivalent powers of the eye and its crystalline lens without resort to phakometry. *Ophthalmic and Physiological Optics,* 8, 53-59.

Berntsen DA, Mutti DO & Zadnick K 2010. Study of theories about myopia progression (STAMP) design and baseline data. *Optometry and Vision Science,* 87, 823-832.

Bjelos Roncevic M, Busic M, Cima I, Kuzmanovic Elabjer B, Bosnar D, et al. 2011. Intraobserver and interobserver repeatability of ocular components measurement in cataract eyes using a new optical low coherence reflectometer. *Graefe's Archive for Clinical and Experimental Ophthalmology,* 249, 83-87.

Bland JM & Altman DG 2007. Agreement between methods of measurement with multiple observations per individual. *J Biopharm Stat,* 17, 571-82.

Bron A, Tripathi R & Tripathi B 1997. Wolff's Anatomy of the Eye and Orbit. *In:* 8th ed: Chapman & Hall Medical, 211-215.

Buckhurst PJ, Wolffsohn JS, Shah S, Naroo SA, Davies LN, et al. 2009. A new optical low coherence reflectometry device for ocular biometry in cataract patients. *British Journal of Ophthalmology,* 93, 949-953.

Calver R, Radhakrishnan H, Osuobeni E & O'Leary D 2007. Peripheral refraction for distance and near vision in emmetropes and myopes. *Ophthalmic and Physiological Optics,* 27, 584-593.

Cameron LA, Gray LS, Seidel D & Day M. 2013. The effect of measurement assumptions when investigating peripheral eye length and peripheral refraction. *Ophthalmic and Physiological Optics,* 34, 112.

Chang RT 2011. Myopia and glaucoma. *International Ophthalmology Clinics,* 51, 53-63.

Charman WN 2011. Myopia: its prevalence, origins and control. *Ophthalmic and Physiological Optics,* 31, 3-6.

Charman WN & Jennings JAM 1982. Ametropia and peripheral refraction. *American Journal of Optometry and Physiological Optics,* 59, 922-923.

Charman WN, Mountford J, Atchison DA & Markwell EL 2006. Peripheral refraction in orthokeratology patients. *Optometry and Vision Science,* 83, 641-648.

Charman WN & Radhakrishnan H 2010. Peripheral refraction and the development of refractive error: a review. *Ophthalmic and Physiological Optics,* 30, 321-338.

Chau A, Fung K, Pak K & Yap M 2004. Is eye size related to orbit size in human subjects? *Ophthalmic and Physiological Optics,* 24, 35-40.

Chen JF, Elsner AE, Burns SA, Hansen RM, Lou PL, et al. 1992. The effect of eye shape on retinal responses. *Clinical and Vision Sciences,* 7, 521–530.

Chen SJ, Lu P, Zhang WF & Lu JH 2012. High myopia as a risk factor in primary open angle glaucoma. *International Journal of Ophthalmology,* 5, 750-753.

Chen X, Sankaridurg P, Donovan L, Lin Z, Li L, et al. 2010. Characteristics of peripheral refractive errors of myopic and non-myopic Chinese eyes. *Vision Research,* 50, 31-35.

Cheng D, Schmid KL, Woo GC & Drobe B 2010. Randomized trial of effect of bifocal and prismatic bifocal spectacles on myopic progression: two-year results. *Archives of Ophthalmology,* 128, 12-19.

Cheng D, Woo GC & Schmid KL 2011. Bifocal lens control of myopic progression in children. *Clinical and Experimental Optometry,* 94, 24-32.

Cheng HM, Singh OS, Kwong KK, Xiong J, Woods BT, et al. 1992. Shape of the myopic eye as seen with high-resolution magnetic resonance imaging. *Optometry and Vision Science,* 69, 698-701.

Cho P, Cheung SW & Edwards M 2005. The longitudinal orthokeratology research in children (LORIC) in Hong Kong: a pilot study on refractive changes and myopic control. *Current Eye Research,* 30, 71-80.

Cho P, Lam AK, Mountford J & Ng L 2002. The performance of four different corneal topographers on normal human corneas and its impact on orthokeratology lens fitting. *Optometry and Vision Science,* 79, 175-183.

Christophe AB 1971. Valley to peak ratio as a measure for the separation of two chromatographic peaks. *Chromatographia,* 4, 455-458.

Chui TY, Yap MK, Chan HH & Thibos LN 2005. Retinal stretching limits peripheral visual acuity in myopia. *Vision Research,* 45, 593-605.

Coleman AL & Brigatti L 2001. The glaucomas. *Minerva Medica,* 92, 365-379.

Cruysberg LP, Doors M, Verbakel F, Berendschot TT, De Brabander J, et al. 2010. Evaluation of the Lenstar LS 900 non-contact biometer. *British Journal of Ophthalmology,* 94, 106-110.

Cummings JR, Muchlinski MN, Kirk EC, Rehorek SJ, DeLeon VB, et al. 2012. Eye size at birth in prosimian primates: life history correlates and growth patterns. *PLoS One,* 7, e36097.

Curcio CA & Allen KA 1990. Topography of ganglion cells in human retina. *The Journal of Comparative Neurology,* 300, 5-25.

Daimon M & Masumura A 2007. Measurement of the refractive index of distilled water from the near-infrared region to the ultraviolet region. *Applied Optics,* 46, 3811-3820.

Davies LN & Mallen EAH 2009. Influence of accommodation and refractive status on the peripheral refractive profile. *British Journal of Ophthalmology,* 93, 1186-1190.

Deller JF, O'Connor AD & Sorsby A 1947. X-ray measurement of the diameters of the living eye. *Proceedings of the Royal Society of London. Series B, Biological Sciences,* 134, 456-467.

Ding X, Wang D, Huang Q, Zhang J, Chang J, et al. 2013. Distribution and heritability of peripheral eye length in Chinese children and adolescents: the Guangzhou Twin Eye Study. *Investigative Ophthalmology and Visual Science,* 54, 1048-1053.

Druault A 1900. Astigmatisme des rayons pénétrant obliquement dans l'œil. Application de la skiascopie (1). *Archives D'Ophtalmologie,* 20, 21-28.

Dunne MCM 1995. A computing scheme for determination of retinal contour from peripheral refraction, keratometry and A-scan ultrasonography. *Ophthalmic and Physiological Optics,* 15, 133-143.

Dunne MCM, Barnes DA & Clement RA 1987. A model for retinal shape changes in ametropia. *Ophthalmic and Physiological Optics,* 7, 159-160.

Dunne MCM, Misson GP, White EK & Barnes DA 1993. Peripheral astigmatic asymmetry and angle alpha. *Ophthalmic and Physiological Optics,* 13, 303-305.

Duong TQ 2011. Magnetic resonance imaging of the retina: A brief historical and future perspective. *Saudi Journal of Ophthalmology,* 25, 137-143.

Edelman R, Hesselink J & Zlatkin M 2006. Advanced imaging techniques. *In: Clinical magnetic resonance imaging.* 3rd ed: W. B. Saunders, 2-22.

Edwards MH 1996. Do variations in normal nutrition play a role in the development of myopia? *Optometry and Vision Science,* 73, 638-643.

Ehrlich DL 1987. Near vision stress: Vergence adaptation and accommodative fatigue. *Ophthalmic and Physiological Optics,* 7, 353-357.

Ehsaei A, Chisholm CM, Pacey IE & Mallen EAH 2012. Off-axis partial coherence interferometry in myopes and emmetropes. *Ophthalmic and Physiological Optics,* 33, 26-34.

Ehsaei A, Chisholm CM, Pacey IE & Mallen EAH 2013. Visual performance fall-off with eccentricity in myopes versus emmetropes. *Journal of Optometry,* 06, 36-44.

Elliott DB 2011. A new horizon for myopia research? *Ophthalmic and Physiological Optics,* 31, 1-2.

Fahle M & Schmid M 1988. Naso-temporal asymmetry of visual perception and of the visual cortex. *Vision Research,* 28, 293-300.

Fan DSP, Lam DSC, Lam RF, Lau JTF, Chong KS, et al. 2004. Prevalence, incidence, and progression of myopia of school children in Hong Kong. *Investigative Ophthalmology and Visual Science,* 45, 1071-1075.

Faria-Ribeiro M, Lopes-Ferreira D, López-Gil N, Jorge J & González-Méijome JM 2014. Errors associated with IOLMaster biometry as a function of internal ocular dimensions. *Journal of Optometry,* 7, 75–78.

Faria-Ribeiro M, Queirós A, Lopes-Ferreira D, Jorge J & González-Méijome JM 2013. Peripheral refraction and retinal contour in stable and progressive myopia. *Optometry and Vision Science,* 90, 9-15.

Fedtke C, Ehrmann K, Falk D & Holden B. 2011. The EyeMapper - Extremely rapid central and peripheral refraction. The 89th annual meeting of the American Academy of Optometry, Eabstract.

Fedtke C, Ehrmann K, Falk D & Holden B. 2012. Validation of a quasi real-time global aberrometer: the EyeMapper. *Ophthalmic Technologies XXII,* 8209, 82090C1-82090C7.

Feldkamper M & Schaeffel F 2003. Interactions of genes and environment in myopia. *Developments in Ophthalmology,* 37, 34-49.

Ferree CE & Rand G 1933a. Interpretation of refractive conditions in the peripheral field of vision. *Archives of Ophthalmology,* 9, 925-938.

Ferree CE, Rand G & Hardy C 1931. Refraction for the peripheral field of vision. *Archives of Ophthalmology,* 5, 717-731.

Ferree CE, Rand G & Hardy C 1932. Refractive asymmetry in the temporal and nasal halves of the visual field. *American Journal of Ophthalmology,* 15, 513–522.

Ferree CE, Rand G & Hardy C 1933b. An important factor in space perception in the peripheral field of vision. *The American Journal of Psychology,* 45, 228-247.

Fledelius HC & Goldschmidt E 2010. Eye shape and peripheral visual field recording in high myopia at approximately 54 years of age, as based on ultrasonography and Goldmann kinetic perimetry. *Acta Ophthalmologica,* 88, 521-526.

French AN, Morgan IG, Burlutsky G, Mitchell P & Rose KA 2013. Prevalence and 5- to 6-year incidence and progression of myopia and hyperopia in Australian school children. *Ophthalmology,* 120, 1482-1491.

Ghosh A, Collins MJ, Read SA & Davis BA 2012. Axial length changes with shifts of gaze direction in myopes and emmetropes. *Investigative Ophthalmology and Visual Science*, 53, 6465-6471.

Gilmartin B, Nagra M & Logan NS 2013. Shape of the posterior vitreous chamber in human emmetropia and myopia. *Investigative Ophthalmology and Visual Science,* 54, 7240-7251.

Gilmartin B, Nagra M, Logan NS & Patel HD 2011. Regional variation in ocular dimensions in human myopia. *Investigative Ophthalmology and Visual Science,* 52, E-Abstract 6315.

Goh PP, Abqariyah Y, Pokharel GP & Ellwein LB 2005. Refractive error and visual impairment in school-age children in Gombak District, Malaysia. *Ophthalmology*, 112, 678-685.

Gozum N, Cakir M, Gucukoglu A & Sezen F 1997. Relationship between retinal lesions and axial length, age and sex in high myopia. *European Journal of Ophthalmology*, 7, 277-282.

Greene PR 1980. Mechanical considerations in myopia: relative effects of accommodation, convergence, intraocular pressure, and the extraocular muscles. *American Journal of Optometry and Physiological Optics,* 57, 902-914.

Guo YH, Lin HY, Lin LL & Cheng CY 2012. Self-reported myopia in Taiwan: 2005 Taiwan National Health Interview Survey. *Eye,* 26, 684-689.

Gwiazda J, Hyman L, Hussein M, Everett D, Norton TT, et al. 2003. A randomized clinical trial of progressive addition lenses versus single vision lenses on the progression of myopia in children. *Investigative Ophthalmology and Visual Science,* 44, 1492-1500.

Haigis W, Lege B, Miller N & Schneider B 2000. Comparison of immersion ultrasound biometry and partial coherence interferometry for intraocular lens calculation according to Haigis. *Graefe's Archive for Clinical and Experimental Ophthalmology,* 238, 765-773.

Hammond CJ, Snieder H, Gilbert CE & Spector TD 2001. Genes and environment in refractive error: the twin eye study. *Investigative Opthalmology and Visual Science,* 42, 1232-1236.

Hartwig A, Atchison DA & Radhakrishnan H 2013. Higher-order aberrations and anisometropia. *Current Eye Research,* 38, 215-219.

Hasebe S, Ohtsuki H, Nonaka T, Nakatsuka C, Miyata M, et al. 2008. Effect of progressive addition lenses on myopia progression in Japanese children: A

prospective, randomized, double-masked, crossover trial. *Investigative Ophthalmology and Visual Science,* 49, 2781-2789.

Hashemi H, Khabazkhoob M, Jafarzadehpur E, Yekta AA, Emamian MH, et al. 2012. High prevalence of myopia in an adult population, Shahroud, Iran. *Optometry and Vision Science,* 89, 993-999.

Hitzenberger CK 1991. Optical measurement of the axial eye length by laser Doppler interferometry. *Investigative Ophthalmology and Visual Science,* 32, 616-624.

Holzer MP, Mamusa M & Auffarth GU 2009. Accuracy of a new partial coherence interferometry analyser for biometric measurements. *British Journal of Ophthalmology,* 93, 807-810.

Hoogerheide J, Rempt F & Hoogenboom WP 1971. Acquired myopia in young pilots. *Ophthalmologica,* 163, 209-215.

Hsiang HW, Ohno-Matsui K, Shimada N, Hayashi K, Moriyama M, et al. 2008. Clinical characteristics of posterior staphyloma in eyes with pathologic myopia. *American Journal of Ophthalmology,* 146, 102-110.

Huang J, Hung LF & Smith EL III 2011. Effects of foveal ablation on the pattern of peripheral refractive errors in normal and form-deprived infant rhesus monkeys (Macaca mulatta). *Investigative Ophthalmology and Visual Science,* 52, 6428-6434.

Hyung SM, Kim DM, Hong C & Youn DH 1992. Optic disc of the myopic eye: relationship between refractive errors and morphometric characteristics. *Korean Journal of Ophthalmology,* 6, 32-35.

Inui T, Mimura O & Kani K 1981. Retinal sensitivity and spatial summation in the foveal and parafoveal regions. *Journal of the Optical Society of America,* 71, 151-163.

Ip JM, Huynh SC, Kifley A, Rose KA, Morgan IG, et al. 2007a. Variation of the contribution from axial length and other oculometric parameters to refraction by age and ethnicity. *Investigative Ophthalmology and Visual Science,* 48, 4846-4853.

Ip JM, Huynh SC, Robaei D, Rose KA, Morgan IG, et al. 2007b. Ethnic differences in the impact of parental myopia: findings from a population-based study of 12-year-old Australian children. *Investigative Ophthalmology and Visual Science,* 48, 2520-2528.

Ip JM, Saw SM, Rose KA, Morgan IG, Kifley A, et al. 2008. Role of near work in myopia: findings in a sample of Australian school children. *Investigative Ophthalmology and Visual Science,* 49, 2903-2910.

Ishii K, Iwata H & Oshika T 2011. Quantitative evaluation of changes in eyeball shape in emmetropization and myopic changes based on elliptic Fourier descriptors. *Investigative Ophthalmology and Visual Science,* 52, 8585-8591.

Iyamu E, Iyamu J & Obiakor CI 2011. The role of axial length-corneal radius of curvature ratio in refractive state categorization in a Nigerian population. *ISRN Ophthalmology,* 2011, 1-6.

Jaeken B, Lundström L & Artal P 2011. Fast scanning peripheral wave-front sensor for the human eye. *Optics Express,* 19, 7903-7913.

Jones CE, Atchison DA, Meder R & Pope JM 2005. Refractive index distribution and optical properties of the isolated human lens measured using magnetic resonance imaging (MRI). *Vision Research,* 45, 2352-2366.

Kang P, Fan Y, Oh K, Trac K, Zhang F, et al. 2012. Effect of single vision soft contact lenses on peripheral refraction. *Optometry and Vision Science,* 89, 1014-1021.

Kang P, Gifford P, McNamara P, Wu J, Yeo S, et al. 2010. Peripheral refraction in different ethnicities. *Investigative Ophthalmology and Visual Science,* 51, 6059-6065.

Kang P & Swarbrick H 2011. Peripheral refraction in myopic children wearing orthokeratology and gas-permeable lenses. *Optometry and Vision Science,* 88, 476-482.

Kang P & Swarbrick H 2013. Time course of the effects of orthokeratology on peripheral refraction and corneal topography. *Ophthalmic and Physiological Optics,* 33, 277-282.

Kempen JH, Mitchell P, Lee KE, Tielsch JM, Broman AT, et al. 2004. The prevalence of refractive errors among adults in the United States, Western Europe, and Australia. *Archives of Ophthalmology,* 122, 495-505.

Kim EC, Morgan IG, Kakizaki H, Kang S & Jee D 2013a. Prevalence and risk factors for refractive errors: Korean national health and nutrition examination survey 2008-2011. *PLoS ONE,* 8, e80361.

Kim SY, Cho SY, Yang JW, Kim CS & Lee YC 2013b. The correlation of differences in the ocular component values with the degree of myopic anisometropia. *Korean Journal of Ophthalmology,* 27, 44-47.

Kimura S, Hasebe S, Miyata M, Hamasaki I & Ohtsuki H 2007. Axial length measurement using partial coherence interferometry in myopic children: repeatability of the measurement and comparison with refractive components. *Japanese Journal of Ophthalmology,* 51, 105-110.

Kolb H 1995. Simple anatomy of the retina. *Webvision: The Organization of the Retina and Visual System,* http://www.ncbi.nlm.nih.gov/books/NBK11533/.

Krishnaiah S, Srinivas M, Khanna RC & Rao GN 2009. Prevalence and risk factors for refractive errors in the South Indian adult population: The Andhra Pradesh Eye disease study. *Clinical Ophthalmology,* 3, 17-27.

Kumah BD, Ebri A, Abdul-Kabir M, Ahmed AS, Koomson NY, et al. 2013. Refractive error and visual impairment in private school children in Ghana. *Optometry and Vision Science,* 90, 1456-1461.

Kuo AN, McNabb RP, Chiu SJ, El-Dairi MA, Farsiu S, et al. 2013. Correction of ocular shape in retinal optical coherence tomography and effect on current clinical measures. *American Journal of Ophthalmology,* 156, 304-311.

Lam AK, Chan R & Pang PC 2001. The repeatability and accuracy of axial length and anterior chamber depth measurements from the IOLMaster. *Ophthalmic and Physiological Optics,* 21, 477-483.

Lam CSY, Lam CH, Cheng SCK & Chan LYL 2012. Prevalence of myopia among Hong Kong Chinese schoolchildren: changes over two decades. *Ophthalmic and Physiological Optics,* 32, 17-24.

Lan W, Zhao F, Lin L, Li Z, Zeng J, et al. 2013. Refractive rrrors in 3–6 year-old Chinese children: A very low prevalence of myopia? *PLoS ONE,* 8, e78003.

Land MF & Tatler BW 2009. Looking and acting: vision and eye movements in natural behaviour. *In: Oxford, UK.* Oxford University Press, 297-300.

Latham K & Whitaker D 1996. Relative roles of resolution and spatial interference in foveal and peripheral vision. *Ophthalmic and Physiological Optics,* 16, 49-57.

Lee RY, Kasuga T, Cui QN, Huang G, Wang SY, et al. 2013. Ethnic differences in intraocular pressure reduction and changes in anterior segment biometric parameters following cataract surgery by phacoemulsification. *Clinical and Experimental Ophthalmology,* 41, 442-449.

Lee TT & Cho P 2013. Relative peripheral refraction in children: twelve-month changes in eyes with different ametropias. *Ophthalmic and Physiological Optics,* 33, 283-293.

Leung JT & Brown B 1999. Progression of myopia in Hong Kong Chinese school children is slowed by wearing progressive lenses. *Optometry and Vision Science,* 76, 346-354.

Lim LS, Chong GH, Tan PT, Chong YS, Kwek K, et al. 2013. Distribution and determinants of eye size and shape in newborn children: a magnetic resonance imaging analysis. *Investigative Ophthalmology and Visual Science,* 54, 4791-4797.

Lim LS, Gazzard G, Low YL, Choo R, Tan DT, et al. 2010. Dietary factors, myopia, and axial dimensions in children. *Ophthalmology,* 117, 993-997.

Lim LS, Yang X, Gazzard G, Lin X, Sng C, et al. 2011. Variations in eye volume, surface area, and shape with refractive error in young children by magnetic resonance imaging analysis. *Investigative Ophthalmology and Visual Science,* 52, 8878-8883.

Lim MC, Gazzard G, Sim EL, Tong L & Saw SM 2009. Direct costs of myopia in Singapore. *Eye,* 23, 1086-1089.

Lim R, Mitchell P & Cumming RG 1999. Refractive associations with cataract: the blue mountains eye study. *Investigative Ophthalmology and Visual Science,* 40, 3021-3026.

Lin LL, Shih YF, Hsiao CK & Chen CJ 2004. Prevalence of myopia in Taiwanese school children: 1983 to 2000. *Annals of the Academy of Medicine Singapore,* 33, 27-33.

Lin Z, Martinez A, Chen X, Li L, Sankaridurg P, et al. 2010. Peripheral defocus with single-vision spectacle lenses in myopic children. *Optometry and Vision Science,* 87, 4-9.

Logan NS, Gilmartin B, Wildsoet CF & Dunne MCM 2004. Posterior retinal contour in adult human anisomyopia. *Investigative Ophthalmology and Visual Science,* 45, 2152-2162.

Lotmar W & Lotmar T 1974. Peripheral astigmatism in the human eye: Experimental data and theoretical model predictions. *Journal of the Optical Society of America,* 64, 510-513.

Loyo-Berrios NI & Blustein JN 2007. Primary-open glaucoma and myopia: a narrative review. *Wisconsin Medical Journal,* 106, 85-89 and 95.

Ma L, Atchison DA & Charman WN 2005. Off-axis refraction and aberrations following conventional laser in situ keratomileusis. *Journal of Cataract and Refractive Surgery,* 31, 489-498.

Macfadden LA, Gray LS, Strang NC & Seidel D 2007. The effect of eye rotation on measurements of peripheral retinal shape using the IOLMaster. *Investigative Ophthalmology and Visual Science,* 48, E-abstract 4002.

Mallen EAH & Kashyap P 2007. Technical note: Measurement of retinal contour and supine axial length using the Zeiss IOLMaster. *Ophthalmic and Physiological Optics,* 27, 404-411.

Marcus MW, de Vries MM, Junoy Montolio FG & Jansonius NM 2011. Myopia as a risk factor for open-angle glaucoma: a systematic review and meta-analysis. *Ophthalmology,* 118, 1989-1994.

Martinez AA, Ho A, Sankaridurg PR, Lazon PF, Holden BA, et al. 2011. Myopia control means. United States *patent application* 20110051079.

Mathur A & Atchison DA 2013. Peripheral refraction patterns out to large field angles. *Optometry and Vision Science,* 90, 140-147.

Mathur A, Atchison DA & Charman WN 2009a. Myopia and peripheral ocular aberrations. *Journal of Vision,* 9(10), 15, 1-12.

Mathur A, Atchison DA, Kasthurirangan S, Dietz NA, Luong S, et al. 2009b. The influence of oblique viewing on axial and peripheral refraction for emmetropes and myopes. *Ophthalmic and Physiological Optics,* 29, 155-161.

McBrien NA & Adams DW 1997. A longitudinal investigation of adult-onset and adult-progression of myopia in an occupational group: Refractive and biometric findings. *Investigative Ophthalmology and Visual Science,* 38, 321-333.

McBrien NA & Gentle A 2003. Role of the sclera in the development and pathological complications of myopia. *Progress in Retinal and Eye Research,* 22, 307-338.

McDaniel J & Mutti D 2002. Repeatability and comparability of IOLMaster and ultrasound measures of ocular axial length in young adults. *Investigative Ophthalmology and Visual Science,* 43, E-abstract 356.

Micelli-Ferrari T, Vendemiale G, Grattagliano I, Boscia F, Arnese L, et al. 1996. Role of lipid peroxidation in the pathogenesis of myopic and senile cataract. *British Journal of Ophthalmology,* 80, 840-843.

Miller JM, Wildsoet CF, Guan H, Limbo M & Demer JL 2004. Refractive error and eye shape by MRI. *Investigative Ophthalmology and Visual Science,* 45, E-Abstract 2388.

Millodot M 1981. Effect of ametropia on peripheral refraction. *American Journal of Optometry and Physiological Optics,* 58, 691-695.

Montes-Micó R & Ferrer-Blasco T 2000. Distribution of refractive errors in Spain. *Documenta Ophthalmologica,* 101, 25-33.

Morgan A, Young R, Narankhand B, Chen S, Cottriall C, et al. 2006. Prevalence rate of myopia in schoolchildren in rural Mongolia. *Optometry and Vision Science,* 83, 53-56.

Morgan IG 2003. The biological basis of myopic refractive error. *Clinical and Experimental Optometry,* 86, 276-288.

Moriyama M, Ohno-Matsui K, Hayashi K, Shimada N, Yoshida T, et al. 2011. Topographic analyses of shape of eyes with pathologic myopia by high-resolution three-dimensional magnetic resonance imaging. *Ophthalmology,* 118, 1626-1637.

Murthy GV, Gupta SK, Ellwein LB, Munoz SR, Pokharel GP, et al. 2002. Refractive error in children in an urban population in New Delhi. *Investigative Ophthalmology and Visual Science,* 43, 623-631.

Mutti DO, Hayes JR, Mitchell GL, Jones LA, Moeschberger ML, et al. 2007. Refractive error, axial length and relative peripheral refractive error before and after the onset of myopia. *Investigative Ophthalmology and Visual Science,* 48, 2510-2519.

Mutti DO, Mitchell GL, Moeschberger ML, Jones LA & Zadnik K 2002. Parental myopia, near work, school achievement, and children's refractive error. *Investigative Ophthalmology and Visual Science,* 43, 3633-3640.

Mutti DO, Sholtz RI, Friedman NE & Zadnik K 2000. Peripheral refraction and ocular shape in children. *Investigative Ophthalmology and Visual Science,* 41, 1022-1030.

Mutti DO, Sinnott LT, Mitchell GL, Jones-Jordan LA, Moeschberger ML, et al. 2011. Relative peripheral refractive error and the risk of onset and progression of myopia in children. *Investigative Ophthalmology and Visual Science,* 52, 199-205.

Mutti DO & Zadnik K 2009. Has near work's star fallen? *Optometry and Vision Science,* 86, 76-78.

Naidoo KS, Raghunandan A, Mashige KP, Govender P, Holden BA, et al. 2003. Refractive error and visual impairment in African children in South Africa. *Investigative Ophthalmology and Visual Science,* 44, 3764-3770.

Norton TT & Siegwart JT, Jr. 1995. Animal models of emmetropization: matching axial length to the focal plane. *Journal of the American Optometric Association,* 66, 405-414.

O'Donoghue L, McClelland JF, Logan NS, Rudnicka AR, Owen CG, et al. 2010. Refractive error and visual impairment in school children in Northern Ireland. *British Journal of Ophthalmology,* 94, 1155-1159.

Orr JB, Gray LS, Seidel D & Day M. 2013. The relationship between retinal shape and relative peripheral refractive error in emmetropic, myopic and hyperopic individuals. *Ophthalmic and Physiological Optics,* 34, 109.

Pan C-W, Zheng Y-F, Anuar AR, Chew M, Gazzard G, et al. 2013a. Prevalence of refractive errors in a multiethnic Asian population: The Singapore epidemiology of eye disease study. *Investigative Ophthalmology and Visual Science,* 54, 2590-2598.

Pan C, Ramamurthy D & Saw S 2012. Worldwide prevalence and risk factors for myopia. *Ophthalmic and Physiological Optics,* 32, 3-16.

Pan CW, Klein BE, Cotch MF, Shrager S, Klein R, et al. 2013b. Racial variations in the prevalence of refractive errors in the United States: the multi-ethnic study of atherosclerosis. *American Journal of Ophthalmology,* 155, 1129-1138.

Paradiso MA & Carney T 1988. Orientation discrimination as a function of stimulus eccentricity and size: nasal/temporal retinal asymmetry. *Vision Research,* 28, 867-874.

Pierro L, Camesasca FI, Mischi M & Brancato R 1992. Peripheral retinal changes and axial myopia. *Retina,* 12, 12-17.

Queirós A, González-Méijome JM, Jorge J, Villa-Collar C & Gutiérrez AR 2010. Peripheral refraction in myopic patients after orthokeratology. *Optometry and Vision Science,* 87, 323-329.

Rada JA, Shelton S & Norton TT 2006. The sclera and myopia. *Experimental Eye Research,* 82, 185-200.

Radhakrishnan H & Charman WN 2008. Peripheral refraction measurement: does it matter if one turns the eye or the head? *Ophthalmic and Physiological Optics,* 28, 73-82.

Raju P, Ramesh SV, Arvind H, George R, Baskaran M, et al. 2004. Prevalence of refractive errors in a rural South Indian population. *Investigative Ophthalmology and Visual Science,* 45, 4268-4272.

Ramrattan RS, Wolfs RC, Jonas JB, Hofman A & de Jong PT 1999. Determinants of optic disc characteristics in a general population: The Rotterdam Study. *Ophthalmology*, 106, 1588-1596.

Read SA, Collins MJ & Alonso-Caneiro D 2011. Validation of optical low coherence reflectometry retinal and choroidal biometry. *Optometry and Vision Science*, 88, 855-863.

Redpath TW 1998. Signal-to-noise ratio in MRI. *The British Journal of Radiology*, 71, 704-707.

Rempt F, Hoogerheide J & Hoogenboom WP 1971. Peripheral retinoscopy and the skiagram. *Ophthalmologica*, 162, 1-10.

Rohrer K, Frueh BE, Wälti R, Clemetson IA, Tappeiner C, et al. 2009. Comparison and evaluation of ocular biometry using a new noncontact optical low-coherence reflectometer. *Ophthalmology*, 116, 2087-2092.

Rose KA, Morgan IG, Smith W, Burlutsky G, Mitchell P, et al. 2008. Myopia, lifestyle, and schooling in students of Chinese ethnicity in Singapore and Sydney. *Archives of Ophthalmology*, 126, 527-530.

Rosén R, Lundström L, Unsbo P & Atchison DA 2012. Have we misinterpreted the study of Hoogerheide et al. (1971)? *Optometry and Vision Science*, 89, 1235-1237.

Royston JM, Dunne MCM & Barnes DA 1989. Calculation of crystalline lens radii without resort to phakometry. *Ophthalmic and Physiological Optics*, 9, 412-414.

Rudnicka AR, Owen CG, Nightingale CM, Cook DG & Whincup PH 2010. Ethnic differences in the prevalence of myopia and ocular biometry in 10- and 11-year-old children: the child heart and health study in England (CHASE). *Investigative Ophthalmology and Visual Science*, 51, 6270-6276.

Salouti R, Nowroozzadeh MH, Zamani M, Ghoreyshi M & Salouti R 2011. Comparison of the ultrasonographic method with 2 partial coherence interferometry methods for intraocular lens power calculation. *Journal of the American Optometric Association*, 82, 140-147.

Sankaridurg P, Donovan L, Varnas S, Ho A, Chen X, et al. 2010. Spectacle lenses designed to reduce progression of myopia: 12-month results. *Optometry and Vision Science*, 87, 631-641.

Sankaridurg P, Holden B, Smith E, Naduvilath T, Chen X, et al. 2011. Decrease in rate of myopia progression with a contact lens designed to reduce relative

peripheral hyperopia: one-year results. *Investigative Ophthalmology and Visual Science,* 52, 9362-9367.

Santodomingo-Rubido J, Mallen EAH, Gilmartin B & Wolffsohn JS 2002. A new non-contact optical device for ocular biometry. *British Journal of Ophthalmology,* 86, 458-462.

Santodomingo-Rubido J, Villa-Collar C, Gilmartin B & Gutiérrez-Ortega R. 2011. Myopia control with orthokeratology contact lenses in Spain (MCOS): Refractive and biometric changes. *The 89th annual meeting of the American Academy of Optometry,* The 89th annual meeting of the American Academy of Optometry.

Saw SM, Chua WH, Hong CY, Wu HM, Chia KS, et al. 2002. Height and its relationship to refraction and biometry parameters in Singapore Chinese children. *Investigative Ophthalmology and Visual Science,* 43, 1408-1413.

Saw SM, Gazzard G, Shih-Yen EC & Chua WH 2005. Myopia and associated pathological complications. *Ophthalmic and Physiological Optics,* 25, 381-391.

Saw SM, Hong CY, Chia KS, Stone RA & Tan D 2001. Nearwork and myopia in young children. *Lancet,* 357, 390.

Saw SM, Katz J, Schein OD, Chew SJ & Chan TK 1996. Epidemiology of myopia. *Epidemiologic Reviews,* 18, 175-187.

Saw SM, Shankar A, Tan SB, Taylor H, Tan DT, et al. 2006. A cohort study of incident myopia in Singaporean children. *Investigative Opthalmology and Visual Science,* 47, 1839-1844.

Scherzinger AL & Hendee WR 1985. Basic principles of magnetic resonance imaging-an update. *The Western Journal of Medicine,* 143, 782-792.

Schmid GF 2003a. Axial and peripheral eye length measured with optical low coherence interferometry. *Journal of Biomedical Optics,* 8, 655-662.

Schmid GF 2003b. Variability of retinal steepness at the posterior pole in children 7–15 years of age. *Current Eye Research,* 27, 61-68.

Schmid GF 2011. Association between retinal steepness and central myopic shift in children. *Optometry and Vision Science,* 88, 684-690.

Schulle KL & Berntsen DA 2013. Repeatability of on- and off-axis eye length measurements using the Lenstar. *Optometry and Vision Science,* 90, 16-22.

Schultz AH 1940. The size of the orbit and of the eye in primates. *American Journal of Physical Anthropology,* 26, 389-408.

Seet B, Wong TY, Tan DT, Saw SM, Balakrishnan V, et al. 2001. Myopia in Singapore: taking a public health approach. *British Journal of Ophthalmology,* 85, 521-526.

Seidemann A, Schaeffel F, Guirao A, Lopez GA & Artal P 2002. Peripheral refractive errors in myopic, emmetropic, and hyperopic young subjects. *Journal of the Optical Society of America A,* 19, 2363-2373.

Shah SP, Jadoon MZ, Dineen B, Bourne RR, Johnson GJ, et al. 2008. Refractive errors in the adult pakistani population: the national blindness and visual impairment survey. *Ophthalmic Epidemiology,* 15, 183-190.

Shammas HJ & Hoffer KJ 2012. Repeatability and reproducibility of biometry and keratometry measurements using a noncontact optical low-coherence reflectometer and keratometer. *American Journal of Ophthalmology,* 153, 55-61.

Shankar H, Taranath D, Santhirathelagan C & Pesudovs K 2008. Anterior segment biometry with the Pentacam: Comprehensive assessment of repeatability of automated measurements. *Journal of Cataract and Refractive Surgery,* 34, 103-113.

Sheng H, Bottjer CA & Bullimore MA 2004. Ocular component measurement using the Zeiss IOLMaster. *Optometry and Vision Science,* 81, 27-34.

Shufelt C, Fraser-Bell S, Ying-Lai M, Torres M & Varma R 2005. Refractive error, ocular biometry, and lens opalescence in an adult population: the Los Angeles Latino Eye Study. *Investigative Ophthalmology and Visual Science,* 46, 4450-4460.

Singh KD, Logan NS & Gilmartin B 2006. Three-dimensional modeling of the human eye based on magnetic resonance imaging. *Investigative Ophthalmology and Visual Science,* 47, 2272-2279.

Smith EL, 3rd, Hung LF, Huang J & Arumugam B 2013. Effects of local myopic defocus on refractive development in monkeys. *Optometry and Vision Science,* 90, 1176-1186.

Smith EL, III. 2011. Prentice Award lecture 2010: A case for peripheral optical treatment strategies for myopia. *Optometry and Vision Science,* 88, 1029-1044.

Smith EL, III., Hung LF, Huang J, Blasdel TL, Humbird TL, et al. 2010. Effects of optical defocus on refractive development in monkeys: evidence for local,

regionally selective mechanisms. *Investigative Ophthalmology and Visual Science,* 51, 3864-3873.

Smith EL, III., Kee CS, Ramamirtham R, Qiao-Grider Y & Hung LF 2005. Peripheral vision can influence eye growth and refractive development in infant monkeys. *Investigative Ophthalmology and Visual Science,* 46, 3965-3972.

Smith EL, III., Ramamirtham R, Qiao-Grider Y, Hung LF, Huang J, et al. 2007. Effects of foveal ablation on emmetropization and form-deprivation myopia. *Investigative Opthalmology and Visual Science,* 48, 3914-3922.

Sng CC, Lin X-Y, Gazzard G, Chang B, Dirani M, et al. 2011. Change in peripheral refraction over time in Singapore Chinese children. *Investigative Ophthalmology and Visual Science,* 52, 7880-7887.

Song HT, Kim YJ, Lee SJ & Moon YS 2007. Relations between age, weight, refractive error and eye shape by computerized tomography in children. *Korean Journal of Ophthalmology,* 21, 163-168.

Stone RA & Flitcroft DI 2004. Ocular shape and myopia. *Annals of the Academy of Medicine Singapore,* 33, 7-15.

Strang NC, Winn B & Bradley A 1998. The role of neural and optical factors in limiting visual resolution in myopia. *Vision Research,* 38, 1713-1721.

Sun J, Zhou J, Zhao P, Lian J, Zhu H, et al. 2012. High prevalence of myopia and high myopia in 5060 Chinese university students in Shanghai. *Investigative Ophthalmology and Visual Science,* 53, 7504-7509.

Tabernero J, Ohlendorf A, Fischer MD, Bruckmann AR, Schiefer U, et al. 2011. Peripheral refraction profiles in subjects with low foveal refractive errors. *Optometry and Vision Science,* 88, 388-394.

Tabernero J & Schaeffel F 2009a. Fast scanning photoretinoscope for measuring peripheral refraction as a function of accommodation. *Journal of Optical Society of America A,* 26, 2206-2210.

Tabernero J & Schaeffel F 2009b. More irregular eye shape in low myopia than in emmetropia. *Investigative Ophthalmology and Visual Science,* 50, 4516-4522.

Takano M & Kishi S 1999. Foveal retinoschisis and retinal detachment in severely myopic eyes with posterior staphyloma. *American Journal of Ophthalmology,* 128, 472-476.

Tang W, Collins MJ, Carney L & Davis B 2000. The accuracy and precision performance of four videokeratoscopes in measuring test surfaces. *Optometry and Vision Science*, 77, 483-491.

Tariq YM, Samarawickrama C, Pai A, Burlutsky G & Mitchell P 2010. Impact of ethnicity on the correlation of retinal parameters with axial length. *Investigative Ophthalmology and Visual Science,* 51, 4977-4982.

Thibos LN, Wheeler W & Horner D 1997. Power vectors: an application of Fourier analysis to the description and statistical analysis of refractive error. *Optometry and Vision Science,* 74, 367-375.

Ticak A & Walline JJ 2013. Peripheral optics with bifocal soft and corneal reshaping contact lenses. *Optometry and Vision Science,* 90, 3-8.

Timothy YL 2007. Retinal complications of high myopia. *The Hong Kong Medical Diary*, 12, 18-20.

Verkicharla PK, Mallen EAH & Atchison DA 2013. Repeatability and comparison of peripheral eye lengths with two instruments. *Optometry and Vision Science,* 90, 215-222.

Verkicharla PK, Mathur A, Mallen EAH, Pope JM & Atchison DA 2012. Eye shape and retinal shape, and their relation to peripheral refraction. *Ophthalmic and Physiological Optics,* 32, 184-199.

Verkicharla PK, Suheimat M, Mallen EA & Atchison DA 2014. Influence of eye rotation on peripheral eye length measurement obtained with a partial coherence interferometry instrument. *Ophthalmic and Physiological Optics,* 34, 82-88.

Villarreal GM, Ohlsson J, Cavazos H, Abrahamsson M & Mohamed JH 2003. Prevalence of myopia among 12- to 13-year-old schoolchildren in Northern Mexico. *Optometry and Vision Science,* 80, 369-373.

Vincent SJ, Collins MJ, Read SA & Carney LG 2013. Retinal and choroidal thickness in myopic anisometropia. *Investigative Ophthalmology and Visual Science,* 54, 2445-2456.

Vincent SJ, Collins MJ, Read SA & Carney LG 2014. Myopic anisometropia: ocular characteristics and aetiological considerations. *Clinical and Experimental Optometry,* 97, 291-307.

Vincent SJ, Collins MJ, Read SA, Carney LG & Yap MKH 2011. Interocular symmetry in myopic anisometropia. *Optometry and Vision Science,* 88, 1454-1462.

Vitale S, Ellwein L, Cotch MF, Ferris FL, 3rd & Sperduto R 2008. Prevalence of refractive error in the United States, 1999-2004. *Archives of Ophthalmology,* 126, 1111-1119.

Vohra SB & Good PA 2000. Altered globe dimensions of axial myopia as risk factors for penetrating ocular injury during peribulbar anaesthesia. *British Journal of Anaesthesia,* 85, 242-245.

Vongphanit J, Mitchell P & Wang JJ 2002. Population prevalence of tilted optic disks and the relationship of this sign to refractive error. *American Journal of Ophthalmology,* 133, 679-685.

Waelti R & Schmid GF. 1999. Method and device for measuring the optical properties of at least two regions located at a distance from one another in a transparent and/or diffuse object. A1 WO 01/38820.

Walker TW & Mutti DO 2002. The effect of accommodation on ocular shape. *Optometry and Vision Science,* 79, 424-430.

Wallman J & Winawer J 2004. Homeostasis of eye growth and the question of myopia. *Neuron,* 43, 447-468.

Weishaupt D, Köchli VD & Marincek B 2003. How does MRI work?: an introduction to the physics and function of magnetic resonance imaging, *Springer*, 32.

Wenner Y, Wismann S, Preising MN, Jager M, Pons-Kuhnemann J, et al. 2014. Normative values of peripheral retinal thickness measured with Spectralis OCT in healthy young adults. *Graefe's Archive for Clinical and Experimental Ophthalmology,* 252, 1195-1205.

Wensor M, McCarty CA & Taylor HR 1999. Prevalence and risk factors of myopia in Victoria, Australia. *Archives of Ophthalmology,* 117, 658-663.

Wertheim T 1980 (translated by DUNSKY, IL. Original work published in 1891). Peripheral visual acuity: Th. Wertheim. *Ameican Journal of Optometry and Physiological Optics,* 57, 915-924.

Whatham A, Zimmermann F, Martinez A, Delgado S, de la Jara PL, et al. 2009. Influence of accommodation on off-axis refractive errors in myopic eyes. *Journal of Vision,* 9(3), 14, 1-13.

Wilson A & Woo G 1989. A review of the prevalence and causes of myopia. *Singapore Medical Journal,* 30, 479-484.

Wong TY, Foster PJ, Johnson GJ & Seah SK 2003. Refractive errors, axial ocular dimensions, and age-related cataracts: the Tanjong Pagar survey. *Investigative Opthalmology and Visual Science,* 44, 1479-1485.

Wu MM & Edwards MH 1999. The effect of having myopic parents: an analysis of myopia in three generations. *Optometry and Vision Science,* 76, 387-392.

Yin G, Wang YX, Zheng ZY, Yang H, Xu L, et al. 2012. Ocular axial length and its associations in Chinese: The Beijing Eye Study. *PLoS ONE,* 7, e43172.

You QS, Wu LJ, Duan JL, Luo YX, Liu LJ, et al. 2013. Prevalence of myopia in school children in greater Beijing: the Beijing childhood eye study. *Acta Ophthalmologica,* DOI: 10.1111/aos.12299, In Press.

Younan C, Mitchell P, Cumming RG, Rochtchina E & Wang JJ 2002. Myopia and incident cataract and cataract surgery: The Blue Mountains Eye Study. *Investigative Ophthalmology and Visual Science,* 43, 3625-3632.

Young T 1801. On the mechanism of the eye. *Philosophical Transactions,* 91, 23-88.

Zadnik K 1997. The Glenn A. Fry Award Lecture (1995). Myopia development in childhood. *Optometry and Vision Science,* 74, 603-608.

Zhao J, Chen Z, Zhou Z, Ding L & Zhou X 2013. Evaluation of the repeatability of the Lenstar and comparison with two other non-contact biometric devices in myopes. *Clinical and Experimental Optometry,* 96, 92-99.

Zhou XD, Wang FR, Zhou SZ & Shi JS 1998. A computed tomographic study of the relation between ocular axial biometry and refraction. *In: Tokoro T.* (ed) Myopia Updates: Proceedings of the 6th international conference on myopia, 112–115.

Appendix 1- Ethics Approval Forms

Queensland University of Technology Brisbane Australia	**PARTICIPANT INFORMATION FOR QUT RESEARCH PROJECT**

Development, validation and application of a clinical method for determining retinal shape in myopia

QUT Ethics Approval Number1100001176

Prof. David A Atchison, Vision Domain, IHBI, QUT ph 3138 6152d.atchison@qut.edu.au
A/Prof. Katrina Schmid, Vision Domain, IHBI, QUT ph 3138 6150 k.schmid@qut.edu.au
Prof. Jim Pope, IHBI, QUT ph 3138 2325 j.pope@qut.edu.au
Mr Pavan Kumar Verkicharla, PhD student, Vision Domain, IHBI, QUT ph 3138 6164 pavankumar.verkicharla@student.qut.edu.au

DESCRIPTION

Part of this project is being undertaken as part of the Masters study for Mr Pavan Verkicharla. The purpose of this research is to investigate how the shape of the retina differs between people with ethnicities and spectacle prescriptions. You are invited to participate in this project because you are aged between 18 and 30 years of age.

PARTICIPATION

Your participation in this project is entirely voluntary. If you do agree to participate, you can withdraw from the project at any time without comment or penalty. Your decision to participate, or not participate, will in no way impact upon your current or future relationship with QUT (for example your grades).

Your participation will involve routine eye examination including eye and general medical history, refraction, intraocular distance measurements and biomicroscopy (viewing light reflected from the eye structures). It will also involve some specialist tests including aberrometry (measurements of the eye aberrations), peripheral refraction, phakometry (measurement of reflections from the lens), and off-axis ocular length. We may need to dilate the pupil of one eye with eye drops. The tests will take 2 – 4 hours of your time.

For a limited number of participants, magnetic resonance imaging (MRI) will be undertaken at the Imaging facility at the University of Queensland. MRI is used

routinely as a medical imaging modality without any adverse health effects on people undergoing a scan. All MRI scans will be carried out by qualified radiographers using equipment approved by the USA Therapeutic Goods Administration (TGA). This will take about an hour.

EXPECTED BENEFITS

It is expected that this project will not benefit you directly, although you may be interested in learning more about your eyes. In this study we will refine and evaluate a simple method of determining retinal shape. We will use it to increase our understanding of retinal shape in different population groups and in different parts of the eye. This will in turn be used to inform the design of devices to correct peripheral refractive errors. By achieving these aims we will contribute an important assessment device with applications for understanding myopia development risk and likely optical treatment effectiveness. This study will be of significant benefit to people at risk of myopia development.

To compensate you for your contribution, should you choose to participate, the research team will provide you with out-of-pocket expenses in the form of supermarket vouchers at the rate of $20/hour of participation.

RISKS

There are minimal risks associated with your participation in this project. The drugs that we use are routinely used in clinical eye examinations, and there are minimal risks associated with using them. However, we will screen for the likelihood of possible side effects. One of the drops anaesthetises the eye and so it is possible to scratch the eye without feeling it. Please do not rub your eyes for at least 45 minutes after the drug is placed in the eye. One of the other drops, if needed, paralyses the focusing of the eyes for up to 8 hours and the pupil may be dilated for up to 48 hours. Another dilating drug does not affect focussing and dilation will last for a few hours only. As pupil dilation makes the eye more sensitive to bright light, we recommend that you bring your sunglasses to wear afterwards. If you require, we can provide transport to get you home. Until the pupil size returns to normal, you should not drive or cycle, and take care with walking and using machinery. We recommend wearing your spectacle or contact lens correction for these tasks.

PRIVACY AND CONFIDENTIALITY

All comments and responses are anonymous and will be treated confidentially. The names of individual persons are not required in any of the responses.

CONSENT TO PARTICIPATE

We would like to ask you to sign a written consent form (enclosed) to confirm your agreement to participate.

QUESTIONS / FURTHER INFORMATION ABOUT THE PROJECT

Please contact the researcher team members named above to have any questions answered or if you require further information about the project.

CONCERNS/ COMPLAINTS REGARDING THE CONDUCT OF THE PROJECT

QUT is committed to research integrity and the ethical conduct of research projects. However, if you do have any concerns or complaints about the ethical conduct of the project you may contact the QUT Research Ethics Unit on [+61 7] 3138 5123 or email ethicscontact@qut.edu.au. The QUT Research Ethics Unit is not connected with the research project and can facilitate a resolution to your concern in an impartial manner.

Thank you for helping with this research project. Please keep this sheet for your information.

Queensland University of Technology Brisbane Australia	CONSENT FOR QUT RESEARCH PROJECT

Development, validation and application of a clinical method for determining retinal shape in myopia

QUT Ethics Approval Number 1100001176

Prof. David A Atchison	**Mr. Pavan Verkicharla**
Vision Domain, IHBI , QUT	**Vision Domain, IHBI, QUT**
3138 6152	**3138 6164**
d.atchison@qut.edu.au	**Pavankumar.verkicharla@student.qut.edu.au**

Statement of consent

By signing below, you are indicating that you:

- Have read and understood the participant information document regarding this project
- Have had any questions answered to your satisfaction
- Understand that if you have any additional questions you can contact the research tem
- Understand that you are free to withdraw at any time, without comment or penalty
- Understand that you can contact the Research Ethics Officer on +61 7 31385123 or ethicscontact@qut.edu.au if you have concerns about the ethical conduct of the project
- Agree and voluntarily consent your participation in this research project

Full Name: _____

Participant's Signature: _____ Date: ___/___/___

University Human Research Ethics Committee

HUMAN ETHICS APPROVAL CERTIFICATE

NHMRC Registered Committee Number EC00171

QUT - Approval Certificate - Date of Issue: 23/9/11(supersedes all previously issued certificates)

Dear Prof David Atchison

A UHREC should clearly communicate its decisions about a research proposal to the researcher and the final decision to approve or reject a proposal should be communicated to the researcher in writing. This Approval Certificate serves as your written notice that the proposal has met the requirements of the *National Statement on Research involving Human Participation* and has been approved on that basis. You are therefore authorised to commence activities as outlined in your proposal application, subject to any specific and standard conditions detailed in this document.

Within this Approval Certificate are:

Project Details

Participant Details

Conditions of Approval (Specific and Standard)

Researchers should report to the UHREC, via the Research Ethics Coordinator, events that might affect continued ethical acceptability of the project, including, but not limited to:

(a) serious or unexpected adverse effects on participants; and
(b) Proposed significant changes in the conduct, the participant profile or the risks of the proposed research.

Further information regarding your ongoing obligations regarding human based research can be found via the Research Ethics website http://www.research.qut.edu.au/ethics/ or by contacting the Research Ethics Coordinator on 07 3138 2091 or ethicscontact@qut.edu.au

If any details within this Approval Certificate are incorrect please advise the Research Ethics Unit within 10 days of receipt of this certificate.

PROJECT DETAILS

Category of Approval:	Human non-HREC		
Approved From:	23/09/2011	**Approved Until:**	23/09/2014 (subject to annual reports)
Approval Number:	1100001176		
Project Title:	Development, validation and application of a clinical method for determining retinal shape in myopia		
Experiment Summary:	Investigate how the shape of the retina differs amongst people with different ethnicities and spectacle prescriptions.		

Investigator Details

Chief Investigator:	Prof David Atchison	
Other Staff/Students:		
Investigator Name	**Type**	**Role**
A/Prof Katrina Schmid	Internal	Associate Investigator
Adj/Prof James Pope	Internal	Associate Investigator
Mr Pavan Kumar Verkicharla	Student	Ethics- Student-Course-Masters
Dr Edward Mallen	External	Associate Investigator
A/Prof Ian Morgan	External	Associate Investigator
Dr Ming guang He	External	Associate Investigator
Prof W Neil Charman	External	Associate Investigator

Participants:
Approximately 150 in Australia and 1200 in China

Location/s of the Work:

QUT

Conditions of Approval

Specific Conditions of Approval:
No special conditions placed on approval by the UHREC. Standard conditions apply.
Standard Conditions of Approval:
The University's standard conditions of approval require the research team to:

1. Conduct the project in accordance with University policy, NHMRC / AVCC guidelines and regulations, and the provisions of any relevant State / Territory or Commonwealth regulations or legislation;
2. Respond to the requests and instructions of the University Human Research Ethics Committee (UHREC);
3. Advise the Research Ethics Coordinator immediately if any complaints are made, or expressions of concern are raised, in relation to the project;
4. Suspend or modify the project if the risks to participants are found to be disproportionate to the benefits, and immediately advise the Research Ethics Coordinator of this action;
5. Stop any involvement of any participant if continuation of the research may be harmful to that person, and immediately advise the Research Ethics Coordinator of this action;
6. Advise the Research Ethics Coordinator of any unforeseen development or events that might affect the continued ethical acceptability of the project;
7. Report on the progress of the approved project at least annually, or at intervals determined by the Committee;
8. (Where the research is publicly or privately funded) publish the results of the project is such a way to permit scrutiny and contribute to public knowledge; and
9. Ensure that the results of the research are made available to the participants.

Modifying your Ethical Clearance:

Requests for variations must be made via submission of a Request for Variation to Existing Clearance Form

(http://www.research.qut.edu.au/ethics/forms/hum/var/var.jsp) to the Research Ethics Coordinator. Minor changes will be assessed on a case by case basis.

It generally takes 7-14 days to process and notify the Chief Investigator of the outcome of a request for a variation.

Major changes, depending upon the nature of your request, may require submission of a new application.

Audits:

All active ethical clearances are subject to random audit by the UHREC, which will include the review of the signed consent forms for participants, whether any modifications / variations to the project have been approved, and the data storage arrangements.

End of Document

THE UNIVERSITY OF QUEENSLAND

PARTICIPATE IN RESEARCH

Information for Prospective Participants

Development, validation and application of a clinical method for determining retinal shape in myopia

Research Team Contacts

Principal Researchers

Prof David A Atchison, Vision Domain, IHBI, QUT
ph 3138 6152d.atchison@qut.edu.au

Prof Jim Pope, IHBI, QUT ph 3138 2325j.pope@qut.edu.au

Mr Parvan Verkicharla, PhD student, Vision Domain, IHBI, QUT
ph 3138 6164 pavankumar.verkicharla@student.qut.edu.au

Please contact the researcher team members to have any questions answered or if you require further information about the project.

What is the purpose of the research?

The purpose of this research is to investigate how the shape of the retina differs between people with different ethnicities and spectacle prescriptions. This is important to the understanding of the progression of myopia as ethnic Chinese have a higher prevalence of myopia thanb European populations.

Are you looking for people like me?

The research team is looking for people aged between 18 and 30 years of age, in good ocular and general health, of either European/Caucasian or Chinese ancestry, and with a range of spectacle prescriptions.

What will you ask me to do?

This is part of a study being conducted through the Queensland University of Technology that involves magnetic resonance imaging (MRI) at the Centre for Advanced Imaging at the University of Queensland. MRI is used routinely as a medical imaging modality without any adverse health effects on people undergoing a scan. All MRI scans will be carried out by a qualified radiographer using equipment approved by the Therapeutic Goods Administration TGA. This

will take a maximum of an hour.

Are there any risks for me in taking part?

Certain items should not be taken into the magnetic field. A checklist will be used to screen for this.

Are there any benefits for me in taking part?

It is expected that this project will not benefit you directly, although you may be interested in learning more about your eyes. In this study we will refine and evaluate a simple method of determining retinal shape. We will use it to increase our understanding of retinal shape in different population groups and in different parts of the eye. This will in turn be used to inform the design of devices to correct peripheral refractive errors. By achieving these aims we will contribute an important assessment device with applications for understanding myopia development risk and likely optical treatment effectiveness. This study will be of significant benefit to people at risk of myopia development.

We will provide you with copies of your eye images.

Will I be compensated for my time?

To compensate you for your contribution, the research team will provide you with out-of-pocket expenses in the form of supermarket vouchers for $20 and will provide you with transportation to and from the Centre for Advanced Imaging.

I am interested – what should I do next?

If you would like to participate in this study, please contact the research team. You will be provided with further information to ensure that your decision and consent to participate is fully informed. Please note that you are free to withdraw from the study at any time without penalty

QUT Ethics Approval Number: *1100001176*

Information of a personal nature obtained in this study will not be shared with others. In any publications or reports, no information will be included that could identify you.

This study adheres to the Guidelines of the ethical review process of The University of Queensland. Whilst you are free to discuss your participation in this study with project staff (contactable on 3138 6152), if you would like to speak to an officer of the University not involved in the study, you may contact the Ethics Officer on 3365 3924.

THE UNIVERSITY OF QUEENSLAND

CONSENT FORM FOR RESEARCH PROJECT

Development, validation and application of a clinical method for determining retinal shape in myopia

QUT Ethics Approval Number 1100001176

UQ Ethics Approval 2012000175

Research Team

Principal Researchers

Prof David A Atchison, Vision Domain, IHBI, QUT

ph 3138 6152 d.atchison@qut.edu.au

Prof Jim Pope, IHBI, QUT ph 3138 2325 j.pope@qut.edu.au

Mr Pavan Verkicharla, PhD student, Vision Domain, IHBI, QUT

ph 3138 6164 pavankumar.verkicharla@student.qut.edu.au

Statement of consent

By signing below, you are indicating that you:

- have read and understood the information document regarding this project
- have had any questions answered to your satisfaction
- understand that if you have any additional questions you can contact the research team
- understand that you are free to withdraw at any time, without comment or penalty
- understand that you can contact the UQ *Ethics Officer on 3365 3924* if you have concerns about the ethical conduct of the project
- agree to participate in the project

Name .....

Signature .....

Date _____

Please return this sheet to the investigator.

THE UNIVERSITY OF QUEENSLAND
AUSTRALIA

Centre for Advanced Imaging

MRI INVESTIGATION

METALS CHECK/INTERIM

MEDICAL

The University of Queensland
Level 2, Gehrmann Laboratories
Research Road
Brisbane Qld 4072 Australia
Telephone +61 7 3365 4100
Internet www.cai.uq.edu.au

Subject/Visitor Name: _____DOB:_____
Date: _____Time: _____Checked By: _____

Contact Phone Number_____

DO YOU HAVE	YES	NO	ARE YOU WEARING	YES	NO
Pacemaker or a Heart valve			Hairpins, slides, wig, hair bands		
Syringe Driver			Ear rings		
Brain clip, aortic clip or neurostimulators			Necklace/Chains		
Metal mesh Implants/Clips/wire sutur			Safety pins/Broaches/Badges		
Medicated Skin Patches			Watch		
Hearing Aid/Implant			Bracelets		
Glass Eye			Body piercing		
Joint Replacement			Braces with metal clips		
Bullet/Shrapnel Wound			Mobile phone/Pager		
Metal Fragments in Eye, Head, Skin			Coins		
Artificial Limb or			Credit Cards		
Do you work with metals?			Wallet		
Do you suffer claustrophobia?			Penknife		
Could you be pregnant?			Keys		
Do you have an IUD?					
Fractured bones treated with Metal?					
Have you had any major surgery?			Do you consent to undergo the MRI?	YES/NO	
A Shunt, spinal or Ventricular?			I have read the MRI Information Sheet	YES/NO	
Do you have any tattoos?			Signed:		
Dental Bridge or Dentures with wires			Volunteer: _____		
Do you have a history of kidney disease/disorder?			Authorised MRI Supervisor: _____		

Blood Pressure: _____Pulse_____
Height_____Weight_____

_____

Appendix 2- Publications

The following are the journal articles and presentations which have arisen from the work presented in thesis at the time of its submission. The first, second and third journal articles are preliminary investigations found in section 3.5.5 and the fourth journal article is an early version of the literature review (section 2.4.2).

Journal Articles

1. Suheimat M, **Verkicharla PK,** Mallen EAH, Rozema J and Atchison DA. Submitted: June 2014. "Refractive indices used by the Haag-Streit Lenstar to calculate axial biometric dimensions". *Ophthalmic and Physiological Optics*. 35(1): 90-96.
2. **Verkicharla PK,** Suheimat M, Mallen EAH, and Atchison DA. 2014. "Technical note: Influence of eye rotation on the peripheral eye length measurements obtained using partial coherence interferometry". *Ophthalmic and Physiological Optics*, 34(1): 82-88.
3. **Verkicharla PK**, Mallen EAH, and Atchison DA. 2013. "Repeatability and comparison of peripheral eye lengths with two instruments". *Optometry and Vision Science*, 90(3):215-22.
4. **Verkicharla PK**, Mathur A, Mallen EAH, Pope JM, and Atchison DA. 2012. "Eye shape and retinal shape, and their relation to peripheral refraction". *Ophthalmic and Physiological Optics*, 32(3): 184-199.

Conference Abstracts

1. Verkicharla PK, Atchison DA, Suheimat M, Schmid KL, Mathur A, Mallen EAH, Wei X, Brennan NA May 2014. Is retinal shape different in Asians and Caucasians? Estimation from peripheral refraction and peripheral eye length methods. *Investigative Ophthalmology and Visual Science* 55:3592. *The Association for Research in Vision and Ophthalmology (ARVO) annual meeting 2014,* Orlando, Florida.

2. **Verkicharla PK**, Atchison DA, Mallen EAH, Suheimat M, Mathur A, Schmid KL, and Dunne MCM, Wei X, Brennan NA August 2013. "Retinal shape estimation from peripheral refraction and peripheral eye length methods". *International Myopia Conference*, California. Ophthalmic and Physiological Optics, 33(6), Appendix S1. http://onlinelibrary.wiley.com/doi/10.1111/opo.12088/suppinfo

3. **Verkicharla PK** and Atchison DA. November 2012. "Intra and inter session repeatability of IOLMaster and Lenstar for measuring peripheral eye lengths". Institute of Health and Biomedical Innovation's *IHBI Inspires postgraduate student conference*, Gold Coast, Australia.

4. **Verkicharla PK**, Mathur A, Mallen EAH, and Atchison DA. September 2012. "Comparison of two partial coherence interferometry instruments for measuring peripheral eye lengths". *14th Scientific Meeting and 8th Educators' Meeting in Optometry*, Melbourne, Australia.